University of Calgary

PRISM Repository **https://prism.ucalgary.ca**

The Vault Open Theses and Dissertations

2017

Comprehensive Analytical Modelling of SAGD and Its Variations

Zargar, Zeinab

Zargar, Z. (2017). Comprehensive Analytical Modelling of SAGD and Its Variations (Doctoral thesis, University of Calgary, Calgary, Canada). Retrieved from https://prism.ucalgary.ca. doi:10.11575/PRISM/25387 http://hdl.handle.net/11023/4195

Downloaded from PRISM Repository, University of Calgary

UNIVERSITY OF CALGARY

Comprehensive Analytical Modelling of SAGD and Its Variations

by

Zeinab Zargar

A THESIS

SUBMITTED TO THE FACULTY OF GRADUATE STUDIES

IN PARTIAL FULFILMENT OF THE REQUIREMENTS FOR THE

DEGREE OF DOCTOR OF PHILOSOPHY

GRADUATE PROGRAM IN CHEMICAL AND PETROLEUM ENGINEERING

CALGARY, ALBERTA

SEPTEMBER, 2017

© Zeinab Zargar 2017

Abstract

A comprehensive analytical model of the Steam-Assisted Gravity Drainage (SAGD) process was developed, encompassing steam chamber rise, sideways expansion, and the confinement phases. Results were validated using experimental and field data. The deficiencies of the previous models are pointed out, none of which treated the SAGD process in its entirety, as done in this work. Also, a new mathematical model of the solvent-SAGD process for the sideways expansion of the vapour chamber was developed.

During steam chamber rise, the Cumulative Steam-Oil ratio (CSOR) decreases, with an increasing oil production rate. The rise velocity increases with an increase in permeability and temperature.

The sideways steam chamber expansion is treated in two widely different ways in this study, called Constant Volumetric Displacement (CVD) where injection rate must be increased continuously for a constant oil rate, and Constant Heat Injection (CHI). In CVD, interface temperature gradient decreases with time, but the heat penetration depth increases. In CHI, heat injection rate is constant, but oil rate declines with time. Also, the oil rate decreases with an increase in operating pressure, in contrast to previous studies.

In the final stage, adjacent chambers interfere, reducing the effective head for gravity drainage. For a small well spacing, confinement occurs earlier, heat loss starts decreasing sooner, resulting in a lower CSOR, than for a large spacing. After chambers coalescence, the oil rate declines faster in CVD than CHI model.

The above models were combined to obtain the Comprehensive Constant Volumetric Displacement (CCVD) and Comprehensive Constant Heat Injection (CCHI) models. Excellent agreement was obtained with laboratory and field results.

Also developed was a new solvent-SAGD model. Results show an increase in heat penetration, and decrease in the interface temperature and concentration with time. Mass transfer scale is of the order of centimetres, while heat transfer occurs over metres.

The solvent-SAGD process would yield a higher oil recovery, if viscosity reduction from dilution at a lower temperature is greater than viscosity reduction by temperature in the plain SAGD process, for the same total rate. In most cases, the additional bitumen recovery was less than the volume of the solvent injected.

Acknowledgments

My deepest gratitude goes first to my supervisor, Dr. Farouq Ali, who has never stopped being a compassionate teacher, a provident mentor, and a caring friend. His unwavering enthusiasm for petroleum engineering kept me constantly engaged with my research and his scholarly guidance and inspiring suggestion helped me in carrying out the present research work. I could not have imagined having a better advisor and mentor for my Ph.D. study. I am especially grateful to him for his thoughtfulness during the hardest time of my life when I lost my father.

I would like to thank all the members of my supervisory committee and the examination committee. Financial support provided by Zandmer and Queen Elizabeth II Scholarships and HOR Heavy Oil Recovery Technology Ltd. is greatly acknowledged.

At last but not the least, I wish to express my deep sense of appreciation towards my wonderful husband, Mehdi, for his great patience, understanding, and constant encouragement throughout these years. My love and special thanks go to my dear Mother who has the greatest power to make me calm and relaxed during the difficult times!

Dedication

To memory of my dearest father who motivated me to start this journey …

Table of Contents

Abstract ii

Acknowledgments iv

Table of Contents vi

List of Tables x

List of Figures and Illustrations xi

Nomenclature xix

1. INTRODUCTION 1

1.1 Heavy Oil and Oil Sands 1

1.2 Steam-Assisted Gravity Drainage (SAGD) Process 4

1.3 Solvent SAGD Process 8

1.4 Statement of the Problem 10

1.5 Thesis Layout 12

2. REVIEW OF THE LITRETURE 16

2.1 Steam-Assisted Gravity Drainage (SAGD) Process 16

2.1.1 Introduction 16

2.1.2 Analytical Modelling of the Steam Chamber Rise Phase 17

2.1.3 Analytical Modelling of the Sideways Expansion Phase 20

2.1.4 Analytical Modelling of the Confinement Phase 26

2.1.5 Comprehensive Analytical Modelling of the SAGD Process 26

2.2 Solvent-SAGD Process 29

2.2.1 Introduction 29

2.2.2 Analytical Modelling of Solvent-SAGD Process 33

3. ANALYTICAL MODELLING OF STEAM CHAMBER RISE STAGE 36

3.1 Introduction 36
3.2 Analytical Model 37
3.2.1 Model Assumptions 37
3.2.2 Analytical Model 37
3.3 Results and Discussion 53
3.3.1 Results for Steam Chamber Rise Velocity 53
3.3.2 Results for Oil Production 56
3.3.3 Results for Heat Distribution and Thermal Efficiency 58
3.3.4 Reservoir Rock Permeability 61
3.4 Validation of the Theory with Field Data 64
4. ANALYTICAL TREATMENTS OF LATERAL SPREADING PHASE OF SAGD CHAMBER 71
4.1 Introduction 71
4.2 Analytical Model - Constant Volumetric Displacement Model 73
4.2.1 Model Assumptions 73
4.2.2 Methodology 73
4.2.3 Results of the CVD Model 88
4.2.4 Discussion of Butler's Original Model 96
4.3 Analytical Model - Constant Heat Injection Model 98
4.3.1 Modelling Assumptions 98
4.3.2 Methodology 99
4.3.3 Results of the CHI Model 102
4.3.4 Discussion of Butler's 1985 SAGD Model 110
4.4 Comparison of CHI and CVD Models 111

5. ANALYTICAL TREATMENT OF THE CONFINEMENT PHASE OF SAGD 115

5.1 Introduction 115

5.2 Analytical Model – Confinement Effect on CVD Model 115

5.2.1 Modelling Assumptions 116

5.2.2 Mathematical Formulation 116

5.2.3 Results 123

5.3 Analytical Model – Confinement Effect on CHI Model 133

5.3.1 Modelling Assumptions 133

5.3.2 Mathematical Formulation 133

5.3.3 Results 135

6. COMPREHENSIVE ANALYTICAL MODEL OF SAGD 141

6.1 Introduction 141

6.2 Comprehensive CVD Model - Summary of the Governing Equations 142

6.2.1 Results 143

6.2.2 Validation of Theory with Experimental Data 149

6.2.3 Validation of Theory with Field Data 160

6.3 Comprehensive CHI Model - Summary of Governing Equations 164

6.3.1 Results 165

7. NEW MATHEMATICAL TREATMENT OF THE SOLVENT-SAGD PROCESS 170

7.1 Introduction 170

7.2 Analytical Model 171

7.2.1 Modelling Assumptions 171

7.2.2 Mathematical Formulation 172
7.3 Results and Discussion 180
7.3.1 Solvent-SAGD Performance Evaluation 180
7.3.2 Effect of Total Injection Rate 196
7.3.3 Effect of Solvent Diffusion Coefficient 199
7.3.4 Oil Recovery Mechanism 202
8. CONCLUSIONS 209
A. Steam-Assisted Gravity Drainage (SAGD) 209
B. Solvent-SAGD Model 212
9. RECOMMENDATIONS FOR FURTHUR WORK 214
REFERENCES 215
APPENDIX A 226
APPENDIX B 231

List of Tables

Table 1.1: Definitions of heavy oil and oil sands (Farouq Ali, 2015). 2
Table 3.1: Closmann and Smith's data for Athabasca. 54
Table 3.2: Comparison of steam chamber rise velocity from Closmann and Smith, Butler and this work to observed field data. 54
Table 3.3: Comparison of steam chamber rise velocity from Butler, Gotawala, and Gates, and this work to the average rise velocity of Athabasca and Lloydminster field data. 55
Table 3.4: Effect of steam temperature on chamber rise velocity. 56
Table 3.5: Typical Athabasca rock and fluid properties. 57
Table 3.6: Some additional results are calculated from the proposed approach of the rise period of SAGD. 58
Table 3.7: Reservoir rock, fluid, and injected steam properties of Surmont project (ConocoPhillips Canada, 2015). 65
Table 3.8: Additional results determined by the proposed approach in this work about the steam chamber development in Well 101-08 in the Athabasca oil sands. 67
Table 4.1: Experimental data from Butler, McNab, and Lo (1981). 89
Table 4.2: Data for oil flow rate calculations (Cenovus Energy, 2015). 91
Table 4.3: Comparison of oil production rate from the CVD model, Butler's original model, TANDRAIN theory, and Reis (1992) with field data (Sharma, 2011). 95
Table 6.1: Summary of all governing equations of the CCVD approach. 142
Table 6.2: Rock and fluid properties of SAGD experiments (Chung and Butler 1987). 150
Table 6.3: Well and reservoir specifications (Cenovus Energy, 2012-2013). 161
Table 6.4: Summary of all governing equations of the CCHI approach. 165
Table 7.1: Andrade's constants used in this study. 181
Table 7.2: Rock and fluid properties used in this study. 183
Table 7.3: Results of the solvent-SAGD model for different solvents and mass fraction over a 1000-day time interval (day 1 to day 1000). 195

List of Figures and Illustrations

Figure 1.1: The world's Largest Oil Reserves (Worldatlas, 2014). 1
Figure 1.2: Variation of Athabasca oil sand's viscosity with temperature (Mehrotra and Svrcek, 1986). 3
Figure 1.3: Schematic representation of SAGD process (courtesy of Japan and Canada Oil Sands Limited). 5
Figure 1.4: Schematic of steam and heated oil flows in and around the steam chamber in SAGD process. 6
Figure 1.5: Steam chamber development in SAGD process including rise, lateral spreading, and confinement phases (Chung and Butler, 1987). 7
Figure 1.6: Effect of solvent (hexane) concentration on Athabasca bitumen viscosity reduction (Shu's Correlation, 1984). 9
Figure 1.7: Schematic representation of the organization of this thesis. 15
Figure 2.1: Interface positions of Butler's original model (Butler and Dargie, 1994). 21
Figure 2.2: Modified interface positions of Butler's original model to represent TANDRAIN theory interface positions. 22
Figure 2.3: Modified interface positions of Butler's original model to represent LINDRAIN theory interface positions. 23
Figure 2.4: Schematic of steam chamber development including rise (green lines), sideways expansion (black lines), and confinement by neighbouring steam chambers (red lines) phases. 28
Figure 3.1: The approximate shape of the steam chamber during rise phase. 38
Figure 3.2: Upper steam chamber interface movement from t_n to t_{n+1} assuming a counter current flow of steam and oil. 42
Figure 3.3: Rising steam chamber interface at the top and heat distribution in the system during rise phase including heat to the steam zone, Q_{sz}, heat to the oil zone at sides of steam chamber, Q_{ozs}, and to the overhead, Q_{ozo}. 46
Figure 3.4: Cumulative oil and oil production rate during steam chamber rise. 57

Figure 3.5: Calculated heat distribution in the system as a function of time during the rise period using data in Table 3.5. 59
Figure 3.6: Cumulative oil production and steam injection from the model versus time. 60
Figure 3.7: Predicted declining CSOR as a function of time during the rise stage of SAGD. 61
Figure 3.8: Comparison of oil production rate and cumulative oil as a function of time for two different rock permeabilities; 1 and 2 D. 62
Figure 3.9: Cumulative steam injection variation with time for two different rock permeabilities; 1 and 2 D during the rise period. 63
Figure 3.10: Comparison of CSOR for rock permeabilities of 1 and 2 D. 64
Figure 3.11: Comparison of cumulative oil production from the proposed of the steam chamber in this work (Equation 3.14) with the reported field data of Surmont project Well 101-08 in the Athabasca oil sands. 66
Figure 3.12: Comparison of cumulative steam injection from this work with the reported field data of Surmont project Well 101-08 in the Athabasca oil sands. 66
Figure 3.13: Cumulative Steam-Oil Ratio from this model (Equation 3.48) is validated against the field data of Surmont project Well 101-08 in the Athabasca oil sands. 67
Figure 3.14: Investigating the effect of modifying the heat distribution in the system to include the heat loss to the underburden. 68
Figure 3.15: Effect of including heat loss to the underburden on CSOR. 69
Figure 3.16: Heat distribution in the reservoir during the rise period for Well 101-08 in the Athabasca oil sands. 70
Figure 4.1: Schematic of heat and fluid flow ahead of an arbitrary interface at $t = tn$ and position $\theta = \theta_n$. 74
Figure 4.2: For each steam chamber interface (rotating around the fixed point, producer), heat front moves normal to it. 76
Figure 4.3: The relation between maximum steam chamber movement at the top, ($x'_H \times dt$), and heat front movement ($U \times dt$) is shown. The steam chamber movement should be equal to the heat front to have the same steam volume invasion. 76

Figure 4.4: Heat front velocity, U, decreases with time for a moving steam chamber interface fixed at the producer. 77
Figure 4.5: Front velocity as a function of reservoir thickness and time. 78
Figure 4.6: Variation of dimensionless temperature as a function of the distance from the steam chamber interface and time in the CVD model. 88
Figure 4.7: Oil production rate comparison by the use of data from Butler, McNab, and Lo (1981). 89
Figure 4.8: Comparison of oil-flow rate as a function of y along the steam chamber interface from the CVD model (Equation 4.24) and Butler original model (Equation 2.1). 92
Figure 4.9: Cumulative heat to steam zone, loss and accumulated ahead of front for CVD model. 93
Figure 4.10: CSOR for CVD model by use of data in Table 4.2. 94
Figure 4.11: Material balance element in Butler's theory (Butler and Dargie, 1994). 96
Figure 4.12: Calculated oil production rate from the Constant Heat Injection (CHI) model by use of data in Table 4.2. 104
Figure 4.13: Distribution of the injected heat rate in the CHI model in three forms: heat rate to steam zone, heat loss rate, and rate of heat outflow into the oil zone ahead of the steam chamber interface by use of data in Table 4.2. 105
Figure 4.14: Calculated CSOR from the CHI model by use of data in Table 4.2. 106
Figure 4.15: Effect of reservoir thickness ($H = 22, 26, and\ 30\ m$) on cumulative oil during a 1000-day period by use of data in Table 3.5. 107
Figure 4.16: Effect of reservoir thickness ($H = 22, 26, 30\ m$) on CSOR in SAGD, during sideways expansion phase, using the CHI model. 108
Figure 4.17: Effect of steam pressure ($P = 2.35, 2.8, and\ 4.8\ MPa$) on cumulative oil during a 1000-day period by use of data in Table 3.5. 109
Figure 4.18: Effect of steam pressure ($P = 2.35, 2.8, and\ 4.8\ MPa$) on CSOR in SAGD with constant rate a of steam injection, during sideways expansion phase. 110

Figure 4.19: Comparison between oil production rate from the CVD model with CHI model..... 112
Figure 4.20: Cumulative oil production from the CHI model is compared with the result of the CVD model by use of data in Table 4.2..... 113
Figure 4.21: Calculated steam chamber interface positions from the two approaches (CVD and CHI) are compared at four different times; 200, 400, 800, and 1000 days..... 114
Figure 5.1: Maximum steam chamber movement under confinement effect occurs on an imaginary vertical line passing through the halfway of well spacing between two neighbouring steam chambers (Lc). Under the confinement effect, the relation between maximum steam chamber movement, ($y'_{Lc} \times dt$), and heat front movement ($U \times dt$) can be seen. To have consistency between the two movements to illustrate the same steam volume invasion, steam chamber movement should be equal to front movement. 117
Figure 5.2: Unsteady dimensionless temperature profiles versus the distance from the steam-oil interface with and without confinement effect - CVD model..... 123
Figure 5.3: Maximum steam chamber velocity versus time with and without confinement effect - CVD model..... 124
Figure 5.4: Oil production rate as a function of time with and without confinement effect – CVD model. 125
Figure 5.5: Comparing cumulative oil production with and without confinement effect over 2000-day time interval – CVD model..... 126
Figure 5.6: Angle between steam-oil interface and the horizon with and without the effect of confinement – CVD model..... 127
Figure 5.7: Calculated interface positions in confined (dashed lines) and unconfined (solid lines) reservoirs at three different times; 1027 (red), 1500 (green), and 2000 (black) days. 128
Figure 5.8: Cumulative heat distribution in the system in forms of loss, into the steam zone, and oil zone with and without confinement effect – CVD model. 129
Figure 5.9: Comparing cumulative steam injection with and without confinement effect over time – CVD model..... 130

Figure 5.10: Calculated CSOR with and without confinement effect – CVD model..... 131
Figure 5.11: Effect of the well spacing on the oil production rate as a function of time.132
Figure 5.12. Effect of the well spacing on CSOR..... 133
Figure 5.13: Maximum steam chamber velocity as a function of time with and without confinement effect – CHI model..... 136
Figure 5.14: Comparing oil production rate with and without confinement effect over 2000-day time interval – CHI model..... 137
Figure 5.15: Steam chamber interface angle with horizontal with and without confinement effect over time – CHI model. 138
Figure 5.16: Heat rate in the system in forms of loss, into the steam zone, and outflow into oil zone with and without confinement effect – CHI model..... 139
Figure 5.17: Comparison of CSOR with and without confinement effect over time – CHI model..... 140
Figure 6.1: Maximum steam chamber velocity of the CCVD approach over the three phases of SAGD process. 144
Figure 6.2: Effective height for oil drainage as a function of time over the three phases of SAGD process..... 144
Figure 6.3: Oil production rate as a function of time over the three phases of SAGD process. 145
Figure 6.4: Cumulative oil production of SAGD process (CCVD approach) over a 2000-day time interval. 146
Figure 6.5: Cumulative steam injection of the CCVD approach per unit length of horizontal well as a function of time..... 147
Figure 6.6: CSOR varies with time over rise, sideways expansion, and confinement phases of SAGD. 148
Figure 6.7: Variation of the angle between the steam chamber interface and the horizon with time in SAGD. 149
Figure 6.8: Comparison of the predicted steam chamber shape from the comprehensive approach at 20 minutes (red solid line triangle) and at 50 minutes (red-dashed line triangle),

and the steam chamber boundaries (black-dashed curve) from experimental work of Chung and Butler (1987) – Rise phase. 151
Figure 6.9: Comparison of the predicted steam chamber shape from the comprehensive approach at 90 minutes (red solid line triangle), and the steam chamber boundaries (black-dashed curve) from experimental work of Chung and Butler (1987) – Rise phase. 152
Figure 6.10: Comparison of the predicted steam chamber shape from the comprehensive approach at 150 minutes (red solid line), and the steam chamber boundaries (black-dashed curve) from experimental work of Chung and Butler (1987) – Sideways expansion phase. 153
Figure 6.11: Comparison of the predicted steam chamber shape from the comprehensive approach at 210 minutes (red solid line), and the steam chamber boundaries (black-dashed curve) from experimental work of Chung and Butler (1987) – Confinement phase. 154
Figure 6.12: Oil production rate from experimental work of Chung and Butler (1987) is compared with the results of comprehensive approach during the three phases of SAGD. 155
Figure 6.13: Oil recovery factor from experimental work of Chung and Butler (1987) is compared with the results of comprehensive model. 156
Figure 6.14: Variation of oil production rate as a function of recovery factor from experimental work of Chung and Butler (1987) is compared with the results of comprehensive model during the three phases of SAGD. 157
Figure 6.15: Comparison of the effective height for drainage from experimental work of Chung and Butler (1987) (red squares) with the results of the comprehensive approach during the three phases of SAGD. 158
Figure 6.16: Calculated maximum steam chamber velocity based on CCVD model by use of data of Chung and Butler (1987) during rise, sideways expansion, and confinement phases of SAGD. 159
Figure 6.17: Comparison of oil production rate from the analytical comprehensive model and well production data of Christina Lake Well A01-6. 161

Figure 6.18: Cumulative oil production data of Christina Lake Well A01-6 is compared with the analytical comprehensive model. 162
Figure 6.19: Comparison of oil production rate from the analytical comprehensive model and well production data of Christina Lake Well A01-4. 163
Figure 6.20: Cumulative oil production data of Christina Lake Well A01-6 is compared with the analytical comprehensive model. 164
Figure 6.21: Oil production rate of the CCHI approach as a function of time over the three phases of SAGD process. 166
Figure 6.22: Cumulative oil production of SAGD process (CCHI approach) over a 2000-day time interval. 167
Figure 6.23: Cumulative steam injection of the CCHI approach per unit length of horizontal well as a function of time. 168
Figure 6.24: CSOR varies with time over rise, sideways expansion, and confinement phases of SAGD. 168
Figure 6.25: Calculated Oil production rate, steam injection rate, and CSOR from the CCHI approach as functions of time. 169
Figure 7.1: Mixture viscosity model as a function of temperature for various solvents, butane, pentane, and hexane and different solvent volume fractions with bitumen; 5 and 10%. 182
Figure 7.2: Comparison of oil production rate from solvent 9%-SAGD with SAGD.... 185
Figure 7.3: Comparison of CSOR of solvent 9%-SAGD with SAGD. 186
Figure 7.4: Solvent and bitumen production rate over a 1000-day period for different solvent at the same mass fraction (9%)..... 187
Figure 7.5: Comparison of cumulative steam-oil ratio versus cumulative bitumen production for different solvent co-injection (at the same mass fraction 9%) with steam and steam only. 188
Figure 7.6: Effect of solvent mass fraction on oil production rate for various solvents. 189
Figure 7.7: Effect of solvent mass fraction on total solvent and bitumen production rate for various solvents. 190

Figure 7.8: Cumulative steam oil ratio over a 1000-day period for different solvents and different solvent mass fraction (5 and 9%). 191
Figure 7.9: Comparison of additional cumulative oil to cumulative injected solvent number versus cumulative oil production for butane at two different mass fractions 5 and 9%. 192
Figure 7.10: Variation of oil production rate with time for three different total injection rates; 300, 400, and 500 kg/day per unit length of horizontal well. 197
Figure 7.11: Comparison of CSOR as a function of time for three different total injection rates; 300, 400, and 500 kg/day per unit length of horizontal well. 198
Figure 7.12: Comparison of solvent loss rate as a function of time for three different total injection rates; 300, 400, and 500 kg/day per unit length of horizontal well. 199
Figure 7.13: Comparison of cumulative oil production as a function of time for three diffusion coefficients; 8.04×10^{-4}, 8.04×10^{-3}, and 8.04×10^{-2}m^2/day. 201
Figure 7.14: Comparison of CSOR as a function of time for three diffusion coefficients; $8.04 \times 10^{-4}, 8.04 \times 10^{-3},$ and 8.04×10^{-2} m^2/day. 202
Figure 7.15: Comparison of temperature profiles for two scenarios with the base case ($D_{so} = 8.04 \times 10^{-4} m^2/day$, and $i_{tot} = 400\ kg/(day - m)$); Case A, higher injection rate, $500\ kg/(day - m)$ and Case B, higher diffusion coefficient, $8.04 \times 10^{-4} m^2/day$. 204
Figure 7.16: Comparison of solvent concentration profiles for two scenarios with the base case ($D_{so} = 8.04 \times 10^{-4} m^2/day$, and $i_{tot} = 400\ kg/(day - m)$); Case A, higher injection rate, $500\ kg/(day - m)$ and Case B, higher diffusion coefficient, 8.04×10^{-4} m^2/day. 205
Figure 7.17: Bitumen viscosity variation for two scenarios with the base case($D_{so} = 8.04 \times 10^{-4} m^2/day$, and $i_{tot} = 400\ kg/(day - m)$); Case A, higher injection rate, $500\ kg/(day - m)$ and Case B, higher diffusion coefficient, $8.04 \times 10^{-2}\ m^2/day$. 206
Figure 7.18: Computed reciprocal of bitumen viscosity as a function of distance from the steam chamber edge. 207

Nomenclature

a	Empirical constant in Reis (1992) equation
A	Area, m^2
A_{inf}	Steam-oil Interface area per unit length of horizontal well, m^2/m
A_o	Available area for oil to drain down at chamber top interface, m^2/m
A_{ob}	Total area in contact with overburden rock, m^2/m
A_s	Available area for steam to move upward at chamber top interface, m^2/m
A_t	Total area at the chamber top interface, m^2/m
C	Solvent volume fraction in solvent-bitumen mixture, vol%
C_{sol}^{inj}	Injected solvent mass fraction
c	Heat capacity, J/(kg. ^oC)
c_o	Oil heat capacity, J/(kg. ^oC)
c_r	Rock heat capacity, J/(kg. ^oC)
c_w	Water heat capacity, J/(kg. ^oC)
D	Vertical depth, m
D_{so}	Mass diffusion coefficient for solvent-oil in oleic phase, m^2/day
E_a	Sweep Efficiency, fraction
f_s	Steam quality
g	Acceleration due to gravity, m/day^2
H	Reservoir thickness, m
i_{tot}	Total rate of mass injection in solvent-SAGD model, kg/(day-m)
L_{int}	Steam-oil interface length, m
K_{ob}	Overburden thermal conductivity, J/(m.day.^oC)
K_{res}	Reservoir thermal conductivity, J/(m.day.^oC)
k	Absolute permeability, m^2
k_o	Effective oil permeability, m^2
k_{ro}	Relative oil permeability, m^2

k_{st}	Effective steam permeability, m^2
m	Dimensionless viscosity-temperature coefficient
m	Mass, kg
L_c	Half of well spacing, m
L_v	Latent heat of condensation, J/kg
Q_{acc}	Cumulative accumulated heat ahead of front, J/m
Q_{inj}	Cumulative heat injection, J/m
Q_{loss}	Cumulative heat loss to overburden, J/m
Q_o	Cumulative oil production, m^3/m
Q_{oy}	Cumulative oil production as a function of y, m^3/m
Q_{oz}	Cumulative heat into oil zone, J/m
Q_{ozo}	Cumulative heat into the overhead interface of chamber, J/m
Q_{ozs}	Cumulative heat into the side interfaces of chamber, J/m
Q_{sz}	Cumulative heat to raise rock and fluid temperature from T_r to T_s, J/m
q_{acc}	Rate of heat accumulation ahead of front, J/(day-m)
q_{inj}	Rate of heat injection, J/(day-m)
q_{loss}	Rate of heat loss, J/(day-m)
q_o	Oil production rate, m^3/(day-m)
q_o^C	Oil production rate for a confined reservoir model, m^3/(day-m)
q_o^{Unc}	Oil production rate for an unconfined reservoir model, m^3/(day-m)
q_{oy}	Oil flow rate in y-direction along the steam chamber interface, m^3/(day-m)
q_{omax}	Maximum oil production, m^3/(day-m)
q_{res}	Heat rate into the reservoir, J/(day-m)
q_{sz}	Heat rate to expand steam chamber, J/(day-m)
q_{sz}^{Unc}	Heat rate to expand steam chamber in an unconfined model, J/(day-m)
S_{oi}	Initial oil saturation of reservoir
S_{or}	Residual oil saturation in steam chamber

S_v	Vapour phase saturation in chamber
S_{wir}	Irreducible water saturation
t	Time, day
t_{con}	Confinement time, day
t_f	Time at which the reservoir is expected to be depleted in a confined model, day
t_r	Time at which steam chamber reaches the top of reservoir, day
T	Temperature, ^oC
T_D	Dimensionless temperature
T_r	Reservoir temperature, ^oC
T_s	Steam temperature, ^oC
U_f	Heat front velocity in this research, m/day
V_b	Bitumen volume fraction in mixture
V_{sol}	Solvent volume fraction in mixture
V_{oD}	Darcy velocity, m/day
V_{sz}	Depleted reservoir volume, m^3
w	Model width in Butler, McNab and Lo experiment, m
x	Distance from production well in x axis, m
x_b	Compositional parameter for bitumen in Lederer's correlation
x_H	Maximum steam chamber movement at the top of the reservoir, m
x_{sol}	Compositional parameter for solvent in Lederer's correlation
$x'_{\Delta y}$	Steam chamber velocity over an element, m/day
x'_H	Steam chamber velocity at the top of the reservoir, m/day
x'_y	Steam chamber velocity at special y, m/day
y	Distance from production well in y axis, m
y_{Lc}	Distance from production well in y axis at $x = Lc$, m
y'_{Lc}	Maximum steam chamber velocity of SAGD confinement phase, m
Γ	Heat front location at any time with respect to the original coordinate

α	Reservoir thermal diffusivity, m^2/day
α_{ob}	Overburden thermal diffusivity, m^2/day
α_A	Dimensionless coefficient, areal flow ratio of oil to steam
α_{LS}	Dimensionless coefficient, Lateral Spreading Coefficient
δ	Total available width for liquid streams at chamber top interface, m
η	Moving coordinate in y direction, m
θ	Angle of steam-oil interface to horizon
θ_n	Angle of steam-oil interface to horizon at a particular time
μ_b	Bitumen viscosity, kg/(day-m)
μ_{mix}	Mixture viscosity, kg/(day-m)
μ_o	Dynamic oil viscosity, kg/(day-m)
μ_{sol}	Solvent viscosity, kg/(day-m)
ν_o	Kinematic oil viscosity, m^2/day
υ_{os}	Kinematic oil viscosity at steam temperature, m^2/day
ξ	Coordinate perpendicular to steam/oil interface, m
ρ_b	Bitumen density, kg/m^3
ρ_o	Oil density, kg/m^3
ρ_g	Steam density, kg/m^3
ρ_r	Reservoir rock density, kg/m^3
ρ_{sol}	Liquid solvent density, kg/m^3
ρ_{sol}^v	Solvent density in vapour phase, kg/m^3
ρ_w	Water density, kg/m^3
$(\rho c)_{res}$	Volumetric heat capacity, J/ (m^3. ^{o}C)
$\Delta\rho$	Density difference between steam and oil, kg/m^3
ψ	Normal coordinate to the steam chamber interface during sideways expansion phase

1. INTRODUCTION

1.1 Heavy Oil and Oil Sands

The proved oil reserves are "the estimated quantities of oil which geographical and engineering data demonstrate with reasonable certainty to be recoverable in future years from known reservoirs under current economics and operating conditions" (www.opec.org). The proved oil reserves around the world were reported to be 1697.6 billion barrels in 2015 (BP Global, 2017). Figure 1.1 illustrates the distribution of the proved oil for different countries. Canada, the third place in the graph, has about 172.9 billion barrels of proven oil reserves. In Canada, more than 97 percent of the total in-situ oil reserves are unconventional oil and more than one-half of the oil production is from oil sands. The Athabasca oil sands, located in northeastern Alberta, are the largest deposit of bitumen which is around 80 percent of the total. The reservoir is shallow and is known for high permeability and porosity, and initial oil saturation.

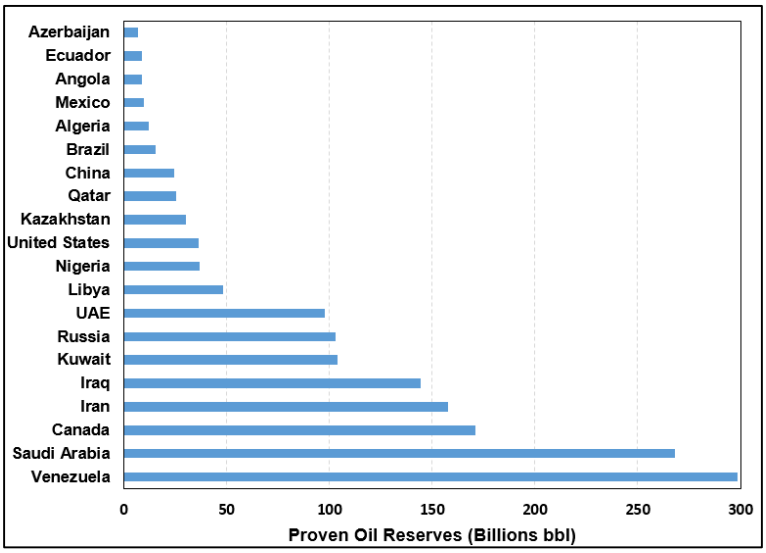

Figure 1.1: The world's Largest Oil Reserves (Worldatlas, 2014).

Unconventional oil reserves such as heavy oil and oil sands are becoming an important source of the oil supply of the world in recent years because of higher oil price, and advancements in technology that make them possible to be extracted. The heavy oil resources of the world total about 10 trillion barrels, nearly three time the conventional oil in place in the world. Canada and Venezuela have the largest share of heavy oil in the world. Conventional oil is recognized as oil with an API gravity of about $25°$ or higher. Table 1.1 provides some specific characteristics of heavy oil and oil sands.

Table 1.1: Definitions of heavy oil and oil sands (Farouq Ali, 2015).

	API Gravity	Density, ρ $(\frac{kg}{m^3})$	Viscosity, $\mu(cp)$
Heavy Crude	20-10	934-1000	100-10000
Tar Sand Crude	< 10	1000	> 10000

The high viscosity of the unconventional oils makes them practically immobile at reservoir conditions so that conventional methods of oil recovery are almost ineffective. Bitumen (or tar sands) is a solid or semisolid form of the oil at initial reservoir pressure and temperature.

Thermal recovery methods are very effective in recovering the heavy oil resources due to high sensitivity of the oil to temperature and so, decreasing oil viscosity. Figure 1.2 shows the viscosity reduction of a Canadian reservoir, Athabasca bitumen, with temperature enhancement. It is seen that bitumen viscosity plunges from millions of centipoise at reservoir temperature (usually between 7 and 15℃) to less than 10 cp at 190℃.

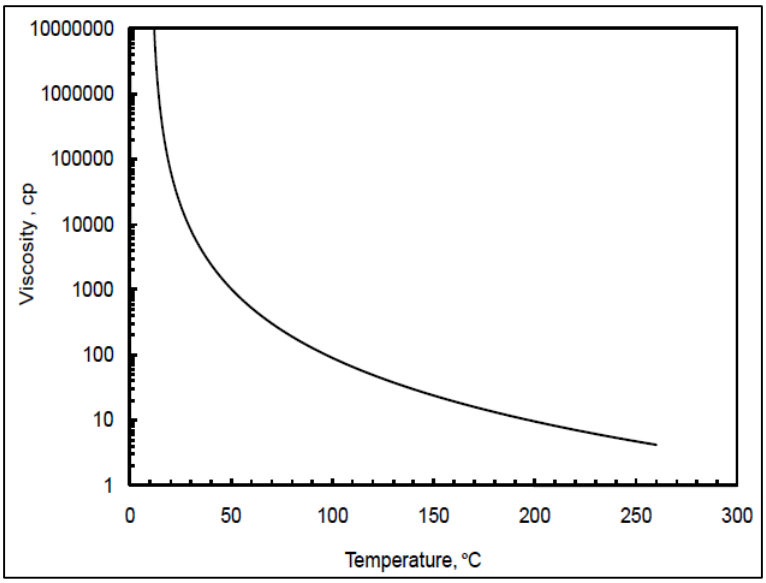

Figure 1.2: Variation of Athabasca oil sand's viscosity with temperature (Mehrotra and Svrcek, 1986).

Alternative recovery methods for heavy oil are mining, thermal, and non-thermal in-situ recovery. Less than 20 percent of Alberta's tar sand deposits at shallow depth (less than 80 m) are potentially mineable. Non-thermal recovery methods are applied for deep and thin formations with low permeability and average oil viscosity between 50 and 200 cp. Polymer flooding, waterflooding, surfactant flooding, CO_2 flooding and light hydrocarbon flooding are the conventional approaches in this category. The effectiveness of these methods for heavy oil recovery is not proven due to the cost of injection fluids.

In Western Canada, thermal recovery methods are the most practical option for the heavy oil and bitumen recovery. In thermal methods, heat is introduced into the reservoir (at an initial temperature typically between 8 and 15℃) by steam, hot water, in-situ combustion or electrical heating. As a result, oil viscosity is lowered and mobile oil moves to a production well.

Steam injection approach, which is the most common thermal recovery method for heavy oil recovery, can be divided into three different processes; Cyclic Steam Stimulation (CSS),

Steamflooding and Steam-Assisted Gravity Drainage (SAGD). In these processes, a fraction of latent and sensible heat of the injected steam is transferred into the oil and serves to lower the oil viscosity.

1.2 Steam-Assisted Gravity Drainage (SAGD) Process

For an oil sands reservoir, reservoir temperature is very low and connate water is immobile. Oil viscosity is too high at initial reservoir conditions so that oil phase velocity is of the order of feet per year even under huge pressure gradients. This makes the application of conventional steam flooding inappropriate for oil sands (Edmunds et al., 1994). SAGD, which is a variation of steamflooding, was introduced for recovering bitumen or extremely viscous oils by Butler, McNab, and Lo (1981). Horizontal wells are utilized to provide an adequate drive to move the heated bitumen at an economic rate by providing a large contact with the reservoir compared to conventional wells and also avoiding gas coning (Butler, 1994, 2001; Edmunds and Peterson, 2007). In this process, high quality steam is continuously injected into the reservoir through a horizontal well located several metres above a horizontal producer at the base of formation. Typically, the length of the horizontal production and injection wells are less than 1000 m. The schematic of the process is shown in Figure 1.3.

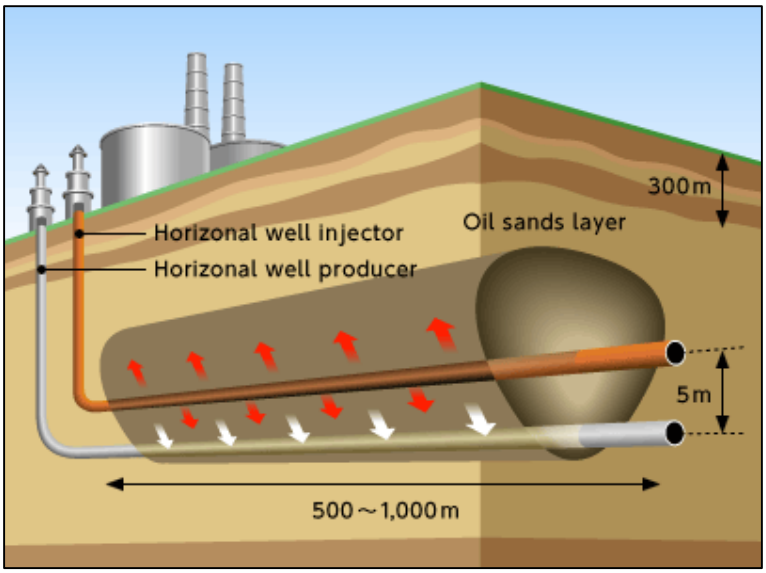

Figure 1.3: Schematic representation of SAGD process (courtesy of Japan and Canada Oil Sands Limited).

In SAGD, the injected steam flows to the edges of the steam chamber and releases its latent heat to the bitumen. This results in heating oil zone beyond the chamber edge and consequently, the viscosity of bitumen is lowered. The mobilized oil flows to the horizontal production well under gravity force (Figure 1.4).

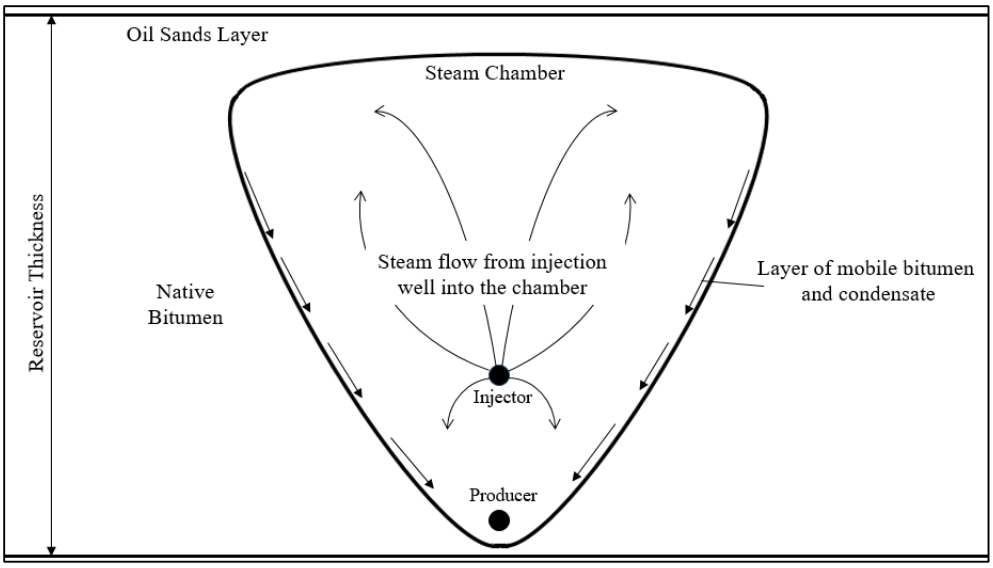

Figure 1.4: Schematic of steam and heated oil flows in and around the steam chamber in SAGD process.

As observed from laboratory experiment test (Chung and Butler, 1987; Sasaki et al., 2002) and the results of the Underground Test Facility (UTF), Phase A reported by Edmunds et al. (1994) and Chalaturnyk (1996), steam chamber development occurs in three different stages. The first phase of steam chamber development in the SAGD process is the upward growth of the chamber until it reaches the top of the reservoir. The next phase is the lateral spreading of the chamber which depends on the spacing between the well pairs in a pattern. After a particular time, the expanding steam chambers in a pattern coalesce, and at the top of the reservoir, all the steam chambers are connected. This is called confinement phase of steam chamber development in SAGD. Figure 1.5 shows the experimental results of Chung and Butler (1987) indicating the three stages of SAGD.

It should be noted that in practice, there is another phase of SAGD which is called preheating of the reservoir. This phase can be considered as a very first phase of SAGD in which steam is circulated in the horizontal well pair to establish the fluid communication between the injector and the producer. Duration of this phase depends strongly on the interwell spacing (Edmunds and Gittins, 1993).

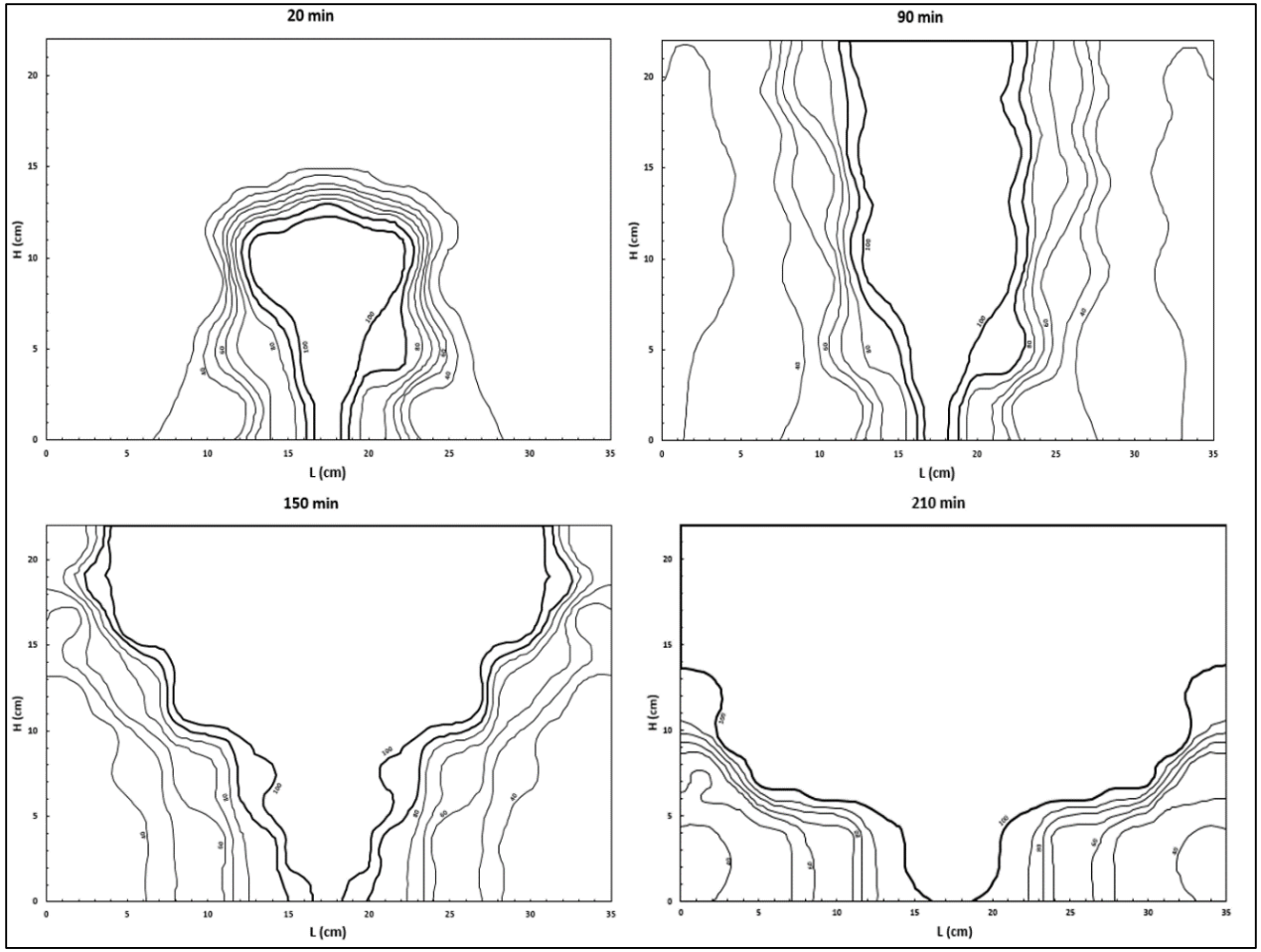

Figure 1.5: Steam chamber development in SAGD process including rise, lateral spreading, and confinement phases (Chung and Butler, 1987).

A liquid pool at the base of the chamber surrounds the production well and acts as a steam trap. This operating condition prevents the injected steam to be produced directly from the production well without contributing to reservoir heating. The SAGD process operates at steam temperature (or pressure). To minimize the direct steam channelling into the producer, the pressure difference between the wells is kept low, less than 500 kPa. This implies that only the latent heat of the injected steam is used to expand the steam chamber (Farouq Ali, 2016).

The process can be applied even in case of the most viscous bitumen because the oil remains heated as it drains down to the producer (Butler, 1994). This is the main advantage of SAGD process compared to conventional steamflooding. In the steam injection processes, the dominant mechanisms of oil recovery are viscosity reduction, oil expansion and steam distillation. In SAGD, with gravity drainage as the driving force, viscosity reduction is responsible for bitumen recovery.

SAGD process is highly successful in Athabasca-like reservoirs. However, the application of SAGD to other heavy oil reservoirs beyond the Canadian borders was shown by numerical simulation to bring new challenges into SAGD technology (Alvarez, Moreno, and Sawatzky, 2014).

1.3 Solvent SAGD Process

SAGD process is widely used to recover extremely heavy oil and bitumen where no other recovery method is proven to be economical. Despite the success of SAGD, high energy and water consumption, water pollution, greenhouse gas emission, and the need to further dilute the produced fluid are some concerns which inspired some researchers to look for alternative methods. Solvent-aided gravity drainage processes are suggested as potential alternatives to the current thermal recovery methods. However, the mechanism of the oil recovery by steam and added solvent is not clear. Over the years, on several occasions - as at the present time - the oil industry has resorted to the use of solvents with steam in thermal recovery operations.

In addition to heat, solvent can also dilute the oil phase viscosity and so, making the bitumen phase mobile. Figure 1.6 illustrates that Athabasca bitumen viscosity declines considerably as a function of the mole fraction of hexane. By comparing Figures 1.2 and 1.6, it can be concluded that Athabasca bitumen at the reservoir temperature can reach the viscosity less than 10 cp if it is diluted by solvent such as hexane by concentration as high as 80% or if it is heated by increasing its temperature as high as 190℃.

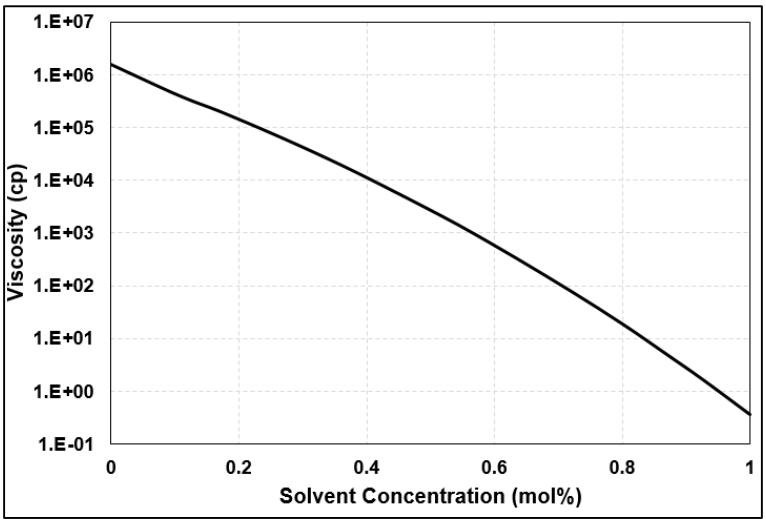

Figure 1.6: Effect of solvent (hexane) concentration on Athabasca bitumen viscosity reduction (Shu's Correlation, 1984).

In a solvent-SAGD process, a small amount of solvent is injected with steam into the formation. In this type of the thermal recovery method, steam is intended to provide heat to the reservoir and solvent dilutes the oil. The combination of these two factors are expected to reduce the oil viscosity above what is achieved by heat alone.

Gates and Chakrabarty (2006) pointed out that the key benefits of applying a solvent-SAGD process to recover bitumen instead of SAGD are:

1- Reduces steam requirement

2- Lowers greenhouse gas emission due to reduced amounts of natural gas consumption
3- Lowers the operating temperatures
4- Improves the overall thermal efficiency due to lower heat losses

It was also mentioned that if the solvent and bitumen can be separated, the solvent could be recycled. This reduces the solvent requirement.

1.4 Statement of the Problem

The primary objective of this work is to improve our fundamental understanding of steam and hybrid solvent-steam gravity drainage processes by proposing new analytical treatments of these processes. This work consists of fundamental and theoretical examination of the original SAGD process models, developing new analytical models for SAGD process during steam chamber rise period and sideways expansion phase. The new SAGD models are extended to include the effect of confinement by adjacent steam chambers. A new approach is also developed for the solvent-SAGD process.

In this work, the original theory is evaluated on the basis of fundamental concepts, and new mathematical models are derived that remove shortcomings of the previous models. All of the work proposed is based upon analytical mathematics. No numerical simulations using external software were carried out. Analytical models provide an answer that is a continuum, unlike numerical methods that give answers for discrete points in space and time. Analytical models include all major mechanisms. Numerical methods, because of their nature, can account for spatial detail, for example, rock property variation. Often this is not a limitation in analytical models, as they provide a good average answer. This was observed in simulations of experimental and field data in this study. Numerical simulation would require the input of selected field data before field results can be reproduced. Besides, numerical simulation requires much data which has uncertainty, such as relative permeabilities; it suffers from numerical dispersion and other numerical effects. Even if

numerical simulation results are available, analytical models provide a good answer to compare with, free of such uncertainties as relative permeabilities.

Specifically, the objectives of this research are as follows:

1. Evaluate the previous SAGD theories, and discuss their deficiencies.

2. Develop new SAGD models in which the primary unknown is the maximum steam chamber velocity. Represent them for the two stages of the steam chamber development as:

1. Steam Chamber Rise (SCR) model
2. Sideways expansion of the steam chamber:
    a. Constant Volumetric Displacement (CVD) model
    b. Constant Heat Injection (CHI) model

3. Evaluate the effect of SAGD well pair confinement by neighbouring wells, via two models developed for the sideways advance phase of SAGD.

4. Introduce a comprehensive analytical model of the SAGD process, encompassing all phases.

5. Model the process of solvent injection with steam, with the aim of predicting: vapour chamber growth, oil production rate, solvent production rate, solvent loss (or solvent retention) rate, unsteady temperature and concentration profiles and investigating the effect of solvent type and concentration on the solvent-SAGD process. Given the controversy regarding the use of solvents with steam, this model is also intended to explain whether solvent injection with steam increases oil recovery. If so, by what mechanism, and by how much.

6. Compare the results of the proposed analytical models with laboratory experimental data and field data.

7. Discuss the novelty and improvement of the proposed models compared with the previous works.

1.5 Thesis Layout

This thesis consists of 8 chapters:

Chapter 1 presents general information and description of heavy oil deposits, SAGD and Solvent-SAGD processes. Also, the main objectives of this research are outlined.

Chapter 2 gives an extensive literature review of SAGD and solvent-SAGD including the main mechanism, effective parameters of these processes, analytical studies, experimental works and field applications.

In **Chapter 3**, a new analytical model for predicting steam chamber rise velocity and oil production rate during this period is developed. In this theory, by combining volumetric oil displacement with Darcy oil rate considering the indirect effect of frontal instability, the rise velocity, and the steam chamber height is calculated. The model is extended to predict oil production, heat or steam injection rate, heat consumption and Cumulative Steam-Oil Ratio (CSOR) during this phase. Moreover, an estimate of injected steam sweep efficiency and the angle between the steam chamber and the horizon can be made. Results are validated with experimental and field data.

Chapter 4 presents the two analytical approaches of the sideways expansion phase of SAGD in an unconfined reservoir, taking into account the development of the steam chamber; Constant Volumetric Displacement (CVD) model and Constant Heat Injection (CHI) model. In the CVD model, it is postulated that the front movement is such that the steam chamber growth is constant over time. In all previous works, the bitumen rate is obtained with no recourse to the steam injection rate – which is worked out after the fact. In real applications, steam is injected into the system so; it is the input to the problem. In the CHI model, heat is injected at a constant rate into the system (input), which provides heat for the growing steam chamber size, increasing heat loss to the overburden, and heat flow by conduction ahead of the front. In this model, the front velocity that satisfies heat balance and mass balance for a constant heat injection rate is computed. The mathematical

derivation of these two approaches are explained in this chapter. This chapter also includes a discussion of previous SAGD oil production rate equations for sideways expansion.

In practical cases of SAGD, well pairs are confined in a repeated pattern. The developing steam chamber during the sideways expansion is affected by the neighbouring steam chambers. In an unconfined model (models presented in Chapter 4), the expanding steam chamber at the top of the reservoir is constantly exposed to the cold overburden but with a confinement effect, this exposure stops and this reduces the heat requirement in this system. The objective of **Chapter 5** is to introduce an analytical treatment of confinement phase of SAGD for the first time in order to have a better understanding of this phase of SAGD.

A comprehensive analytical model of SAGD including rise, lateral spreading, and confinement phases is introduced in **Chapter 6**. The list of equations used in Comprehensive Constant Volumetric Displacement (CCVD) and Comprehensive Constant Heat Injection (CCHI) is given. The results are validated against experimental and field data.

The objective of **Chapter 7** is to develop a new analytical model of solvent-SAGD process for describing the process performance based on the combination of an overall solvent mass balance, heat balance and volumetric oil displacement and Darcy oil rate using a mixture viscosity model as a function of temperature and solvent concentration ahead of front which satisfy the equilibrium in the system. Unlike previous works, the results of this approach are based on the mass and heat balances over the system. These are coupled because of their dependency on the steam chamber velocity. The model predicts: vapour-steam chamber growth, oil production rate, solvent production rate, solvent loss (or solvent retention) rate, and the effect of solvent type and concentration on the solvent-SAGD process. On the whole, the results of this approach give a better understanding of the mechanism of oil production by interconnecting vapour chamber conditions and the conditions of heated and diluted oil ahead of the interface.

The findings and conclusions of this research are summarized in **Chapter 8**.

Recommendations for future research are also listed in **Chapter 9**.

Figure 1.7 illustrates the organization diagram of this thesis.

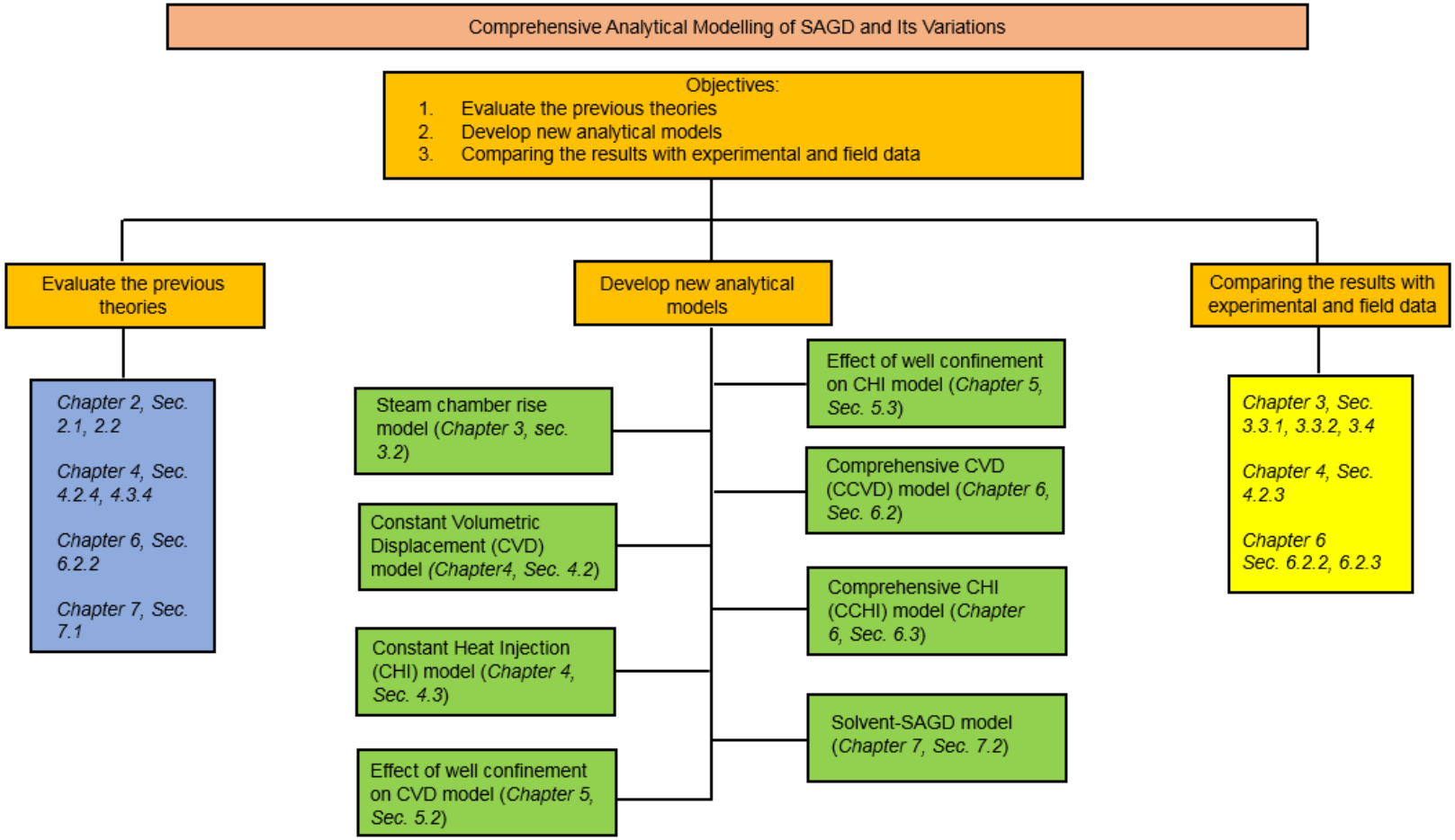

Figure 1.7: Schematic representation of the organization of this thesis.

2. REVIEW OF THE LITRETURE

2.1 Steam-Assisted Gravity Drainage (SAGD) Process

2.1.1 Introduction

There are a number of works on the performance of the SAGD process using numerical simulation and pilot testing (Chow and Butler, 1996; Kisman and Yeung, 1995; Ito and Suzuki, 1996; Ito, Suzuki, and Yamada, 1998; Ito and Hirata, 1999; Komery et al., 1998; Suggett, Gittins, and Youn, 2000; Edmunds and Chhina, 2001; Ito, Hirata, and Ichikawa, 2004). Several analytical or numerical treatments of the SAGD have also been proposed for calculating the oil production rate. The first analytical model was introduced by Butler, McNab, and Lo (1981). Some assumptions were made in developing the model such as heat transfer by conduction only. Farouq Ali (1997) pointed out that this assumption is a point of concern due to the presence of steam condensate with a volume two to five times as large as the volume of heated oil. Following his paper, several works investigated the relative roles of conduction and convection in the SAGD process (Edmunds, 1999; Sharma and Gates, 2011; Irani and Ghannadi, 2013; Irani and Gates, 2013; Li and Chen, 2015).

Chung and Butler (1987) and Sasaki et al. (2002), based on experimental works, showed that the steam chamber development occurs in three stages. Moreover, the results of the Underground Test Facility (UTF), Phase A reported by Edmunds et al. (1994) and Ito, Hirata, and Ichikawa (2001) corroborated the experimental observations. The first phase in developing a steam chamber in SAGD process is the upward growth of the chamber until it reaches the top of the reservoir. The next phase is the lateral spreading of the chamber which depends on the spacing between the well pairs in a pattern. After a certain time, the expanding steam chambers in a pattern coalesce, and at the top of the reservoir, all the steam chambers get connected (see Figure 2.4). This is called the *confinement phase* in this work. It should be noted that in practice, there is another phase of SAGD which is called preheating of the reservoir. This phase can be considered as the very first phase of SAGD in which steam is circulated in both of the horizontal wells in a pair to establish fluid

communication between the injector and the producer. The duration of this phase depends strongly on the interwell spacing (Edmunds and Gittins, 1993). Since in this stage, there is no steam chamber development, the analytical modelling of this phase is not included in this research. However, it will be shown that this phase has an effect on the early oil production rate. In fact, in practice, the success of a SAGD operation depends on the initial heating (or circulation) period. In this chapter, the literature review of SAGD is organized based on the steam chamber development phases which will be followed by selected reviews of publications on the solvent-SAGD process.

2.1.2 Analytical Modelling of the Steam Chamber Rise Phase

Several analytical models have been proposed for predicting steam chamber rise velocity, and a few for computing oil production rate at early times. As mentioned above, the steam chamber grows upwards, and oil drains downwards. It is hard to model the process at this stage due to the frontal instability between steam and the liquid phases in the system. Stability is affected by factors such as the direction of displacement and viscosity difference between gas/steam and liquid. Steam condensation, on the other hand, has a stabilizing effect. The rise velocity and uniform steam distribution along the well pair at the early time of the SAGD process are the key parameters for evaluating the performance and economics of SAGD projects (Butler, 1987; Edmunds et al., 1994; Gotawala and Gates, 2012).

Closmann and Smith (1983) measured the rate of steam chamber rise above a horizontal fracture in a steam injection project in the Athabasca oil sands and recorded the resulting temperature profile. Temperatures above the injection point were much higher than could be described by heat conduction alone. They proposed that a higher rate of temperature increase could be explained by assuming that the steam front was moving upwards with a constant velocity. The measured steam rise was 0.021 m/day (0.070 ft /day) for a heat source at 198°C. It was suggested that conduction was the dominant mechanism of heat transfer above the rising steam zone. They also did numerical and analytical analyses

showing good agreement with the observed upward movement of the steam front. Butler (1987) developed a model to predict the constant upward steam front velocity. Steam flow into steam fingers and downward movement of heated oil around these fingers were postulated. The predicted steam chamber rise velocity was proportional to reservoir permeability, steam temperature, and oil viscosity and it also depended on the width of the steam finger. The model predicted a considerably lower velocity (0.0047 m/day) than the observations of Closmann and Smith. Chung and Butler (1987) conducted an experimental study using a 2D visual scaled reservoir model. Two well configurations were designed to represent the steam-assisted gravity drainage process. In the first scheme, the injector was horizontal and close to the horizontal producer near the base of the reservoir model which is a typical SAGD configuration in recovering heavy oil and bitumen in Alberta. The second scheme consists of a single horizontal production well and vertical wells close to the top of the formation. The laboratory study showed that in the first scheme, steam chamber starts to rise until it reaches the reservoir top. The measured oil production rate showed an increasing trend during this period. The rise velocity was not reported. However, the chamber grew fast during the first 20 minutes of the experiment, but slowed down thereafter, till touching the top.

Chow and Butler (1996) performed a numerical study, using a commercial simulator (STARS), on SAGD process during the rise and lateral spreading phases of the steam chamber. The aim of the numerical simulation was to match the oil recovery and interface positions as reported in Chung and Butler's (1987) experimental data. The rising steam chamber could not be modelled properly even by adjusting the relative permeability. It is concluded that the lack of built-in physics such as steam fingering, and water/oil emulsification in the simulator caused this mismatch.

Birrell and Putnam (2000) suggested a graphical method to estimate the location and growth rate of the steam chamber during the rise period by interpreting thermocouple data above the steam chamber. Ito and Ipek (2005) discussed steam fingering during the rise time through the numerical history matches of measured field data. They believed that the dimension of steam fingers are of the order of a few metres, similar to what Butler (1987)

concluded. They thought a geomechanical change of formation at the early time of SAGD has a profound effect on the generation of the steam fingers in addition to viscosity and density differences. It was discussed that as the operating pressure increased the rise velocity increased, and the important role of steam fingers on the rise velocity was noted in their conclusion.

Gotawala and Gates (2008) extended the Butler (1987) theory of steam fingers and concluded that the length of steam fingers from their model was smaller than that of the Butler's. They also claimed that the rise rate from their model was closer to the reported field data compared with Butler's model. The two-phase counter-current flow of Butler's (1987) was extended by Dehghanpour, Murtaza, and He (2013) to include water-oil coupling at the edge of steam fingers to find the steam rise velocity that was higher than predicted.

Butler (1991) developed a model for steam chamber rise velocity and oil production rate during the steam chamber rise period by use of the original oil rate equation. Two curve fitted parameters were introduced to match experimental oil rate and steam chamber height to the model responses. In addition, no model was proposed for evaluating the thermal efficiency of SAGD process during rise period. Sasaki et al. (2002) studied the expansion and vertical rise of the steam chamber, and drainage mechanism close to the chamber edge by conducting an experiment. The oil production rate and steam chamber shape were reported. Oil production rate from their experiment increased during the rise period and reached a maximum.

Baker et al. (2010) conducted a numerical simulation study of SAGD process at early times of the project. It was concluded that the steam chamber during the rise period was unstable. They also mentioned that it is critical to control the volumetric sweep efficiency of the injected steam as it has a significant impact on project economics. Azad and Chalaturnyk (2012) proposed a circular geometry for representing the steam chamber to model the steam chamber rise phase. The model results were validated against Chung and Butler's (1987) experimental data and they showed there was a good match between the predicted oil rate

from the model and the experimental results. The steam chamber geometry reported from the Chung and Butler's experiment, shown in Figure 1.5, is very close to an inverted triangle as mentioned by the authors. The predicted oil production rate from the model increased monotonically. We believe there are other factors affecting the measured oil production rate and the reason is not the steam chamber geometry. This will be explained in detail in Chapter 6.

There is currently no analytical model describing all aspects of rise stage of SAGD process. A new analytical approach is proposed in this study, to predict the rise velocity, oil production rate, steam injection rate, and CSOR during the rise period of SAGD process. In this approach, counter-current flow of steam and the liquid phase is assumed, and oil at the steam temperature contributes to the oil production only. The indirect effect of frontal instability on the process is also included in the model derivation. This model can also estimate sweep efficiency and steady steam-oil interface position during the early time of SAGD life. The proposed model is validated against experimental and several field data.

2.1.3 Analytical Modelling of the Sideways Expansion Phase

Butler, McNab, and Lo published an analytical treatment of SAGD in 1981. The basic physics of drainage mechanism of SAGD was introduced and simple theories derived from the early experimental and mathematical works (Butler, McNab, and Lo, 1981; Butler and Stephens, 1981; Butler, 1985; Chung and Butler, 1987; Ferguson and Butler, 1988; Reis, 1992; Reis, 1993; Butler, 1991). Butler's original theory relates the oil production rate per unit length of the horizontal well as a function of rock and fluid properties and steam temperature:

$$q_o = 2\sqrt{\frac{2k_o g\alpha\,\phi\,H\,\Delta S_o}{m\nu_{os}}} \qquad \left(\text{or as function of y;}\;\; q_o = 2\sqrt{\frac{2k_o g\alpha\,\phi\,(H-y)\,\Delta S_o}{m\nu_{os}}}\right) \tag{2.1}$$

The equation indicates that oil production rate, q_o, is proportional to square root of porosity, ϕ, reservoir thickness,H, thermal diffusivity,α, effective permeability,k_o, and difference between initial and residual oil saturation, ΔS_o, while it has a reciprocal proportionality with kinematic viscosity of oil at steam temperature, ν_{os}, and a viscosity-temperature constant, m. The effect of multiphase flow is incorporated via effective oil permeability.

This model was developed for predicting oil production rate during the steady-state stage of the SAGD process. It is assumed that heat transfers beyond the chamber interface by conduction only and the steam chamber expands sideways from a vertical plane through the producer and injector (excluding the rise stage). Butler's original theory gives too high an oil rate as the steam chamber interface moves away from the producer and also moves away to infinity at the top of the reservoir (See Figure 2.1).

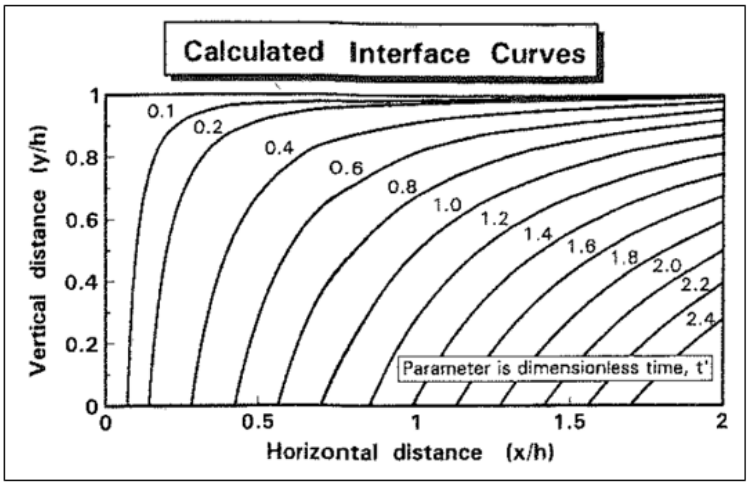

Figure 2.1: Interface positions of Butler's original model (Butler and Dargie, 1994).

Several attempts were made to solve this problem by finding a multiplier empirically, experimentally, or adding new concepts to the model to make the equation predict lower rates. Butler and Stephens (1981) revised the model and changed the coefficient in the original oil production rate to include the effect of horizontal movement of interface away

from the production well by modifying the interface curve of the original theory and introduced the so-called TANDRAIN theory:

$$q_o = 2\sqrt{\frac{1.5k_o g\alpha\ \phi\ H\ \Delta S_o}{m v_{os}}} \tag{2.2}$$

Figure 2.2 shows the revised steam chamber interface considered in the TANDRAIN theory. The tangents are drawn from the producer to the interface curves of the original method.

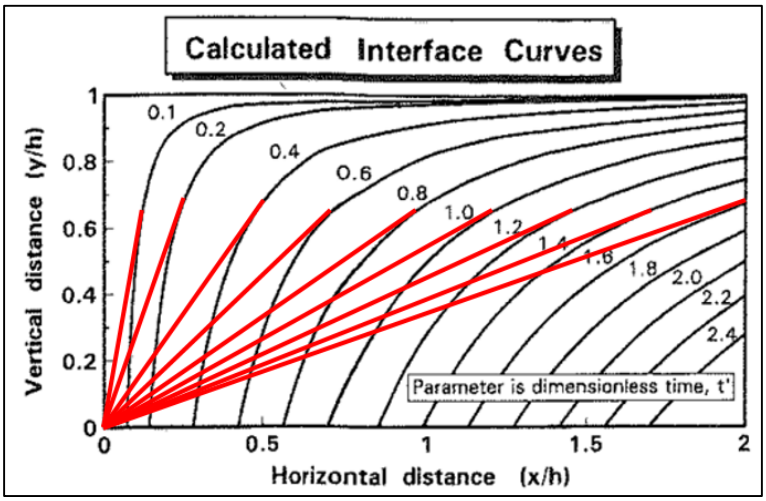

Figure 2.2: Modified interface positions of Butler's original model to represent TANDRAIN theory interface positions.

As a result, the lower part of the new steam chamber interface is a straight line but still goes to infinity at the top of the reservoir and oil production rate is still high. Later, Butler (1991) proposed the so-called LINDRAIN theory. In this theory, as seen in Figure 2.3, the tangent in TANDRAIN theory is extended to the top of the reservoir. As a result, the original oil production rate changes to:

$$q_o = 2\sqrt{\frac{1.3k_o g\alpha\ \phi\ H\ \Delta S_o}{m\nu_{os}}} \tag{2.3}$$

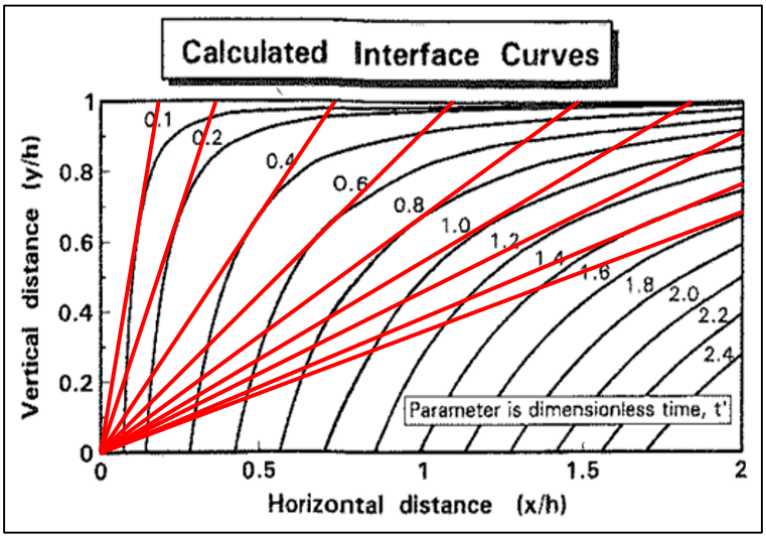

Figure 2.3: Modified interface positions of Butler's original model to represent LINDRAIN theory interface positions.

Butler (1985) developed a numerical approach to calculate the oil production rate which describes the spreading phase of the steam chamber, excluding the steam chamber rise period, based on the same principles as introduced in the original model. Steam chamber interface expanded laterally from a vertical plane. A differential equation was derived for heat penetration depth, extracted from an energy balance, ahead of the interface. For each time, the interface was divided into small elements, and the calculations were done for each element over time. The heat penetration equation varied between two limiting cases; steady state case where the front velocity was constant (this condition was applied to most of the elements) and unsteady state case where the front velocity was zero (this condition was used for the small elements near the well). In this model, the steam chamber interface was assumed to be fixed at the producer. The oil production rate was calculated depending on the heat penetration depth at each time for all the elements.

A numerical approach was developed by Ferguson and Butler (1988) to investigate the impact of varying steam injection rate and pressures on SAGD. An approximate mathematical approach was used to calculate the heat transfer. It was concluded that the higher injection pressures accelerate the production rate with no considerable reduction on cumulative oil-steam ratio. Reis (1992) proposed an analytical model for predicting oil production rate. In this approach, the steam chamber geometry was assumed to be an inverted triangle. This geometry is observed in Hele-Shaw and sand pack laboratory experiments (Chung and Butler, 1987). The oil production rate from this model is given by:

$$q_o = 2\sqrt{\frac{k_o g\alpha\ \phi\ H\ \Delta S_o}{2am\nu_{os}}} \tag{2.4}$$

where a is a constant empirical coefficient equal to 0.4. In a similar manner, Reis (1993) derived a model assuming an inverted cone in the case of a vertical injector. Based on extensive numerical simulations, Ito, Suzuki, and Yamada (1998) proposed an oil production rate equation with an empirical constant based on rock-fluid properties. The oil production rate and reservoir thickness had linear proportionality up to a certain reservoir thickness (30 m). Pooladi-Darvish, Tortike, and Ali (1995) modified Butler's 1985 model. The Heat Integral Method (HIM) was applied to solve the unsteady-state temperature profile to obtain a differential equation for the heat penetration depth ahead of the advancing front. Unlike the Butler approach, the unsteady state temperature was assumed for all the steam chamber interface elements in the numerical model.

The primary mechanism of oil production in SAGD models is viscosity reduction due to reservoir heating. However, other mechanisms may be active, such as steam distillation and asphaltene deposition. These were accounted for in the proposed model by Akin (2005). He concluded that at late times of SAGD process, these two are dominant. Edmunds and Peterson (2007) proposed an analytical model to estimate CSOR by modifying the Reis (1992) model using field data. It was shown that the CSOR model

predicted the field results fairly. Heidari et al. (2009) modified Pooladi-Darvish's model to consider heat conduction in the normal direction and fluid flow along the interface.

In Butler's original model, the effective permeability is assumed to be constant. Sharma and Gates (2010) added the effect of multiphase flow or relative permeability effects to Butler's original model by assuming a linear saturation profile ahead of the steam chamber edge. In this way, a new constant appears in Butler's original model which indicates the effect of two-phase flow (steam condensate and oil) at the edge of the steam chamber. Azom, Kamp, and Srinivasan (2013) built on Butler's model to include the effect of multiphase flow at the edge of the steam chamber in a different way from that proposed by Sharma and Gates (2010). The temperature gradient ahead of the steam chamber interface resulted in the interfacial tension gradient. Consequently, the thermo-capillary imbibition of condensate into the bitumen phase occurred which was scale dependent. It was concluded that this behaviour explains the difference between the results of oil production rate from field and experiment. However, it was also mentioned that the only accurate way to validate the multiphase flow in SAGD is by including a high-resolution imaging technique in the SAGD experiment which is extremely difficult.

Almost all analytical models of the SAGD have modified Butler's original oil rate equation to get a better match with the experimental and field results by proposing a multiplier experimentally or empirically. As discussed in Chapter 4, it is believed that the development of oil production rate equation in the original theory needs to be modified. Zargar and Farouq Ali (2016) introduced two new models for assessing SAGD performance during the lateral expansion of the steam chamber for two operating schemes; Constant Volumetric Displacement (CVD) and Constant Heat Injection (CHI). In these models, the main unknown was the steam chamber velocity. It was shown that the cause of constant or variable steam chamber velocity in the lateral spreading phase of SAGD was the steam injection strategy. In the CVD model, it was shown that the steam injection rate had to be increased continuously to produce at a constant maximum oil rate. The CHI model showed that by injecting steam at a steady rate, steam chamber growth and oil production rate decreased over time. This approach could handle the effect of varying

steam injection rate. It was the first time that an analytical model was introduced for the SAGD process which showed the effect of steam injection rate on oil production rate. Most importantly, for the first time, the correct effect of pressure was shown on the SAGD performance (Farouq Ali, 2016; Zargar and Farouq Ali, 2016).

2.1.4 Analytical Modelling of the Confinement Phase

Most of the analytical works on SAGD are concerned with the sideways expansion of the steam chamber in a semi-infinite reservoir. However, in a practical sense, the steam chamber growth is limited at the top by the reservoir caprock and on the sides by the growing steam chambers in a series of parallel patterns. The effect of confinement was first introduced theoretically by Butler, and Stephens (1981). A numerical calculation was done to describe the confinement effect. Afterwards, no attempt was made to model this phase of SAGD. This research presents an analytical model for the SAGD confinement phase for the first time which leads to a better comprehension of this phase of the SAGD process.

The analytical SAGD theory introduced in this work for a semi-infinite reservoir is extended to describe the effect of confinement by neighbouring steam chambers. It will be shown in Chapter 5; that this theory predicts the steam chamber shape, oil production rate, and oil recovery accurately by validating the model results with experimental work of Chung and Butler (1987).

2.1.5 Comprehensive Analytical Modelling of the SAGD Process

All analytical works on SAGD have focused on a part of the process. The present comprehensive approach is designed to analytically evaluate the SAGD process with regard to the production rate, recovery and thermal efficiency of the process from the beginning to the end (steam chamber rise, sideways expansion, and confinement phases). Currently, no analytical model available, and it is the first time that a comprehensive

analytical model of SAGD is proposed. The schematic of all three stages of SAGD is shown in Figure 2.4.

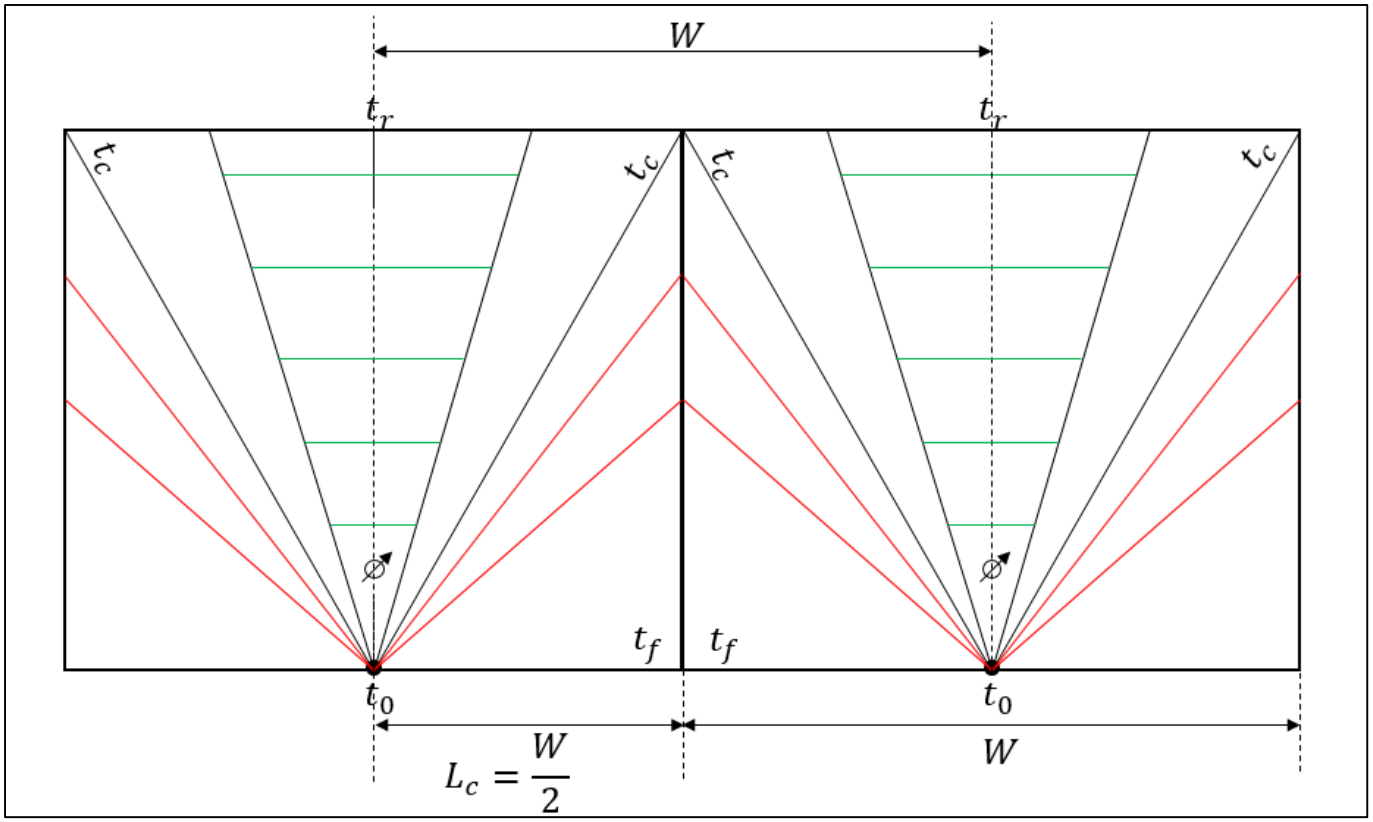

Figure 2.4: Schematic of steam chamber development including rise (green lines), sideways expansion (black lines), and confinement by neighbouring steam chambers (red lines) phases.

2.2 Solvent-SAGD Process

2.2.1 Introduction

Farouq Ali and Snyder (1973) proposed the idea of hot miscible displacement using solvents. Use of light solvent in CSS to recover heavy oils was introduced by Allen (1974) and extensive work was done afterwards in this area in 1960-70's by Allen and Redford (1976), Nenniger (1979), and Dunn, Nenniger, and Rajan (1989). However, the production rates from their works were discouraging.

Alikhan and Farouq Ali (1974), and Farouq Ali and Abad (1976) proposed and investigated the performance of injecting light hydrocarbons with steam for Athabasca oil sand. The results of their experiments showed that the process was not economical due to the high solvent-to-oil ratios. Doscher et al. (1979) did an investigation on the use of a solvent in a steam stimulation process. It was shown that there were no economic benefits in using solvent. Frauenfeld et al. (1998) showed through experimental work that solvent-assisted process could be potentially economic.

With advances in drilling technology and introduction of horizontal wells, the SAGD process was adopted to recover extremely viscous oils. There are some limitations in applying SAGD for oil sands, such as high steam requirement with steam generation resulting in significant greenhouse gas emissions. In addition, some reservoir properties such as thin or deep formations, unfavourable mineralogy, and the presence of thief zones make bitumen extraction by common techniques such as mining and thermal processes such as CSS and SAGD unsuitable. Therefore, the use of solvent was revisited in 1990's. Butler and Mokrys (1989) introduced the Vapour Extraction process (VAPEX) injecting a mixture of hot water, and a low-boiling vaporized solvent into the reservoir to create a solvent-vapour chamber. In this process, solvent vapour replaces the steam chamber in SAGD but at considerably lower temperatures. VAPEX is not a thermal method; the main recovery mechanism is mass transfer instead of heat transfer unlike SAGD, which is several orders of magnitude slower than heat transfer (Butler and Mokrys, 1993; Cuthiell et al., 2006; Nenniger and Dunn, 2008; Bayestehparvin, Abedi, and Farouq Ali, 2015).

Afterwards, several research projects were initiated in this area (Butler and Mokrys, 1991;Butler and Mokrys, 1993; Das and Butler, 1996; Yazdani and Maini, 2004; Yazdani and Maini, 2006). Experimental studies were performed by Das and Butler, 1995 and 1998 to evaluate VAPEX performance. The results showed that the performance of VAPEX was considerably improved by using vaporized solvent than liquid due to the higher gravity force and lower solvent retention. It was observed that the maximum oil recovery was achieved with propane or butane and the oil production rate depended on the solvent injection rate. Butler, Mokrys, and Das (1995) investigated the solvent requirement for VAPEX recovery and reported the practical values of cumulative solvent to oil ratio between 0.12 to 0.3 m^3/m^3. However, the oil production rate was not encouraging compared to SAGD. The process had limited success in the field.

Therefore, as in the past, the attention was given to use warm VAPEX to take advantage of both heat (latent heat of condensation of solvent) and mass transfer to reduce the heavy oil viscosity. Butler and Jiang (2000) and Karmaker and Maini (2003) performed experimental work to investigate the process. 21.5% and 18% increases in oil production rate were observed by increasing the operating temperature from 21 to 27 and 10 to 19℃ in the experiments, respectively. Rezaei, Mohammadzadeh, and Chatzis (2010) showed higher oil production rates by using a superheated solvent in a VAPEX process via an experimental work. Nenniger and Dunn (2008) proposed an empirical correlation for oil production rate depending on raw bitumen viscosity and the grain size parameter. The correlation indicated a strong potential for enhancing oil production rate by applying N-Solv (a condensing solvent process with high chamber temperature because of latent heat of vaporization of solvent).

In recent years, co-injection of a small amount of solvent, mostly light to medium hydrocarbons, with steam has been investigated as an alternate heavy oil recovery method to improve the efficiency of steam only (SAGD) or solvent only (VAPEX) gravity drainage processes by combining them. This was named variously as Expanding Solvent Steam-Assisted Gravity Drainage (ES-SAGD), Solvent Aided Process (SAP), Liquid Addition to

Steam for Enhanced Recovery (LASER), etc. This co-injection was aimed to reduce steam requirement, water treatment, heat losses, and greenhouse gas emissions of SAGD.

The incremental oil rate of the process, if any, depends on the operating conditions, solvent type and concentration but the economics of the process depend on the oil production rate, solvent requirement and solvent retention in view of the high cost of solvents. There are some research which indicate that solvent-SAGD method increases oil recovery compared with SAGD (Nasr and Isaacs, 2001; Nasr et al., 2003; Ivory et al., 2008; Li and Mamora, 2010; Keshavarz, Okuno, and Babadagli, 2015). However, it is important to have similar operating conditions to make a fair comparison. Nasr and Isaacs (2001) introduced ES-SAGD process. Nasr and Ayodele (2006) discussed the mechanism of the process. The process was tested in the field, and it showed better thermal efficiency, lower water requirement, and oil recovery improvement compared to SAGD. It was suggested that the solvent should condense or evaporate at conditions similar to that for water at the operating pressure.

Gupta, Gittins, and Picherack (2004) showed through simulations that a higher oil production rate by applying Solvent Aided Process (SAP) with the lighter hydrocarbons and larger its amount. The importance of solvent retention in a porous medium and its adverse effect on the economics of SAP process are also discussed in work. Gates and Chakrabarty (2006) presented a simulation work on optimization of the solvent-SAGD process by adjusting the injection pressure and solvent fraction in the injected stream. It was concluded that the key to optimizing solvent and steam recovery processes is to determine the injection volumes so that no excess steam or solvent is delivered to the bitumen edges. The results also showed that solvent can significantly reduce the steam requirement of SAGD, yet produce the same volumes of oil. Gates (2007) performed a simulation study on solvent-SAGD performance. The study showed that the solvent-SAGD recovery method required less steam to produce the same amount of bitumen that of SAGD and also stated that the operating temperature is lower than that of SAGD which resulted in lower heat losses and better thermal efficiency. The solvent recovery was also estimated to be 80%.

Experimental work of Ardali, Barrufet, and Mamora (2012) indicated that the choice of solvent in the solvent-SAGD process depends on its impact on oil phase viscosity reduction which in turn is affected by reservoir properties and operational conditions. Frauenfeld et al. (2008), and Frauenfeld et al. (2012) did experimental and numerical studies of the solvent-SAGD process. It was concluded that there is not a large difference between oil rates from SAGD and solvent-SAGD. However, solvent-SAGD could be more economical in view of lower CSOR. The results of experiments show that a lower oil production rate and steam-oil ratio in the case of hybrid solvent (propane and butane) compared with steam only. High steam injection rates resulted in higher CSOR and required higher pressure (to produce higher oil production rates) to use propane optimally and to balance the reduced solubility at higher temperatures. The results of their experimental work showed that the low injection rate for a certain pressure in a solvent SAGD process resulted in a very low temperature and so, the chamber did not grow. It was also shown that the lower steam quality at the same injection rate and injection pressure resulted in lower oil production rates. Gupta et al. (2010) did a numerical evaluation of Solvent Aided Process (SAP) for different butane injection strategies (continuous constant, ramp-up, and ramp-down, and pulse injection). They reported the solvent concentration at the interface increased with time. Pulse injection strategy was found to have better performance, and the optimal butane concentration was 10% wt of the steam injection rate.

Some reported field observations indicate an improvement in oil recovery by adding solvent to steam. In Cold Lake, Imperial Oil reported almost 100% incremental oil production (Leaute, 2002; Leaute and Carey, 2007) by the addition of diluent to steam in selected wells in their last cycles of CSS which was named Liquid Addition to Steam Enhanced Recovery (LASER). In another project, EnCana (2002) reported 50% improved oil recovery compared to SAGD by co-injecting butane with steam in phase-C well pairs at Senlac and Christina Lake (Gupta, Gittins, and Picherack, 2002; Gupta, Gittins, and Picherack, 2004; Gupta and Gittins, 2005; Gupta and Gittins, 2007). The process was called Solvent Aided Process (SAP). However, Orr (2009) reported no bitumen improvement in Nexen Jet B project (Long Lake) using a mixture of C_7 to C_{12} at a 10% concentration and

Suncor Firebag project applying naphtha. The observation of Imperial Oil Resources's solvent-SAGD project injecting a light hydrocarbon with steam was analyzed by Dittaro, Dickson, and Boone (2013). Oil production rate improved approximately 90% (from 40 to 75 m^3/day). However, the SOR remained constant at approximately 3.5 m^3/m^3. This indicates that to achieve a higher oil production rate, steam injection rate was increased. The reported field production rate was the total hydrocarbon production (bitumen and solvent). This is an important point because if the oil production of the solvent-SAGD and SAGD process is to be compared, it should be bitumen production rate only. Dickson et al. (2011), and Dickson et al. (2013) have described several analyses of this project.

Gupta et al. (2010), Govind et al. (2008), and Akinboyewa et al. (2010) reported that a larger concentration of injected solvent in a solvent co-injection with steam resulted in the higher oil production rate. Nevertheless, due to the high cost of the solvent, the optimal amount of solvent is required to be determined.

Some studies indicate that the lighter solvents improve the performance of solvent based recoveries (Das and Butler, 1998; Pathak, Babadagli, and Edmunds, 2010; Gupta et al., 2010; Ferguson, Mamora, and Goite, 2001; Dittaro, Dickson, and Boone, 2013; Dickson et al., 2011; Dickson et al., 2013), while there are others which claim the effectiveness of heavier solvents (Shu and Hartman, 1988; Nasr and Isaacs, 2001; Boak and Palmgren, 2007; Sabet, Hassanzadeh, and Abedi, 2017).

2.2.2 Analytical Modelling of Solvent-SAGD Process

In this work, the focus is on mathematical modelling of the solvent-SAGD process. Despite all the simulation and experimental works, field observations in this area, the results are mixed. It remains unclear whether injecting solvent with steam improves oil recovery or not, and which solvent results in higher recovery, if any, compared to the steam-only process, and what would be the optimal amount of solvent concentration in the injected steam. Evaluating the performance of this process has mostly been done by numerical

simulation, but the reliability of simulation models is questionable because of extremely small diffusivity and large numerical dispersion (Nenniger and Dunn, 2008).

There are only a few analytical treatments of this process. Butler and Mokrys (1989) proposed a mathematical model of the VAPEX (Vapour Extraction) process. The oil rate equation was developed based on a steady-state concentration profile from Fick's law with a constant interface velocity. Gupta and Gittins (2011) developed a semi-analytical model for estimating oil rate and optimal solvent consumption by combining the SAGD and VAPEX equations. The oil production rate from the model was not consistent with the field and numerical simulation results. It was suggested that by assuming an artificially increased molecular diffusion coefficient (by almost two orders of magnitude) or by introducing a diffusive solvent layer in between the vapour chamber and oil zone, the oil production rate from the model could be justified. The model predicted that butane and pentane resulted in higher oil rates compared to propane and hexane.

Rabiei Faradonbeh, Harding, and Abedi (2012) extended the numerical model of Butler (1985) to include the solvent co-injection with steam using a linear geometry. The heat integration method was applied to solve the unsteady state temperature and concentration profiles. It was shown by using proper parameters the results of their model were in good agreement with the numerical results by CMG-STARS. It was also concluded that the solvent type and its concentration had a profound effect on oil production rate. Sharma and Gates (2010) solved the concentration and temperature equations to show the profiles beyond the chamber edges. Concentration dependence of diffusion coefficient was considered.

Azom and Srinivasan (2013) extended their thermo-capillary imbibition model for SAGD to include the solvent component. The oil rate from their model was steady, but it was a function of the thermo-capillary number. Within a certain range, there was no improvement in the oil recovery compared to SAGD, but no equation or comparison was proposed for thermal efficiency. It was also concluded that the ES-SAGD process had a high dependency on the reservoir or operating pressure and viscosity ratio of solvent to bitumen

at the vapour-chamber interface. Rabiei Faradonbeh, Harding, and Abedi (2014) proposed a numerical model for calculating oil rate using a curved interface in a similar approach as in Rabiei Faradonbeh, Harding, and Abedi (2012).

The above discussion and the mixed results of solvent-SAGD processes indicate that the overall interactions of heat and solvent mass transfer are still unclear. In particular, the effect of operating conditions on these two means of transfer and their relative roles on the performance of the solvent-SAGD process is a mystery. Zargar and Farouq Ali (2017) proposed a new analytical model of the solvent-SAGD process based on the combination of the overall solvent mass balance, heat balance and volumetric oil displacement and Darcy oil rate using a mixture viscosity model as a function of temperature and solvent concentration ahead of front satisfying the equilibrium in the system, unlike the previous works. The heat and mass balances in the system were coupled because of their dependency on steam chamber velocity. It showed that the total injection rate (steam and solvent) had a profound effect on the performance of the process. It also showed that if the dilution effect of solvent on bitumen could offset the lower temperature effect on oil viscosity reduction, a higher oil production rate could be possible in the solvent-SAGD compared to SAGD.

3. ANALYTICAL MODELLING OF STEAM CHAMBER RISE STAGE

3.1 Introduction

When steam is injected continuously in a SAGD operation, a steam chamber starts to develop, as observed in the field and laboratory experiments. Initially, the vertical growth of the steam chamber is considerably greater than the sideways growth, which it is called the steam chamber rise period. The upward growth is limited by the top of the reservoir, and afterwards, the steam chamber grows sideways. In the final stage, the steam chamber coalesces with neighbouring steam chambers. This stage is called the confinement stage in this work. Physics of the steam chamber development in the first and the two last stages are different, and are modelled separately. Most of the available theoretical analyses of SAGD are concerned with the lateral spreading stage of the steam chamber development but there are a few works on mathematical modelling of the steam chamber rise. The rate of the upward growth of the steam chamber has a profound effect on the performance of SAGD project because after the chamber reaches the top of the reservoir heat loss starts to play a significant role in the thermal efficiency of the process.

There are a few analytical models to determine the steam chamber rise velocity, oil production rate and thermal efficiency of SAGD process at early times. As mentioned above, the steam chamber grows upwards, and oil drains downwards. It is hard to model the process at this stage due to the frontal instability between steam and the liquid phases in the system. Stability is affected by factors such as the direction of displacement to gravity and viscosity difference between gas/steam and liquid phases.

In this theory, by combining volumetric oil displacement with Darcy oil rate considering the indirect effect of frontal instability, the rise velocity and the steam chamber height were calculated. The model is extended to predict oil production, heat or steam injection rate, heat consumption and CSOR during this phase. Moreover, an estimate of injected steam

sweep efficiency and the angle between the steam chamber and the horizon are achieved. This theory is tested via comparison with several field data and experimental data to show the adequacy of the model.

3.2 Analytical Model

3.2.1 Model Assumptions

In developing this model, the following assumptions were made:

1. The steam chamber is assumed to be an inverted triangle with a vertex fixed at the production well.
2. The steam chamber maintains a similar geometry as it grows.
3. The steam chamber expands sideways and upwards but the upward rate is much larger than the sideways growth. In this model, the sideways expansion is ignored.
4. Counter-current flow of steam and liquid phase is assumed. Steam flows up, and liquid stream flows down inside the steam chamber.
5. The pressure gradient is neglected as it is very small.
6. Porous medium is homogenous.
7. Bitumen at the steam temperature contributes to production.
8. Heat transfer is directed normal to the steam chamber interface at the top (triangle base).
9. In the steam invaded zone, the remaining oil is residual oil saturation to steam.

3.2.2 Analytical Model

3.2.2.1 *Steam Chamber Rise Velocity*

A model is developed to predict steam chamber rise velocity for SAGD process. Steam is injected from the injector into the cold reservoir. Gravity causes steam to move upwards, while heated oil and condensate drain down (counter-current flow of steam and oil). During

this stage, steam chamber expands upwards and sideways, but the upwards rate is much larger than the sideways growth.

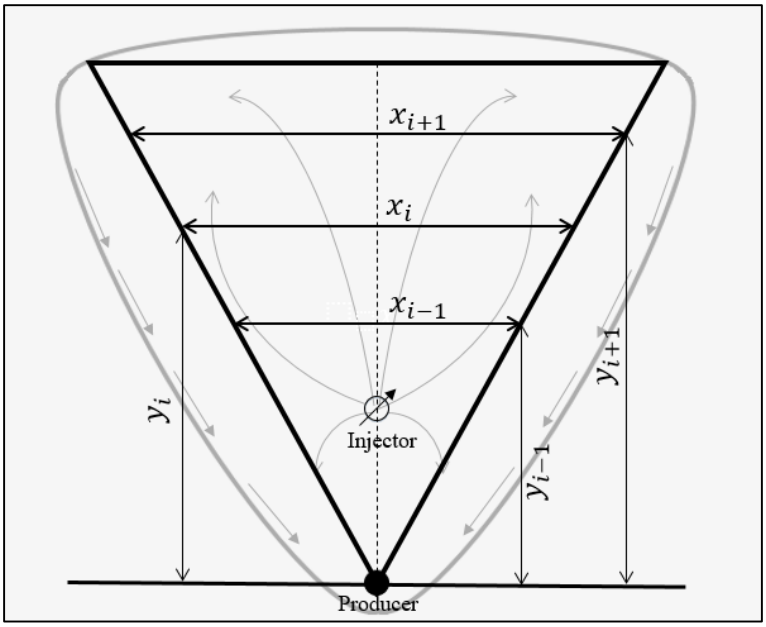

Figure 3.1: The approximate shape of the steam chamber during rise phase.

In this model, heated oil at steam temperature contributes to the production only. The pressure gradient is neglected as it is very small. It was observed from the experimental work of Butler and Chung (1987) that when steam is injected through a horizontal well at the bottom of the formation close to the horizontal producer, an inverted triangle shape steam chamber grows upwards, and it keeps a similar geometry as it rises (Figure 1.5). This geometry is assumed in our steam chamber rise approach (Figure 3.1). The base of the triangle, the steam chamber top interface, is proportional to its height by a dimensionless coefficient which named *Lateral Spreading Coefficient*, α_{LS}. So, the cross-section area of the rising steam chamber (per unit length of the horizontal well) is:

$$x = \alpha_{LS} y(t) \quad , \quad A(t) = \frac{1}{2} x.y = \frac{1}{2} \alpha_{LS} y(t)^2 \tag{3.1}$$

where $y(t)$ is the steam chamber height as a function of time, and x is the base of the steam chamber or the upper steam chamber interface which is a function of time as well. Volumetric oil displacement over the steam-invaded zone during the rise period can be calculated per unit length of the horizontal well as:

$$Q_o = \phi \Delta S_o \, V_{SC}$$

$$q_o = \frac{dQ_o}{dt} = \phi \Delta S_o \, \frac{dA(t)}{dt}$$

$$q_o = \alpha_{LS} \phi \Delta S_o y \, \frac{dy}{dt}$$

(3.2)

Note that cumulative oil production, Q_o, is equivalent to the total steam chamber volume, V_{SC}, at each time. Darcy oil rate per unit length of the horizontal well is also given by:

$$q_o = V_{oD} \delta(t) = \frac{k_o}{\mu_o} \left(\frac{\partial p}{\partial y} + \rho g \frac{\partial D}{\partial y} \right) \delta(t)$$

(3.3)

where V_{oD} is Darcy velocity in the direction normal to the upper interface, k_o and μ_o are effective permeability and dynamic viscosity of oil, respectively. In Equation 3.3, the first term in the bracket indicates the pressure gradient and the second term represents the gravity force in the normal direction to the upper steam chamber interface.

Butler and Chung (1987) observed steam fingers at the boundary of the steam chamber as the steam chamber rises. Heated oil and injected steam form a two-phase counter-current flow within the steam chamber. Applying the assumptions above and neglecting ρ_g compared to ρ_o ($\rho_g \ll \rho_o$), Equation 3.3 can be rewritten as:

$$q_o = \frac{k_o}{\mu_o} \left(\rho_o - \rho_g \right) g \, \delta(t) = \frac{k_o}{\upsilon_{os}} g \delta(t)$$

(3.4)

$\delta(t)$ is the total available width for the liquid streams at the top of the steam chamber to allow the downward drainage at a particular time ($\sum_j \delta_{nj} = \delta_n$ where n is the time index and j is, the number of liquid streams). This concept can be well understood by looking at Figure 3.2. It is assumed that the fingers move at the same velocity. In this approach, the limiting factor in Darcy oil rate is the ability of oil to drain down. Oil kinematic viscosity at the injected steam temperature, υ_{os} , is defined as the ratio of absolute viscosity to its density at the same temperature.

A new coefficient is introduced which is defined as the volumetric ratio (per unit length of horizontal well) of the displaced oil to the steam at each particular time. It is considered that this ratio is the same in both volumetric and Darcy models. This coefficient is called the areal flow ratio of oil to steam, α_A. As a result, $\delta(t)$ in Darcy oil rate equation is given by:

$$\delta(t) = \frac{1}{2}\alpha_A x(t) = \frac{1}{2}\alpha_A \alpha_{LS}\, y(t) \qquad 0 < \alpha_A \leq 1$$

(3.5)

By substituting Equation 3.5 into Equation 3.4, Darcy oil rate from this approach is calculated by:

$$q_o = \frac{k_o g}{2\upsilon_{os}}\alpha_A \alpha_{LS} y$$

(3.6)

It is expected that at each time the oil rate is unique. Therefore, the following expression can be derived for the constant rise velocity:

$$\frac{dy}{dt} = \frac{\alpha_A k\, k_{ro} g}{2(\phi \Delta S_o \upsilon_{os})}$$

(3.7)

The rise velocity in this approach is a result of a balance between volumetric displacement and Darcy oil rate. The heated oil at steam temperature drains down on a limited portion

of the rising front in the vertical direction and inside the chamber parallel to the upward movement of steam streams (Figure 3.2).

Maximum vertical interface velocity occurs in the case of $\alpha_A = 1$. As can be seen from Equation 3.7, rise velocity depends on reservoir rock and fluid properties, steam temperature and α_A. Areal flow ratio of oil to steam, α_A, depends on the number, size and spacing of the fingers. One of the limitations of this model is that it cannot predict the condition of the fingers. A large α_A indicates a large area available for oil to flow down implying a higher front rise velocity.

The height of steam chamber can be calculated from Equation 3.7 as follow:

$$\int_0^y dy = \int_0^t \frac{\alpha_A k\, k_{ro} g}{2(\phi \Delta S_o \upsilon_{os})}\, dt \quad \rightarrow \quad y = \frac{\alpha_A k\, k_{ro} g}{2(\phi \Delta S_o \upsilon_{os})} t \tag{3.8}$$

The above equation shows that the steam chamber height is a linear function of time. From the model developed above, the time (t_r) at which the steam chamber reaches the top of the reservoir can be determined knowing the areal flow ratio of oil to steam. In case of $\alpha_A = 1$ (correspond to the largest interface velocity), t_r is given by:

$$t_r = \frac{2(\phi \Delta S_o H \upsilon_{os})}{k_o g} \tag{3.9}$$

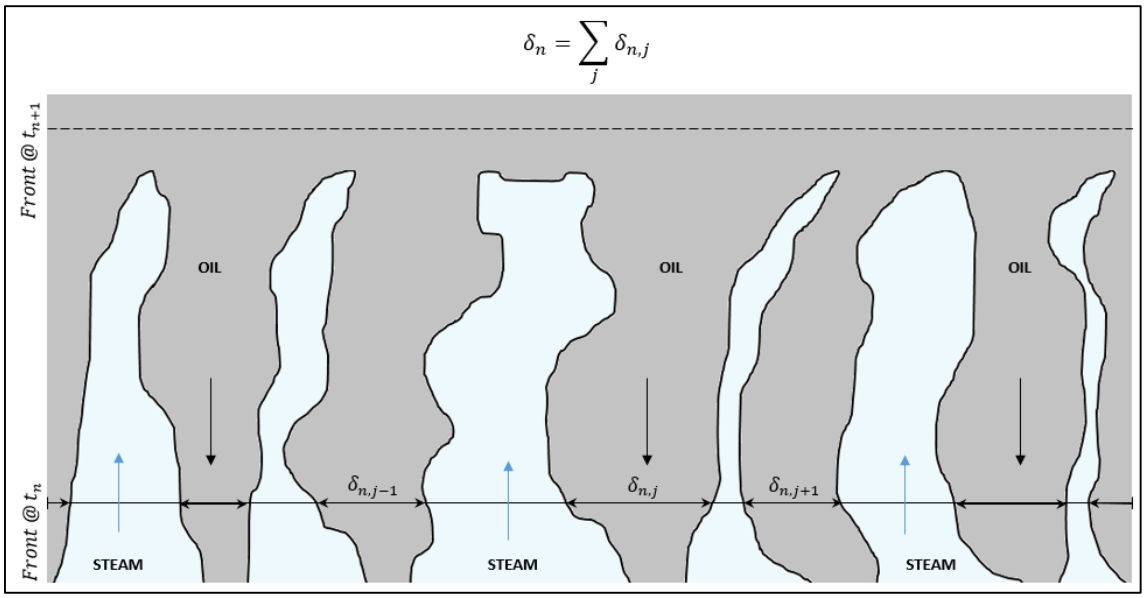

Figure 3.2: Upper steam chamber interface movement from t_n to t_{n+1} assuming a counter current flow of steam and oil.

3.2.2.2 *Oil Production Rate*

To calculate the oil production rate during this period, we need to find α_{LS}. The rate reaches a maximum when steam chamber rises to the top of the reservoir. We postulate that the maximum oil production rate comes from Constant Volumetric Displacement (CVD) model (Section 4.2.23) having the below oil rate:

$$q_{omax} = 2\sqrt{\frac{\phi \Delta S_o k_o g \alpha H}{m \upsilon_{os}}} \tag{3.10}$$

And from the steam chamber rise model, the maximum oil production rate is:

$$q_{omax} = \frac{k_o g}{2\upsilon_{os}} \alpha_{LS} \alpha_A H \tag{3.11}$$

Therefore,

$$\alpha_{LS} = ({}^{4}/_{\alpha_A}) \sqrt{\frac{\phi \Delta S_o \alpha \upsilon_{os}}{m k_o g H}}$$

(3.12)

Hence, the oil production rate and cumulative oil production as chamber rises $(0 < t < t_r)$ are calculated as:

$$q_o = \left(\frac{k_o g}{\upsilon_{os}}\right)^{3/2} \left(\frac{\alpha}{\phi \Delta S_o m H}\right)^{1/2} \alpha_A \, t$$

(3.13)

$$Q_o = 0.5 \left(\frac{k_o g}{\upsilon_{os}}\right)^{3/2} \left(\frac{\alpha}{\phi \Delta S_o m H}\right)^{1/2} \alpha_A t^2$$

(3.14)

Equation 3.13 shows that the oil production rate during the rise period is a function of properties such as effective permeability, oil kinematic viscosity at steam temperature, and thermal diffusivity. One of the parameters affecting the oil production rate is areal flow ratio of oil to steam. This parameter can be obtained from history matching or experiment. In this approach, the angle between side oil-steam interface of the steam chamber and the horizon is different from one reservoir to another and can be calculated by lateral spreading coefficient, α_{LS}, as below:

$$\theta = \arctan\left(\frac{2}{\alpha_{LS}}\right)$$

(3.15)

Also, areal flow ratio, α_A, can be used to estimate sweep efficiency, E_a, in the steam chamber, assuming uniform steam and oil streams distribution along the horizontal well. The relation is given by:

$$E_a = \frac{A_s}{A_t} = \frac{1}{1 + A_o/A_s}$$

(3.16)

So, the sweep efficiency and areal flow ratio of oil to steam are related as below:

$$\alpha_A = \frac{1}{E_a} - 1$$

(3.17)

3.2.2.3 *Energy Balance and CSOR Calculations*

During the transient steam chamber rise period, initially there is no heat ahead of the rising front, but as the front rises with time, heat accumulates ahead of the front. Upward movement of the front means that the heat is transferred to the top of the steam chamber and into the oil zone. This heat can be considered as the heat loss term in this stage of SAGD because in the oil production model it was assumed that heated bitumen at the steam temperature is contributed in the production only. Heat balance for this model is given by:

$$Q_{inj} = Q_{sz} + Q_{oz}$$

(3.18)

The injected heat into the system, Q_{inj} , during the rise period is distributed in two ways. Q_{sz} is the heat to raise the reservoir rock and fluid temperature from the reservoir temperature, T_r, to the steam temperature, T_s. Q_{oz} is the heat into the reservoir from the steam chamber interfaces which can be divided into two portions; Q_{ozo} which is accumulated heat overhead of the rising oil-steam interface, and Q_{ozs} which is the heat transfer into the reservoir from the extending sides of steam chamber by conduction only. Therefore,

$$Q_{oz} = Q_{ozo} + Q_{ozs}$$

(3.19)

Heat into the steam zone (per unit length of the horizontal well) is calculated as:

$$Q_{sz} = mC(T_s - T_r)$$

$$= \frac{1}{2} xy(\rho C)_{res} \Delta T$$

$$= \left\{ \frac{1}{2} \alpha_{LS} (\rho C)_{res} \Delta T \left(\frac{dy}{dt}\right)^2 \right\} t^2$$

(3.20)

So, the heat rate to the steam zone is given by:

$$q_{sz} = \left\{ \alpha_{LS} (\rho C)_{res} \Delta T \left(\frac{dy}{dt}\right)^2 \right\} t$$

(3.21)

Heat is transferred ahead of the rising steam-oil interface at the top of the steam chamber. Overhead heat transfer, Q_{ozo}, can be evaluated from integrating over the temperature distribution beyond the rising interface at each time. In this case, there is a moving boundary problem as shown in Figure 3.3.

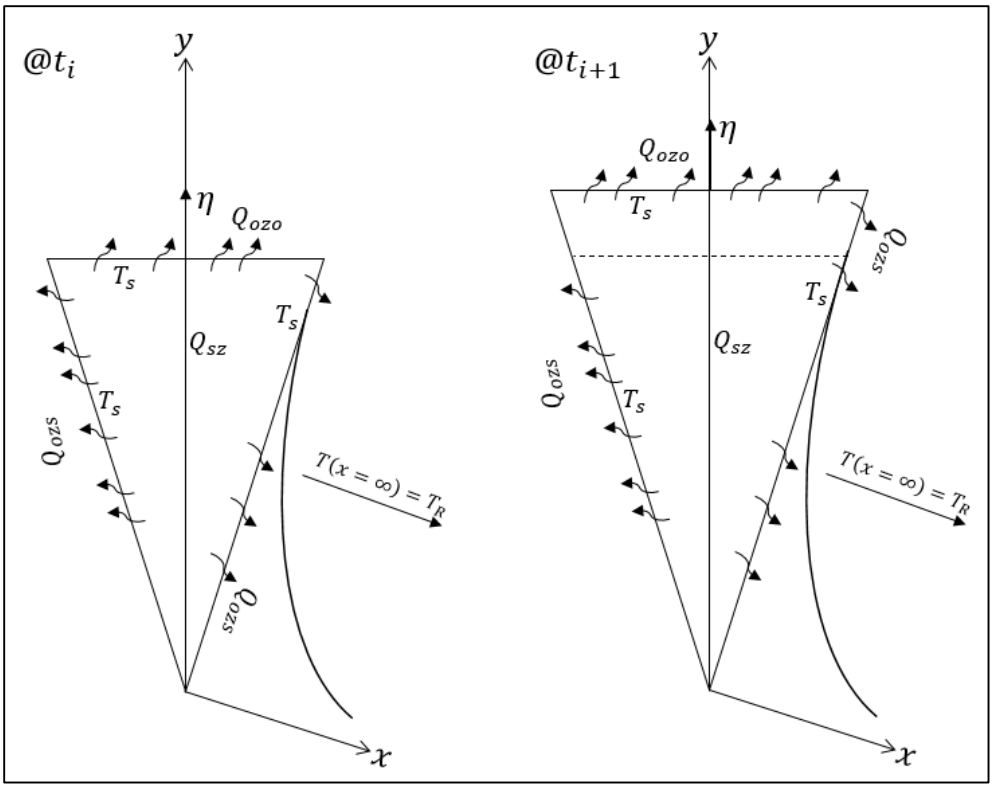

Figure 3.3: Rising steam chamber interface at the top and heat distribution in the system during rise phase including heat to the steam zone, Q_{sz}, heat to the oil zone at sides of steam chamber, Q_{ozs}, and to the overhead, Q_{ozo}.

Heat transfer by conduction is based on Fourier's heat conduction equation:

$$\frac{\partial^2 T}{\partial x^2}+\frac{\partial^2 T}{\partial y^2}+\frac{\partial^2 T}{\partial z^2}=\frac{1}{\alpha}\frac{\partial T}{\partial t} \tag{3.22}$$

where α is the thermal diffusivity and is defined as the ratio of thermal conductivity (K) to volumetric heat capacity (ρc):

$$\alpha=\frac{K}{\rho c} \tag{3.23}$$

Where ρ is the mass density and c is the specific heat capacity. The temperature gradient in directions parallel to the rising interface and along the horizontal well is negligible compared to that in the normal direction to the interface. So, the three-dimensional Fourier's equation for this problem reduces to:

$$\frac{\partial^2 T}{\partial y^2} = \frac{1}{\alpha}\frac{\partial T}{\partial t} \tag{3.24}$$

This is a moving boundary problem meaning that the heat source plane is rising with time with a constant velocity, dy/dt. The treatment of this type of problem is different from problems with static source of heat. A new coordinate, η, (See Figure 3.3) with the following variable transformation is defined:

$$\eta = y - (dy/dt).t \tag{3.25}$$

Applying this transformation and the chain rule gives:

$$\frac{\partial T}{\partial \eta} = \frac{\partial T}{\partial y}\frac{\partial y}{\partial \eta} + \frac{\partial T}{\partial t}\frac{\partial t}{\partial \eta} \Rightarrow \frac{\partial T}{\partial \eta} = \frac{\partial T}{\partial y} \tag{3.26}$$

Similarly, the second derivative to space can be obtained as:

$$\frac{\partial^2 T}{\partial \eta^2} = \frac{\partial^2 T}{\partial y^{\,2}} \tag{3.27}$$

And also for time derivative,

$$\frac{\partial T}{\partial t} = \frac{\partial T}{\partial \eta}\frac{\partial \eta}{\partial t} + \frac{\partial T}{\partial t}\frac{\partial t}{\partial t} \Longrightarrow \frac{\partial T}{\partial t} = -(dy/dt)\frac{\partial T}{\partial \eta} + \frac{\partial T}{\partial t} \tag{3.28}$$

Substituting the temperature derivatives from Equations 3.27 and 3.28 in the new coordinates, Equation 3.24 can be rewritten as:

$$\frac{\partial^2 T}{\partial \eta^2} = \frac{1}{\alpha}\left(-(dy/dt)\frac{\partial T}{\partial \eta} + \frac{\partial T}{\partial t}\right)$$

(3.29)

The above equation can be simplified by assuming pseudo steady-state temperature profile:

$$\frac{d^2 T}{d\eta^2} + \frac{1}{\alpha}(dy/dt)\frac{dT}{d\eta} = 0$$

(3.30)

Two boundary conditions are required in the above equation to find the temperature distribution; steam temperature, T_s, at the interface and reservoir temperature, T_r, at a distance far from the interface. Dimensionless temperature also can be defined as:

$$T_D = \frac{T - T_r}{T_s - T_r}$$

(3.31)

By solving Equation 3.30 with the aforementioned boundary conditions, the pseudo steady-state dimensionless temperature distribution beyond a rising interface with a constant velocity can be calculated as:

$$T_D = exp(-\frac{dy/dt}{\alpha}\eta)$$

(3.32)

The accumulated heat beyond the rising front over a differential interval,$d\eta$, at each time is given by:

$$dQ_{ozo} = d\big(mc(T - T_r)\big)$$

(3.33)

By integrating Equation 3.33, the accumulated heat over the entire area beyond the front can be calculated as:

$$Q_{ozo} = x(\rho c)_{res}\Delta T \int_0^{\infty} T_D d\eta$$

(3.34)

where, $(\rho c)_{res}$is the volumetric heat capacity of formation and is defined as:

$$(\rho c)_{res} = \phi\rho_w c_w S_{wir} + \phi\rho_o c_o S_{oi} + (1-\phi)\rho_r c_r$$

(3.35)

where, S_{wir} is the irreducible water saturation, S_{oi} is the initial oil saturation, ρ_w, ρ_o, and ρ_r are density of water, oil, and rock respectively, c_w, c_o, and c_r are also specific heat capacity of water, oil and rock respectively.

By substituting for T_D from Equation 3.32 and x from Equation 3.1, accumulated heat overhead of the rising interface is found as a linear function of time as below:

$$Q_{ozo} = \alpha_{LS} K_{res}\Delta T t$$

(3.36)

Heat rate to the overhead oil zone is given by:

$$q_{ozo} = \alpha_{LS} K_{res}\Delta T$$

(3.37)

Another portion of the heat transfer in this model is the heat transfer into the oil zone around the sides of the steam chamber,Q_{ozs}, which is assumed to be by conduction. It is mentioned in the assumptions, the sideways expansion of the steam chamber is neglected in the rise period so, the heat transfer from the sides is modelled as heat flux into a semi-infinite reservoir from an extending plane as a static source at the steam temperature (See Figure 3.3). It is worth mentioning that the heat transfer to the sides of the chamber is considered

to be the heat loss in this stage because it does not contribute to heating bitumen but it preheats the oil zone for later production during the lateral spreading phase.

First, the temperature distribution is derived to find the heat transfer into the sides of the rising steam chamber by conduction. The one-dimensional heat conduction equation and the initial and boundary conditions for this problem (Figure 3.3) are given by:

$$\frac{\partial^2 T}{\partial x^2} = \frac{1}{\alpha}\frac{\partial T}{\partial t}$$

$$T(x, t = 0) = T_r$$

$$T(x = 0, t) = T_s$$

$$T(x \to \infty, t) = T_r$$

(3.38)

The solution to this second order partial differential equation (Strang and Aarikka, 1986) is:

$$T = T_r + (T_s - T_r) erfc(\frac{x}{2\sqrt{\alpha t}})$$

(3.39)

Or it can be rewritten in dimensionless temperature form as:

$$T_D = erfc(\frac{x}{2\sqrt{\alpha t}})$$

(3.40)

Heat flow rate into a differential surface,dl_{int}, of the chamber at its side (per unit length of the horizontal well) is given by:

$$dq_{oz,S} = -K_{res} dl_{int} \frac{\partial T}{\partial x}|_{x=0}$$

(3.41)

The side of the steam chamber can be measured versus time as:

$$dl_{int} = \sqrt{1 + \frac{{\alpha_{LS}}^2}{4}}\,(dy/dt)dt$$

(3.42)

The rise velocity,(dy/dt), in the above equation is constant. The derivative term can be calculated from Equation 3.40:

$$\frac{\partial T}{\partial x}|_{x=0} = -\frac{(T_s - T_r)}{\sqrt{\pi \alpha t}}$$

(3.43)

By substituting Equations 3.42 and 3.43 into Equation 3.41, and taking double integral on time as below:

$$Q_{ozs} = \int_0^t \int_0^t dq_{ozs}$$

$$= \int_0^t \int_0^t K_{res} \sqrt{1 + \frac{{\alpha_{LS}}^2}{4}}\,(dy/dt)\frac{(T_s - T_r)}{\sqrt{\pi \alpha t}}dt$$

(3.44)

So, the cumulative heat flow into both sides of the steam chamber is derived as:

$$Q_{ozs} = \frac{8}{3}\sqrt{1 + \frac{{\alpha_{LS}}^2}{4}}\, K_{res}\Delta T\,(dy/dt)(1/\sqrt{\pi\alpha})t^{3/2}$$

(3.45)

And heat rate,

$$q_{ozs} = 4\sqrt{1 + \frac{{\alpha_{LS}}^2}{4}}\, K_{res}\Delta T\,(dy/dt)(1/\sqrt{\pi\alpha})t^{1/2}$$

(3.46)

CSOR is a criterion used to evaluate the performance of SAGD and is defined as the ratio of cumulative injected steam to cumulative produced oil and is given by:

$$CSOR = \frac{Q_{inj}}{\rho_w f_s L_v Q_o}$$

(3.47)

where $\rho_w$is the water density, f_s is the steam quality, L_v and Q_o are latent heat of condensation of steam and cumulative oil production, respectively. By substituting from Equations 3.14, 3.20, 3.36, and 3.45 into the above equation, CSOR as a function of time during the rise period can be calculated as:

$$CSOR = \frac{\left\{\frac{1}{2}\alpha_{LS}(\rho c)_{res}\Delta T(\frac{dy}{dt})^2\right\}t^2 + \alpha_{LS}K_{res}\Delta T t + \frac{8}{3}\sqrt{1 + \frac{{\alpha_{LS}}^2}{4}}\, K_{res}\Delta T\,(dy/dt)(1/\sqrt{\pi\alpha})t^{3/2}}{\rho_w f_s L_v 0.5\left(\frac{k_o g}{\upsilon_{os}}\right)^{3/2}\left(\frac{\alpha}{\phi\Delta S_o m H}\right)^{1/2}\alpha_A t^2}$$

(3.48)

As can be seen from the CSOR equation, it is a function of several reservoir variables but most importantly it is a function of time. The behaviour of CSOR with respect to time can be shown in a simple form as:

$$CSOR = A + \frac{B}{t} + \frac{C}{\sqrt{t}}$$

(3.49)

where A, B, and C are constants depending on the rock and fluid properties, rise velocity, steam properties. As it is expected, CSOR is decreasing with time during this phase.

3.3 Results and Discussion

In this chapter, a steam chamber rise model is introduced. This model evaluates the SAGD process at early times. The model determines several parameters such as rise velocity, oil production rate, cumulative oil production, heat distribution in the system, temperature profile ahead of the rising front and ahead of the static interface at the sides of the steam chamber, steam injection rate, CSOR, thermal efficiency, sweep efficiency of the injected steam, and the time interval of the rise period. The areal flow ratio of oil to steam is a matching parameter, and it embraces the effect of frontal instability. In the steam chamber rise model, introduced in this work, the steam temperature has a crucial impact on the oil production rate because only the heated oil at steam temperature contributes to the production in this stage. Therefore, a higher steam temperature results in a lower oil viscosity and so a higher oil production rate.

3.3.1 Results for Steam Chamber Rise Velocity

During the steam chamber rise period, the rise velocity has a significant effect on the performance of the SAGD process. After the steam chamber reaches the top of the reservoir, the heat loss to the overburden comes into play. This reduces the thermal efficiency of SAGD.

Closmann and Smith (1983) measured the rate of steam chamber rise above a horizontal fracture in a steam injection project in the Athabasca oil sands. Closmann and Smith's (1983) field test data is shown in Table 3.1. The predicted rise velocity of Closmann and

Smith (1983), Butler's models and the new approach are compared with the observed field data in Table 3.2.

Table 3.1: Closmann and Smith's data for Athabasca.

Initial reservoir temperature, T_r, ^oC	4
Injected steam temperature, T_s , ^oC	198
Viscosity of oil at steam temperature, μ_{os}, cp	11
Oil density, ρ_o, g/cm^3	1.005
Porosity, ϕ	0.39
Permeability, k, Darcy	0.5
Initial oil saturation, S_{oi}	0.8
Residual oil saturation, S_{or}	0.0
Irreducible water saturation, S_{wi}	0.2
Thermal diffusivity, α, m^2/day	0.061

Table 3.2: Comparison of steam chamber rise velocity from Closmann and Smith, Butler and this work to observed field data.

	Field Data	**Closmann and Smith**	**Butler (1987) Case A**	**Butler (1987) Case B**	**Butler (1987) Case C**	**This Model**
Effective oil permeability, (m^2)		0.2	0.2	0.25	0.5	0.2
Effective steam permeability, (m^2)		0.04	0.04	0.2	0.4	-
Residual oil saturation, S_{or}		0.0	0.0	0.15	0.15	0.0
Steam rise velocity (m/day)	0.029	0.0222	0.0047	0.015	0.031	0.0247

Table 3.2 shows that this approach predicts a maximum vertical front velocity which is close to the maximum observed rise velocity. Butler's model predicts significantly lower rise velocity. Butler suggested that by increasing the effective permeability to oil and residual oil saturation like Cases B and C in the table, a fair match can be obtained with

the observed field data. Gotawala and Gates (2008) proposed a model to estimate the average rise velocity. The rise velocity from their model and Butler (1987) and this work are compared in Table 3.3 for Athabasca and Lloydminster oils. The results are listed for the three different cases of A, B, and C. In Case A, the effective permeability to oil and the difference between initial and residual oil saturations are 0.1 and 0.8, respectively. In Cases B, and C, the residual oil saturation is assumed to be 0.15, and so the difference between initial and residual oil is 0.65. The effective permeability with respect to oil is considered to be 0.125 and 0.25 in Cases B, and C respectively. The data used in the calculations is the same as in Table 3.1 except for those shown in Table 3.3. The rise velocity for Lloydminster oil from field data is higher due to its lower initial oil viscosity and so, lower oil viscosity at the steam temperature. The predicted rise velocity is also higher compared to the heavier Athabasca oil. The results of this work show a closer agreement with the field data, in particular for the Athabasca oil.

Table 3.3: Comparison of steam chamber rise velocity from Butler, Gotawala and Gates, and this work to the average rise velocity of Athabasca and Lloydminster field data.

Reservoir Data	Athabasca Oil			Lloydminster Oil		
	Case A	Case B	Case C	Case A	Case B	Case C
$v_{os}(m^2/day)$	1.59			0.95		
$k\ (m^2)$	5E-13					
k_{ro}	0.2	0.25	0.5	0.2	0.25	0.5
ΔS_{oi}	0.8	0.65		0.8	0.65	
m	4			2		
Rise Velocity (cm/day) Comparison						
This work	**0.74**	**1.13**	**2.27**	**1.23**	**1.90**	**3.80**
Butler (1987)	0.22	0.69	1.4	0.37	1.2	2.3
Gotawala and Gates (2008)	0.21	0.47	0.93	0.98	3.3	6.5
Field data	1 - 6			4 - 13		

It can be concluded from Equation 3.7, that rise velocity increases with the steam temperature. The effect of steam temperature on rise velocity is investigated for our model by the use of data in Table 3.1, and the results are shown in Table 3.4. As expected, a higher steam temperature leads to a higher front velocity which is consistent with its effect on bitumen viscosity reduction.

Table 3.4: Effect of steam temperature on chamber rise velocity.

Steam temperature (°C)	ν_{os} (m^2/s)	Chamber rise velocity (m/day)
121	9.49E-05	0.003
198	1.10E-05	0.025
260	4.30E-06	0.063

3.3.2 Results for Oil Production

Oil production rate from this approach (Equation 3.13) depends on rock and fluid properties, steam temperature and is a linear function of time. Figure 3.4 shows the oil rate and cumulative oil production versus time using typical Athabasca rock and fluid properties data in Table 3.5. In this stage of SAGD, oil production rate increases as the steam chamber continues to expand upwards as reported from the results of the Underground Test Facility (UTF) by (Edmunds et al., 1994; Chalaturnyk, 1996; Ito, Hirata, and Ichikawa, 2001) and experimental data (Butler, Stephens, and Weiss, 1980; Chung and Butler 1987). It can be estimated that for a horizontal well with around 1000 m length in Athabasca like reservoir, bitumen production rate at the end of the rise period is almost 96 m^3 per day with a cumulative oil production around 15,000 m^3 over the time interval of 301 days.

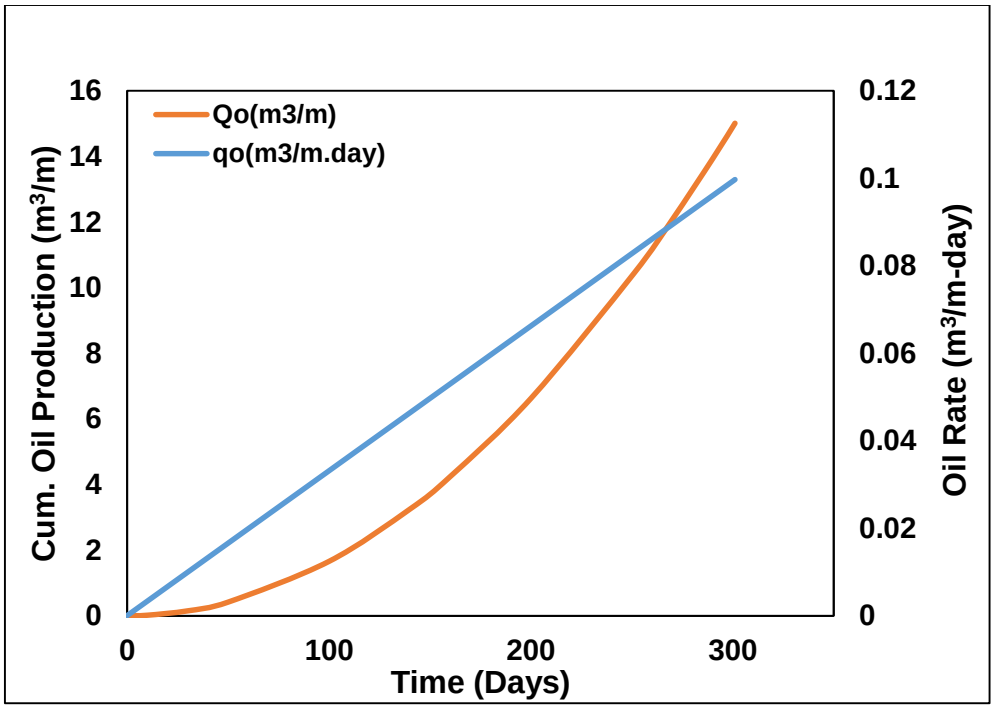

Figure 3.4: Cumulative oil and oil production rate during steam chamber rise.

Table 3.5: Typical Athabasca rock and fluid properties.

Porosity, ϕ	0.35
Residual oil saturation, S_{or}	0.14
Initial oil saturation, S_{oi}	0.75
Permeability, $k,\ m^2$	1E-12
Injected steam temperature, T_s ,^{o}C	213
Initial reservoir temperature, T_r, ^{o}C	13
Oil density, ρ_o , kg/m^3	1014
Water density, ρ_w , kg/m^3	1000
Oil viscosity at T_s , μ_{os} , kg/m-s	0.0109
Reservoir thickness, h, m	22
Thermal diffusivity, α, m^2/day	0.0543
Volumetric heat capacity, ρC, kJ/m^3-^{o}C	1935
Viscosity-temperature Constant, m	3.6

Using data in Table 3.5 and assuming the areal flow ratio of oil to steam to be one, rise velocity and lateral spreading coefficient, the angle between the oil-steam side interface and horizon, time at which the steam chamber hits the top of the reservoir are calculated as shown in Table 3.6. The results indicate that the steam chamber rises with a maximum velocity of 7.3 cm per day and with this velocity, approaches the reservoir top ($H = 22\ m$) in 300 days.

Table 3.6: Some additional results are calculated from the proposed approach of the rise period of SAGD.

Rise velocity, m/day	0.073
Lateral spreading coefficient	0.29
Angle, degrees	81.7
End of the rise period, days	300.9

3.3.3 Results for Heat Distribution and Thermal Efficiency

As mentioned in the previous subsections, injected heat into the reservoir for SAGD process during the rise period is distributed in three ways; heat into the steam zone, heat into the oil zone beyond the rising interface, heat into the oil zone at the sides of the chamber. Heat into the sides and overhead of the rising front are considered as heat loss in this stage. Figure 3.5 illustrates the heat distribution during the rise period using data of Table 3.5. The results show that a significant portion of injected heat is lost to the oil zone from the two sides of the steam chamber. Figure 3.5 also shows that the effective heat which is the heat into the steam zone is larger than heat to the top of the steam chamber but lower than the corresponding heat to the sides.

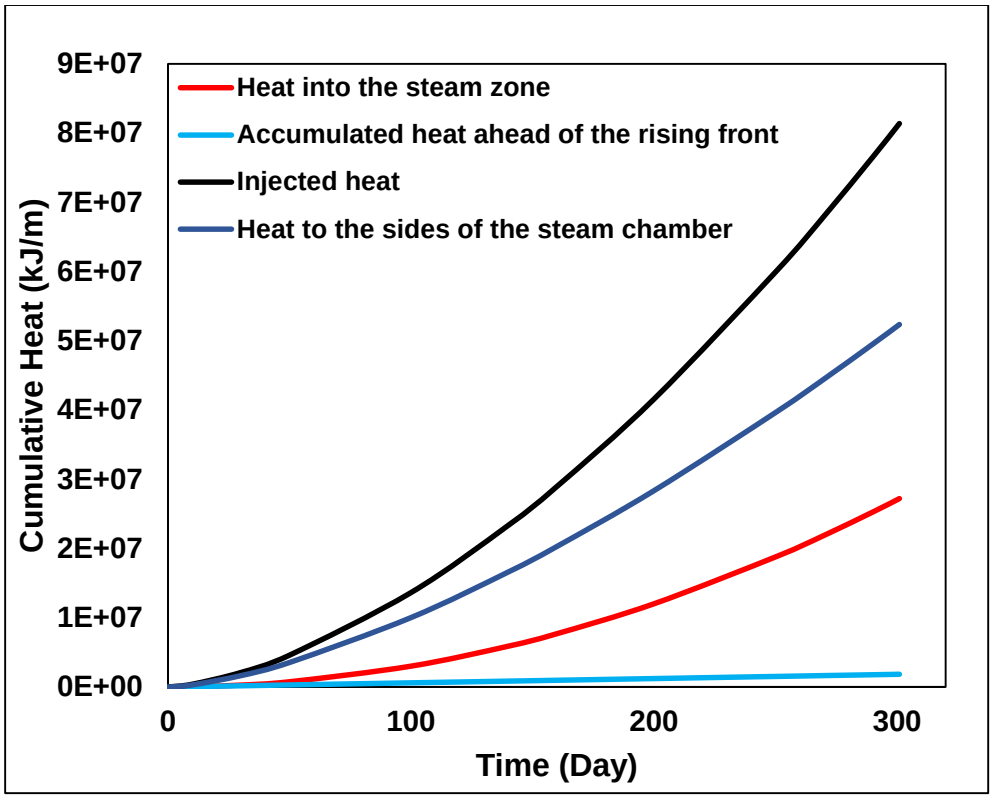

Figure 3.5: Calculated heat distribution in the system as a function of time during the rise period using data in Table 3.5.

In Figure 3.6 the cumulative steam injection and oil production per unit length of a horizontal well are shown. As can be seen from this figure, at the end of the rise period (after 300 days) cumulative injected steam is almost four times of the cumulative produced oil.

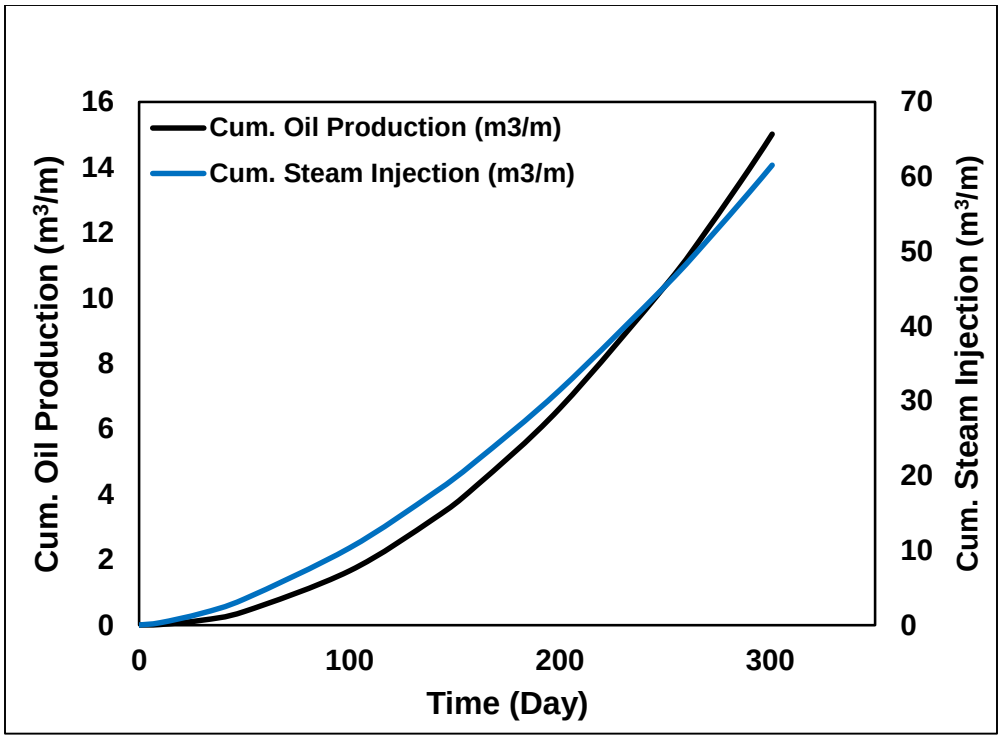

Figure 3.6: Cumulative oil production and steam injection from the model versus time.

CSOR in Equation 3.48 depends on several rock and fluid and steam properties but most importantly it is a function of time. Figure 3.7 shows the behaviour of CSOR during the steam chamber rise period. As is evident from this figure, CSOR is a monotonically decreasing function of time. It reaches a plateau close to the end (CSOR~4).

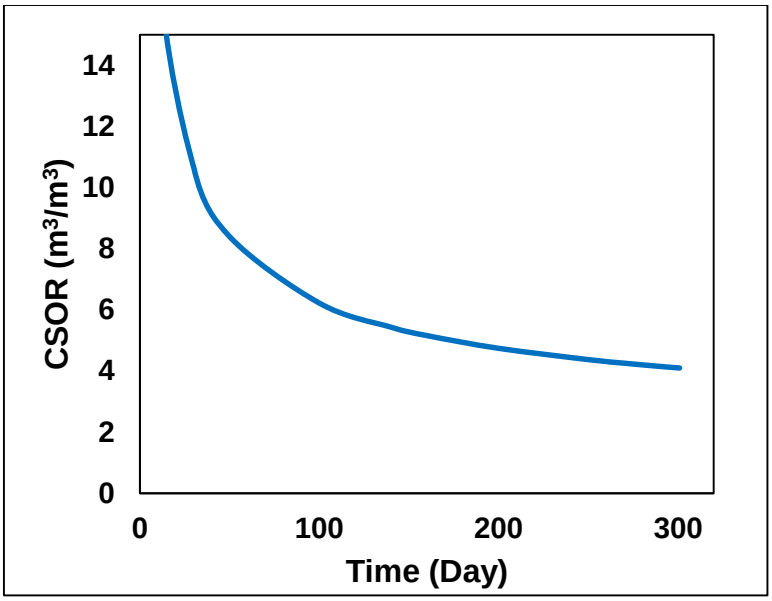

Figure 3.7: Predicted declining CSOR as a function of time during the rise stage of SAGD.

3.3.4 Reservoir Rock Permeability

Rock permeability has a great impact on the success of a steamflood project especially in the case of SAGD with two horizontal wells at the base of the formation. In this situation, as it was mentioned before, the steam chamber grows upward at the early time (rise phase). It is expected from general knowledge of reservoir engineering that a larger rock permeability results in a higher rise velocity. Here, the performance of SAGD during the steam chamber rise period is investigated for two different permeabilities ($k = 1$ and 2 Darcy) with the all other reservoir properties remain unchanged. Equation 3.7 indicates that the rise velocity has a linear proportionality with permeability. Rise velocity is 7.3 cm/day and 14.6 cm/day for rock permeability of 1 and 2 Darcy, respectively. As the reservoir thickness is assumed to be the same in both cases ($H = 22\ m$), the time at which the growing steam chamber reaches the top is doubled in case of the lower rise velocity. Figure 3.8 compares the oil production rate and cumulative oil as a function of time for these two situations.

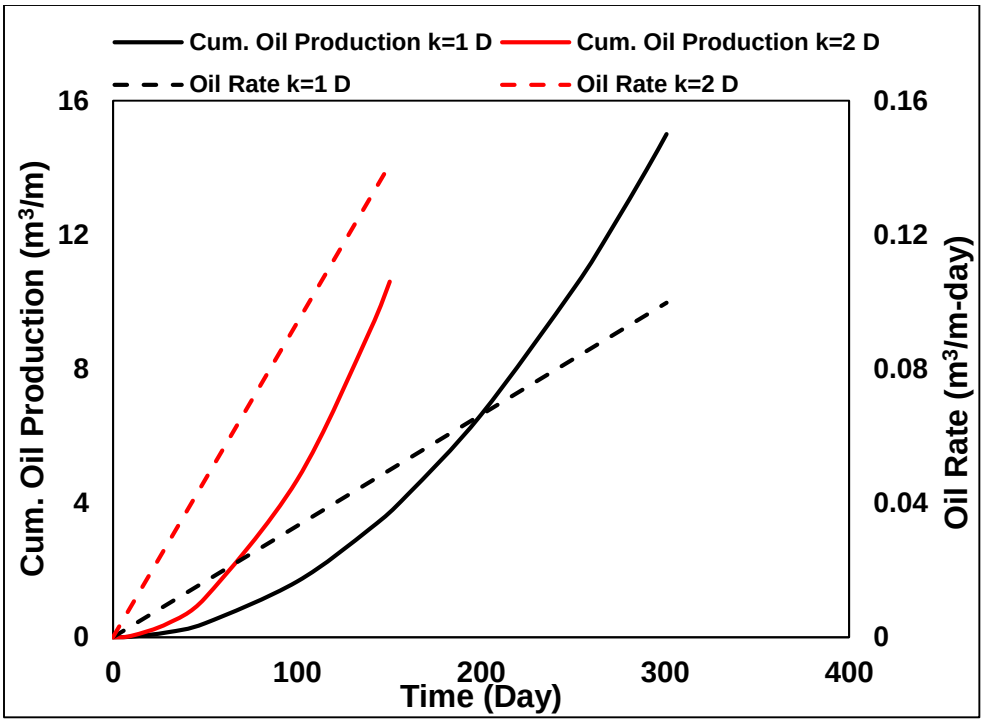

Figure 3.8: Comparison of oil production rate and cumulative oil as a function of time for two different rock permeabilities; 1 and 2 D.

It is seen that a higher permeability reservoir results in a higher oil production rate but for a shorter period compared with a lower permeability reservoir. Oil recovery is greater in the reservoir with a lower permeability although it takes a longer time to reach the reservoir top. The cumulative steam injection of these two reservoirs is compared in Figure 3.9. It shows that the cumulative steam injection in the reservoir with lower reservoir permeability($k = 1\ D$) is much lower at the end of rise period for the higher reservoir permeability ($t = 150\ day$) but at the end of the rise period, the total amount of steam injected is much higher. CSOR for the two cases of permeabilities are shown in Figure 3.10. From an analysis of the effect of rock permeability on SAGD performance during the rise period, one might conclude that a higher reservoir rock permeability may result in an accelerated oil production rate and lower CSOR which is important to the quick project return although the ultimate recovery is lower in this case. Also, for a given vertical permeability, the chamber rise stage velocity will define the chamber height and the angle

subtended at the production well. The lower the vertical permeability, the smaller will be the angle between the steam chamber interface and the horizon, and the chamber would approach a more oblate form.

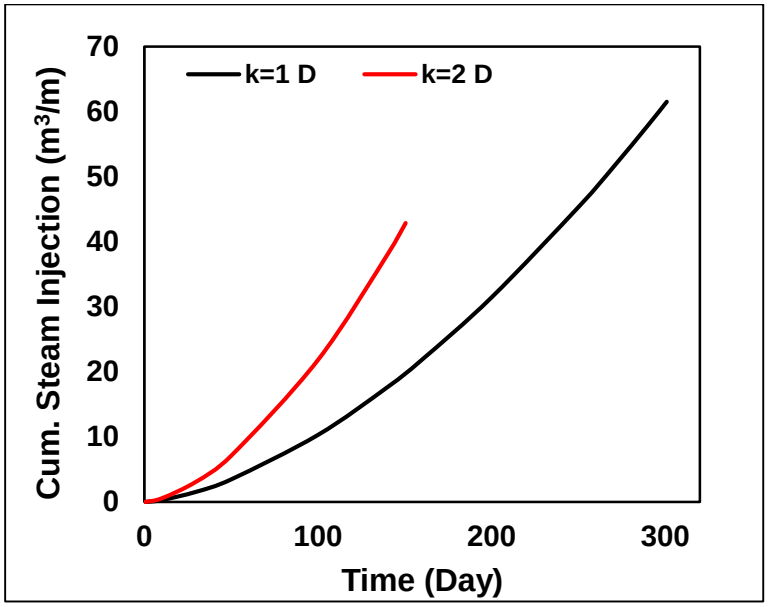

Figure 3.9: Cumulative steam injection variation with time for two different rock permeabilities; 1 and 2 D during the rise period.

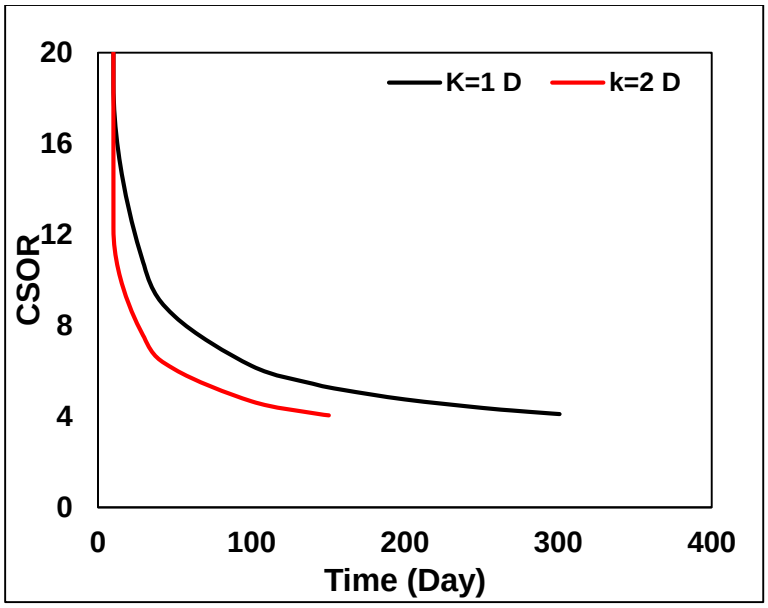

Figure 3.10: Comparison of CSOR for rock permeabilities of 1 and 2 D.

In particular, the faster the steam chamber reaches the top of the reservoir the sooner the heat loss to the overburden comes into play.

3.4 Validation of the Theory with Field Data

The approach introduced for evaluating the performance of SAGD process in its initial stage (steam chamber rise period) including rise velocity, oil production, and thermal efficiency is validated against the field data in this section. The production and injection data of Surmont project Well 101-08 in the Athabasca oil sands of Northeast Alberta which was completed in McMurray formation was reported by ConocoPhillips Canada, 2007. Table 3.7 shows the rock, fluid, and injected steam properties for this field study.

Table 3.7: Reservoir rock, fluid, and injected steam properties of Surmont project (ConocoPhillips Canada, 2015).

Porosity, ϕ	0.33
Residual oil saturation, S_{or}	0.12
Initial oil saturation, S_{oi}	0.82
Permeability, $k,\ m^2$	4E-12
Injected steam temperature, T_s ,ºC	225
Initial reservoir temperature, T_r, ºC	13
Oil density, ρ_o , kg/m^3	1014
Water density, ρ_w , kg/m^3	967
Oil viscosity at T_s , υ_{os} , m^2/s	1.0341E-5
Reservoir thickness, h, m	30
Thermal diffusivity, α, m^2/s	7.06E-7
Volumetric heat capacity, ρC, kJ/m^3.℃	2600
Viscosity-temperature Constant	3.7
Horizontal well length, m	850

As can be seen in Figure 3.11, the cumulative oil production from this approach (Equation 3.14) can predict well data very closely for areal flow ratio of oil to steam of 0.28 ($\alpha_A = 0.28$). Figure 3.12 compares cumulative oil production and cumulative steam injection of the model and well data. Note that the cumulative steam injection at the beginning of the rise period is not zero because of steam consumption during the preheating period. CSOR behaviour as a function of time is depicted in Figure 3.13 for this model (Equation 3.48) and Well 101-08 data.

Some additional results such as rise velocity, the angle between the steam chamber and the horizon, the time interval that chamber hit the overburden, and the estimated injected steam sweep efficiency are listed in Table 3.8 for Well 101-08. The model results show a fair agreement with the observations. Information on when the steam chamber for this well pair reached the top of the reservoir is not available, but the predicted time from this work is 397 days.

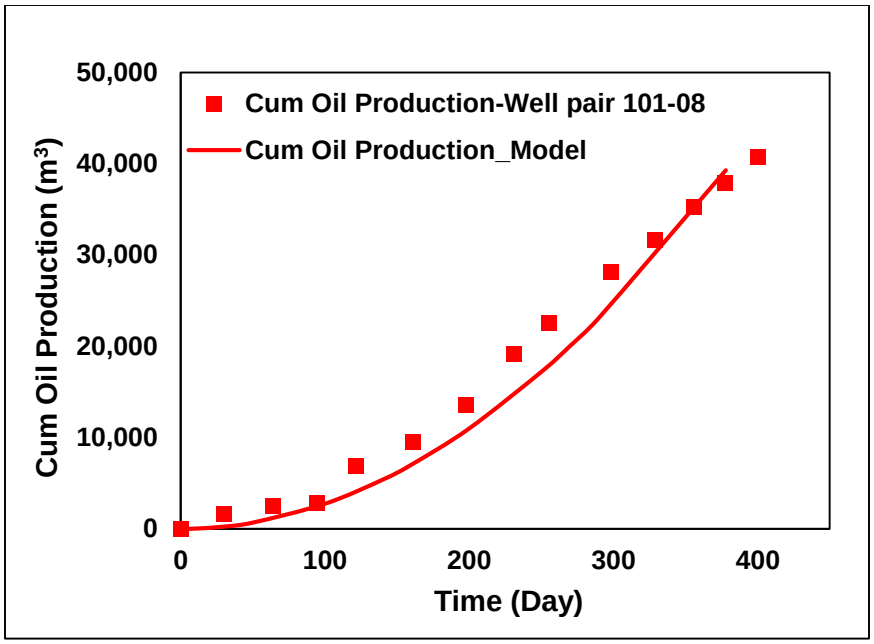

Figure 3.11: Comparison of cumulative oil production from the proposed of the steam chamber in this work (Equation 3.14) with the reported field data of Surmont project Well 101-08 in the Athabasca oil sands.

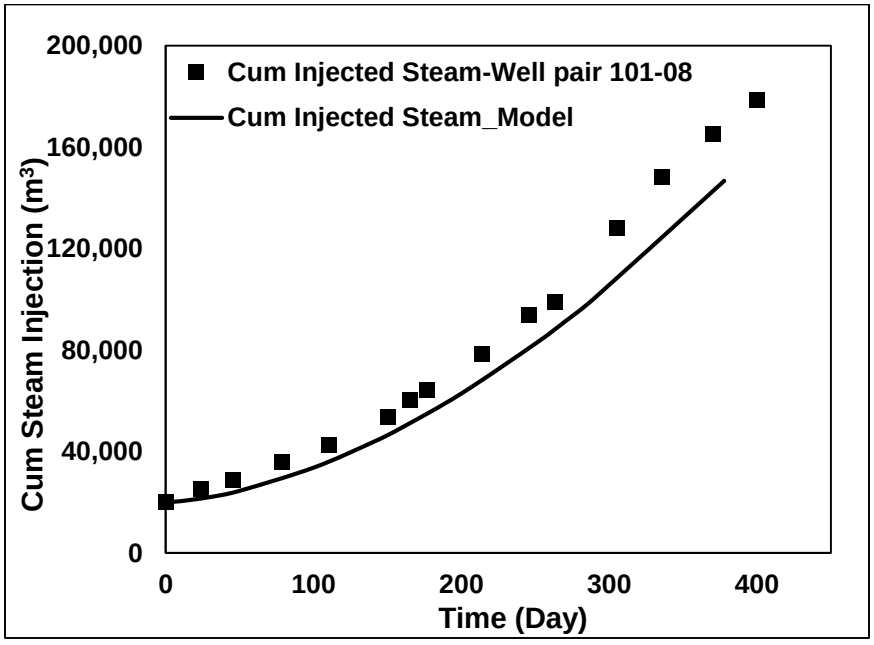

Figure 3.12: Comparison of cumulative steam injection from this work with the reported field data of Surmont project Well 101-08 in the Athabasca oil sands.

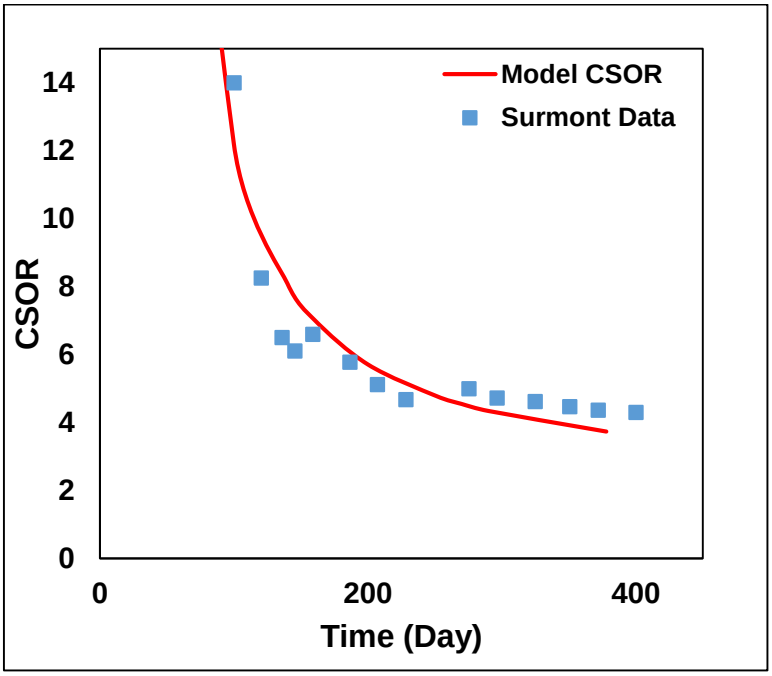

Figure 3.13: Cumulative Steam-Oil Ratio from this model (Equation 3.48) is validated against the field data of Surmont project Well 101-08 in the Athabasca oil sands.

Table 3.8: Additional results determined by the proposed approach in this work about the steam chamber development in Well 101-08 in the Athabasca oil sands.

Rise velocity, m/day	0.079
Lateral spreading coefficient, α_{LS}	0.45
Angle	77.46
Sweep efficiency	0.78

The cumulative steam injection in this model provides heat to the sides of the steam chamber, ahead of the rising chamber, and the steam zone plus, of course, the heat produced. It is apparent from the figure that the steam injection from the well data is higher than the predicted steam from the model. In this thermal evaluation of the rise period, heat

to the underburden area or the production well vicinity is ignored. It is suggested in the literature (Edmunds and Peterson, 2007) that heat to the underburden can be assumed as one-third of heat loss to the surrounding steam chamber.

This suggestion is applied in our calculation, and the results are shown in Figures 3.14 and 3.15. It is seen in Figure 3.14 that the gap between cumulative steam in the model and well data which exists in Figure 3.12 is eliminated. This confirms that in the heat balance model, the heat loss to the underburden should be considered. Heat distribution in the system for this well pair is predicted and shown in Figure 3.16.

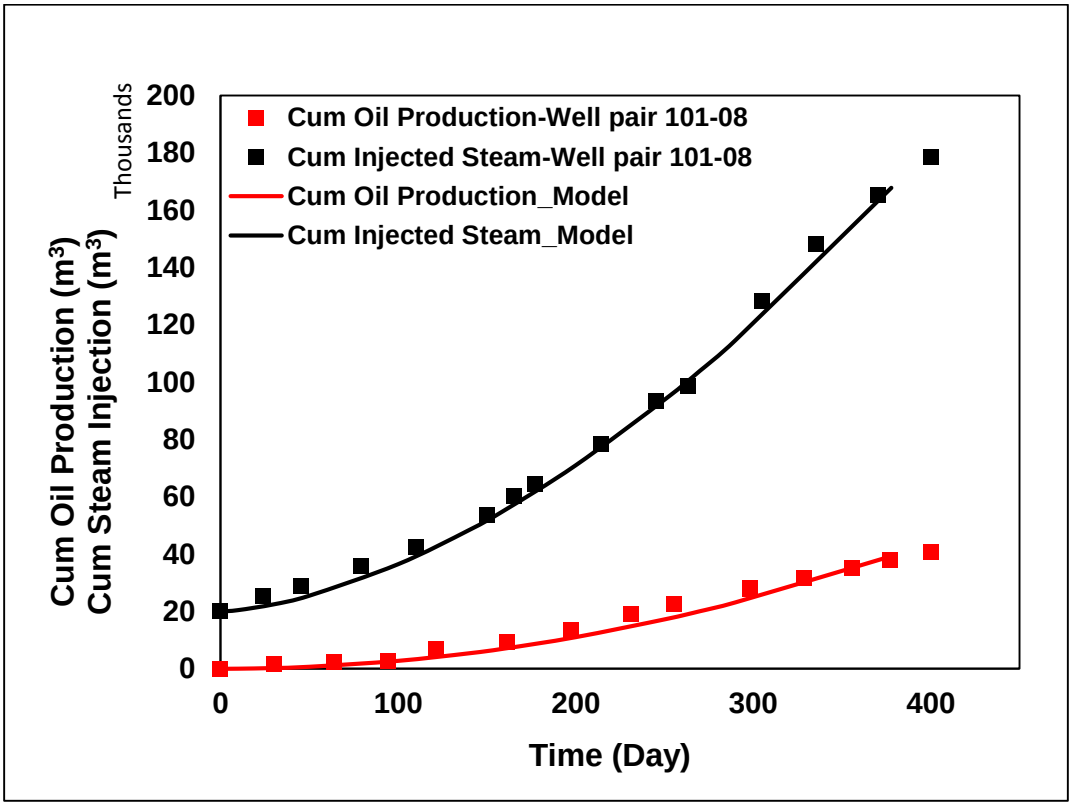

Figure 3.14: Investigating the effect of modifying the heat distribution in the system to include the heat loss to the underburden.

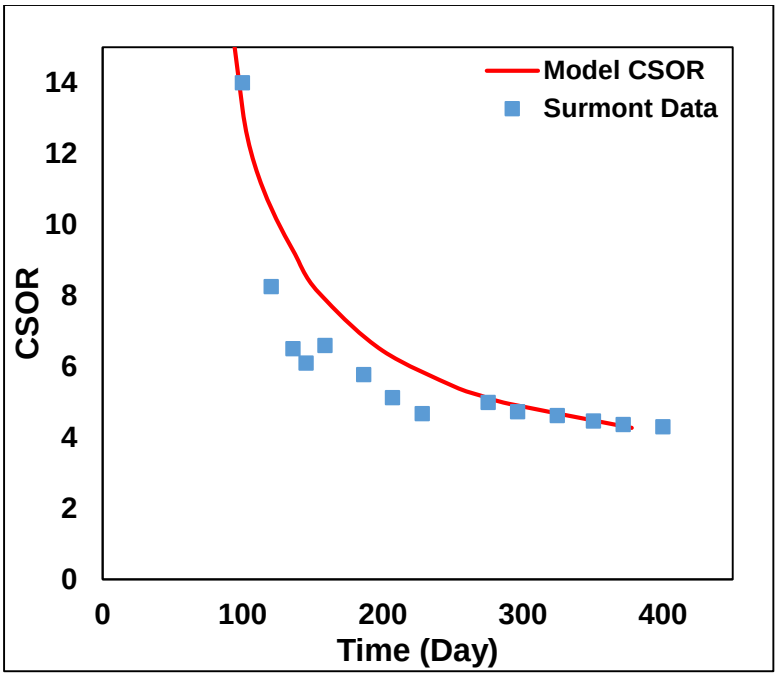

Figure 3.15: Effect of including heat loss to the underburden on CSOR.

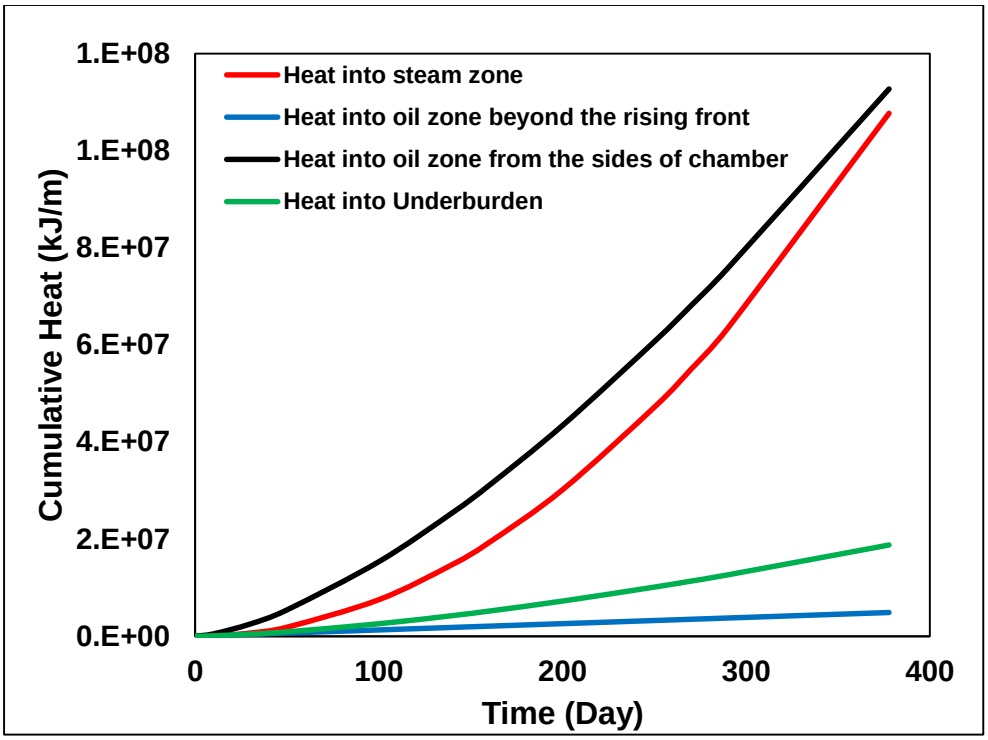

Figure 3.16: Heat distribution in the reservoir during the rise period for Well 101-08 in the Athabasca oil sands.

4. ANALYTICAL TREATMENTS OF LATERAL SPREADING PHASE OF SAGD CHAMBER

4.1 Introduction

The first phase in developing a steam chamber in the SAGD process is the upward growth of the chamber to the top of the reservoir. The next phase is sideways spreading of the chamber which is the focus of this chapter. Butler, McNab, and Lo (1981) developed a model for predicting oil production rate during the sideways expansion of the steam chamber. In this model, it is assumed that heat transfer beyond the chamber interface is by conduction only, with steam chamber expanding sideways from a vertical plane through the producer and injector (after the transient stage) at a constant velocity in a direction normal to the interface. The predicted oil rate from this model, referred here as Butler's original theory, is too high compared to observations. Moreover, the steam chamber interface moves away from the producer and goes to infinity at the top of the reservoir. There were several attempts to solve this problem by finding a multiplier empirically, experimentally, or adding new concepts to the Butler's model to make the equation predict lower rates. Another shortcoming of the previous models is that all of them aim to calculate the oil production rate resulting from a moving heat front. As a result, oil production rate is independent of the steam chamber shape and growth.

In this chapter, sideways expansion phase of SAGD is modelled by two different approaches; Constant Volumetric Displacement (CVD) and Constant Heat Injection (CHI). In the sideways spreading stage, there is a dynamic equilibrium situation. Unlike the steam chamber rise model, the accumulated heat ahead of the front plays a crucial role in this phase of SAGD modelling to find the advancing front velocity. There is a reciprocal relationship between the advancing front velocity and the amount of stored heat ahead of the front. Higher front velocity leads to lower heat accumulation ahead of the front for mobilizing oil ahead and making it drain. By considering the equilibrium situation for thermal recovery methods with dominant gravity drainage driving force, the advancing

front velocity is responsible for heat accumulation ahead of the front, and in turn, this heated oil drains away and determines the advancing the front. Therefore, the key point in the modelling is to determine the advancing interface movement that satisfies heat and mass balances over the system under equilibrium.

In the CVD (Constant Volumetric Displacement) model, we postulate that the front movement is such that the steam chamber growth is constant over time. In this work, it is shown that to obtain a constant oil production rate from a mass balance; the injected heat has to be increased to compensate for the heat loss to the overburden and growing accumulated heat ahead of the front due to interface extension and decreasing front velocity.

In all previous works of SAGD, the bitumen rate is obtained with no recourse to the steam injection rate – which is worked out after the fact. In real applications, steam is injected into the system so; it is the input to the problem. Knowing the steam injection rate, the reservoir behaviour or performance is analyzed. In the CHI (Constant Heat Injection) model, heat is injected at a constant rate into the system, which provides heat for the growing steam chamber size, increasing heat loss to the overburden, and heat flow by conduction ahead of the front. In this model, we are computing the front velocity that satisfies heat balance and mass balance for a constant heat injection rate. Decreasing steam chamber velocity with time from this model leads to reducing oil production rate.

The modelling of SAGD process in this work is different from that in previous works since it is believed that the steam chamber velocity is the key point in SAGD modelling. These approaches consider constant steam chamber expansion (CVD) and constant heat injection rate (CHI), respectively. The results of these two approaches for lateral spreading phase of SAGD show that in the CVD model, the steam injection rate should be increased continuously to provide constant steam chamber velocity, and the CHI model indicates that with a constant rate of steam injection, oil production rate decreases over time (strongly affected by increasing heat loss to the overburden).

4.2 Analytical Model - Constant Volumetric Displacement Model

4.2.1 Model Assumptions

In modelling of the SAGD process, several different mechanisms are involved such as viscosity reduction, steam distillation and asphaltene deposition. The analytical modelling of the process would be impossible if all of these mechanisms are accounted for. Therefore, in developing the analytical model of Constant Volumetric Displacement (CVD) for the sideways expansion of SAGD, taking into account the primary mechanisms, the following assumptions are made:

1. Homogenous porous medium.
2. Heat is transferred ahead of the steam chamber by conduction only.
3. Heat transfer is directed perpendicular to the steam chamber interface, and the heated oil flows parallel to the interface.
4. Steam-oil interface geometry is a straight line with a fixed end at the producer.
5. Inside the steam chamber, saturation temperature and pressure of steam remain constant and are the same as the injection point.
6. The maximum steam chamber interface velocity (at the reservoir top) remains constant over time.
7. The temperature profile is derived based on a pseudo steady-state condition.

4.2.2 Methodology

Recorded isotherms of the steam chamber development from experimental work of SAGD by Chung and Butler (1987) (Figure 1.5) indicate that an inverted triangle is the best geometry to represent the steam chamber shape. In analytical modelling of SAGD it is assumed that heat is conducted beyond and normal to the chamber interface but the temperature gradient in the direction parallel to the chamber interface is considered to be negligible or heat is distributed uniformly. Heated oil drains down to the producer along the interface and so, normal to the steam chamber interface, the heat front moves forward. A schematic of heat and fluid flows ahead of an arbitrary interface is shown in Figure 4.1.

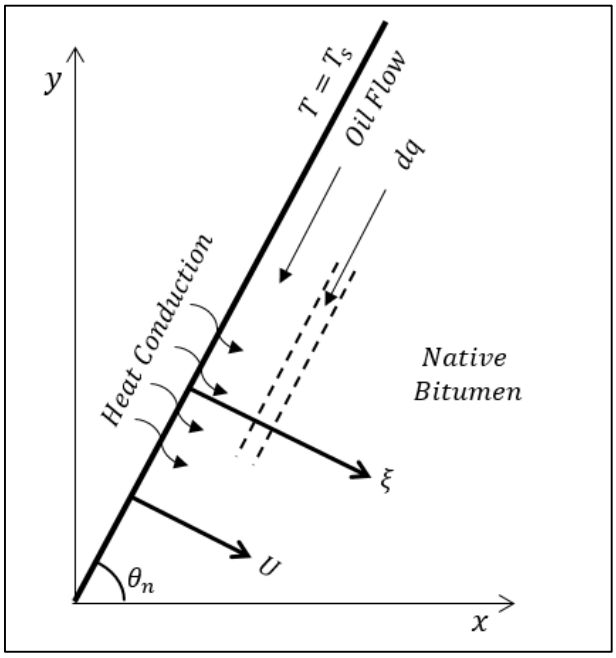

Figure 4.1: Schematic of heat and fluid flow ahead of an arbitrary interface at $t = t_n$ and position $\theta = \theta_n$.

Figure 4.2 shows the schematic of the lateral spreading phase of SAGD considered in our theory. The model is developed for an arbitrary interface at $t = t_n$ and position $\theta = \theta_n$.

In the SAGD process, heat transfer coupled with fluid flow. The governing equations are; Darcy's law, volumetric balance, heat conduction, constitutive equations indicating the temperature dependence of some of the physical properties.

4.2.2.1 *Relation between Heat Front and Steam Chamber Interface*

In this approach, the steam chamber interface bends around the producer with a constant velocity and its maximum velocity is at the top of the reservoir, (x'_H). Displaced oil is calculated from this perspective. In this theory, the steam chamber interface at each particular time moves with a constant velocity at its normal direction which is named as the heat front velocity, U.

Figure 4.2 shows that the front is moving with a constant velocity U (normal to steam chamber interface) for each interface position while the steam chamber interface moves around a fixed point at the producer. In this theory, time scale of reservoir heating starts at the new position of steam chamber interface. The relation between U (heat front velocity) and x'_H (maximum steam chamber velocity) can be expressed as:

$$U = x'_H \, sin\theta_n \qquad where\ \theta_n = \tan^{-1}\left(\frac{H}{x_n}\right) \tag{4.1}$$

As can be seen from the above equation, the heat front velocity, U, is proportional to the maximum steam chamber velocity (x'_H). Figures 4.3 demonstrates this relation. The heat front velocity is a varying parameter due to gravity effect but as mentioned in the model assumptions section, the maximum steam chamber velocity (x'_H) in CVD model is constant.

Given that the front movement should be equivalent to the steam chamber interface movement to represent the same steam invasion volume, the above front velocity is modified to represent the steam chamber interface movement correctly. In Figure 4.3, triangle ABD has the same volume (per unit length of the horizontal well) as the parallelogram ABCF. So,

$$U_f = \frac{1}{2} x'_H \, sin\theta_n \tag{4.2}$$

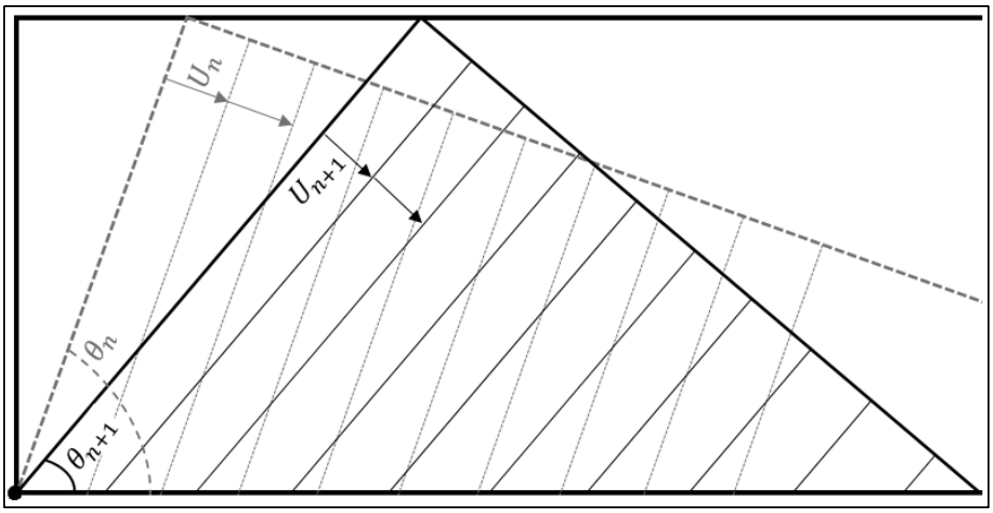

Figure 4.2: For each steam chamber interface (rotating around the fixed point, producer), heat front moves normal to it.

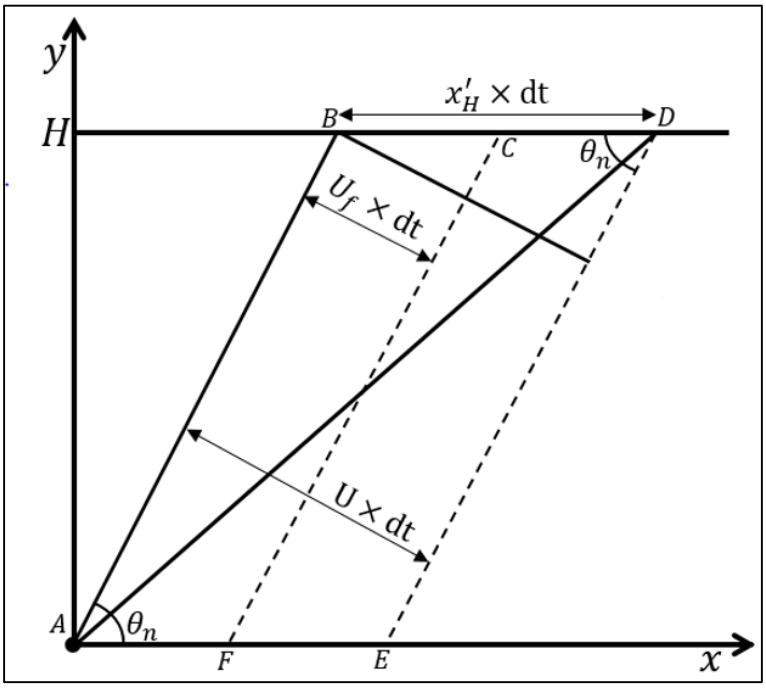

Figure 4.3: The relation between maximum steam chamber movement at the top, ($x'_H \times dt$), and heat front movement ($U \times dt$) is shown. The steam chamber movement should be equal to the heat front to have the same steam volume invasion.

Equation 4.2 indicates that the front velocity depends on the steam chamber interface positions under a constant steam chamber velocity. Figure 4.4 shows that the heat front velocity is not constant due to the new steam chamber interface position, it decreases with time in the CVD model.

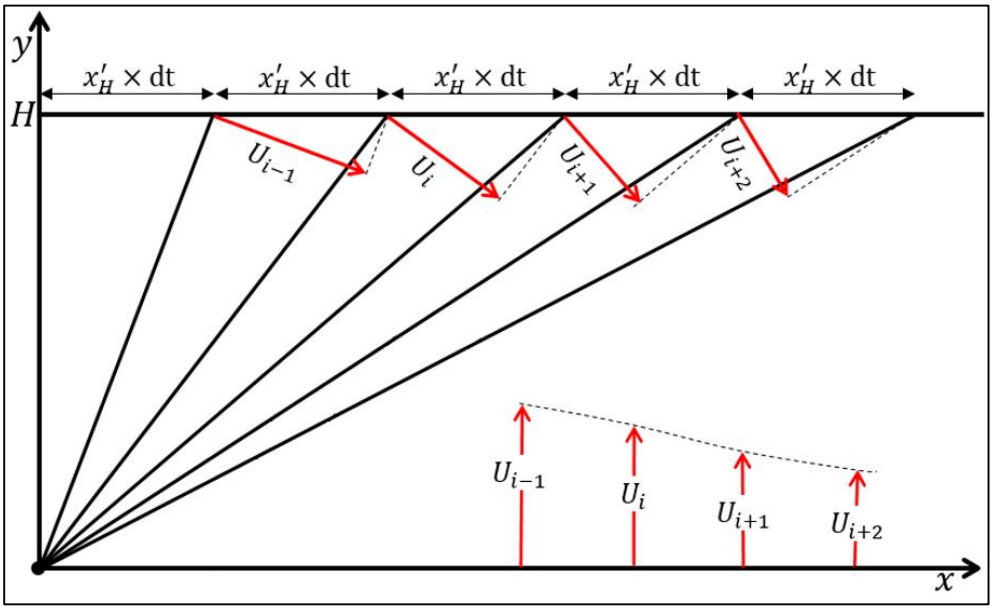

Figure 4.4: Heat front velocity, *U*, decreases with time for a moving steam chamber interface fixed at the producer.

Figure 4.4 shows heat front velocity, U, decreases with time for a moving steam chamber interface with one end attached at the producer. The steam chamber interface position strongly depends on reservoir thickness. The dependence of the front velocity on reservoir thickness is,

$$U_f = \frac{1}{2} \frac{H x'_H}{\sqrt{H^2 + (x'_H t)^2}} \tag{4.3}$$

This dependence is also shown in Figure 4.5. As can be seen from the figure, the variation of the front velocity over time is higher in the case of thinner reservoirs compared to the thicker reservoirs.

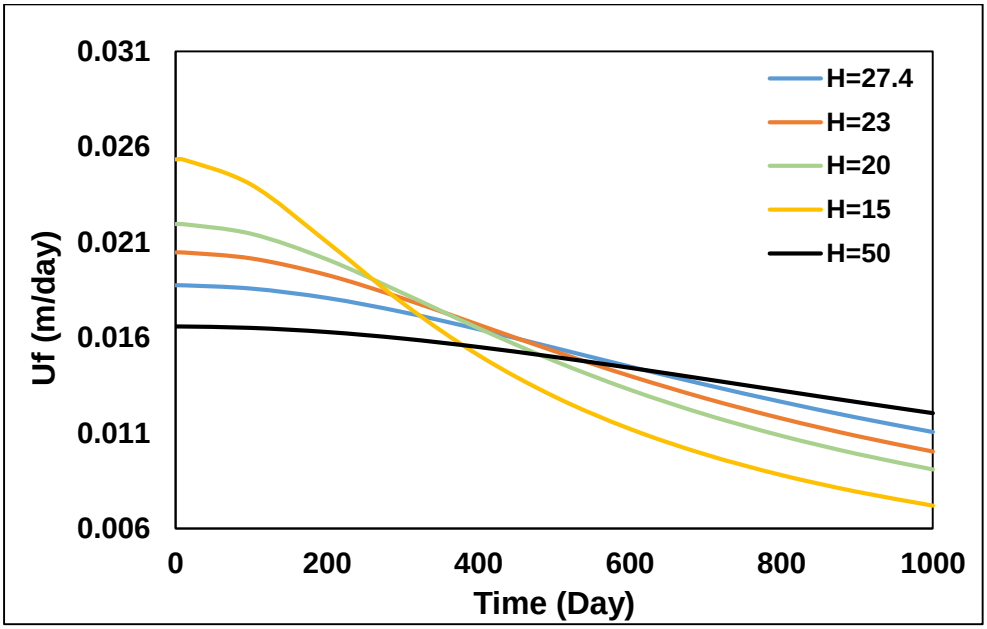

Figure 4.5: Front velocity as a function of reservoir thickness and time.

4.2.2.2 *Temperature Profile in CVD Model*

Temperature profile ahead of the front depends on the steam chamber interface position at each time. Heat conduction equation ahead of the interface and in a direction perpendicular to the interface is as follow:

$$\frac{\partial^2 T}{\partial \psi^2} = \frac{1}{\alpha}\frac{\partial T}{\partial t} \tag{4.4}$$

where α is thermal diffusivity of formation and ψ is the perpendicular coordinate to the steam chamber interface. Initial boundary conditions for this semi-infinite heat conduction model are as follow:

$$T(\psi, t = 0) = T_r \tag{4.5}$$

$$T(\psi = \Gamma(t), t) = T_s \tag{4.6}$$

$$T(\psi \to \infty, t) = T_r \tag{4.7}$$

$\Gamma(t)$, represents the heat front location at any time and its original coordinates is the steam chamber interface at each particular time. As explained in previous chapter, the heat conduction problem in a SAGD process is a moving boundary problem. To solve the above equation with its corresponding boundary and initial conditions, a new coordinate, ξ, is defined to make the front stationary:

$$\xi = \psi - \Gamma(t) \tag{4.8}$$

In the same manner as derived in Chapter 3, applying this coordinate transformation, and the chain rule, a pseudo steady-state temperature equation ahead of a moving front at $t = t_n$ is given by:

$$\frac{d^2T_D}{d\xi^2} + \frac{U_f}{\alpha}\frac{dT_D}{d\xi} = 0$$
$$T_D(\xi = 0, t) = 1$$
$$T_D(\xi \to \infty, t) = 0 \tag{4.9}$$

T_s and T_r are steam temperature and initial reservoir temperature respectively. U_f is the heat front velocity given in Equation 4.2. Solving the above temperature equation and substituting for the heat front velocity, the temperature profile is derived by:

$$T_D = \frac{T - T_r}{T_s - T_r} = \exp\left(-\frac{U_f}{\alpha}\xi\right) = \exp(-\frac{x'_H\, sin\theta_n}{2\alpha}\xi)$$

(4.10)

In the CVD model, temperature profile varies over time due to gravity effect.

4.2.2.3 *Drainage Rate for the CVD Model*

In Constant Volumetric Displacement (CVD) approach, it is assumed that the steam chamber moves with a constant velocity. Therefore, the rate of steam injection has to increase to provide such a constant velocity. The main point in this model is that the heat front movement (normal to the interface) has to be equivalent to the steam chamber interface displacement in a linear geometry as an inverted triangle to represent the same steam volume invasion at each time. The real steam chamber shape is complicated but the inverted triangle fixed at the producer is a reasonable approximation for analytical treatment. The pseudo steady-state temperature profile ahead of the moving front, developed in the previous section, is used for computing oil production. The maximum horizontal steam chamber velocity can be obtained from a mass balance that satisfies the equilibrium in the system.

Oil flow rate ahead of a particular front at $t = t_n$ and position $\theta = \theta_n$ can be calculated from Darcy equation (See Figure 4.1)

$$dq_o = \frac{k_o}{\mu_o}\Delta\rho_o g \sin\theta_n\, d\xi$$

(4.11)

$\Delta\rho_o$is density difference between oil and steam. Steam density is much smaller than the oil density and can be ignored. Moreover, the equation can be simplified by replacing the ratio of the dynamic viscosity to the density by the kinematic viscosity.

$$dq_o = \frac{k_o}{\nu_o} g \sin\theta_n d\xi$$

(4.12)

In the above differential oil rate equation ahead of the interface, viscosity is a function of temperature and in turn, is a function of distance from the interface (ξ). Oil viscosity increases as it goes away from the interface which means that the oil mobility decreases. Fluid flow rate in the heated region is given by:

$$q_o = k_o\, g\, sin\theta_n \int_0^{\infty} \frac{d\xi}{\nu_o}$$

(4.13)

Butler, McNab, and Lo (1981) introduced the below expression for representing the variation of the oil viscosity with temperature which simplifies the mathematical derivation.

$$\frac{\nu_{os}}{\nu_o} = \left(\frac{T - T_r}{T_s - T_r}\right)^m = T_D^m$$

(4.14)

$\nu_{os}$is the kinematic oil viscosity at the steam temperature, and m is the dimensionless heavy oil characteristics. For heavy oil and bitumen, this parameter is between 3 and 4 (Butler, 1991). Combining Equations 4.10, 4.13, and 4.14, the oil production rate is derived,

$$q_o = \frac{k_o}{\nu_{os}}\, g\, sin\theta_n \int_0^{\infty} T_D^m\, d\xi = \frac{k_o}{\nu_{os}}\, g\, sin\theta_n \int_0^{\infty} \exp(-\frac{m x'_H\, sin\theta_n}{2\alpha}\xi) d\xi = \frac{2\, k_o g \alpha}{m \nu_{os}\, x'_H}$$

(4.15)

In the above equation, maximum steam chamber velocity, x'_H , is unknown. Cumulative volume of the displaced oil for a steam chamber interface moving around a fixed point (well) is given by (for one side of the steam chamber):

$$Q_o = \frac{1}{2}\phi\, H\, (S_{oi} - S_{or})\, x_H$$

(4.16)

where, H is the reservoir thickness, ϕ, is the porosity of reservoir rock, S_{or} is residual oil saturation after steaming, and $S_{oi}$is the initial oil saturation in the reservoir. Oil production rate can be derived from Equation 4.16 as:

$$q_o = \frac{dQ_o}{dt} = \frac{1}{2}\phi\, H\, \Delta S_o x'_H$$

(4.17)

It is expected to have the same oil production rate from Darcy oil rate equation and volumetric oil displacement at a particular time. By equating two equations, the maximum steam chamber velocity at the top of the reservoir is derived as:

$$x'_H = 2\sqrt{\frac{k_o g \alpha}{m v_{os} \phi\, H\, \Delta S_o}}$$

(4.18)

As expected from this model, the steam chamber velocity is constant, and it depends on the rock and fluid properties, and the steam temperature. It should be noted that this steam chamber velocity is the maximum horizontal chamber growth which occurs at the top of the chamber. By substituting Equation 4.18 into Equation 4.15 or 4.17, the oil production rate is given by:

$$q_o = \sqrt{\frac{k_o g \alpha\, \phi\, H\, \Delta S_o}{m v_{os}}}$$

(4.19)

It is concluded from the above equation, that the oil production rate in the CVD model is constant and depends on the rock and fluid properties, and the steam temperature. Comparing Equation 4.19 and Butler's original model, Equation 2.1, shows that the coefficient of the oil production rate from this theory changes to one. Constant oil production rate from this model is about 71% of production rate predicted by Butler's

original model. The predicted oil production rate from this theory is in better agreement with experimental and field data compared to the previous theories of SAGD. The horizontal steam chamber interface velocity in this model is a linear function of y, which is maximum at the top of the reservoir (x'_H) and zero at the producer.

$$x'_y = \frac{x'_H}{H}\, y \tag{4.20}$$

The interface equation is given by:

$$y = \frac{H}{x'_H t}\, x \tag{4.21}$$

At any time during the process, the cumulative oil at a specific height of the reservoir can be calculated as:

$$Q_{oy} = \int_y^H \phi \Delta S_o \frac{x'_H t}{H}\, y dy \quad \rightarrow \quad Q_{oy} = \frac{1}{2}\phi \Delta S_o \frac{x'_H t}{H}(H^2 - y^2) \tag{4.22}$$

Moreover, oil flow rate as a function of y is also derived from the cumulative oil production and is given by:

$$q_{oy} = \frac{1}{2}\phi \Delta S_o \left[H\, x'_H - y\, x'_y\right] \tag{4.23}$$

By substituting Equations 4.18 and 4.20, the above equation can be rewritten as:

$$q_{oy} = \sqrt{\frac{k_o g \alpha\ \phi\ H\ \Delta S_o}{m \nu_{os}}}\left[1 - \left(\frac{y}{H}\right)^2\right]$$

(4.24)

The above oil flow rate as a function of y indicates that at the top of the reservoir, $y = H$, oil flow rate from the top of the reservoir is zero and the maximum oil rate occurs at the well.

4.2.2.4 *Energy Balance and CSOR Calculations*

In the CVD model, the front velocity, temperature profile, and oil rate are derived independently of the heat balance in the system. Heat injection rate is required to be increased to provide the SAGD project with constant oil production rate over time. This heat injection rate trend should compensate for the increasing heat loss to the overburden, and the higher accumulated heat ahead of the front to provide constant volumetric displacement due to combined effects of interface extension and decreasing front velocity over time. Latent heat of the injected steam into the chamber is consumed in three ways; heat loss to the overburden, heat to oil zone ahead of advancing heat front, and heat to raise steam chamber and produced oil temperature from reservoir temperature (T_r) to steam temperature (T_s). The heat balance for such a system can be written as:

$$q_{inj} = q_{loss} + q_{acc} + q_{sz}$$

(4.25)

where, q_{inj} is the injected heat from latent heat of condensation of steam, q_{loss}, is the heat loss rate to the reservoir top or overburden, q_{acc}, is the accumulated heat rate into the oil zone ahead of the steam chamber edge, and q_{sz}, is the heat rate to the steam chamber to raise the saturated formation from steam temperature (T_s) to initial reservoir temperature (T_r). There is no fluid flow to the overburden rock and so, heat is transferred or lost to the overburden by conduction only. Heat loss rate is given by heat conduction equation in one dimension as:

$$q_{loss} = -K_{ob} A_{ob} \frac{\partial T}{\partial y}\Big|_{y=H}$$

(4.26)

where, $K_{ob}$is the thermal conductivity of overburden rock, and $A_{ob}$is the cross-sectional area of the overburden rock which is exposed to saturated steam (T_s). Temperature gradient term in the above equation can be substituted from the temperature profile in Equation 3.40 and so, heat loss rate and cumulative heat loss are derived as:

$$q_{loss} = \frac{2\,K_{ob}\Delta T}{\sqrt{\pi\alpha_{ob}t}}x_H$$

(4.27)

$$Q_{loss} = \frac{4\,K_{ob}\Delta T}{\sqrt{\pi\alpha_{ob}}}x_H\sqrt{t}$$

(4.28)

By substituting for the maximum steam chamber velocity from Equation 4.18, the rate of heat loss is computed as:

$$q_{loss} = \frac{2\,K_{ob}\Delta T}{\sqrt{\pi\alpha_{ob}}}x'_H\sqrt{t} = 4\,K_{ob}\Delta T\sqrt{\frac{k_o g}{\pi m \nu_{os}\phi\, H\, \Delta S_o}\left(\frac{\alpha}{\alpha_{ob}}\right)t}$$

(4.29)

Heat loss to the overburden is less than what is calculated from the above model. Vertical heat loss to the overburden at each time is greater close to the advancing front and smaller over the area which has already been exposed to steam. In the above model, it is assumed that all the overburden rock at T_r at each time is exposed to saturated steam at T_s meaning that the steam chamber is exposed instantly to the overburden. This assumption is like what Vogel (1984) made as a conservative approach for modelling steam requirements of a steamflooding project. The additional heat loss from the above model can compensate for the smaller heat loss to the underburden which is not included in this model (steam is not directly in touch with the underburden rock but there is still heat loss at the bottom even if

it is small in comparison to the overburden). The cumulative heat to raise the saturated formation from T_s to T_r is calculated by:

$$Q_{sz} = mc(T_s - T_r)$$

(4.30)

where m is the mass of the saturated reservoir, and c is the formation specific heat capacity. The heat rate to expand the steam chamber (per unit length of horizontal well) from the above equation is derived as:

$$q_{sz} = \frac{\partial}{\partial t}\big(mc(T_s - T_r)\big) = (\rho c)_{res}\Delta T\frac{\partial}{\partial t}(H.x_H)$$

(4.31)

$$q_{sz} = 2(\rho c)_{res}\Delta T\sqrt{\frac{k_o g\alpha H}{m\nu_{os}\phi\ \Delta S_o}}$$

(4.32)

As expected from the CVD model, the amount of heat rate required to raise the reservoir rock and fluid from T_r to T_s during steam chamber expansion is constant in a homogenous reservoir rock.

Accumulated heat (per unit length of the horizontal well) in the oil zone ahead of each steam chamber front with a predetermined steady-state temperature profile is;

$$Q_{acc} = \int_0^\infty d(mc(T - T_r)) = \int_0^\infty L_{int}(\rho c)_{res}\ (T_s - T_r)\ T_D d\xi$$

(4.33)

where, L_{int} is the length of the steam chamber interface at a particular time:

$$L_{int} = \frac{H}{\sin\theta}$$

(4.34)

The dimensionless temperature in Equation 4.33 is the pseudo steady-state temperature profile in a moving boundary problem derived in Equation 4.10. By substituting for temperature profile, and the length of interface Equation 4.33 can be rewritten as:

$$Q_{acc} = \int_0^{\infty} \frac{H}{\sin\theta} (\rho c)_{res} \Delta T \exp(-\frac{x'_H \, sin\theta_n}{2\alpha} \xi) \, d\xi$$

(4.35)

Therefore, the accumulated heat for both sides of the steam chamber is given by:

$$Q_{acc} = 4\alpha \, H \, (\rho c)_{res} \Delta T \left(\frac{1}{x'_H \, sin^2\theta}\right)$$

(4.36)

By substituting for the maximum steam chamber velocity and $sin\theta$, the accumulated heat as a function of time is given by:

$$Q_{acc} = 2(\rho C)_{res} \Delta T \, H \sqrt{\frac{m v_{os} \alpha H \phi \Delta S_o}{k_o g}} \left(\frac{H^2 + (x'_H t)^2}{H^2}\right)$$

(4.37)

And the rate of heat accumulation ahead of the heat front increases linearly with time, given by:

$$q_{acc} = 16 \, (\rho C)_{res} \Delta T \sqrt{\frac{k_o g}{m v_{os} \phi \Delta S_o} \left(\frac{\alpha}{H}\right)^3} \quad t$$

(4.38)

4.2.3 Results of the CVD Model

Figure 4.6 shows dimensionless temperature profile (Equation 4.10) in the CVD model versus the distance from the steam chamber interface for different times. As can be observed from the figure, temperature gradient at the interface decreases with time, but the heat penetration depth increases.

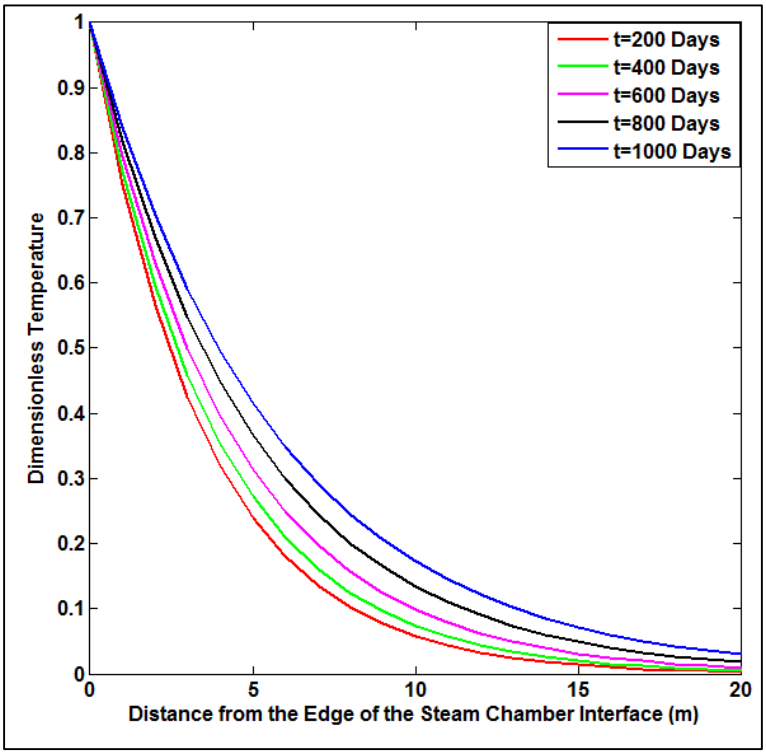

Figure 4.6: Variation of dimensionless temperature as a function of the distance from the steam chamber interface and time in the CVD model.

Figure 4.7 compares the results of Butler models, Reis, and this work to the experimental data of Butler, McNab, and Lo (1981). The rock and fluid data used in their experiment is shown in Table 4.1.

Table 4.1: Experimental data from Butler, McNab, and Lo (1981).

Physical Parameter	Value
S_{oi}	1
S_{or} *(%)*	0
ϕ	0.4
ρ_o*(gm/cc)*	0.98
k (Darcy)	14800
m	3.9
v_{os}*(m²/day)*	12.15
h (m)	0.105
w (m)	0.025
α (m²/day)	0.0557

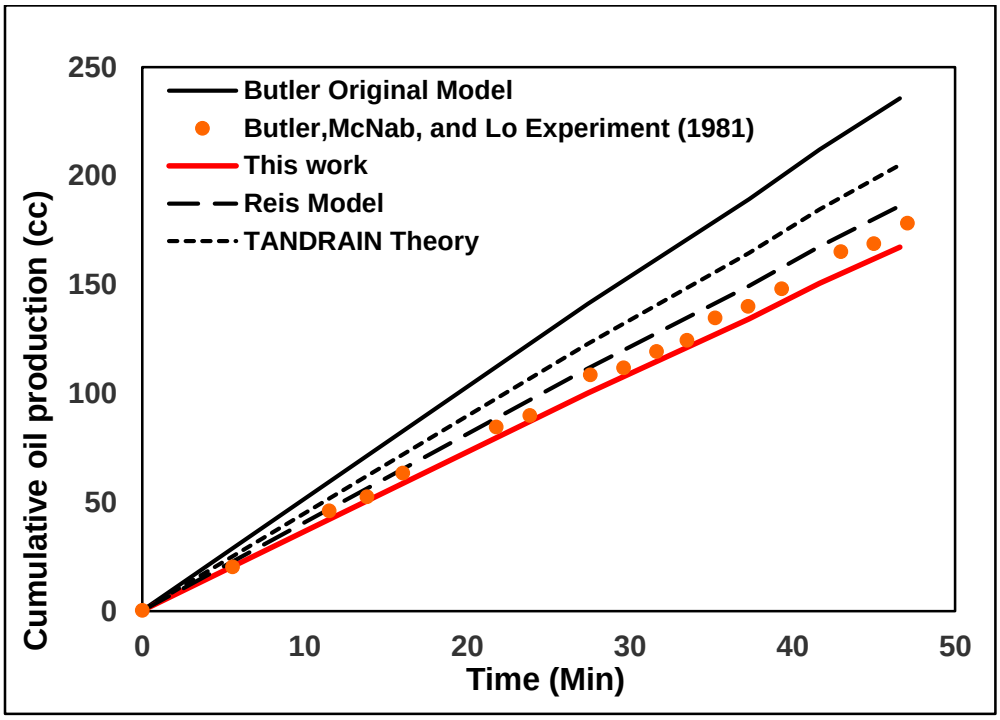

Figure 4.7: Oil production rate comparison by the use of data from Butler, McNab, and Lo (1981).

From this figure, oil production rate from this model is in good agreement with experimental data without using any experimental or empirical constants. The TANDRAIN theory improves the predicted oil production rate from the original model, but still, there is a considerable gap between the experimental results and TANDRAIN theory.

Figure 4.8 compares oil flow rates from Equation 4.24 with Equation 2.1 as a function of y. As is apparent from the figure, this model predicts lower oil flow rates compared to Butler's model along the steam chamber interface. Table 4.2 shows the data used for this comparison which is like those for Christina Lake. Figure 4.8 shows the predicted oil production rates from the CVD model and the original Butler's model are 0.268 and 0.38 m^3/(d-m) at $y = 0$, respectively. For the horizontal well pair A3 in Cenovus Energy Christina Lake project with 690-m length, the predicted oil production rates are 185 and 262 m^3/day, respectively. The well data reported for this well pair A3 is approximately 170 m^3/day by the use of the Cenovus Energy Christina Lake In-situ Oil Sands Scheme 8591 report (Cenovus Energy, 2015), which is close to the production rate predicted by the CVD model compared with Butler's.

Table 4.2: Data for oil flow rate calculations (Cenovus Energy, 2015).

Physical Parameter	**Value**
ϕ	0.33
S_{oi}	0.8
S_{or}	0.1
$k\ (m^2)$	6E-12
$\rho_{os}(kg/m^3)$	880
$h\ (m)$	26
$\alpha\ (m^2/day)$	0.06048
m	3
$\upsilon_{os}(m^2/day)$	0.5883
$(\rho c)_{Res}(kJ/m^3.C)$	1935
$T_s\ (^oC)$	220
$T_r\ (^oC)$	20
f_{st}	0.7
$L_v\ (kJ/kg)$	1849
$L\ (m)$	690

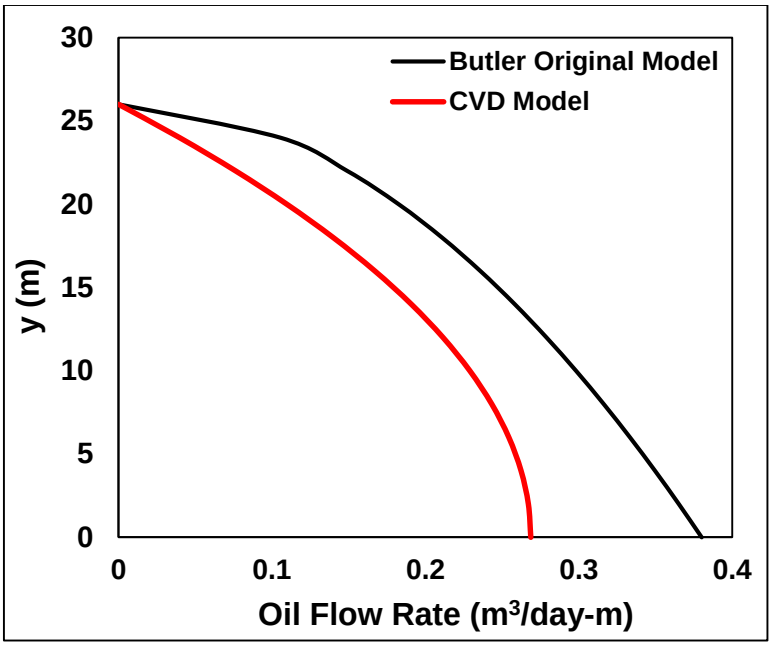

Figure 4.8: Comparison of oil-flow rate as a function of y along the steam chamber interface from the CVD model (Equation 4.24) and Butler original model (Equation 2.1).

Figure 4.9 compares the cumulative heat loss, accumulated heat, and heat to the steam chamber for the CVD model using the data in Table 4.2. The CSOR as a criterion for the efficiency of SAGD is depicted in Figure 4.10. CSOR starts at approximately 1.3 and then reaches a plateau at just above 2.

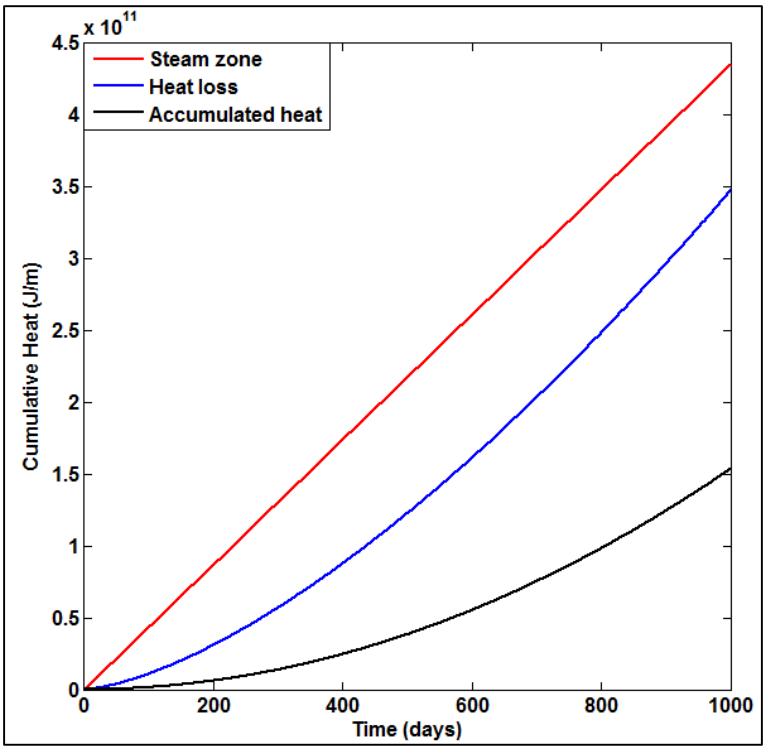

Figure 4.9: Cumulative heat to steam zone, loss and accumulated ahead of front for CVD model.

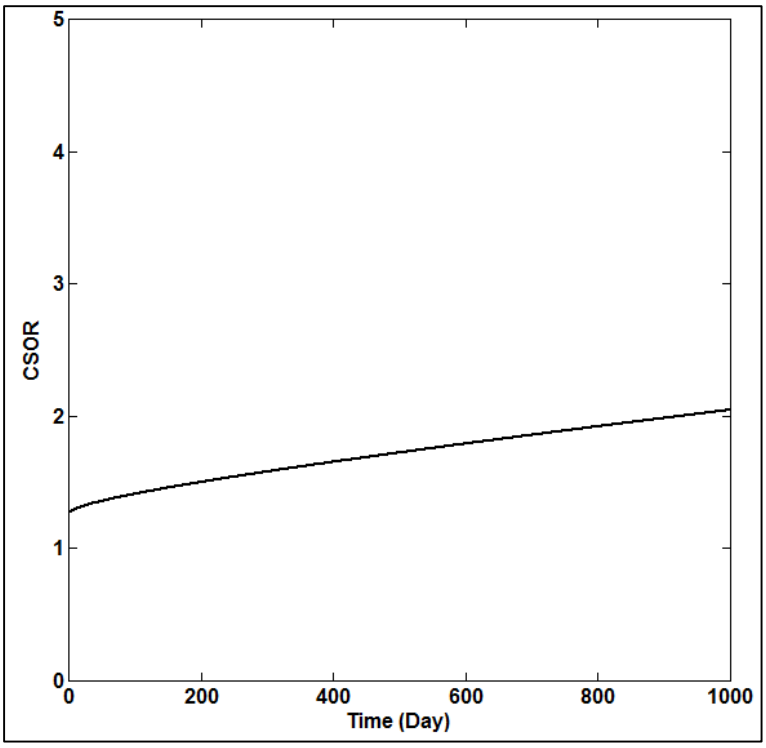

Figure 4.10: CSOR for CVD model by use of data in Table 4.2.

The oil production rate from the CVD model is also compared with Butler's original model (1981), TANDRAIN theory, and Reis (1992) for three others SAGD field data in addition to Christina Lake (See Table 4.3); Dover UTF phase B (Athabasca), Hangingstone (Athabasca), and Wolf Lake (Cold Lake). The results show that the CVD theory estimates the oil production rate better than the previous works.

Table 4.3: Comparison of oil production rate from the CVD model, Butler's original model, TANDRAIN theory, and Reis (1992) with field data (Sharma, 2011).

Reservoir rock and fluid properties	Christina Lake	Dover UTF phase B, Athabasca Res.	Hangingstone, Athabasca Res.	Wolf Lake, Cold Lake
Reservoir Temperature (^oC)	20	7	20	20
Steam Temperature (^oC)	220	220	260	250
Reservoir Height (m)	26	21	25	11
Porosity	0.33	0.33	0.35	0.32
Thermal Diffusivity (m^2/day)	0.061	0.061	0.061	0.061
Permeability (Darcy)	6	7	5	3
Initial Oil Saturation	0.8	0.85	0.77	0.75
Residual Oil Saturation	0.1	0.15	0.1	0.1
Viscosity at Steam Temperature (m^2/day)	0.587	0.687	0.37	0.35
Oil density, kg/m^3	880	880	980	980
Well Length (m)	690	500	500	500
Viscosity-temperature exponent, m	3	4	4	3
Calculated Oil Rates (m^3/day)				
Butler, McNab, and Lo (1981)	262	148	229	131
Butler and Stephens (1981)	227	128	199	114
Reis (1992)	207	117	181	104
CVD Model	**185**	**88**	**162**	**93**
Field data	170	77	82	50

4.2.4 Discussion of Butler's Original Model

The interface positions calculated from Butler's original model are unrealistic; interface curves move away from the well at the bottom and go to infinity at the top of the reservoir, as can be seen in Figure 2.1. The question is how we can be sure of the interface positions between these two limits. Several attempts were made to modify the interface positions from this model (TANDRAIN and LINDRAIN theories by Butler, explained in Chapter 2) to get lower oil production rates. So, in addition to unrealistic interface positions, the oil production rates from this model are too high. Here, we revisit the model equations which led to this result. Based on Darcy oil flow rate, in Butler's original theory the oil rate is given by:

$$q_o = k_o\, g\, \sin\theta \int_0^{\infty} \frac{d\xi}{v_o} = \frac{k_o g \alpha}{m v_{os}} \frac{1}{x'_{\Delta y}} \tag{4.39}$$

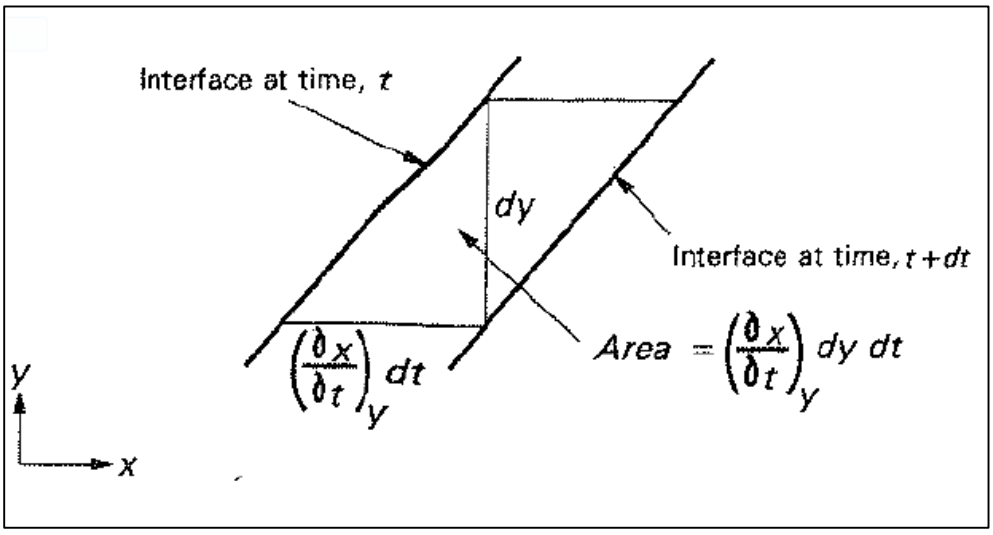

Figure 4.11: Material balance element in Butler's theory (Butler and Dargie, 1994).

Figure 4.11 depicts the material balance element over the small portion of the interface, and the material balance equation for this element is:

$$\left(\frac{\partial q_o}{\partial y}\right)_t = \phi \Delta S_o \left(\frac{\partial x}{\partial t}\right)_{\Delta y}$$

(4.40)

This material balance equation is for a model with horizontal front velocity only; y and t are independent variables. There are two options for finding the oil rate from this set of equations. The first choice is to substitute $x'_{\Delta y}$from one equation into another and finding oil production rate as done in Butler's original model, Equation 2.1. The assumption, which leads to Equation 2.1 from the above two equations, is ignoring the difference between the oil rate from material balance and Darcy's law based on 1D temperature distribution ahead of steam zone. This assumption is not valid because Darcy oil rate for this element is constant due to the constant horizontal velocity but this is not the case in material balance equation.

In the second option (which is in line with the CVD theory), it is believed that oil rate and steam chamber interface velocity are strongly tied together. It is the front velocity which can relate the two equations and so, there should be a front velocity which satisfies both equations. This front velocity has different effects on the two equations. A higher front velocity gives a higher oil displacement from material balance and a lower oil rate from Darcy's equation because of a lower rate of heat accumulation ahead of the front.

$$\left(\frac{\partial x}{\partial t}\right)_{\Delta y} = \sqrt{\frac{k_o g \alpha}{m v_{os} \phi \Delta S_o \Delta y}}$$

(4.41)

And

$$q_o = \sqrt{\frac{k_o g \alpha \, \phi \Delta S_o \Delta y}{m v_{os}}}$$

(4.42)

As can be seen from this approach the front velocity and oil rate depend on the height of the element (Δy) and not on the exact point (y). If with some manipulations, the element is defined in a way that one side is fixed at a reference point like $y = H$, the solution with a little difference would be similar to the first solution but with different concept. It is clear that this horizontal front velocity does not represent the steam chamber positions.

$$\left(\frac{\partial x}{\partial t}\right)_{H-y} = \sqrt{\frac{k_o g \alpha}{m v_{os} \phi \Delta S_o (H-y)}} \tag{4.43}$$

$$q_{oy} = \sqrt{\frac{k_o g \alpha \ \phi \Delta S_o (H-y)}{m v_{os}}} \tag{4.44}$$

Results indicate that the front velocity is an element-wise velocity and is based on these front velocities for which oil flow rates are computed. In general, it is believed that this model can give a proper result for well oil production rate ($over\ \Delta y = H$). In other words, the model does not give the correct relation for oil flow rate as a function of *y*, nor the interface positions based on the above horizontal front velocity.

4.3 Analytical Model - Constant Heat Injection Model

4.3.1 Modelling Assumptions

A second analytical model of the lateral spreading phase of the SAGD process is introduced in this section. This approach is named Constant Heat Injection (CHI) model. The assumptions applied in developing this approach are the same as of ones mentioned for Constant Volumetric Displacement (CVD) model except for the Assumption 6. In this approach, steam chamber velocity is unknown, but it is not assumed to be constant. Instead, the rate of steam or heat injection is constant.

4.3.2 Methodology

This model describes another new treatment of the sideways expansion stage of the SAGD process. In this approach, it is assumed that heat is injected at a constant rate into the reservoir, and steam chamber growth is evaluated under heat and mass balances. As in the CVD model, for a linear steam chamber interface, this model is developed for an arbitrary interface at $t = t_n$ and position $\theta = \theta_n$. From the heat balance, heat loss to the overburden and constant injection rate are expected to have a limiting effect on the growth rate of the steam chamber. In the following sections, it is explained how to obtain temperature profile, bitumen drainage rate, and steam chamber growth of SAGD in the Constant Heat Injection (CHI) approach.

4.3.2.1 *Temperature Profile in CHI Model*

Based on the overall heat balance, constant heat injection rate into the reservoir is distributed into the reservoir in three different ways; heat loss rate to the overburden, raising temperature of saturated steam chamber from T_r to T_s, and outflow of heat into the oil zone ahead of the advancing front, assumed to be by conduction only. Note that constant heat injection rate is known and it is the input of the model. From the overall heat balance:

$$q_{res} = q_{inj} - (q_{loss} + q_{sz}) \tag{4.45}$$

In the same manner as explained for the conservative heat loss model in the CVD approach, heat loss rate, q_{loss} is:

$$q_{loss} = \frac{2\,K_{ob}\Delta T}{\sqrt{\pi \alpha_{ob} t}} x_H \tag{4.46}$$

And heat rate for steam zone expansion is also evaluated as described for the CVD model and is given by:

$$q_{sz} = (\rho c)_{res} \Delta T H x'_H$$

(4.47)

The portion of injected heat which flows into the oil zone by conduction at a rate q_{res} at the steam chamber interface is given by:

$$q_{res} = -K_{res} A_{inf} \left(\frac{dT}{d\xi}\right)_{\xi=0}$$

(4.48)

The above equation indicates that the rate of heat flowing into the oil zone is affected by interface extension and temperature gradient at the front over time. The former has an increasing effect, and the latter has a decreasing effect on the heat rate.

By substituting Equations 4.46, 4.47 and 4.48 into the energy balance equation, the overall heat balance in the system is given by:

$$-2K_{res} \frac{H}{sin\theta} \left(\frac{dT}{d\xi}\right)_{\xi=0} = q_{inj} - \frac{2K_{ob}\Delta T}{\sqrt{\pi \alpha_{ob}}} \frac{x_H}{\sqrt{t}} - H x'_H (\rho C)_{res} \Delta T$$

(4.49)

In the above equation, steam chamber velocity and the temperature gradient at the interface are unknown. The equation is rearranged to obtain the temperature gradient based on the primary unknown which is the maximum steam chamber velocity as follow:

$$\left(\frac{dT}{d\xi}\right)_{\xi=0} = -\frac{sin\theta}{2K_{res}H} \left\{ q_{inj} - \left(\frac{2K_{ob}\Delta T}{\sqrt{\pi \alpha_{ob}}} \frac{x_H}{\sqrt{t}} + H x'_H (\rho C)_{res} \Delta T \right) \right\}$$

(4.50)

This temperature gradient is used as a Neumann boundary condition at the moving interface at each particular time.

Temperature equation ahead of the moving front is evaluated by assuming a pseudo steady-state condition (as described in CVD model) and the two below boundary conditions:

$$\frac{d^2T}{d\xi^2} + \frac{U_f}{\alpha}\frac{dT}{d\xi} = 0$$

$$\left(\frac{dT}{d\xi}\right)_{\xi=0} = -\frac{sin\theta}{2K_{res}H}\left\{q_{inj} - \left(\frac{2K_{ob}\Delta T}{\sqrt{\pi\alpha_{ob}}}\frac{x_H}{\sqrt{t}} + Hx'_H(\rho C)_{res}\Delta T\right)\right\}$$

$$T(\xi \to \infty, t) = T_r$$

(4.51)

By solving the above equation, the temperature profile at each given time or interface position in CHI model is calculated as:

$$T = \frac{\alpha}{K_{res}Hx'_H}\left\{q_{inj} - \left(\frac{2K_{ob}\Delta T}{\sqrt{\pi\alpha_{ob}}}\frac{x_H}{\sqrt{t}} + Hx'_H(\rho C)_{res}\Delta T\right)\right\}e^{-\frac{sin\theta}{2\alpha}x'_H\xi} + T_r$$

(4.52)

Note that over time, the temperature profile from this model is not affected by gravity (as in the case of CVD model) alone, but also strongly by heat injection rate, a variation of maximum steam chamber velocity (at the top), etc. Steam chamber growth at the top of the reservoir, x'_H, is unknown in the temperature equation.

4.3.2.2 *Drainage Rate for the CHI Model*

Oil flow rate can be calculated by combining Darcy's law and the above temperature equation. As a result, oil flow rate is given by:

$$q_o = \frac{2K_o g}{m\upsilon_{os}}\left(\frac{1}{K_{res}H\Delta T}\right)^m\left(\frac{\alpha}{x'_H}\right)^{m+1}\left\{q_{inj} - \left(\frac{2K_{ob}\Delta T}{\sqrt{\pi\alpha_{ob}}}\frac{x_H}{\sqrt{t}} + Hx'_H(\rho C)_{res}\Delta T\right)\right\}^m$$

(4.53)

Another relation for the oil flow rate is the displaced oil calculation, as a result of steam chamber interface movement, by considering an inverted triangle approximation for the steam chamber growth and is given by:

$$q_o = \frac{1}{2} H\phi\Delta S_o x'_H$$

(4.54)

By combining Equations 4.53 and 4.54, the steam chamber interface velocity at the top of the reservoir, x'_H , at each special time which satisfies heat balance and volume balance is found by solving the following nonlinear first order ODE.

$$x_H'^{\,m+2} = \frac{4K_o g}{m\upsilon_{os} H\phi\Delta S_o}\left(\frac{1}{K_{res} H\Delta T}\right)^m (\alpha)^{m+1}\left\{q_{inj} - \left(\frac{2K_{ob}\Delta T}{\sqrt{\pi\alpha_{ob}}}\,\frac{x_H}{\sqrt{t}} + Hx'_H(\rho C)_{res}\Delta T\right)\right\}^m$$

(4.55)

When the steam chamber velocity is obtained from the above equation; oil rate, temperature profile, heat distribution in the system, CSOR will be determined.

4.3.3 Results of the CHI Model

Figure 4.12 shows the predicted oil production rate from the CHI model during the sideways expansion of SAGD using the data from Table 4.2. The oil production rate, for an unconfined reservoir, decreases slightly from 0.2665 (m^3/day-m) to 0.238 (m^3/day-m) over the time interval of approximately three years. The steam injection rate remains constant at 0.675 (m^3/day-m) during this period. At a steady rate of steam injection, over time, the steam chamber expands and in turn, the heat loss to the extending overburden

increases. As a result, the rate of steam chamber growth is limited, and oil production rate decreases over time. Division of the injected heat rate in the system in three different form of heat from the energy balance over the system is illustrated in Figure 4.13. As can be seen, CSOR for this case is evaluated and depicted in Figure 4.14. At the beginning of the phase, CSOR is 2.53 and increases gradually to 2.785 at the end of the 3-year period.

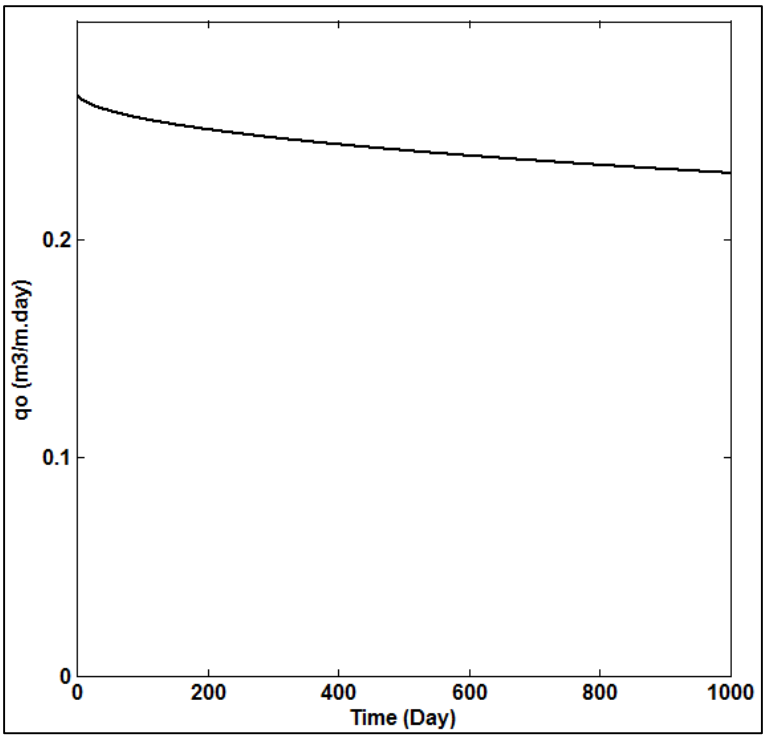

Figure 4.12: Calculated oil production rate from the Constant Heat Injection (CHI) model by use of data in Table 4.2.

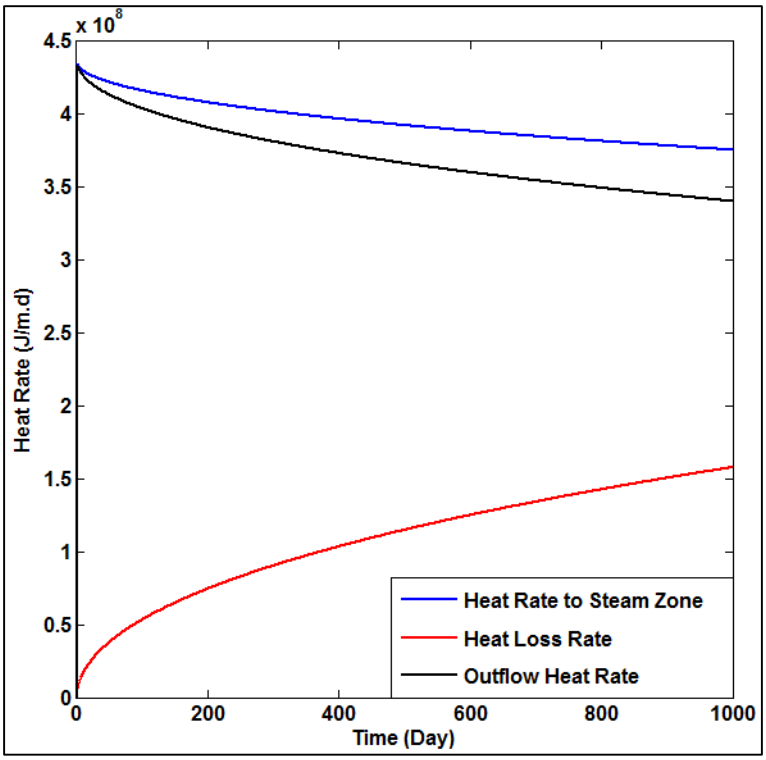

Figure 4.13: Distribution of the injected heat rate in the CHI model in three forms: heat rate to steam zone, heat loss rate, and rate of heat outflow into the oil zone ahead of the steam chamber interface by use of data in Table 4.2.

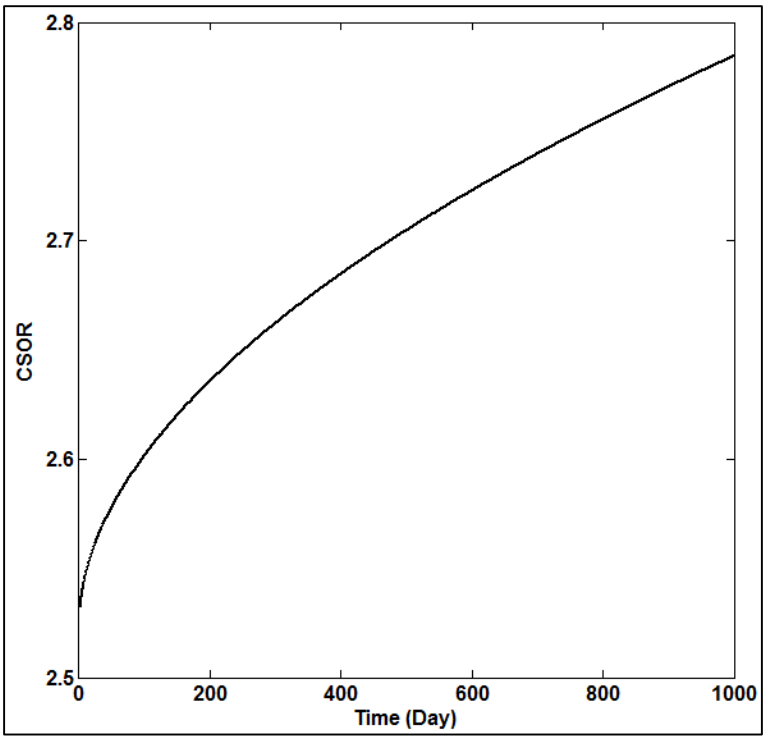

Figure 4.14: Calculated CSOR from the CHI model by use of data in Table 4.2.

Reservoir thickness is one of the key parameters affecting oil recovery in steam injection processes. In the CHI method developed here, the effect of reservoir thickness is investigated to see quantitatively its impact on SAGD. Figure 4.15 compares the effect of reservoir thickness (H=22, 26 and 30 m) on cumulative oil production, at the same steam injection rate, using data in Table 3.5 and it shows that a higher reservoir thickness leads to a higher cumulative oil production over a 1000-day period. In the case of a thinner reservoir, the steam chamber velocity is larger, but the volume of displaced oil is lower. Note that the larger steam chamber velocity also means that the more significant portion of injected heat is lost to the overburden. The results for CSOR in Figure 4.16 for the three cases confirm that a smaller reservoir thickness leads to a higher cumulative steam-oil ratio. The results indicate that the thinner reservoirs are not favourable or sometimes uneconomical due to a high degree of heat loss, resulting in high CSOR and lower oil production rates.

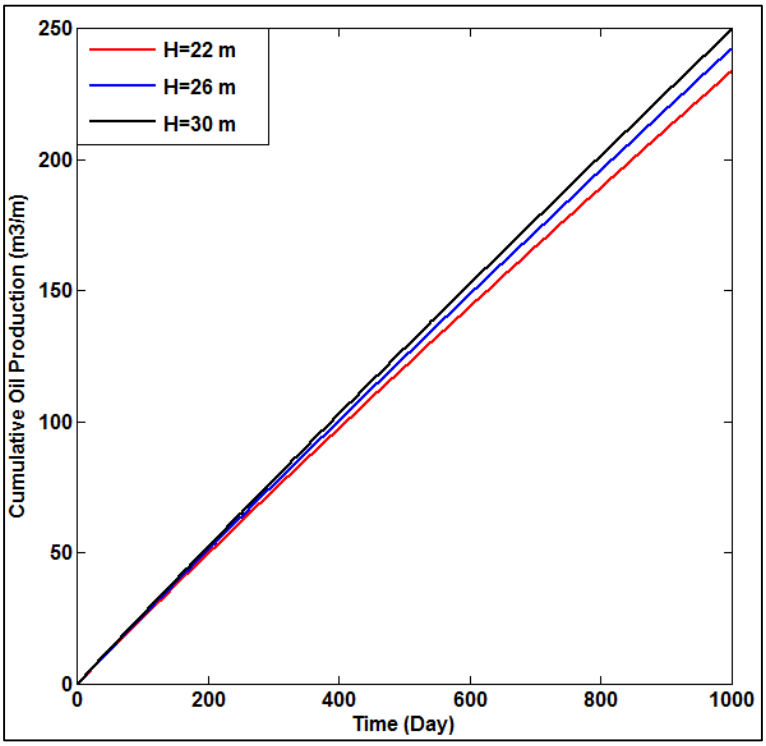

Figure 4.15: Effect of reservoir thickness ($H = 22, 26, and\ 30\ m$) on cumulative oil during a 1000-day period by use of data in Table 3.5.

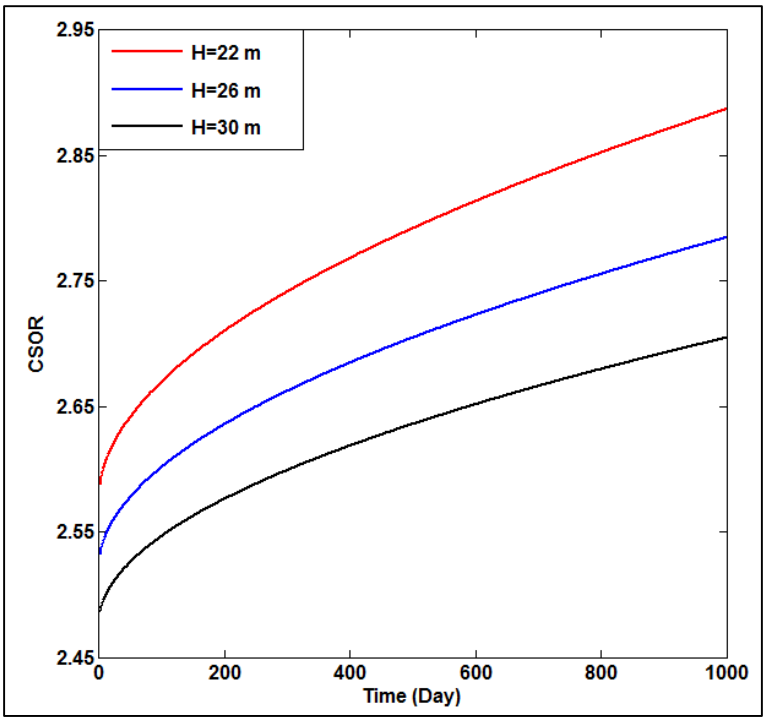

Figure 4.16: Effect of reservoir thickness ($H = 22, 26, 30\ m$) on CSOR in SAGD, during sideways expansion phase, using the CHI model.

The effect of steam pressure is also investigated here. Steam injection rate and steam pressure depend on each other but to see the effect of steam pressure on oil production rate; the steam injection rate is kept constant. A higher steam pressure indicates a higher steam temperature and a lower latent heat of condensation. So, it is not correct to simply judge that higher steam pressure leads to higher oil production rates due to inverse proportionality of oil rate and saturated oil viscosity. In the CHI model, higher steam pressures affect steam chamber growth rate and oil production rate in a nonlinear way. Figures 4.17 and 4.18 show the effect of three different steam pressure (p_s=2.35, 2.8 and 4.8 MPa) on cumulative oil production and CSOR, respectively. As can be seen, higher steam pressures lead to lower oil production, unlike the prediction of Butler's original model in Equation 2.1. Figure 4.18 illustrates that a higher steam pressure gives a higher cumulative steam-oil ratio at a constant steam injection rate.

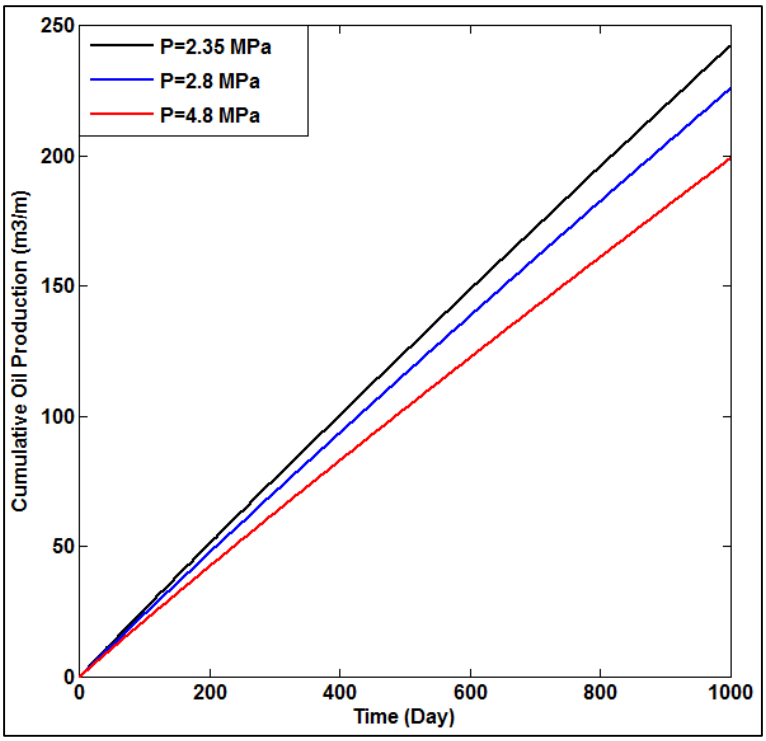

Figure 4.17: Effect of steam pressure ($P = 2.35, 2.8, and\ 4.8\ MPa$) on cumulative oil during a 1000-day period by use of data in Table 3.5.

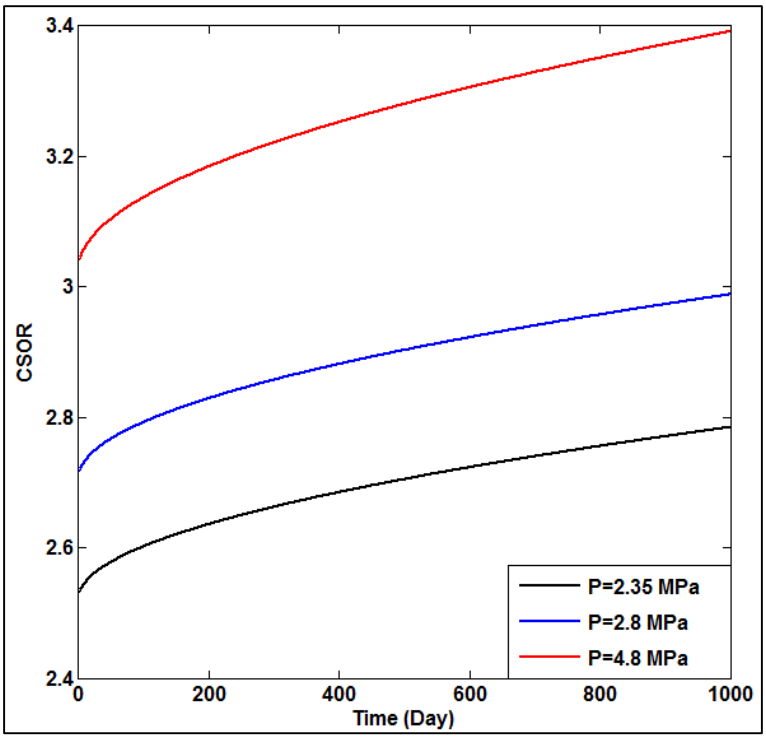

Figure 4.18: Effect of steam pressure ($P = 2.35, 2.8, and\ 4.8\ MPa$) on CSOR in SAGD with constant rate a of steam injection, during sideways expansion phase.

4.3.4 Discussion of Butler's 1985 SAGD Model

In addition to the previous discussion of Butler's original model, there are a few additional points to consider relevant to the model. Bitumen drainage is assumed from around a spreading steam chamber above a horizontal producer. The approach is limited to situations where steam is introduced above the interface (sideways expansion) excluding the steam chamber rise period. The initial rate for the lateral spreading phase of SAGD modelling is believed to be the oil production rate at the end of the steam chamber rise period which is the maximum oil production rate.

The question is: why the predicted oil production rate from this approach starts with zero initial rate and increases to a maximum before starting to decline? In other words, the physical model descriptions and time-dependent oil production rate result are not consistent.

We believe this discrepancy comes from ignoring (1) gravity effect, decreasing interface angle with time which leads to an extension of interface length, and (2) heat loss in the heat balance equation which has a profound effect on SAGD performance and it may come from the definition of heat penetration depth in the steady state Darcy oil flow. Therefore, the lack of interface extension (the numerical solution of the model was adjusted to include the interface extension by multiplying the heat penetration depth of the top element by the ratio of element length at the previous time step to its new value) and the maximum point for oil production rate from this model might be explained in this way.

4.4 Comparison of CHI and CVD Models

Two new analytical approaches were introduced in the previous subsections; Constant Volumetric Displacement (CVD), and Constant Heat Injection (CHI). In the CVD model, steam chamber velocity is assumed to be constant and so, the steam injection rate increases to meet the target which is constant volumetric displacement. In the CHI approach, a constant rate of steam is injected and, so, the oil production rate decreases over time due to the increasing heat loss to the overburden. The performance of SAGD process under these two schemes is compared in this section.

Figure 4.19 compares the oil production rate. As can be seen, oil production rate remains constant over time for the CVD model but it shows a declining trend for the CHI model. As a result, oil recovery over the same period is lower as a consequence of a constant injection rate (See Figure 4.20). The interface position over time is different in applying the two schemes. Figure 4.21 shows that the steam chamber interface positions at the beginning of the process are almost at the same positions for the two schemes, but later the ones from the CHI scheme lag behind the interface positions from the CVD. After 1000 days, the steam chamber interface moves 44 m at the top of the reservoir in the CVD scheme while it is at 40 m from the vertical plane through the producer and injector in case of the constant rate of steam injection.

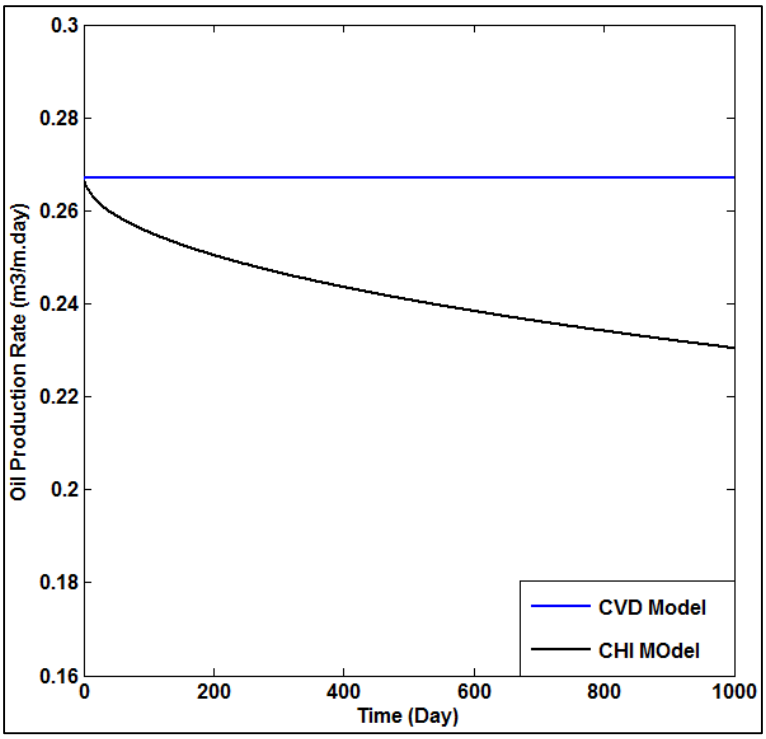

Figure 4.19: Comparison between oil production rate from the CVD model with CHI model.

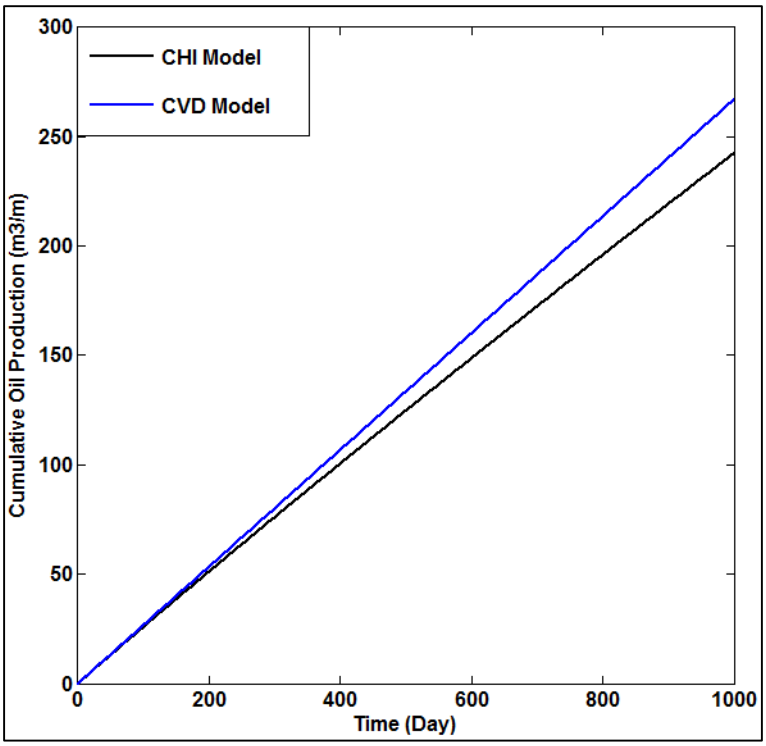

Figure 4.20: Cumulative oil production from the CHI model is compared with the result of the CVD model by use of data in Table 4.2.

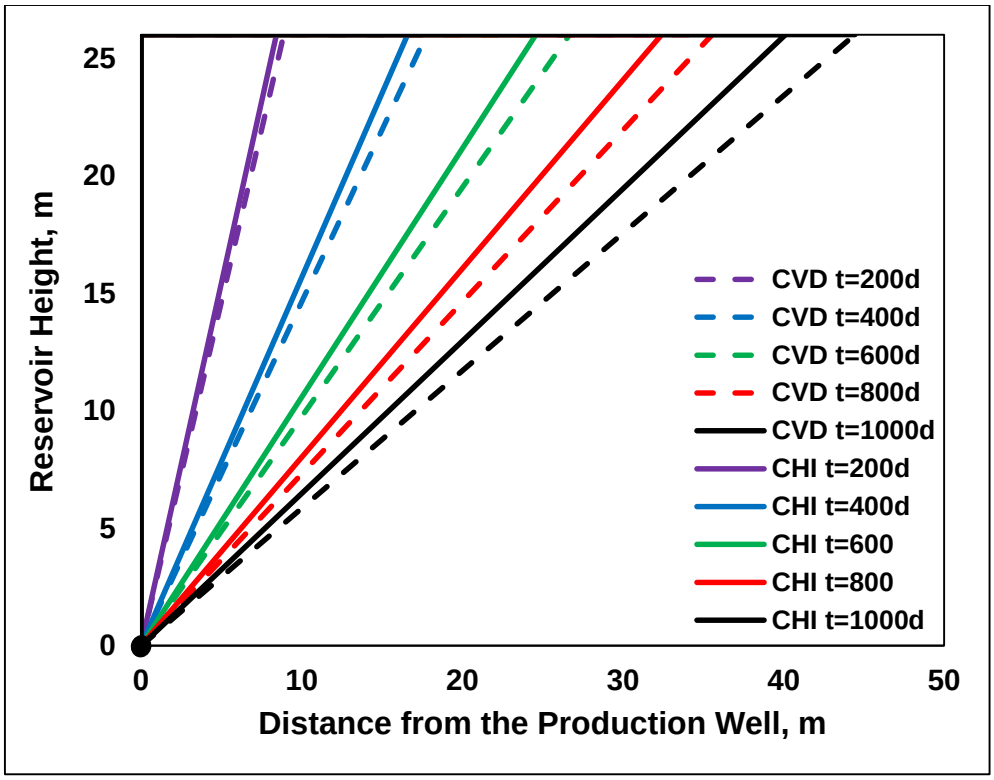

Figure 4.21: Calculated steam chamber interface positions from the two approaches (CVD and CHI) are compared at four different times; 200, 400, 800, and 1000 days.

5. ANALYTICAL TREATMENT OF THE CONFINEMENT PHASE OF SAGD

5.1 Introduction

In practical cases of SAGD, well pairs are confined in a repeated pattern. The developing steam chamber during the sideways expansion is affected by the neighbouring steam chambers. In an unconfined model, the expanding steam chamber at the top of the reservoir is constantly exposed to the cold overburden but with a confinement effect, this exposure stops, and this reduces the heat requirement in the system. In general, the steam chamber in SAGD process develops in three stages: (1) steam chamber rise period; $0 < t < t_r$, (2) lateral expansion period; $t_r < t < t_{con}$, and (3) confinement period; $t_{con} < t < t_f$. Here, the end of rise period is denoted by t_r, the time at which the steam chamber reaches the no flow boundary is called the confined time (t_{con}) and the final time (t_f) is the estimated lifetime of a SAGD well pairs.

The effect of well confinement was first introduced by Butler and Stephens (1981). Using a numerical simulation, this effect was added to their evaluation of SAGD when the steam chamber was confined by the neighbouring steam chambers. In this work, an analytical approach is introduced, for the first time, to evaluate the well confinement effect in the SAGD process which is the final period of the steam chamber development. This analytical approach helps to achieve a better understanding of the final phase of SAGD process. In this stage of SAGD, the effective height or available head for oil drainage decreases and as regards heat distribution, heat loss rate decreases or in a conservative design remains constant. The analytical models of CVD and CHI are extended to include the effect of well confinement.

5.2 Analytical Model – Confinement Effect on CVD Model

As described in previous chapters, the target in the CVD model is that the steam chamber advance velocity is assumed to be constant and the oil rate remains constant which requires

an increasing steam injection rate. The model was developed for a semi-infinite reservoir. In a confined model of a SAGD well pair, the steam chamber sideways expansion is limited by the neighbouring steam chambers in a series of parallel horizontal wells in a reservoir. Here, for the first time, an analytical model is proposed to describe the confinement phase of SAGD.

5.2.1 Modelling Assumptions

The assumptions made in the derivation of well confinement effect on Constant Volumetric Displacement model are similar to those mentioned in Section 4.2.1. The only difference is that there is no restriction on the maximum steam chamber velocity after the confinement is felt by the growing steam chamber.

5.2.2 Mathematical Formulation

Figure 2.4 shows the schematic of the steam chamber development in SAGD process with the effect of growing neighbouring steam chambers. It is clear that the effective height of the drainage rate is decreasing over time. Therefore, oil production rate has a decreasing trend. It is also concluded by comparing with Figure 5.1, the maximum steam chamber movement under confinement effect occurs on an imaginary vertical line passing through the halfway of well spacing between two neighbouring steam chambers. The model is developed for an arbitrary interface at $t = t_n$ and position $\theta = \theta_n$. The governing equations are; Darcy's law, volumetric displacement relation, heat conduction, constitutive equations indicating the temperature dependence of some physical properties.

5.2.2.1 *Relation between Heat Front and Steam Chamber Interface*

For each particular steam chamber interface, heat is conducted normal to the chamber interface, and the temperature variation in a direction parallel to the chamber interface is considered to be negligible. Parallel to the steam chamber interface, heated oil drains down

to the producer and so, normal to the steam chamber interface, the heat front moves forward. From Figure 5.1, the heat front velocity as a function of the maximum steam chamber velocity is given by:

$$U_f = \frac{1}{2} y'_{Lc} \, cos\theta_n \tag{5.1}$$

y'_{Lc}, is the maximum vertical steam chamber velocity at the half well spacing (Lc).

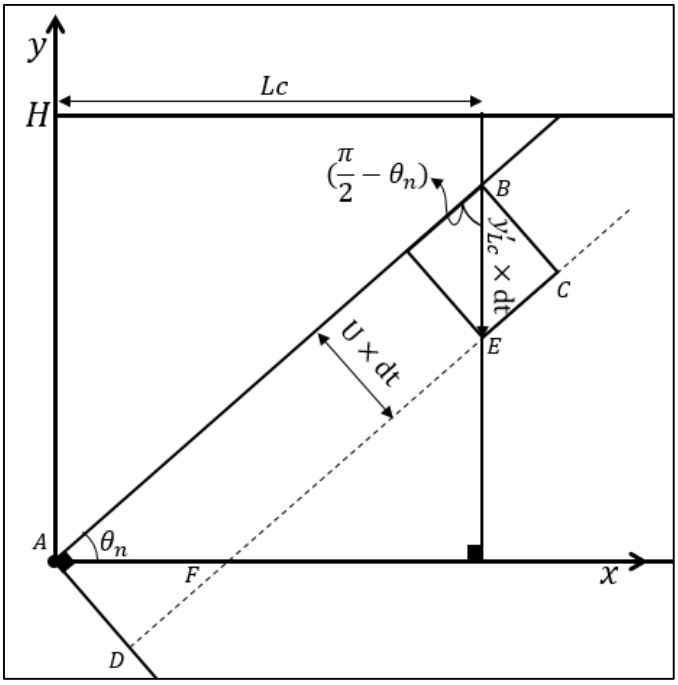

Figure 5.1: Maximum steam chamber movement under confinement effect occurs on an imaginary vertical line passing through the halfway of well spacing between two neighbouring steam chambers (L_c). Under the confinement effect, the relation between maximum steam chamber movement, ($y'_{Lc} \times dt$), and heat front movement ($U \times dt$) can be seen. To have consistency between the two movements to illustrate the same steam volume invasion, steam chamber movement should be equal to front movement.

5.2.2.2 *Temperature Profile in CVD Model*

The temperature profile in this situation is different due to a different heat front velocity from Equation 5.1 which is substituted into the heat conduction equation, Equation 4.9. As a result, the pseudo steady-state temperature profile ahead of the advancing steam chamber interface is computed by:

$$T_D = \exp\left(-\frac{U_f}{\alpha}\xi\right) = \exp(-\frac{y'_{Lc}\, cos\theta_n}{2\alpha}\xi)$$

(5.2)

5.2.2.3 Drainage *Rate for the CVD Model*

Drainage rate can be calculated by applying Darcy oil flow rate, substituting for viscosity-temperature correlation, Equation 4.14, and the pseudo steady-state temperature profile, Equation 5.2:

$$q_o = k_o\, g\, sin\theta_n \int_0^\infty \frac{d\xi}{\nu_o} = \frac{k_o}{\nu_{os}}\, g\, sin\theta_n \int_0^\infty \exp\left(-\frac{m y'_{Lc}\, cos\theta_n}{2\alpha}\xi\right) d\xi = \frac{2\, k_o g\alpha}{m\nu_{os}} \frac{\tan\theta_n}{y'_{Lc}}$$

(5.3)

Substituting for $\tan\theta_n$,

$$q_o = \frac{2\, k_o g\alpha}{m\nu_{os}\, L_c} \frac{y}{y'_{Lc}}$$

(5.4)

As it is clear from Figure 5.1, volumetric oil displacement rate can be calculated by:

$$q_o = \frac{1}{2}\phi\, L_c\, \Delta S_o y'_{Lc}$$

(5.5)

Hence, the maximum steam chamber velocity as a function y is derived as follow:

$$y'_{Lc} = \frac{2}{L_c}\sqrt{\frac{k_o g\alpha}{m\nu_{os}\phi\Delta S_o}}\sqrt{y_{Lc}} = \frac{\sqrt{H}}{L_c}x'_H\sqrt{y_{Lc}}$$

(5.6)

The steam chamber velocity and the interface positions are functions of time, given by:

$$y'_{Lc} = -\frac{H}{L_c}x'_H\left(1 - \frac{1}{2L_c}x'_H(t - t_{con})\right)$$

(5.7)

$$y_{Lc} = H\left(1 - \frac{1}{2L_c}x'_H(t - t_{con})\right)^2$$

(5.8)

Oil production rate as a function of y or t is derived by substituting Equation 5.6 or Equation 5.7 into Equation 5.5, respectively:

$$q_o = \frac{1}{2}\phi\,\Delta S_o x'_H\sqrt{Hy}$$

(5.9)

$$q_o = \frac{1}{2}\phi\,\Delta S_o H x'_H\left(1 - \frac{1}{2L_c}x'_H(t - t_{con})\right)$$

(5.10)

As is evident from the above derivation, the available head for oil production decreases with time during the confinement period. The oil production rate with confinement effect can also be rewritten as:

$$q_o^C = q_o^{Unc}\left(1 - \frac{1}{2L_c}x'_H(t - t_{con})\right)$$

(5.11)

where q_o^{Unc}, is the oil production rate from the unconfined CVD model. The above equation indicates that the oil production rate is a linear function of time.

5.2.2.4 *Estimation of SAGD Well Pair Lifetime*

In general, steam chamber development means reservoir depletion. The lifetime of a SAGD well pair in the confined pattern at which it reaches complete depletion (for the analytical purpose, it is assumed to reach zero oil rate) can be estimated from the previous section derivation as:

$$\text{SAGD lifetime} = \frac{3L_c}{x'_H}$$

(5.12)

The above equation indicates that lifetime of a SAGD well pair for a CVD scenario depends on well spacing from the adjacent well pairs and maximum horizontal steam chamber velocity. Using the same data as in Table 4.2 and the well spacing of 92 m, lifetime for this well pair is 3083 days.

5.2.2.5 *Energy Balance and CSOR Calculations*

Under the confinement effect, when the interference of adjacent steam chambers occurs, the steam chamber expansion stops. As a result, heat loss rate decreases afterwards, or in a

conservative design, we may say it remains constant. Under the confinement effect, rate of heat loss, accumulated heat, and heat to raise the rock and fluid temperature from T_s to T_r are given by the equations below in which heat loss rate is calculated in two forms:

1. In a non-conservative form:

$$q_{loss} = \frac{2\,K_{ob}\Delta T}{\sqrt{\pi\alpha_{ob}}} x'_H \left(\sqrt{t_{con}} - \sqrt{t - t_{con}}\right) \tag{5.13}$$

2. In a conservative form:

$$q_{loss} = \frac{2\,K_{ob}\Delta T}{\sqrt{\pi\alpha_{ob}}} \sqrt{L_c x'_H} \tag{5.14}$$

Heat rate into the steam zone to raise the temperature by ΔT is given by:

$$q_{sz} = (\rho C)_{res}\Delta T \frac{\partial}{\partial t}(L_c \Delta y) = (\rho C)_{res}\Delta T H x'_H \left(1 - \frac{1}{2L_c} x'_H (t - t_{con})\right)$$

$$= q_{sz}^{Unc}\left(1 - \frac{1}{2L_c} x'_H (t - t_{con})\right) \tag{5.15}$$

where $q_{sz}^{Unc}$is the heat rate into the steam zone for the unconfined model. The portion of the injected heat which accumulates ahead of the front is:

$$Q_{acc} = 4\alpha\, L_c\, (\rho C)_{res} \Delta T \left(\frac{1}{y'_{Lc} cos^2\theta}\right)$$

$$= 4\alpha\, L_c\, (\rho C)_{res} \Delta T \left(\frac{1}{\frac{H}{L_c} x'_H \left(1 - \frac{1}{2L_c} x'_H (t - t_{con})\right)} + \frac{H}{L_c x'_H}\left(1 - \frac{1}{2L_c} x'_H (t - t_{con})\right)^3\right)$$

(5.16)

And the rate of heat accumulation ahead of the heat front is:

$$q_{acc} = 4\alpha\, L_c\, (\rho C)_{res} \Delta T \left(\frac{1}{2H} \frac{1}{\left(1 - \frac{1}{2L_c} x'_H (t - t_{con})\right)^2} - \frac{3}{2} \frac{H}{{L_c}^2}\left(1 - \frac{1}{2L_c} x'_H (t - t_{con})\right)^2\right)$$

$$= 2\alpha\, L_c\, (\rho C)_{res} \Delta T \left(\frac{1}{y} - \frac{3}{{L_c}^2} y\right)$$

(5.17)

From the above equations, steam injection rate and CSOR can be evaluated for $t_{con} < t < t_f$ respectively as below:

$$i_{st} = \frac{q_{inj}}{\rho_w L_v f_s} = \frac{q_{loss} + q_{acc} + q_{sz}}{\rho_w L_v f_s} \quad and \quad CSOR = \frac{Q_{inj}}{Q_o}$$

(5.18)

where $Q_{inj}$is the cumulative steam injection, and $Q_o$is the cumulative oil production.

5.2.3 Results

Using the same data as in CVD section, Table 4.2, and assuming the well spacing of 92 m, the results of Constant Volumetric Displacement model with and without confinement effect (confined and unconfined models, respectively) are compared. Figure 5.2 compares the unsteady temperature profiles. As can be seen, because of the confinement effect lower temperatures are predicted ahead of the interface.

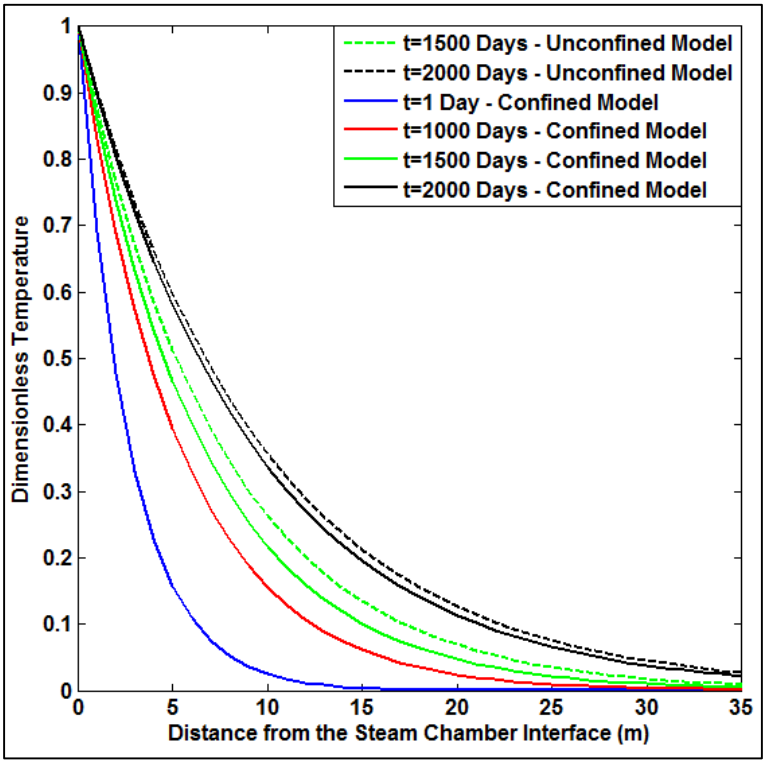

Figure 5.2: Unsteady dimensionless temperature profiles versus the distance from the steam-oil interface with and without confinement effect - CVD model.

Figure 5.3 shows that the maximum horizontal chamber velocity is 4.5 cm per day, but it drops to approximately one-half, around 2.5 cm per day, after confinement. Afterwards, it continues declining linearly. Note that in a confined model, the maximum steam chamber

velocity before confinement occurs at the top of the reservoir, but after confinement, it changes direction and occurs in the vertical direction.

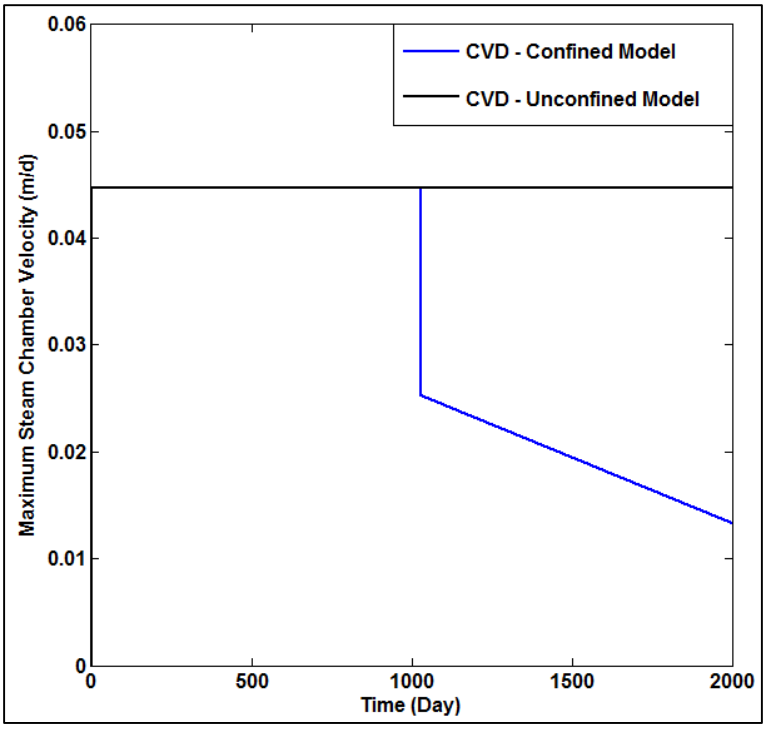

Figure 5.3: Maximum steam chamber velocity versus time with and without confinement effect - CVD model.

Figure 5.4 shows that the oil production rate does not remain constant and begins to decrease linearly in a confined model. The growing steam chamber in this example, reaches the neighbouring steam chamber at about half the well spacing after 1027 days. Oil is produced at a constant rate of 0.27 m^3/day per unit length of well but it decreases to 0.14 m^3/day per unit length of well after 973 days of the start date of confinement. This results in a lower cumulative oil production in a confined model than an unconfined model.

Figure 5.5 shows that the predicted cumulative oil production is 475 m^3 per unit length of well in a confined model which is approximately 50 m^3 lower than an unconfined model after 2000 days of production.

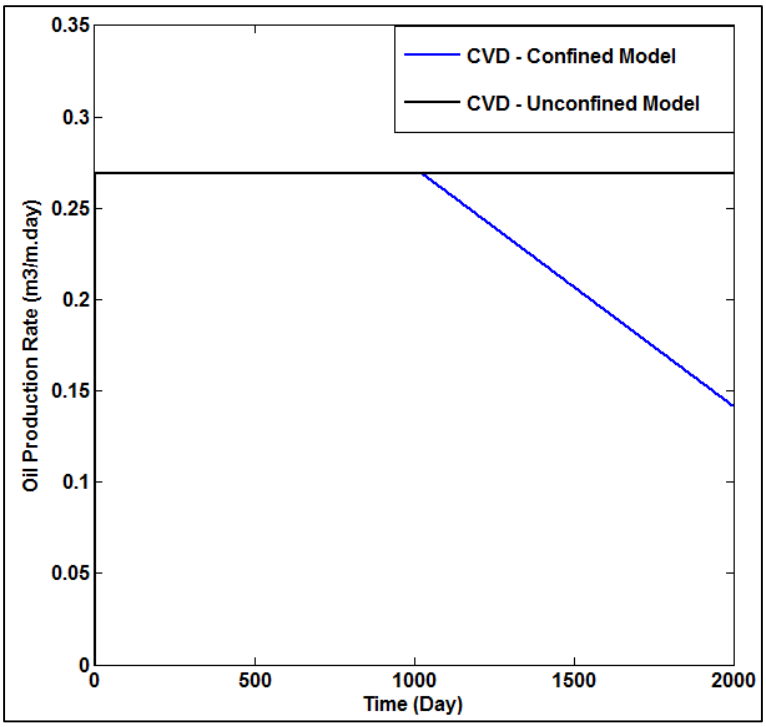

Figure 5.4: Oil production rate as a function of time with and without confinement effect – CVD model.

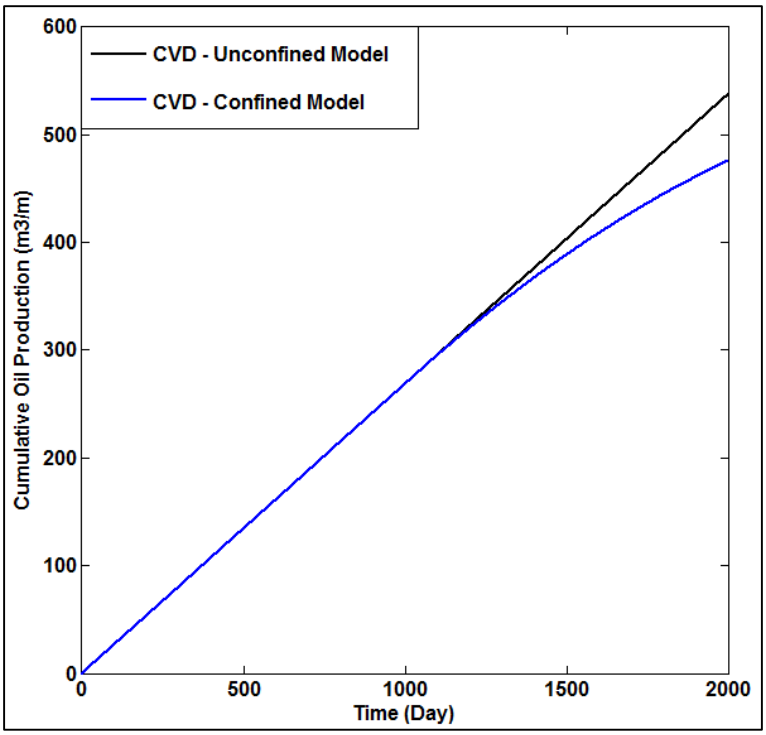

Figure 5.5: Comparing cumulative oil production with and without confinement effect over 2000-day time interval – CVD model.

In Figure 5.6, the predicted angle between the steam chamber interface and the horizontal are compared. With confinement effect, the angle tends to decrease faster. This means that the reservoir would be depleted at a faster rate in a confined pattern compared with the unconfined reservoir. The well spacing is 92 m.

Figure 5.7 depicts the interface positions in the confined (dashed lines) and unconfined (solid lines) approaches at three different times; 1027, 1500, and 2000 days. In an unconfined model, the steam chamber interface extends in its length and moves as if there is no limitation. However, in a confined model, after confinement time (1027 days), which happens at the half-way point of the well spacing, the steam chamber coalesces with the neighbouring steam chamber interface, and it starts to shrink in length. Note that by comparing the interface positions at the same time for the two models, it is clear that the reservoir depletes faster in a confined model.

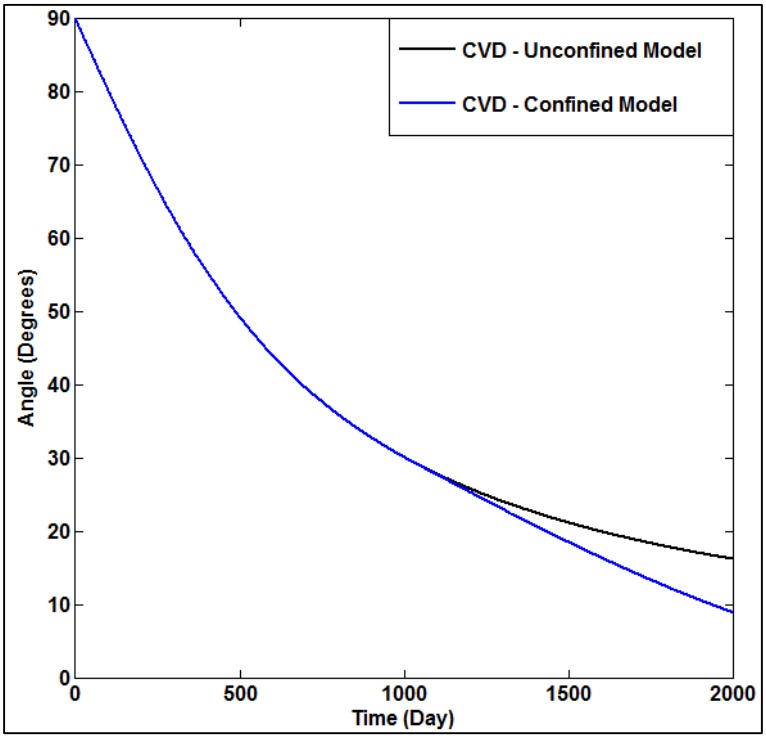

Figure 5.6: Angle between steam-oil interface and the horizon with and without the effect of confinement – CVD model.

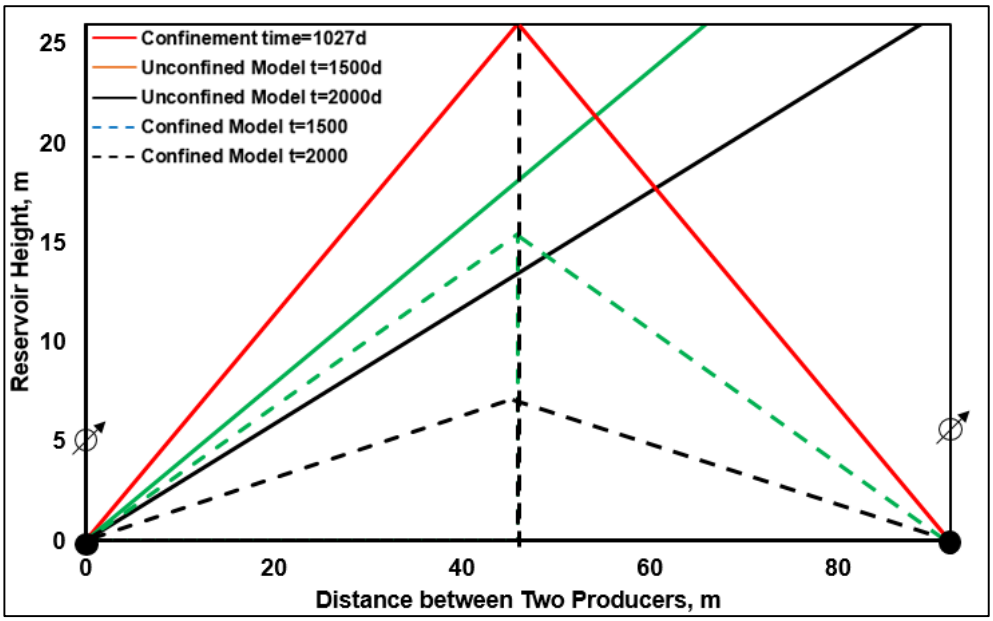

Figure 5.7: Calculated interface positions in confined (dashed lines) and unconfined (solid lines) reservoirs at three different times; 1027 (red), 1500 (green), and 2000 (black) days.

The predicted cumulative heat distributions in the system are depicted in Figure 5.8. As mentioned in the energy balance section, the injected heat is assumed to be consumed in three ways; raising the rock and fluid from reservoir temperature to steam temperature, accumulated heat ahead of the steam-oil interface, and the heat loss to the overburden rock. After 2000 days, Figure 5.8 shows the heat loss to the overburden is even higher than heat to the steam zone in an unconfined reservoir (solid lines) which indicates an excessive heat loss in this model. Thermal efficiency is low in this situation. However, in a confined model, the thermal efficiency improves.

As can be seen in Figure 5.8, heat loss is considerably lower than the heat to steam zone in a confined model (dashed lines). The cumulative injected steam to provide the required heat in the system is estimated and depicted in Figure 5.9. As expected, the steam injection is lower in a confined reservoir compared with the unconfined one.

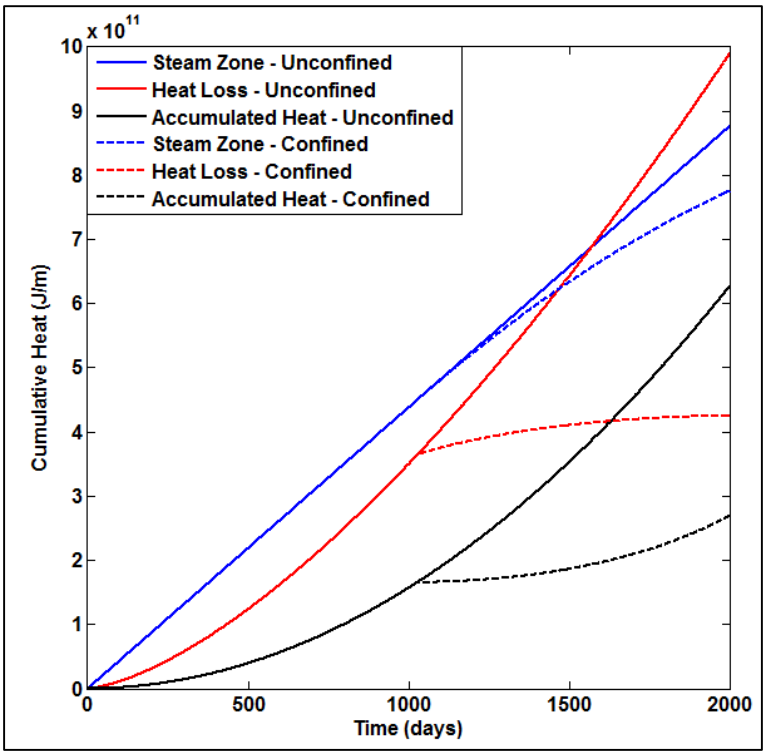

Figure 5.8: Cumulative heat distribution in the system in forms of loss, into the steam zone, and oil zone with and without confinement effect – CVD model.

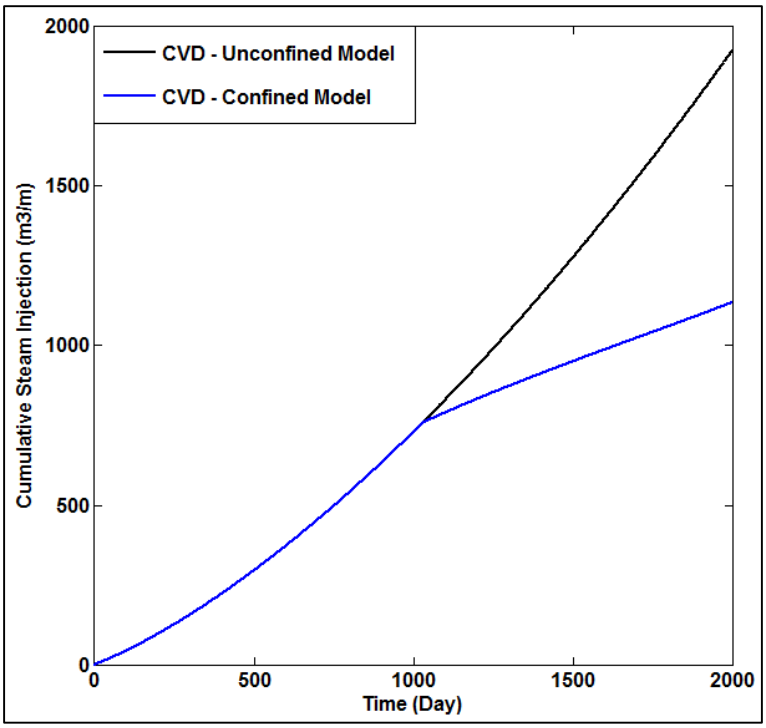

Figure 5.9: Comparing cumulative steam injection with and without confinement effect over time – CVD model.

Figure 5.10 compares the CSOR. A lower CSOR is estimated for a confined reservoir relative to an unconfined one. This behaviour is due to the combined impact of the lower oil recovery and steam injection requirement in the confined model. The predicted CSOR from the confined model reaches a plateau of 2.39 after 2000 days.

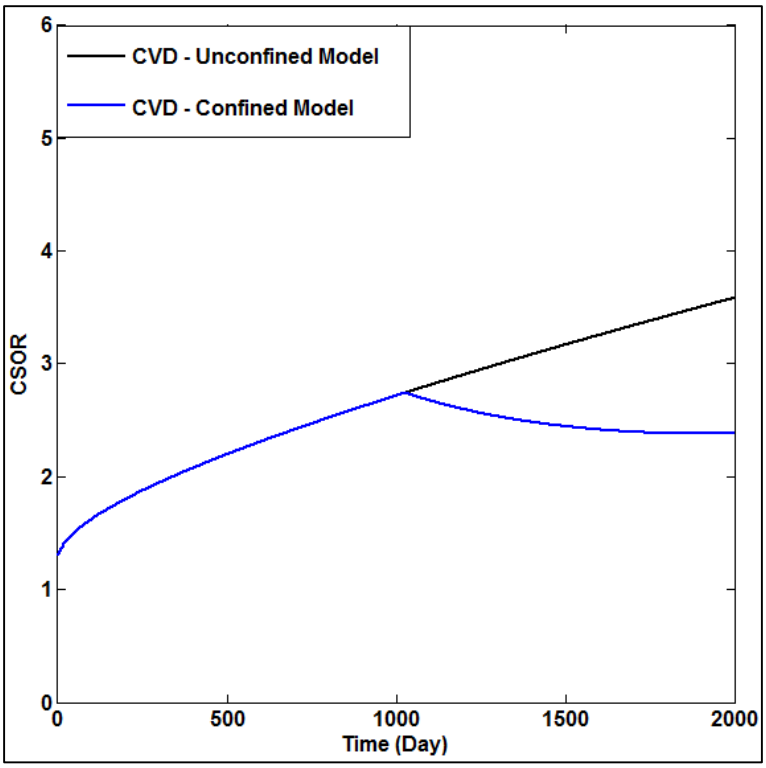

Figure 5.10: Calculated CSOR with and without confinement effect – CVD model.

One of the factors affecting the economics of the SAGD project is the well spacing. Figures 5.11 and 5.12 show the effect of well spacing. Performance of an unconfined reservoir is compared with a confined reservoir for 90 and 120 m as the well spacing value. Oil production rate starts to decrease at the time of confinement for both cases compared to the unconfined reservoir as is seen in Figure 5.11. Cumulative steam-oil ratios are also shown in Figure 5.12. Lower ratios are achieved with the well confinement effect in particular for the smaller well spacing. The confinement occurs at the shorter period, 1027 and 1340 days after production starts for well pacing of 90 and 120 m respectively. Consequently, the heat loss to the overburden begins to decrease sooner. A higher recovery factor of 43.61% results for the well spacing of 90 m compared to 35.79% for the well spacing of 120 m, after 2000 days of production.

The results of the proposed approach also indicate that the SAGD lifetime (complete depletion) is shorter in the case of smaller pattern size. It takes 11 years for the well spacing of 120 m and nearly 8 years and a half for the well spacing of 90 m.

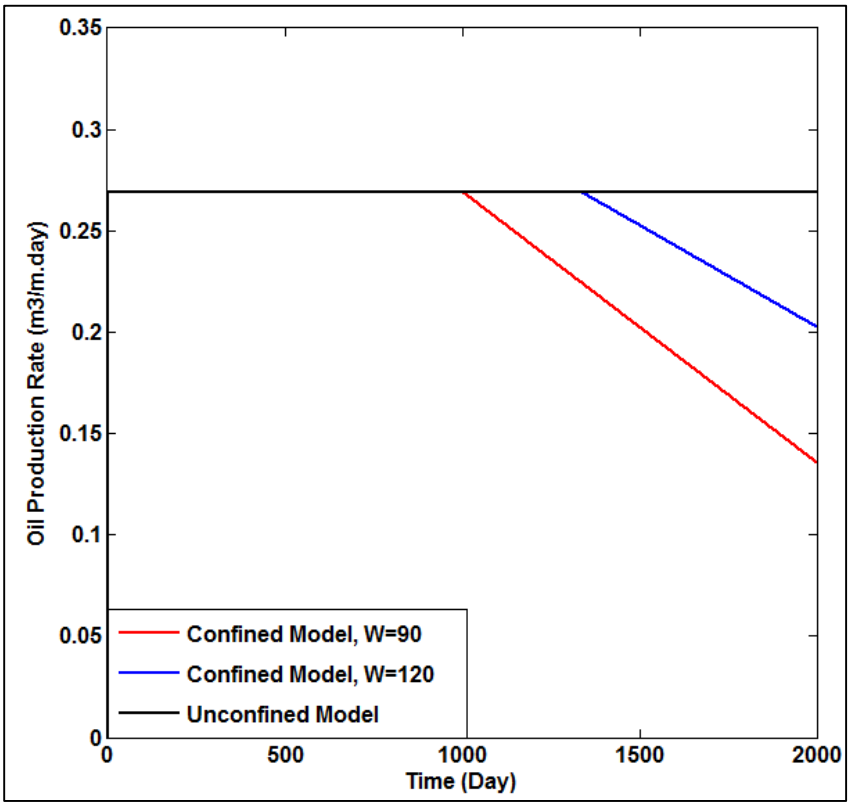

Figure 5.11: Effect of the well spacing on the oil production rate as a function of time.

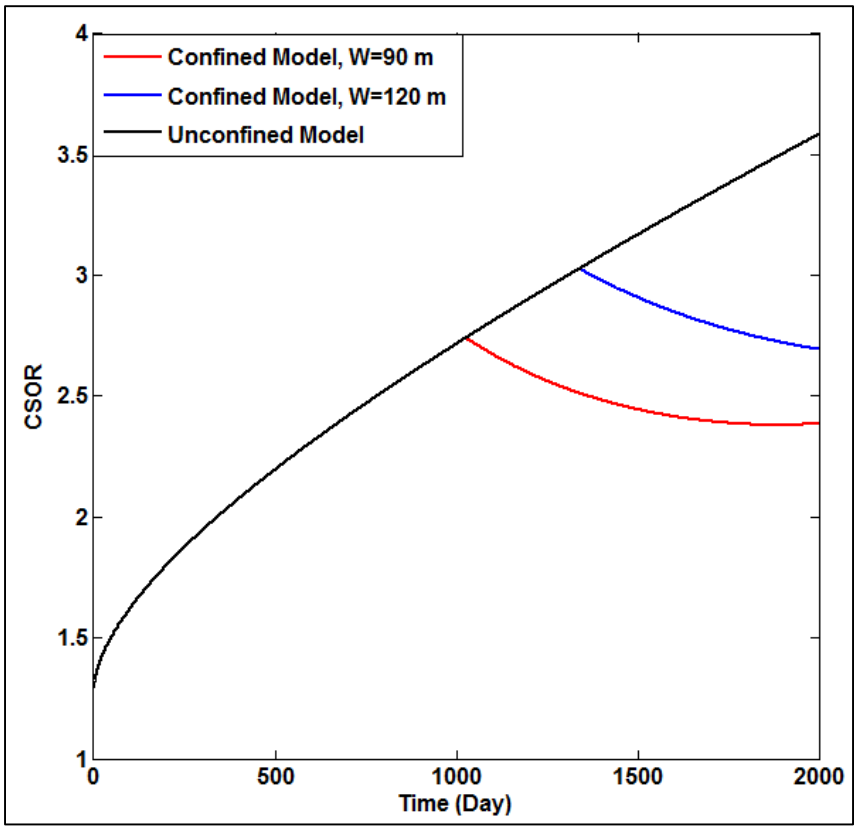

Figure 5.12. Effect of the well spacing on CSOR.

5.3 Analytical Model – Confinement Effect on CHI Model

5.3.1 Modelling Assumptions

The assumptions were made in developing the analytical model of the confinement effect on the CHI scheme are similar to those in developing the CHI model. However, the model geometrical description is different as is evident from Figure 5.1. Moreover, the heat loss rate in this model is assumed to remain constant as the process proceeds.

5.3.2 Mathematical Formulation

In this section, the analytical model of the confinement phase is added to the lateral spreading - CHI model which is described in detail in previous sections. In developing the

energy balance for a confined steam chamber, the heat injection rate is constant, and the heat loss rate stops increasing. This has a direct effect on oil production rate. Moreover, the effective height for the drainage rate and the length of the steam chamber interface decreases with time as shown in Figure 5.1. All these factors affect the drainage rate and thermal efficiency of the SAGD process.

From the heat balance (Equation 4.45) and the conservative heat loss (Equation 5.14), heat to the growing steam zone (Equation 4.47) and heat outflow to the oil zone (Equation 4.48), the temperature gradient at the steam chamber interface as a Neumann boundary condition for the heat conduction equation at a particular time is given by:

$$\left(\frac{dT}{d\xi}\right)_{\xi=0} = -\frac{cos\theta}{2K_{res}L_c}\left\{q_{inj} - \frac{2\,K_{ob}\Delta T}{\sqrt{\pi\alpha_{ob}}}\sqrt{L_c x'_H} - L_c y'_{Lc}(\rho C)_{res}\Delta T\right\} \tag{5.19}$$

After the coalescence of the growing steam chambers occurs the pseudo-steady state temperature distribution ahead of the moving steam chamber interface, at each given time, can be calculated as:

$$T = \frac{\alpha}{K_{res}L_c y'_{Lc}}\left\{q_{inj} - \frac{2\,K_{ob}\Delta T}{\sqrt{\pi\alpha_{ob}}}\sqrt{L_c x'_H} - L_c y'_{Lc}(\rho C)_{res}\Delta T\right\} e^{-\frac{cos\theta}{2\alpha}y'_{Lc}\xi} + T_r \tag{5.20}$$

Applying Darcy oil rate model gives the oil rate as:

$$q_o = \frac{2K_o g}{m v_{os}} \left(\frac{1}{K_{res} L_c \Delta T}\right)^m \left(\frac{\alpha}{y'_{Lc}}\right)^{m+1} \tan\theta \left\{ q_{inj} - \frac{2\, K_{ob} \Delta T}{\sqrt{\pi \alpha_{ob}}} \sqrt{L_c x'_H} - L_c y'_{Lc} (\rho C)_{res} \Delta T \right\}^m \tag{5.21}$$

$$\tan\theta = \frac{y}{L_c} \tag{5.22}$$

Combining the above oil rate equation with Equation 5.5, the steam chamber velocity in y-direction can be calculated from;

$$\frac{{y'_{Lc}}^{m+2}}{y} = \frac{4K_o g}{m v_{os} \phi \Delta S_o} \left(\frac{1}{K_{res} \Delta T}\right)^m \left(\frac{1}{L_c}\right)^{m+2} (\alpha)^{m+1} \left\{ q_{inj} - \frac{2\, K_{ob} \Delta T}{\sqrt{\pi \alpha_{ob}}} \sqrt{L_c x'_H} - L_c y'_{Lc} (\rho C)_{res} \Delta T \right\}^m \tag{5.23}$$

The above non-linear first order ODE is solved for y'_{Lc}using an iterative method. Knowing the steam chamber velocity, oil production rate, unsteady temperature profile ahead of front, steam chamber position, heat distribution, and CSOR can be predicted.

5.3.3 Results

There are two options in evaluating the CHI model with confinement effect; keeping the same rate of injection from the beginning of the sideways expansion phase and using the lower injection rate. In generating the following results, the former option is used. In this approach, the steam chamber velocity comes from the heat and mass balances over the system.

The predicted maximum steam chamber velocities from the CHI model, with and without confinement effect, are compared in Figure 5.13. The data in Table 4.2 is used to generate these results. In applying this approach, the spreading steam chamber reaches the neighbouring steam chambers after 1148 days. As is apparent from the figure, after the confinement is felt, there is a gap between the results of the two models due to the switching from the maximum horizontal velocity to the vertical one in the confined model. The steam chamber velocity drops from 3.8 cm per day to 2 cm per day.

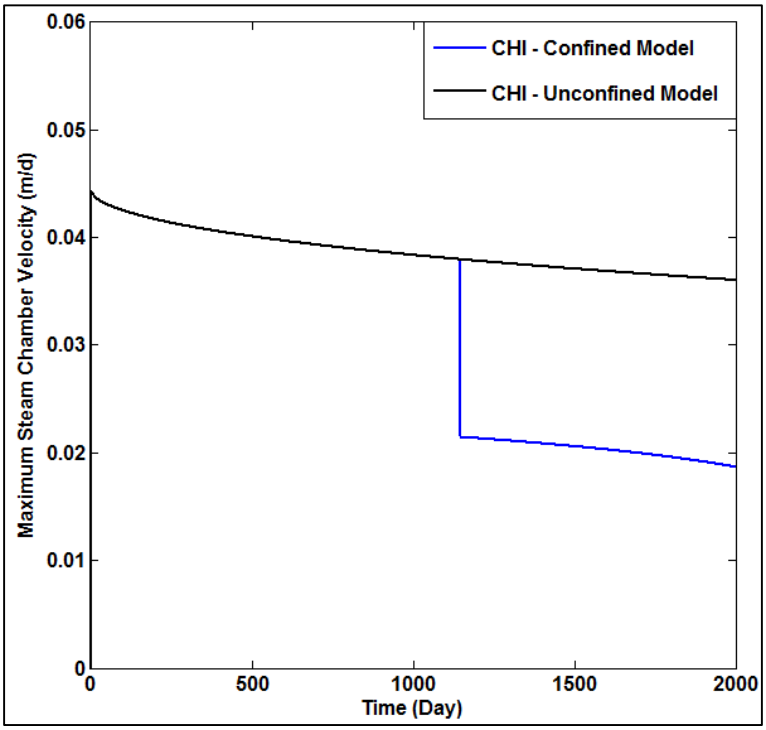

Figure 5.13: Maximum steam chamber velocity as a function of time with and without confinement effect – CHI model.

Figure 5.14 illustrates the oil production rates predicted from the CHI model in confined and unconfined conditions. After coalescence, the oil production rate begins to drop more in the case of the confined model. Oil rate is maximum at the beginning, 0.2665 m^3/day

per unit length of well and it decreases to 0.2164 and 0.1985 m^3/(d-m) in the unconfined and confined models, respectively.

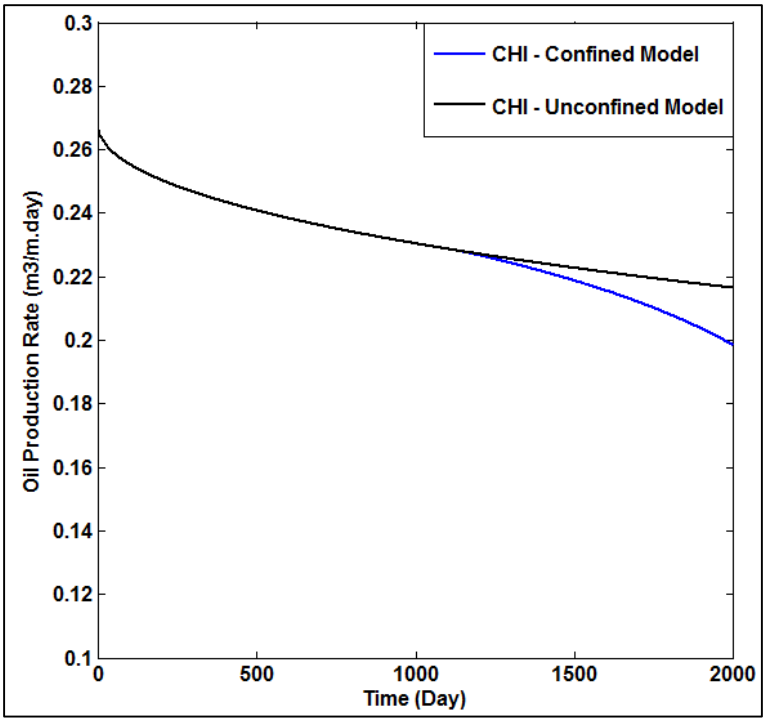

Figure 5.14: Comparing oil production rate with and without confinement effect over 2000-day time interval – CHI model.

The angle between the steam chamber interface and the horizon is 8 degrees smaller in the confined model compared with the unconfined at the end of 2000-day period (See Figure 5.15). This indicates that under the confinement, the reservoir depletes faster.

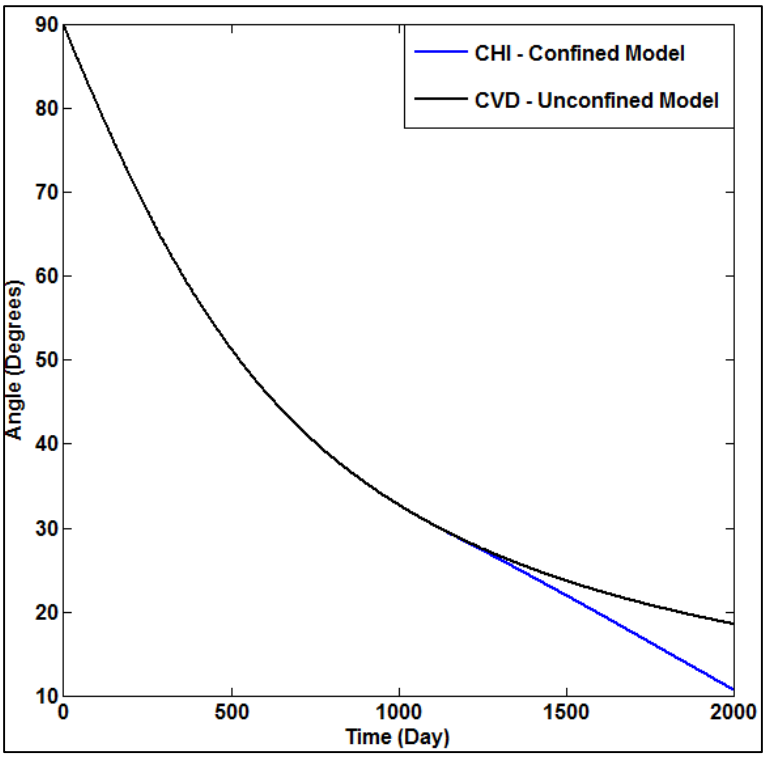

Figure 5.15: Steam chamber interface angle with horizontal with and without confinement effect over time – CHI model.

These results are generated by assuming a constant rate of steam injection from the beginning to the end. Therefore, the excess heat in the system due to the constant heat loss to the overburden in the confined model should be redistributed in the system to reach the balance. As a result, the rate of heat transfer at the steam chamber edge increases but the rate of heat to raise the rock and fluid decreases.

Figure 5.16 compares the rate of heat loss, the outflow of heat into the oil zone and heat to the steam zone for the confined and unconfined conditions.

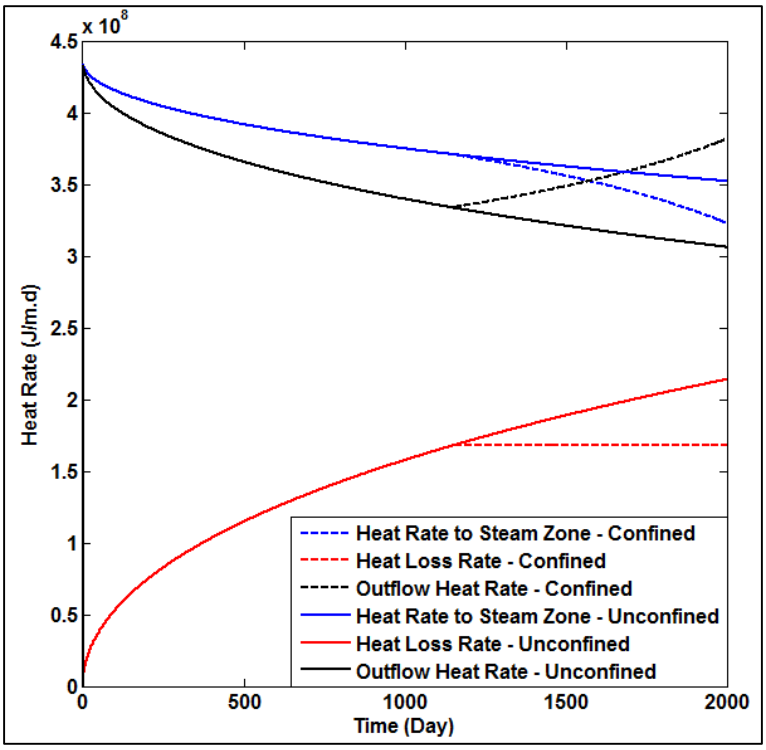

Figure 5.16: Heat rate in the system in forms of loss, into the steam zone, and outflow into oil zone with and without confinement effect – CHI model.

Finally, it can be concluded from Figure 5.17 that there is not a significant difference between CSOR for confined and unconfined conditions in a Constant Heat Injection (CHI) scheme if there is no change in the rate of steam injection after confinement. It is seen that in the case of the confined model, the cumulative steam-oil ratio is even slightly higher compared to the unconfined model, unlike the CVD model results. In this approach, steam injection rate does not change before and after the confinement phase starts. This means that the cumulative steam injection is the same under both conditions. As seen in Figure 5.14, the oil production rate is slightly lower for the confined state and so is the cumulative oil production. This is the reason for no improvement in SAGD performance during the confinement phase.

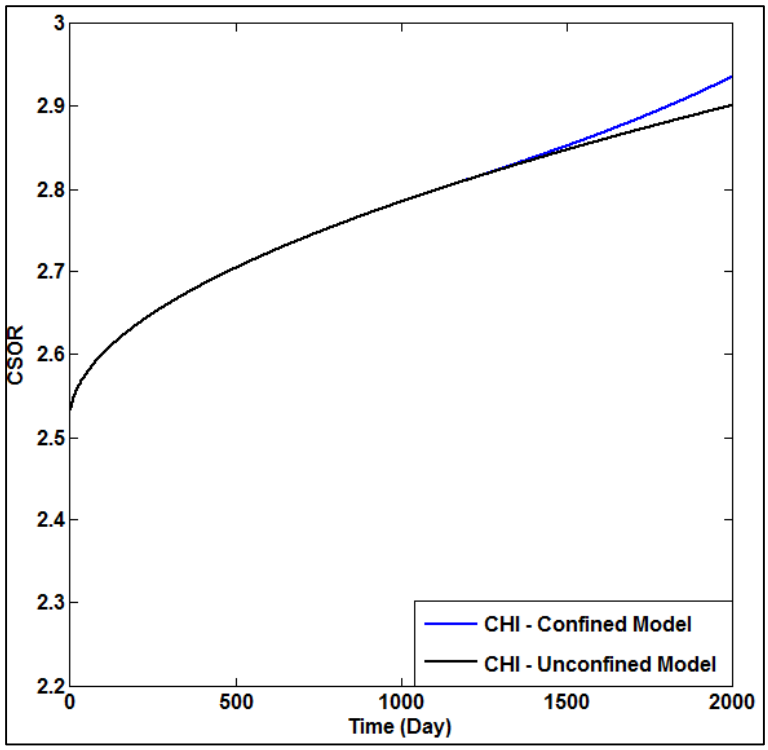

Figure 5.17: Comparison of CSOR with and without confinement effect over time – CHI model.

6. COMPREHENSIVE ANALYTICAL MODEL OF SAGD

6.1 Introduction

This is the first time that a comprehensive analytical model of Steam-Assisted Gravity Drainage (SAGD) process, describing the complete process is introduced. Steam is continuously injected into the reservoir through a horizontal well located several metres above a horizontal producer near the base of the formation. It was observed in experiments and in the UTF pilot test that the steam chamber mainly grows upwards initially, until it reaches the top of the reservoir, after which the steam chamber continues to expand laterally.

In a confined pattern, the steam chamber expansion is limited after a while by its coalescence with the neighbouring steam chambers. The experimental results of Butler and Chung (1987), Figure 1.5, indicate that a linear geometry is a reasonable approximation of the growing chamber. In this research, as is seen in Figure 2.4, the steam chamber is assumed to be an inverted triangle with a fixed vertex at the producer. All three phases of SAGD are included in the models presented below. The comprehensive model is an analytical tool that simulates steam chamber growth from the beginning to the end.

In this chapter, the proposed models in the last three chapters for the rise, lateral spreading, and confinement effect are combined to introduce the Comprehensive Constant Volumetric Displacement (CCVD) model and Comprehensive Constant Heat Injection (CCHI) model. It is believed that these comprehensive models provide a better understanding of the SAGD process and also provide a tool for evaluating a SAGD well pair among patterns. The model is validated against experimental and field data.

The predicted oil production rate, oil recovery and steam chamber shape from the comprehensive analytical approach are in good agreement with experimental work of Chung and Butler (1987) and field data.

6.2 Comprehensive CVD Model - Summary of the Governing Equations

The Comprehensive Constant Volumetric Displacement (CCVD) model of SAGD process includes three sets of equations for the rise, sideways expansion, and confinement periods derived in the previous chapters. In generating the results in this chapter, all these equations are applied in the same order as listed in Table 6.1.

Table 6.1: Summary of all governing equations of the CCVD approach.

Model Name	Equation Number
Rise velocity – Rise period	Eq (3.7)
Steam chamber height – Rise period	Eq (3.8)
End time of the steam chamber – Rise period	Eq (3.9)
The constant angle between steam chamber and the horizon	Eq (3.15)
Oil production rate – Rise period	Eq (3.13)
Cumulative oil production – Rise period	Eq (3.14)
Heat rate to steam zone – Rise period	Eq (3.21)
Heat rate to overhead oil zone – Rise period	Eq (3.37)
Heat rate to the oil zone at the sides of the steam chamber – Rise period	Eq (3.46)
Heat front velocity – Sideways expansion	Eq (4.2)
Temperature profile beyond the steam chamber edge – Sideways expansion	Eq (4.10)
Maximum horizontal velocity of the steam chamber – Sideways expansion	Eq (4.18)
Oil production rate – Sideways expansion	Eq (4.19)
Cumulative oil production rate – Sideways expansion	Eq (4.16)
Heat loss rate to the top boundary of the reservoir – Sideways expansion	Eq (4.29)
Heat rate to the steam chamber – Sideways expansion	Eq (4.32)
Accumulated heat rate ahead of the steam chamber edge – Sideways expansion	Eq (4.38)
Heat front velocity – Confinement period	Eq (5.1)
Temperature profile beyond the steam chamber edge – Confinement period	Eq (5.2)
Angle between the steam-oil interface and the horizon – Confinement period	Eq (5.22)
Maximum steam chamber velocity in vertical direction – Confinement period	Eq (5.7)
Steam chamber height – Confinement period	Eq (5.8)
Oil production rate – Confinement period	Eq (5.10)
Heat loss rate – Confinement period	Eq (5.13)
Heat rate to the steam chamber – Confinement period	Eq (5.15)
Accumulated heat rate – Confinement period	Eq (5.17)

6.2.1 Results

It is expected that the comprehensive analytical theory provides a reasonably accurate tool to investigate SAGD performance. In this section results are generated by use of data in Table 4.2.

Figure 6.1 shows the calculated maximum steam chamber velocity from this approach over the three phases of the SAGD process. During the rise period, the rise velocity is constant at 9 cm/day. After the steam chamber reaches the top of the reservoir, the steam chamber velocity is in horizontal direction. It is seen from the figure that there is a big drop in switching from the vertical velocity to the horizontal one. The maximum steam chamber velocity remains constant (CVD model) at 4.48 cm/day during this phase. At the end of sideways expansion (1171 days), the maximum steam chamber velocity changes direction and values. It drops from 4.48 to 2.53 cm/day and linearly declines afterwards. Figure 2.4 provides better visualization of the phases and directions of the maximum steam chamber velocities. Figure 6.2 also shows the effective height for the oil drainage as a function of time.

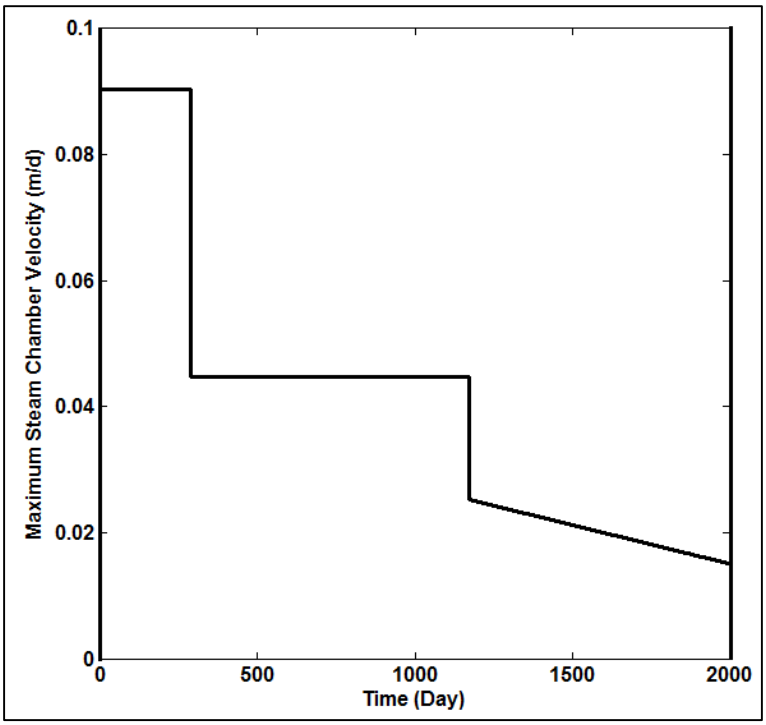

Figure 6.1: Maximum steam chamber velocity of the CCVD approach over the three phases of SAGD process.

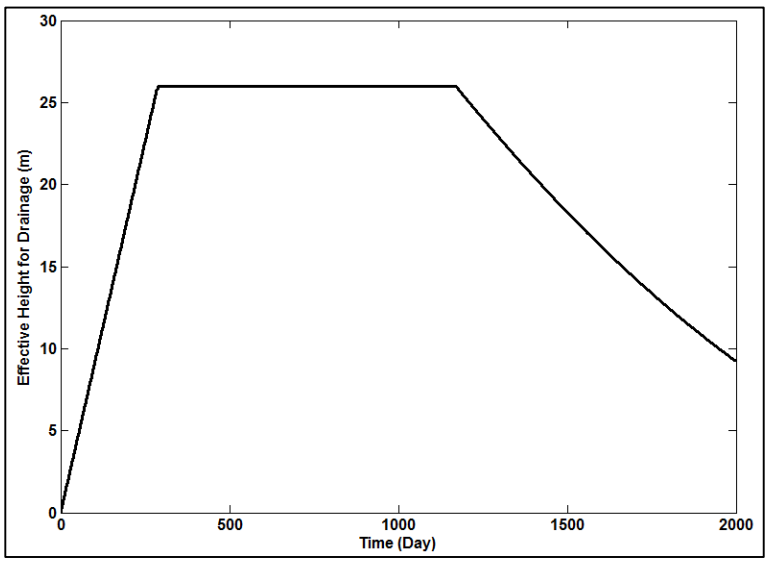

Figure 6.2: Effective height for oil drainage as a function of time over the three phases of SAGD process.

Oil production rate as a function of time is shown in Figure 6.3 by use of data in Table 4.2. The oil production rate increases during the rise period and it reaches a peak at 0.2665 m^3/day per unit length of the well after 287 days. For the next 884 days, the oil production rate remains constant during the lateral spreading time. It starts to decline when the steam chamber coalesces with the neighbouring steam chambers at the half way distance of the well spacing. Figure 6.3 shows that oil production rate declines to 0.16 m^3/day per unit length of the horizontal well at the end of 2000-day time interval.

Cumulative oil production over the 2000-day time interval is displayed in Figure 6.4. This model predicts that the cumulative oil volume of approximately 454 m^3 is produced per unit length of the well after 2000 days. For instance, a horizontal well with the length of 1000 m, is expected to produce 450,000 m^3 of bitumen after almost 5 years and half.

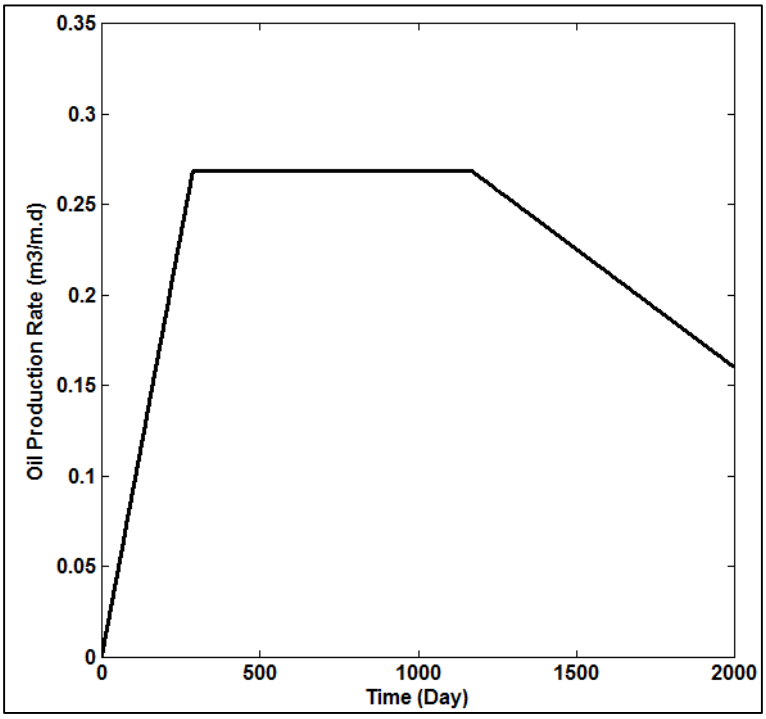

Figure 6.3: Oil production rate as a function of time over the three phases of SAGD process.

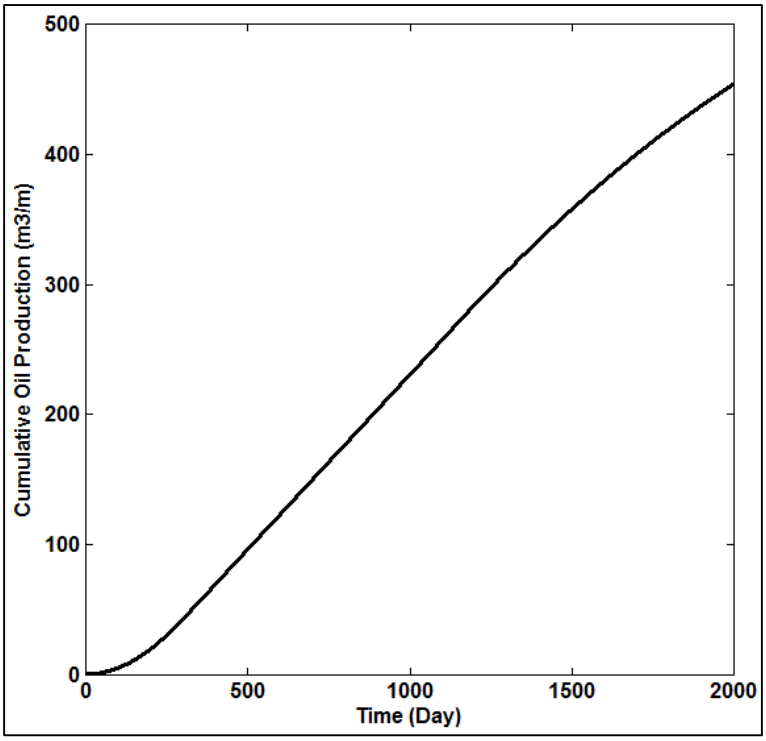

Figure 6.4: Cumulative oil production of SAGD process (CCVD approach) over a 2000-day time interval.

The calculated cumulative steam injection required to provide the above oil production in SAGD as a function of time is shown as in Figure 6.5. Consequently, CSOR for this set of data and using the comprehensive analytical CVD model is calculated and displayed in Figure 6.6. It is evident that CSOR decreases initially to approximately 2.5 m^3/m^3 and then increases slightly during the sideways expansion. It declines gradually during the confinement phase and finally reaches a plateau at near 2.1 m^3/m^3.

It is seen from Figure 6.7 that the angle between the steam-oil (chamber) interface and the horizon is constant during the rise period $(\theta = 76.24)$ and after that, it decreases nonlinearly over time and reaches 11.36 degrees after 2000 days of steam chamber establishment.

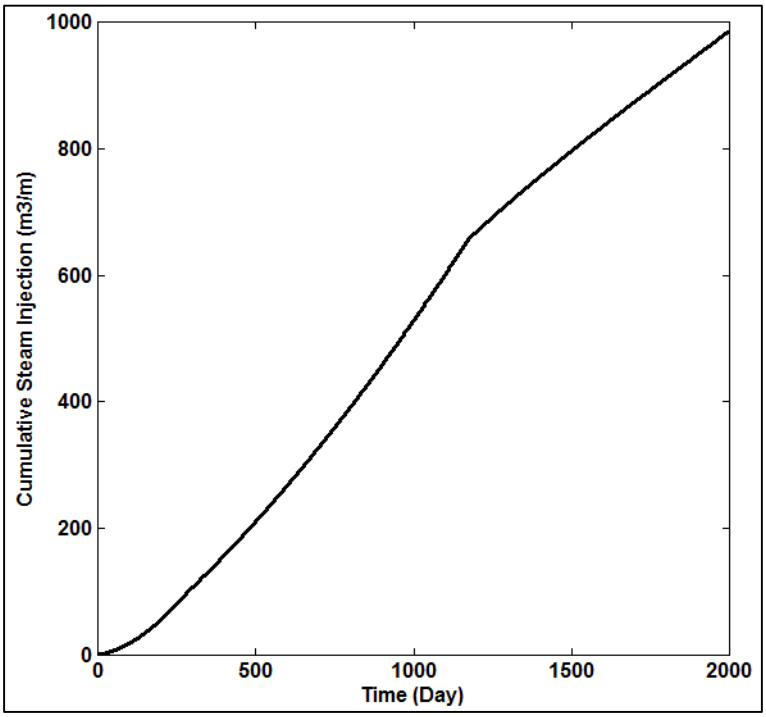

Figure 6.5: Cumulative steam injection of the CCVD approach per unit length of horizontal well as a function of time.

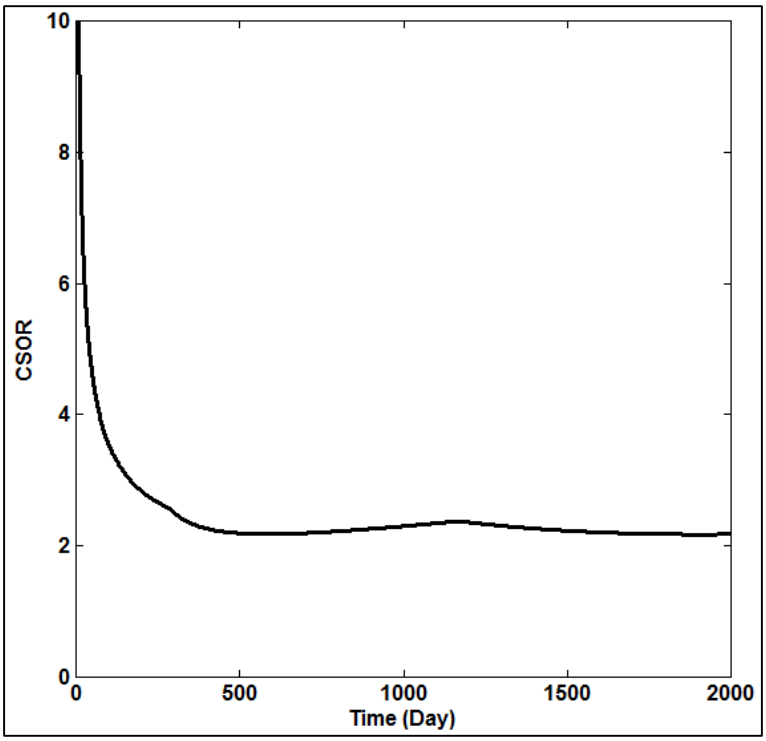

Figure 6.6: CSOR varies with time over rise, sideways expansion, and confinement phases of SAGD.

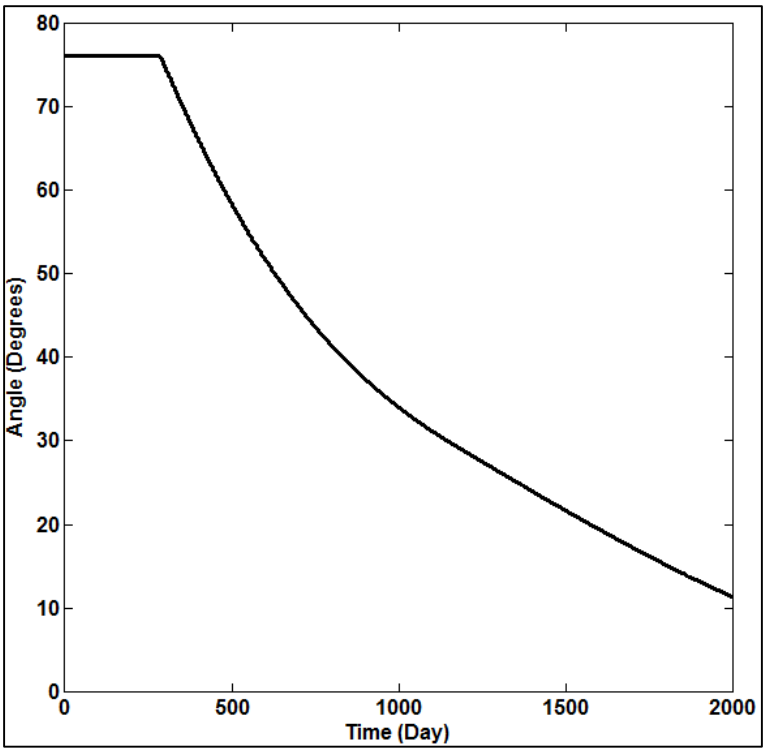

Figure 6.7: Variation of the angle between the steam chamber interface and the horizon with time in SAGD.

6.2.2 Validation of Theory with Experimental Data

Chung and Butler (1987) conducted a laboratory study on the steam-assisted gravity drainage process with Cold Lake Bitumen injecting steam at a pressure of 153 kPa. The main goal of the experiment was to figure out the effect of well configuration on water/oil emulsion production. However, the results also show the steam chamber development based on temperature isotherms, and oil production rate for the two well configuration experiments. The first configuration was designed to simulate SAGD process with two horizontal wells close to each other at the base of the formation. The second one was a vertical well at the top of the reservoir with a horizontal well near the base. Although some authors focused to validate the SAGD model with the results of the second experiment, the proposed comprehensive SAGD approach in this work is validated against the results of the first well configuration, which truly represents a SAGD process. The results for steam

chamber development, oil production rate, and recovery factor are reported from their work. Table 6.2 lists the properties and specifications of their experiment set up. The same values are used for the model validation.

Table 6.2: Rock and fluid properties of SAGD experiments (Chung and Butler 1987).

Effective permeability (m^2)	0.944×10^{-9}
Porosity	0.39
Difference between initial and residual saturation	0.95
Oil viscosity at steam temperature (m^2/day)	9
Oil density (kg/m^3)	980
Steam temperature (^{o}C)	109
Initial temperature (^{o}C)	20
Thermal diffusivity (m^2/day)	0.0507
Height of the model (m)	0.21
Thickness of the model (m)	0.03
Width of the model (m)	0.175
Viscosity-temperature coefficient, 'm'	3.6

Figure 1.5 shows the isotherms around the expanding steam chamber at 20, 90, 150, and 210 minutes. The innermost isotherm which is at 100℃ represents the approximate boundary of the steam chamber.

The red solid triangle in Figure 6.8 is the steam chamber shape predicted from the Comprehensive Constant Volumetric Displacement model at 20 minutes. At this time, there is a mismatch between the recorded steam chamber boundaries and the calculated steam chamber interfaces from the CCVD model. The CCVD model calculates the steam chamber shape very close to the reported chamber boundaries at 20 minutes after 50 minutes (red dashed line triangle). The reason is that the reservoir model (in the experiment) had been heated by steam circulation in both horizontal wells for 30 minutes before the continuous steam injection into the reservoir model started. This phase is not modelled in the CCVD theory. It is believed that this effect makes the preheated oil around the wells drain down much faster at the early time of the process.

By comparing the Figure 6.8 and 6.9, it can be concluded that in the beginning of the experiment, the steam chamber rises very fast (almost half way of reservoir height in 20 minutes) due to preheating effect. However, beyond a certain radius which heat penetration was minimal during the preheating phase, the steam chamber growth slows down. It took 70 minutes for the steam chamber to rise upwards the other half of the model height.

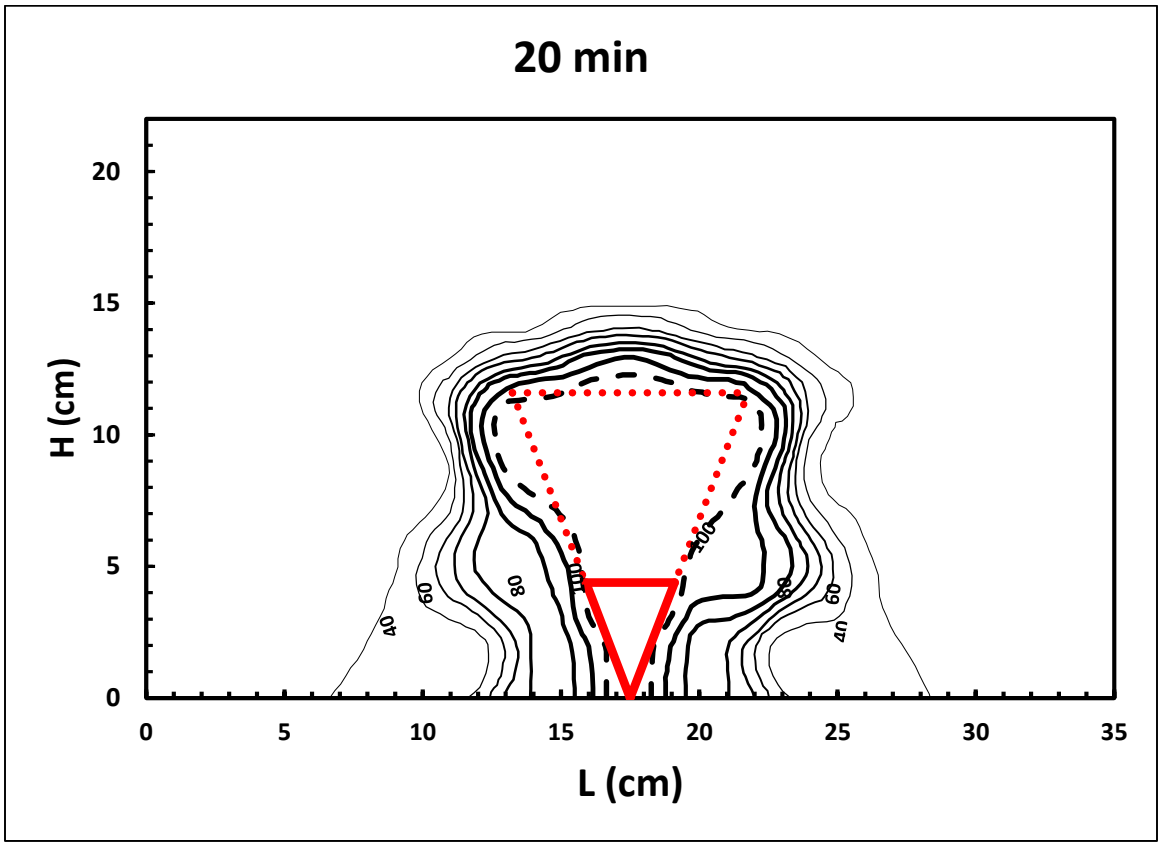

Figure 6.8: Comparison of the predicted steam chamber shape from the comprehensive approach at 20 minutes (red solid line triangle) and at 50 minutes (red-dashed line triangle), and the steam chamber boundaries (black-dashed curve) from experimental work of Chung and Butler (1987) – Rise phase.

After 90 minutes, the steam chamber reaches the top of the model. Figure 6.9 compares the steam chamber shape predicted by the CCVD model and the approximate shape of the

steam chamber from recorded isotherm (100℃) at 90 minutes. It is seen that the predicted final time of rise period and the steam chamber shape from the CCVD model and observed from the experiment are very close.

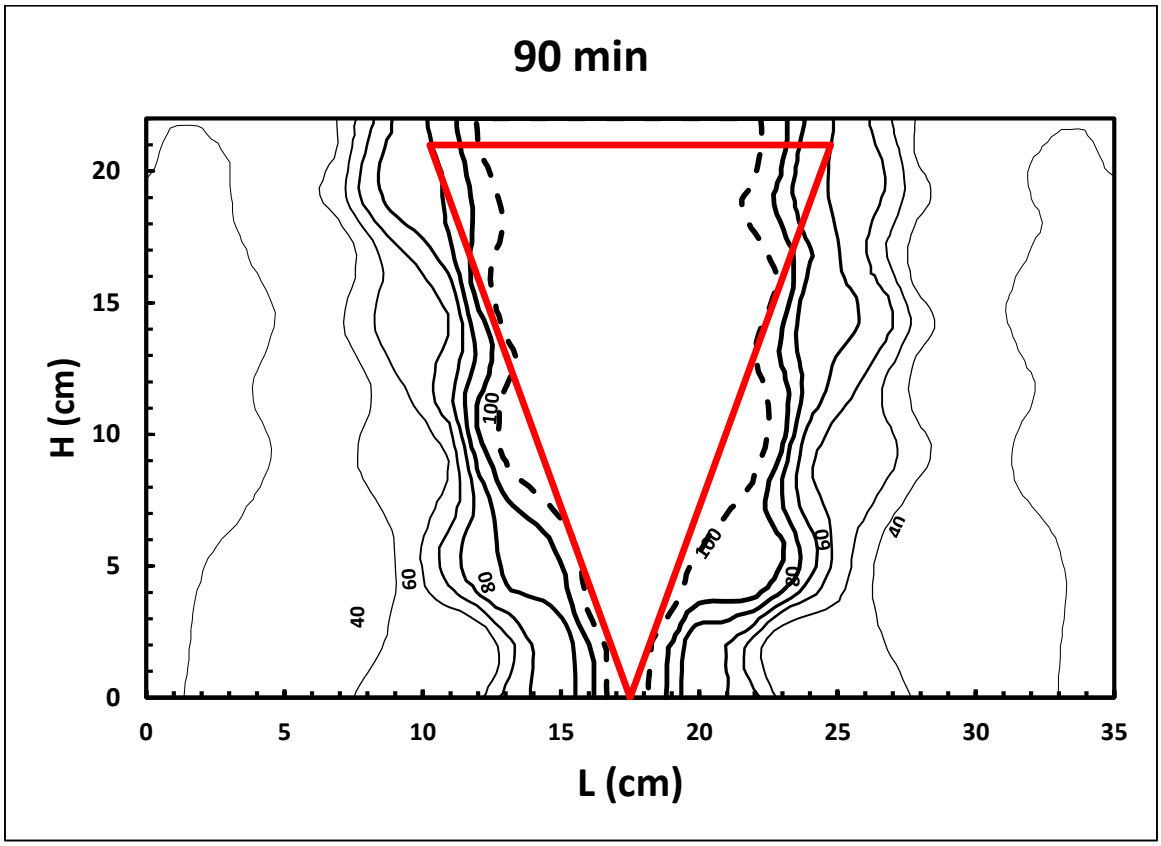

Figure 6.9: Comparison of the predicted steam chamber shape from the comprehensive approach at 90 minutes (red solid line triangle), and the steam chamber boundaries (black-dashed curve) from experimental work of Chung and Butler (1987) – Rise phase.

At 150 and 210 minutes, the CCVD model also predicts the steam chamber boundaries perfectly, as shown in Figures 6.10 and 6.11, respectively. These results confirm that the theories and models introduced in the CCVD approach represent the major mechanism of

SAGD process during rise, sideways expansion and confinement phases. Thus, the CCVD model provides an accurate tool to investigate SAGD performance.

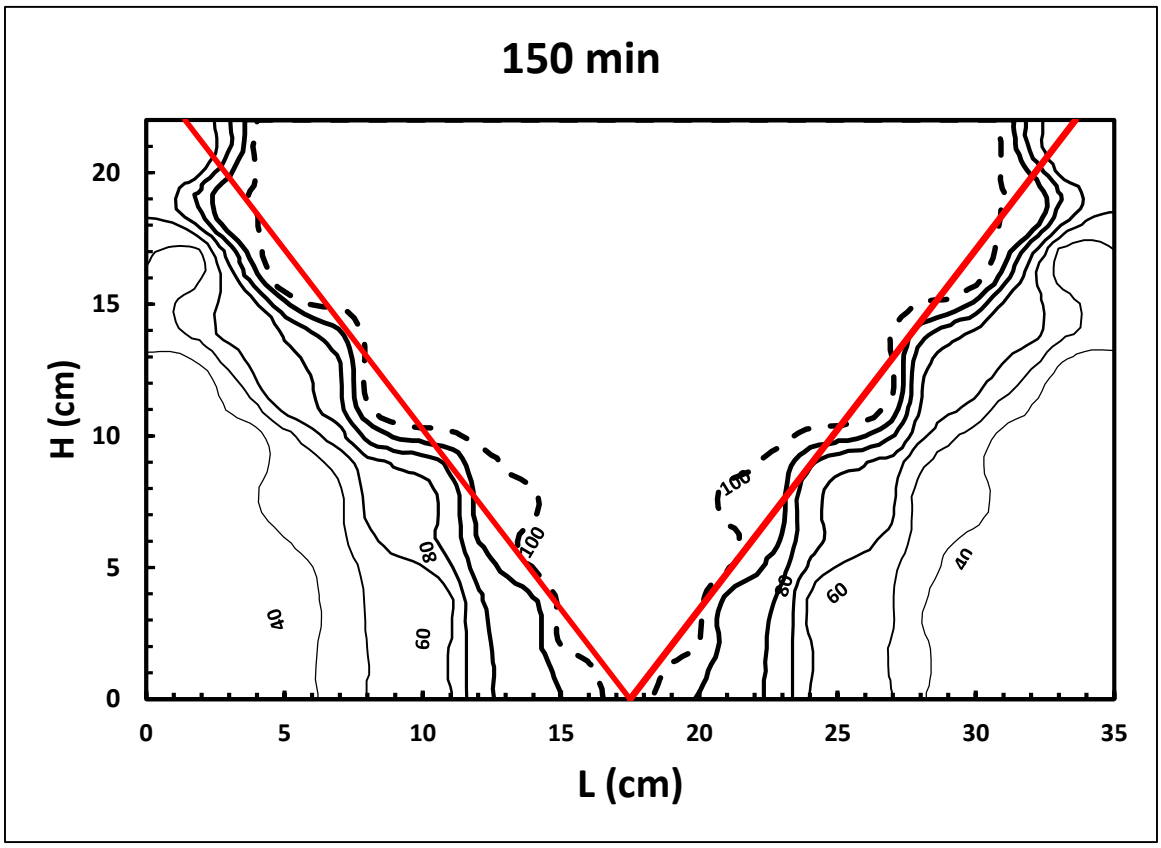

Figure 6.10: Comparison of the predicted steam chamber shape from the comprehensive approach at 150 minutes (red solid line), and the steam chamber boundaries (black-dashed curve) from experimental work of Chung and Butler (1987) – Sideways expansion phase.

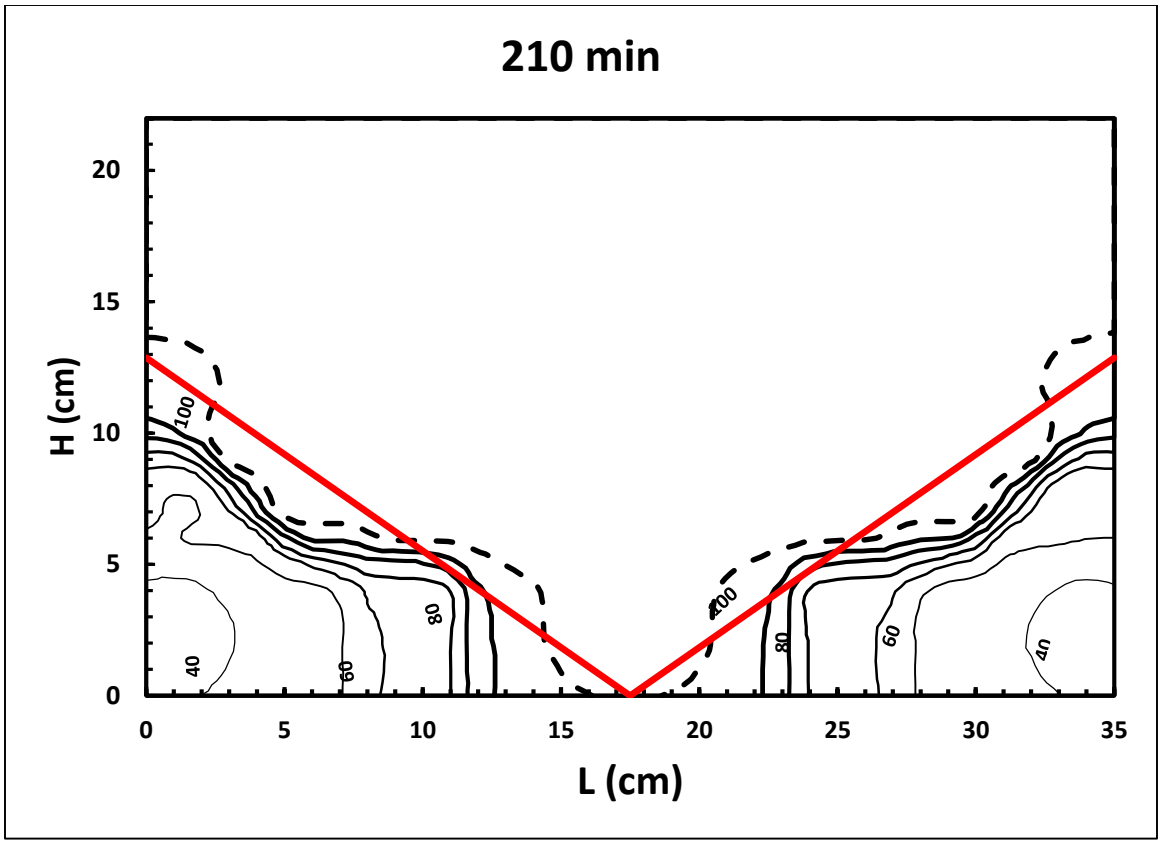

Figure 6.11: Comparison of the predicted steam chamber shape from the comprehensive approach at 210 minutes (red solid line), and the steam chamber boundaries (black-dashed curve) from experimental work of Chung and Butler (1987) – Confinement phase.

Figure 6.12 compares the oil production rate from the Comprehensive Constant Volumetric Displacement (CCVD) model and Chung and Butler (1987) experimental data. The oil production rate from the experiment at the early time of SAGD process is higher than the predicted oil rate from the CCVD model which is believed to be a result of the preheating period. However, both show an increasing trend and they reach a maximum and then start declining. There is a good match between the experiment and the CCVD prediction, especially, during the confinement phase.

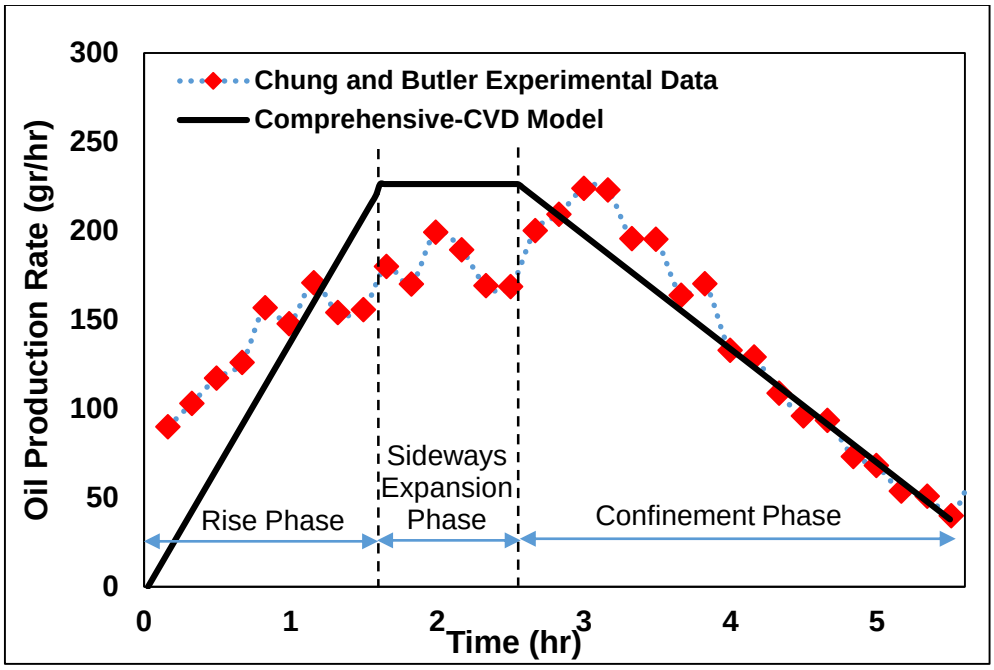

Figure 6.12: Oil production rate from experimental work of Chung and Butler (1987) is compared with the results of comprehensive approach during the three phases of SAGD.

Recovery factor versus time is shown in Figure 6.13 for the CCVD model and the experimental data. There is a very close match between the model prediction and reported experimental data. This indicates that even if preheating period may accelerate oil production rate at the early times but it has a little effect on overall recovery. For instance, after 4 hours of the experiment, a 75% recovery is resulted from both the experiment and the CCVD model. Note that the Original Oil In Place (OOIP) for this reservoir model can be calculated as:

$$OOIP = \rho_o \phi (L \times h \times W) = 0.98 \times 0.39 \times 21 \times 35 \times 3 = 842 - gm \quad (6.1)$$

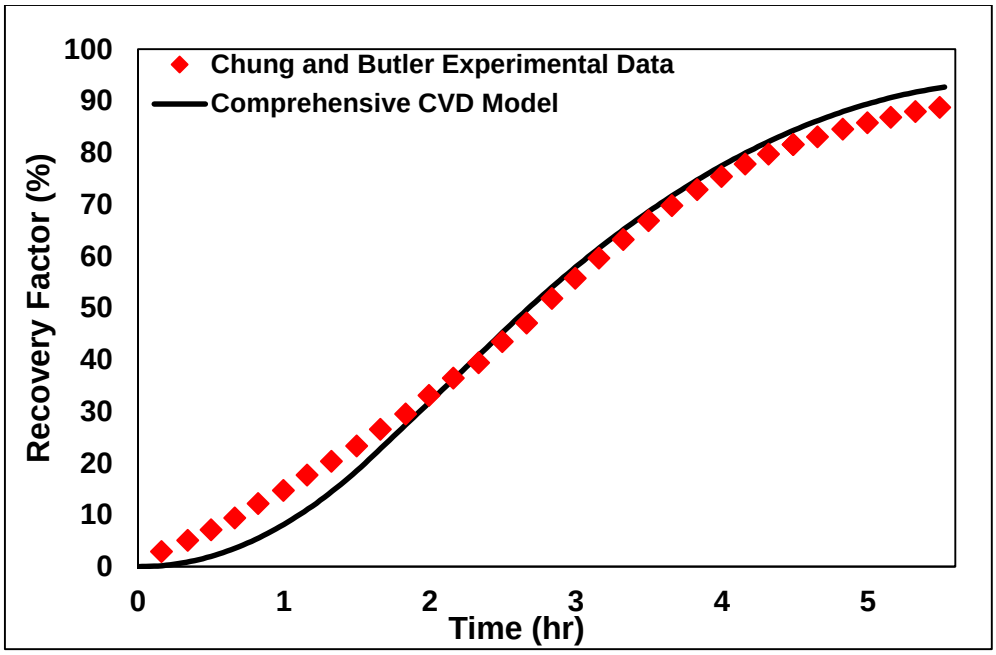

Figure 6.13: Oil recovery factor from experimental work of Chung and Butler (1987) is compared with the results of comprehensive model.

Figure 6.14 shows the oil production rate as a function of recovery factor for the CCVD model and the experimental data. The trend is similar and there is a good match.

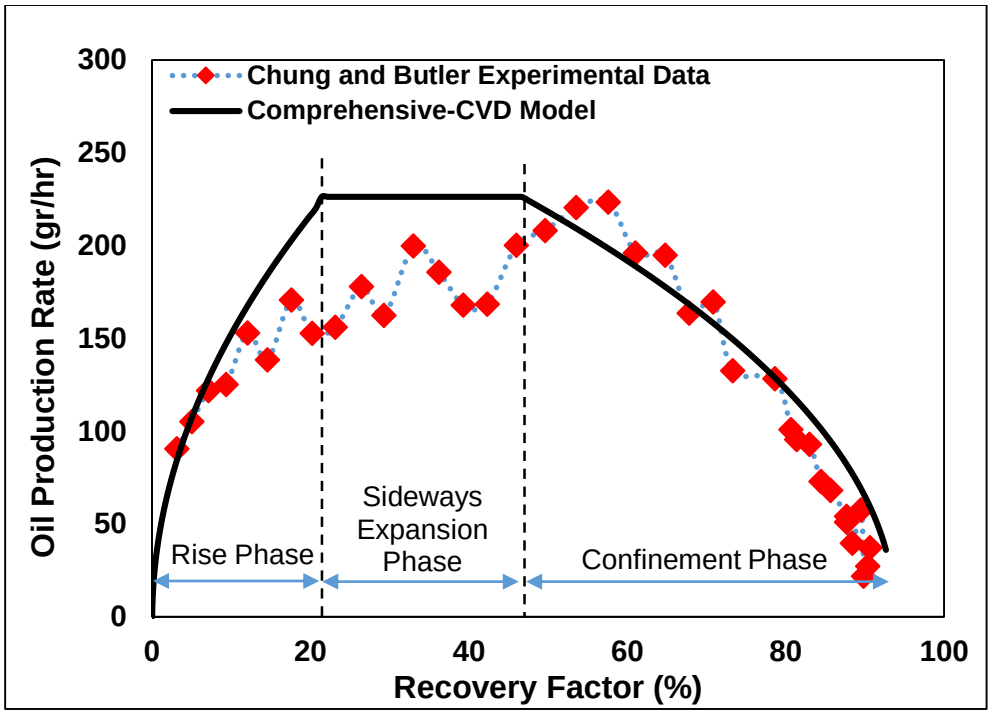

Figure 6.14: Variation of oil production rate as a function of recovery factor from experimental work of Chung and Butler (1987) is compared with the results of comprehensive model during the three phases of SAGD.

From the experiment, the available steam chamber head for drainage is reported at four different times; 20, 90, 150, and 210 minutes. Figure 6.15 compares the calculated steam chamber height from the CCVD model and experimental data (red squares). In CCVD approach, during the rise period, the steam chamber height increases linearly and then reaches the top of the model. Afterwards, the steam chamber height remains at its maximum (reservoir model thickness) before it reaches the model boundary. During the confinement period, the available steam chamber head for drainage decreases nonlinearly. It is apparent that except for the first point, the other three points are almost similar to the predicted steam chamber height.

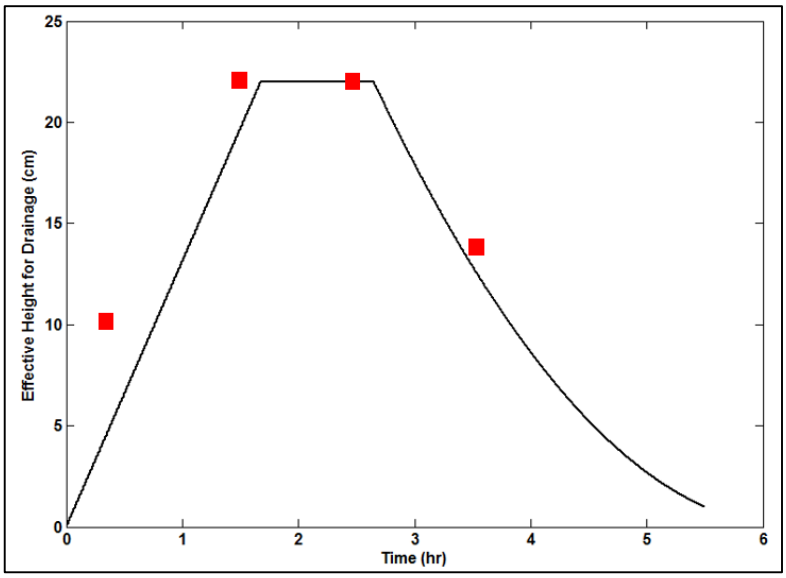

Figure 6.15: Comparison of the effective height for drainage from experimental work of Chung and Butler (1987) (red squares) with the results of the comprehensive approach during the three phases of SAGD.

Steam chamber velocity is different in the direction and magnitude from one stage to another. Figure 6.16 shows that the steam chamber velocity during the rise period is the highest, 13.2 cm/hr, compared with the rest of the process for this experiment. There is a big gap of almost 4 cm/hr, between the constant steam chamber rise velocity during the rise and the constant horizontal velocity of the sideways expansion. At the time that the steam chamber reaches the boundary of the reservoir model, the maximum steam chamber velocity jumps to 12 cm/hr, Figure 6.16, and also changes to the downward vertical direction. The vertical steam chamber velocity decreases linearly with time.

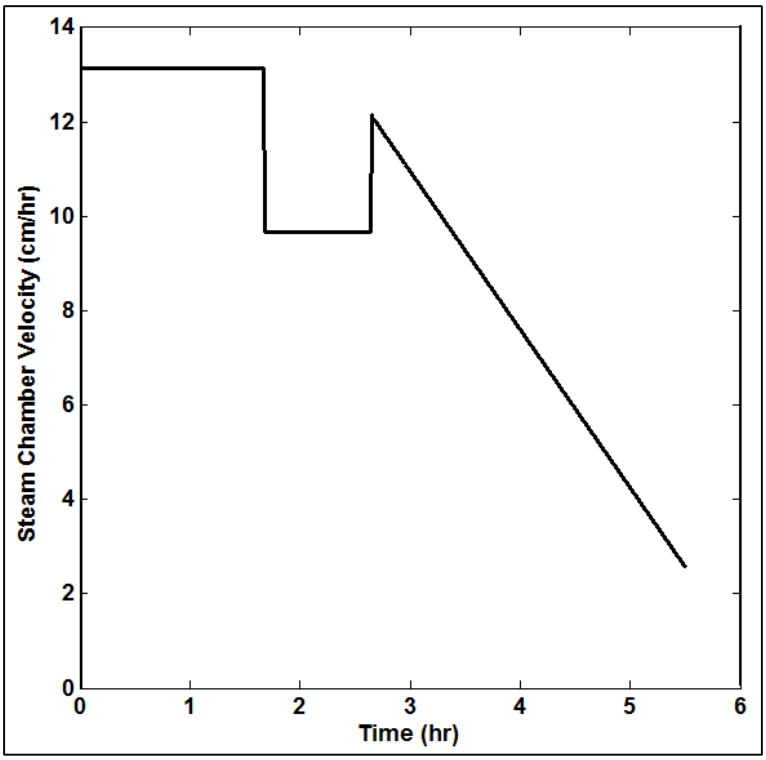

Figure 6.16: Calculated maximum steam chamber velocity based on CCVD model by use of data of Chung and Butler (1987) during rise, sideways expansion, and confinement phases of SAGD.

It was shown in all previous figures that there is a close match between the model results and the experiment. However, those small differences are believed to be due to the following reasons:

1. In the experiment, for 30 minutes steam circulation was performed prior to steam injection. The preheating period of the reservoir model is not included in the comprehensive theory. This is the reason for the small gap between the experimental data and the predicted oil rate from CCVD model at the early time.
2. Error in collecting and calculating the experimental results
3. Steam chamber is approximated as an inverted triangle in our model. As can be seen from Figure 1.5, the inverted triangle it is the most appropriate geometry for the steam chamber shape but the lines are not exactly straight.

4. The steam chamber shapes are approximate because the recorded steam chamber isotherms representing the steam-oil interface are at 100 ^{o}C not 109 ^{o}C.

6.2.3 Validation of Theory with Field Data

Figures 6.17 and 6.18 compare oil production data and cumulative oil of Christina lake Well A01-6 (©geoSCOUT) with the results of the Comprehensive Constant Volumetric Displacement (CCVD) model by use of the well and reservoir specifications in Table 6.3 (Cenovus Energy, 2012-2013). Figure 6.17 shows that the calculated oil production rate from the CCVD model is in a good agreement with the reported well data. Oil rate increases initially during the rise period and reaches a maximum at nearly 150 m^3/day and it stays at this rate for around 2.5 years. Afterwards, the oil production rate decreases to almost zero. It is seen that the lifetime of SAGD well pair from the analytical model is nearly the same as in practice, eight years and four months. The cumulative oil production from the comprehensive model and well data are almost the same and it reaches 303,040 m^3 at the end of the production history as is seen in Figure 6.18. This indicates that the proposed comprehensive approach of SAGD is in a very good agreement with field data in addition to experimental data. Figures 6.19 and 6.20 compare oil production data and cumulative oil for Christina lake Well A01-4 (©geoSCOUT) with the results of the Comprehensive Constant Volumetric Displacement (CCVD) model by use of the well and reservoir specifications in Table 6.3 (Cenovus Energy, 2012-2013). The producible well length of this well pair is 323 m larger than well pair A01-6 but the reservoir thickness is 2 m shorter. The comprehensive model shows a close match with the well data for this well pair as well. The oil production rate of the model overestimates the Well A01-4 oil rate during the confinement phase (See Figure 6.19). This overestimation can also be seen in Figure 6.20 at the late times of the SAGD operation. The likely reasons are the effect of reservoir heterogeneity, operating conditions, and steam distribution along the horizontal well. However, the foremost reason for the lack of agreement (as in Christina Lake Well A01-4) between field and model results (analytical or numerical simulation) is steam distribution along the injector. Given a 1000 m long injector, steam distribution is not

uniform, and there are many instances of discontinuous steam chambers. In the present model predictions, absolutely no data adjustments were carried out, and chamber conformance (continuity) was assumed to be 100%. Similarly, the lifetime of SAGD well pair from the analytical model is nearly the same as in practice, ten years and five months.

Table 6.3: Well and reservoir specifications (Cenovus Energy, 2012-2013).

Well No.	Net SAGD Pay (m)	Drilled Length (m)	Spacing (m)	Average porosity	Average initial oil saturation	Average reservoir permeability (Darcy)
A01-4	26.95	723.33	115	0.35	0.78	6
A01-6	29.05	399.08	115	0.34	0.81	6

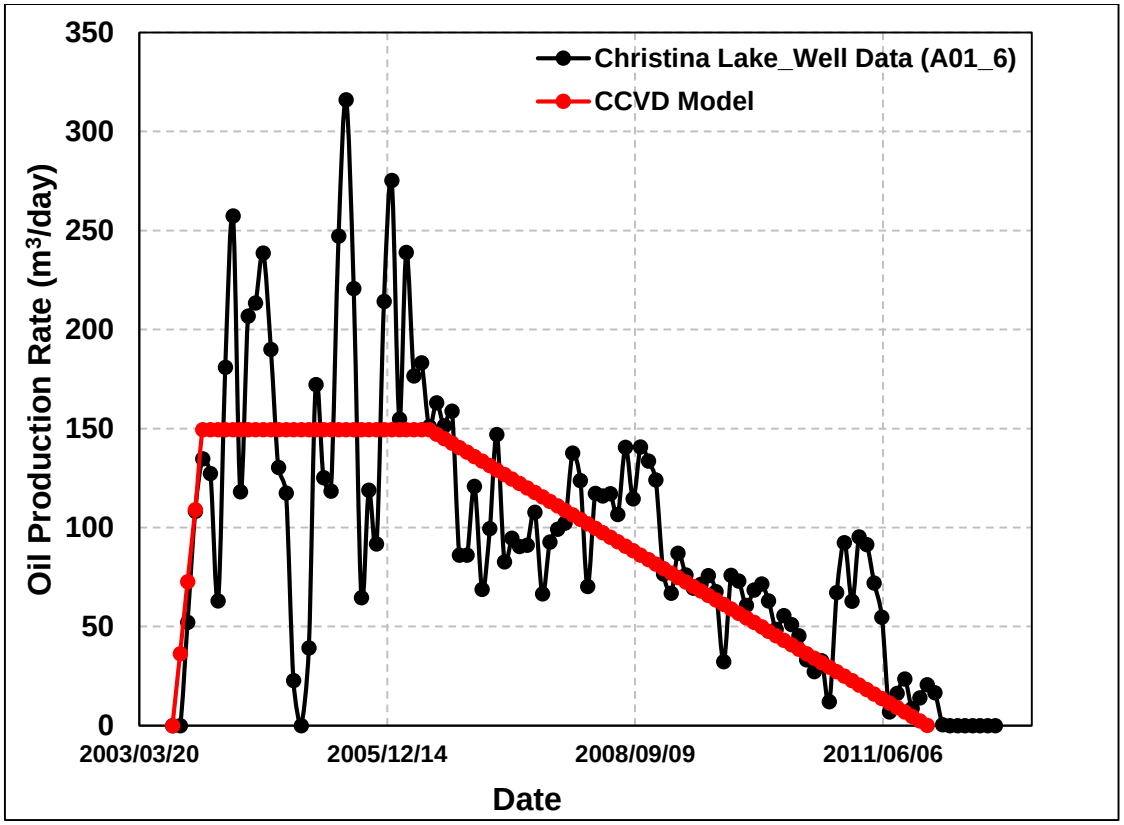

Figure 6.17: Comparison of oil production rate from the analytical comprehensive model and well production data of Christina Lake Well A01-6.

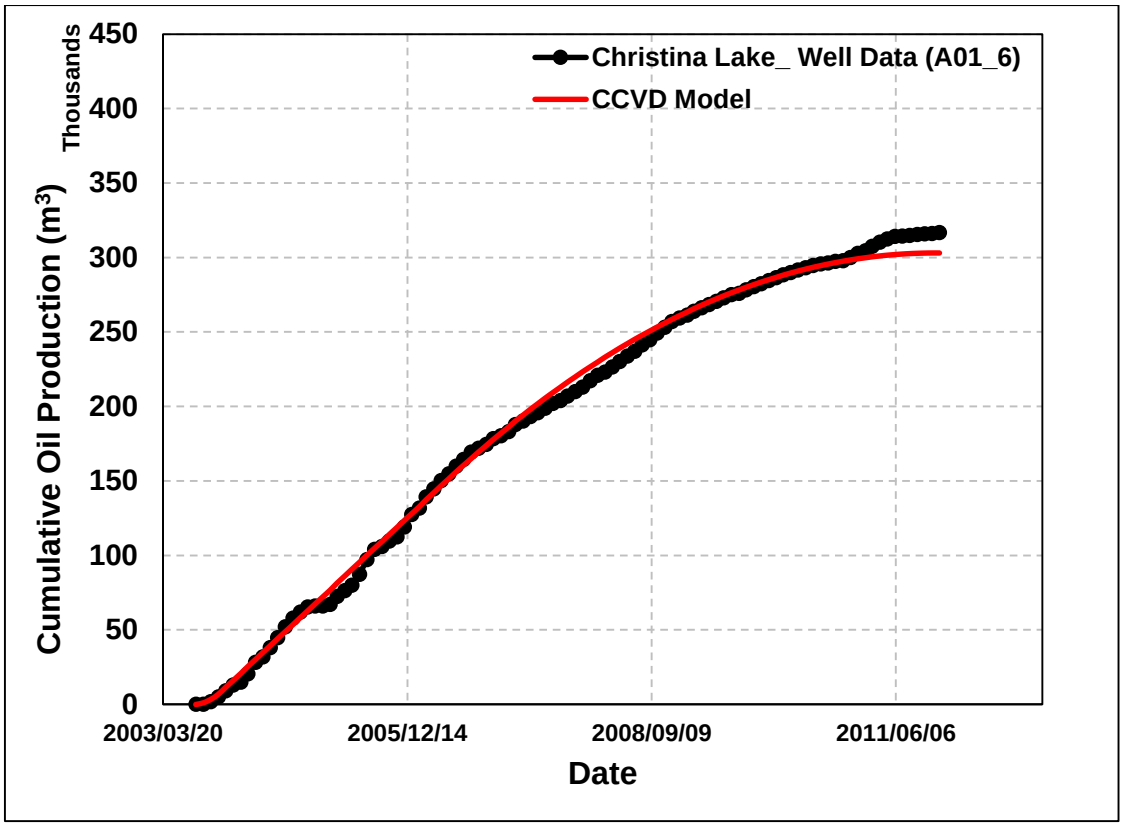

Figure 6.18: Cumulative oil production data of Christina Lake Well A01-6 is compared with the analytical comprehensive model.

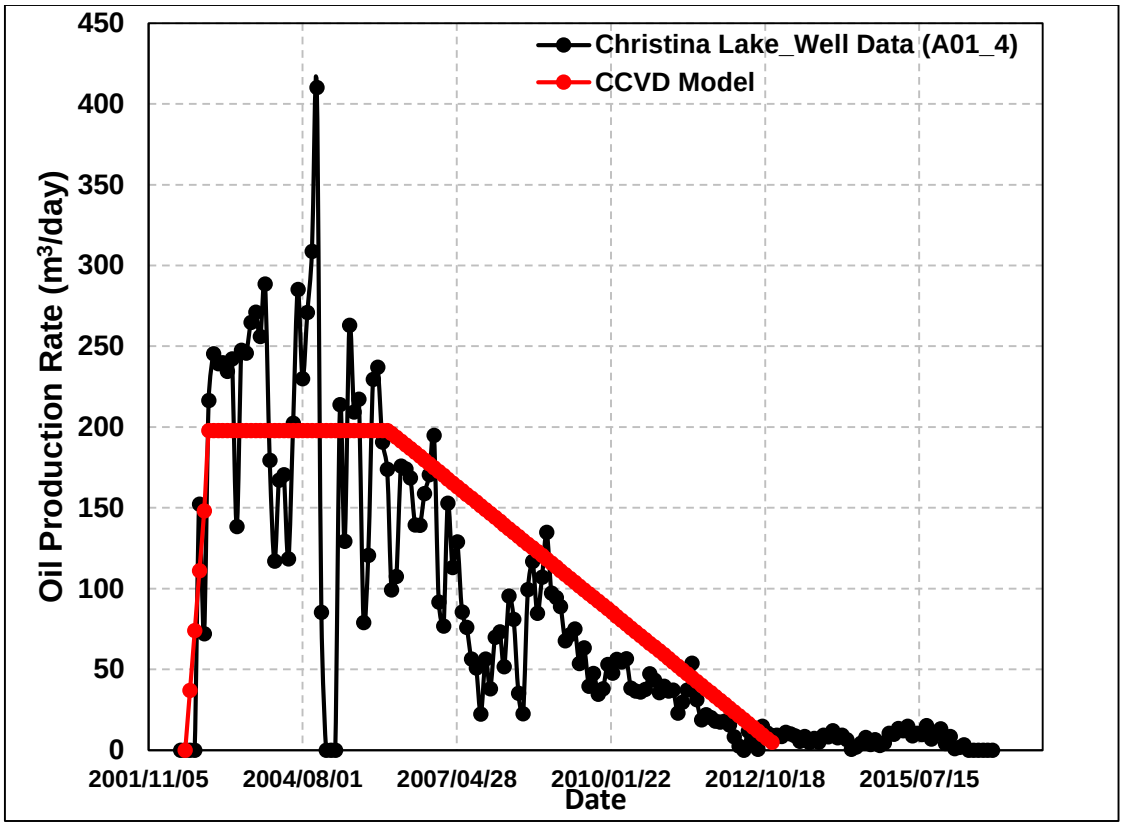

Figure 6.19: Comparison of oil production rate from the analytical comprehensive model and well production data of Christina Lake Well A01-4.

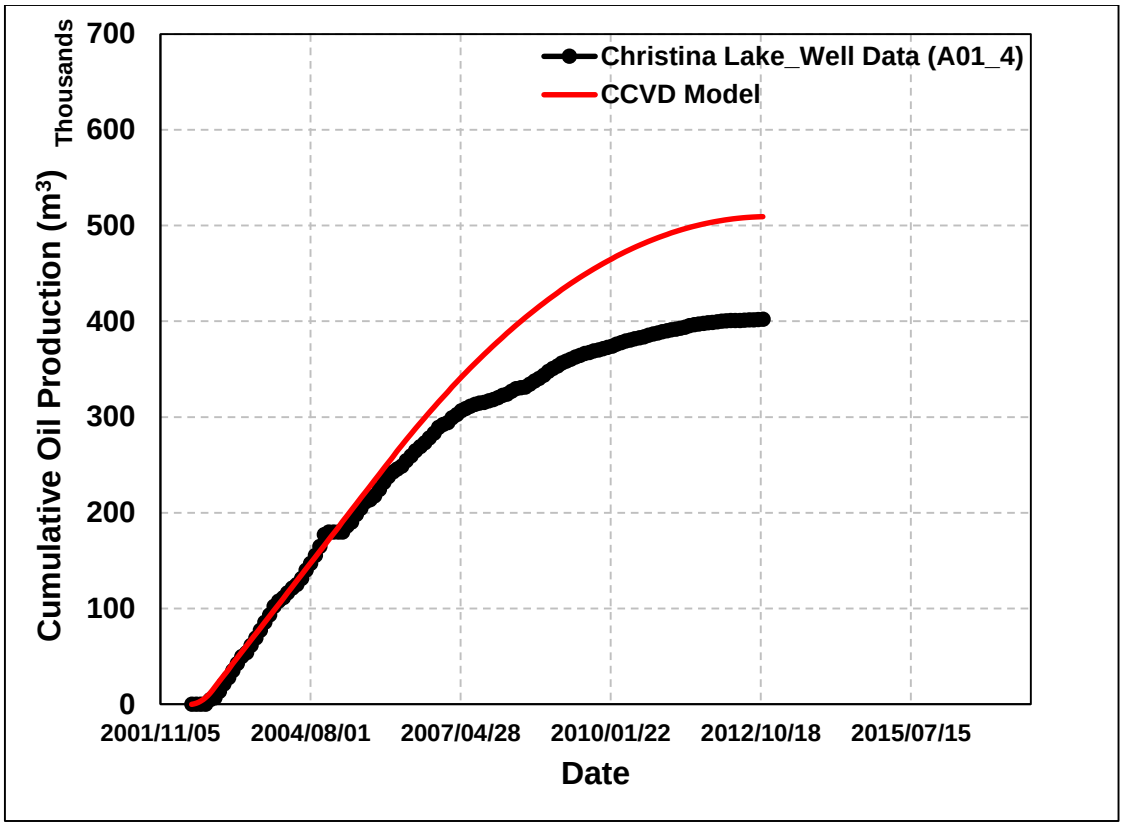

Figure 6.20: Cumulative oil production data of Christina Lake Well A01-6 is compared with the analytical comprehensive model.

6.3 Comprehensive CHI Model - Summary of Governing Equations

The Comprehensive Constant Heat Injection (CCHI) model of SAGD process also consists of three sets of equations for the rise, sideways expansion, and confinement phases derived in the previous chapters. The equations are summarized in Table 6.4.

Table 6.4: Summary of all governing equations of the CCHI approach.

Model Name	Equation Number
Rise velocity – Rise period	Eq (3.7)
Steam chamber height – Rise period	Eq (3.8)
End time of the steam chamber rise period	Eq (3.9)
The constant angle between steam chamber and the horizon	Eq (3.15)
Oil production rate – Rise period	Eq (3.13)
Cumulative oil production – Rise period	Eq (3.14)
Heat rate to steam zone – Rise period	Eq (3.21)
Heat rate to overhead oil zone – Rise period	Eq (3.37)
Heat rate to the oil zone at the sides of the steam chamber – Rise period	Eq (3.46)
Maximum chamber movement at the top of reservoir – Sideways expansion	Eq (4.55)
Oil production rate – Darcy's law – Sideways expansion	Eq (4.53)
Volumetric oil displacement rate – Darcy's law – Sideways expansion	Eq (4.54)
Temperature profile ahead of the steam – oil interface – Sideways expansion	Eq (4.52)
Heat loss rate – Sideways expansion	Eq (4.27)
Outflow heat rate – Sideways expansion	Eq (4.48)
Heat rate to the steam chamber – Sideways expansion	Eq (4.47)
Maximum steam chamber velocity in vertical direction – Confinement period	Eq (5.23)
Oil production rate – Darcy's law – Confinement period	Eq (5.21)
Volumetric oil displacement rate – Confinement period	Eq (5.5)
Angle between the steam-oil interface and the horizon – Confinement period	Eq (5.22)
Temperature profile beyond the steam chamber edge – Confinement period	Eq (5.20)

6.3.1 Results

The Comprehensive Constant Heat Injection (CCHI) approach is applied to calculate oil production rate, cumulative steam injection, and CSOR by use of data in Table 4.2. Oil production rate as a function of time is shown in Figure 6.21. The oil production rate increases during the rise period and reaches a peak of 0.2665 m^3/day per unit length of well after 287 days. Afterwards, in CCHI approach, steam is injected at a constant rate of 0.705 (m^3/day-m) therefore unlike the oil production rate from the CCVD, oil production rate decreases.

The steam chamber velocity decreases in this approach (as explained in Chapter 4). As a result, the confinement time at which the expanding steam chamber reaches half-way spacing between wells occurs after 1237 days. Thereafter, the oil production rate decreases with a higher rate as seen in Figure 6.21. Note that the oil production rate at the end of the run time (2000 days) is 0.21 m^3/day-m which is 30% higher than corresponding oil rate at the end of CCVD. However, during the sideways expansion phase, the constant oil rate from CCVD approach is higher than the calculated oil rate from CCHI model. In total, the cumulative oil production from the CCVD and CCHI approaches are almost the same after 2000 days (See Figure 6.22).

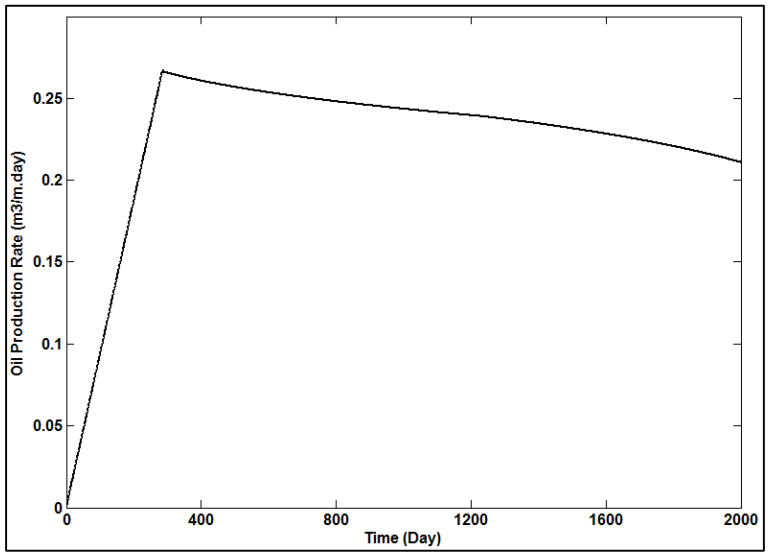

Figure 6.21: Oil production rate of the CCHI approach as a function of time over the three phases of SAGD process.

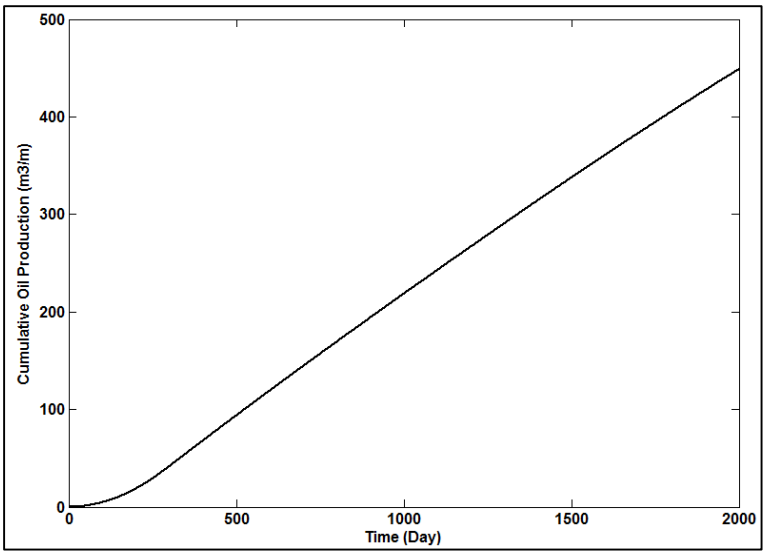

Figure 6.22: Cumulative oil production of SAGD process (CCHI approach) over a 2000-day time interval.

Figure 6.23 shows the calculated cumulative steam injection as a function of time. After approximately five years and half, the cumulative steam injected (excluding the preheating period) in the SAGD well pair in a confined model is 1298.5 m^3/m. CSOR decreases in the beginning to a minimum of 2.57 m^3/m^3, but it increases slowly afterwards till the end of the run time (See Figure 6.24). The steam injection rate, oil production rate, and CSOR are also displayed in Figure 6.25.

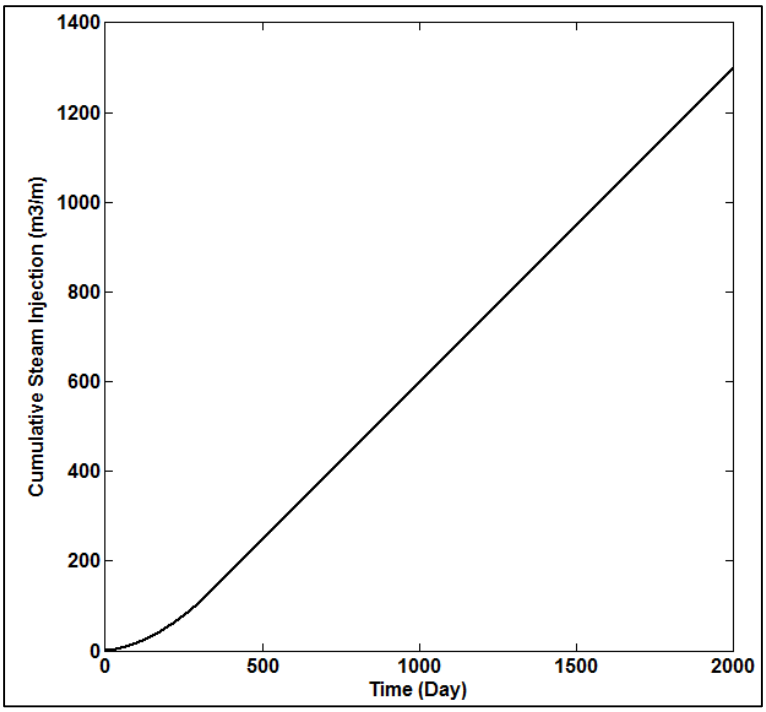

Figure 6.23: Cumulative steam injection of the CCHI approach per unit length of horizontal well as a function of time.

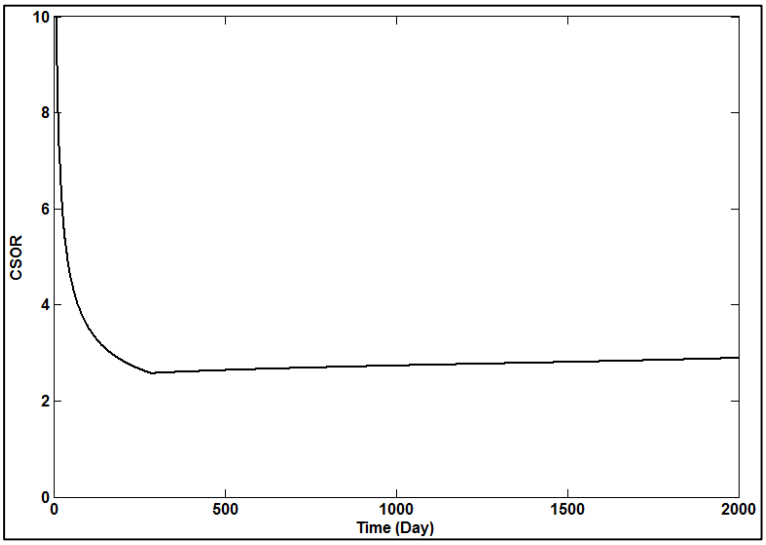

Figure 6.24: CSOR varies with time over rise, sideways expansion, and confinement phases of SAGD.

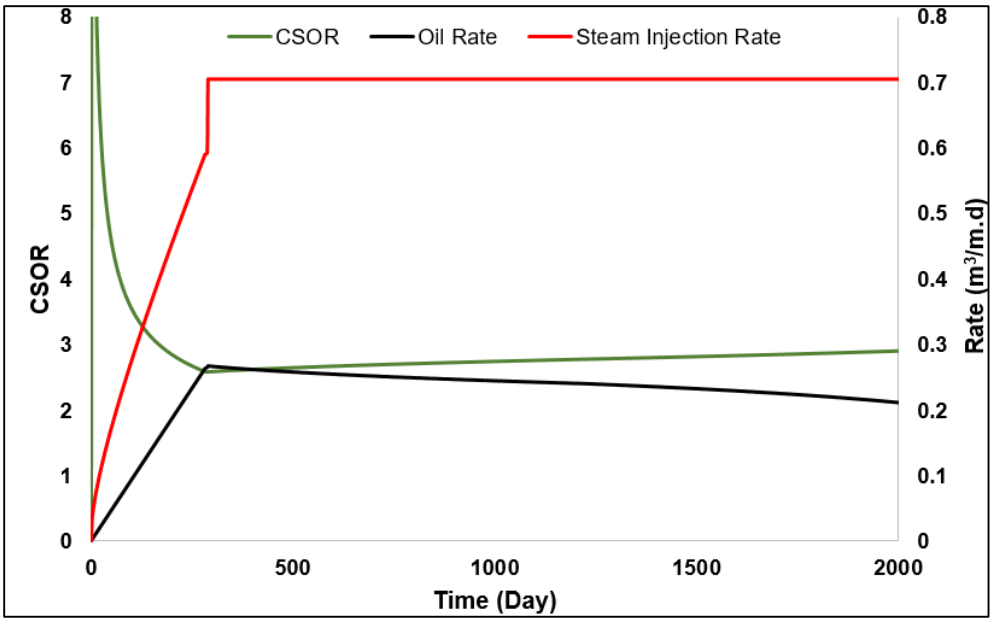

Figure 6.25: Calculated Oil production rate, steam injection rate, and CSOR from the CCHI approach as functions of time.

7. NEW MATHEMATICAL TREATMENT OF THE SOLVENT-SAGD PROCESS

7.1 Introduction

Steam Assisted Gravity Drainage (SAGD) has a few undesirable aspects, such as high steam requirement and steam generation resulting in significant greenhouse gas emissions. The oil industry is developing new processes to overcome this shortcoming. Adding a small amount of condensable gas as a solvent to steam was proposed as one of the solutions, named variously as Expanding Solvent Steam-Assisted Gravity Drainage (ES-SAGD), Solvent Aided Process (SAP), or Liquid Addition to Steam for Enhanced Recovery (LASER), etc. The economics of these processes depend on the oil production rate, solvent requirement and solvent retention in view of the high cost of solvents. In addition, it remains unclear which solvent gives better recovery, if any, compared to the steam only process, and what would be the optimal amount of solvent concentration in the injected steam. Evaluating the performance of this process has mostly been done by numerical simulation. However, the simulation models of solvent-SAGD process are somewhat unreliable because of extremely small diffusivity and large numerical dispersion. Only a few analytical treatments of this process are reported.

In the previous mathematical works, the oil production rate in a solvent-SAGD process was calculated without connection with the chamber condition; heat and solvent losses, injection rate, and interface extension. In this chapter, a new analytical model is developed to describe the solvent-SAGD performance based on the combination of an overall solvent mass balance, heat balance and volumetric oil displacement and Darcy oil rate using a mixture viscosity model as a function of temperature and solvent concentration ahead of the front which satisfy equilibrium in the system.

The objectives of this work are to predict: vapour-steam chamber growth, oil production rate, solvent production rate, solvent loss (or solvent retention) rate, and the effect of solvent type and concentration on the solvent-SAGD process. The results show that the

rate of solvent retention increases over time, while the rate of solvent and bitumen production decreases.

The efficiency of this process is evaluated using cumulative steam-oil and solvent-oil ratios, allowing a comparison of the SAGD and solvent-SAGD processes for different solvents. On the whole, the results of this approach give a better understanding of the mechanism of oil production during the solvent-SAGD process by interconnecting the vapour chamber conditions and the conditions of heated and diluted oil ahead of the interface.

7.2 Analytical Model

7.2.1 Modelling Assumptions

In modelling of solvent-SAGD process, several mechanisms are involved. All of these mechanisms cannot be accounted for. Therefore, in developing the analytical model of solvent-SAGD by taking into account the major mechanisms, the following assumptions are made:

1. Heat and solvent mass transfers are directed normal to the steam chamber.
2. Steam-oil interface geometry is a straight line with a fixed end at the producer.
3. Chamber pressure is sum of partial pressures of solvent and steam and it remains constant with time.
4. Constant chamber temperature is the steam temperature corresponding to the steam partial pressure.
5. The model is developed for the condensable gases such as butane, propane, and hexane.
6. Total mass injection rate (steam and solvent) remains constant over time.
7. Temperature and solvent concentration distributions are derived based on a pseudo steady-state condition.

7.2.2 Mathematical Formulation

In this work, by assuming a constant rate of steam and solvent injection and relating this to the vapour chamber and the mobilized oil ahead of the vapour and oil interface, an analytical model is derived for evaluating the solvent-SAGD process. In this analytical approach, unlike previous models, it is assumed that the injected solvent vapour condenses at the chamber edges and the heat and mass fluxes at the vapour-oil interface are the limiting boundary conditions. The injected solvent travels with steam in different directions; there would be an accumulation of solvent around the boundaries of the chamber. The accumulated solvent at the edges of the vapour chamber condenses to keep the vapour chamber at the concentration of the injected solvent. At the advancing front, the condensed solvent mixes with the oil and reduces oil viscosity. The solvent accumulated at the top boundary of the reservoir is assumed to be retained inside the vapour chamber. A conservative solvent loss model is assumed in this approach which is similar to the conservative heat loss term in the energy balance equation.

The Constant Heat Injection (CHI) model introduced in previous chapters is extended to include solvent co-injection with steam at a constant total rate of injection.

The model is developed for an arbitrary interface at $t = t_n$ and position $\theta = \theta_n$. The horizontal vapour chamber velocity at the top of the reservoir (x'_H) is the primary unknown in the set of equations. This maximum horizontal vapour chamber velocity is obtained from a combination of an overall solvent mass balance, heat balance and volumetric oil displacement and Darcy oil rate using a mixture viscosity model as a function of temperature and solvent concentration ahead of the front. It is assumed that mass and heat diffusion occur in a direction normal to the interface.

7.2.2.1 Overall Heat Balance – Temperature profile

It is assumed that the total injection rate (solvent and steam) is constant. The temperature differential equation is developed using overall heat in the system, for a linear vapour chamber interface and an arbitrary interface at $t = t_n$ and position $\theta = \theta_n$.

In this approach, heat loss to the overburden, solvent loss, constant injection rate, and extending steam chamber interface are expected to have a limiting effect on the growth rate of the chamber. Based on the overall heat balance, constant heat injected at a constant rate is distributed in the reservoir in three different ways: heat loss rate to the overburden, rising vapour chamber and the produced oil temperature increase from T_r to T_s, and outflow of heat into the oil zone ahead of the advancing front, assumed to be by conduction only. In the solvent-SAGD process, the injected heat is the sum of the latent heats of vaporization of steam and solvent.

$$q_{inj} = i_{tot}\left\{\left(1 - C_{sol}^{inj}\right)f_s^{st}L_v^{st} + C_{sol}^{inj}f_s^{sol}L_v^{sol}\right\} \tag{7.1}$$

In the above equation i_{tot}, is the total mass rate for the solvent and water and C_{sol}^{inj} is the injected mass fraction of the solvent.

From the above equation, it can be concluded that the heat injection rate in the case of solvent-SAGD is smaller than that of SAGD due to the presence of the solvent in the vapour and, in turn, the considerable lower latent heat of vaporization of the solvent. In a similar manner, as explained in Subsection 4.3.2.1, temperature profile for a solvent-SAGD process is derived as:

$$T(\xi, t) = \frac{\alpha}{K_{res}Hx'_H}\left\{q_{inj} - \left(\frac{2K_{ob}\Delta T}{\sqrt{\pi\alpha_{ob}}}\frac{x_H}{\sqrt{t}} + Hx'_H(\rho C)_{res}\Delta T\right)\right\}e^{-\frac{sin\theta}{2\alpha}x'_H\xi} + T_r \tag{7.2}$$

Note that the maximum steam chamber velocity in the above temperature profile, unlike in SAGD, is affected by heat and mass transfer. Moreover, at the same rate of injection, heat injection rate in this approach is different from the corresponding SAGD process.

7.2.2.2 Overall Solvent Mass Balance – Concentration Profile

It is assumed that the total injection rate (solvent and steam) is constant. The solvent concentration differential equation is developed using overall mass balance in the system, for a linear vapour chamber interface and an arbitrary interface at $t = t_n$ and position $\theta = \theta_n$. Solvent concentration distribution beyond the edge of the vapour-oil chamber interface is derived by solving the above differential equation. The injected solvent in the process can be consumed in three ways: accumulation as a vapour phase in the growing vapour chamber, diffusion into the oil zone, and retention in the system. It is assumed that the solvent concentration in the vapour chamber is equal to the injection point concentration. The overall mass balance for the solvent can be written as:

$$\dot{m}|_{in} - \dot{m}|_{out} = \frac{\partial m_{sol}}{\partial t} \tag{7.3}$$

$$\dot{m}|_{in} = C_{sol}^{inj} i_{tot} \tag{7.4}$$

The solvent injected as a vapour phase travels with steam in all directions. As a result, it accumulates at the boundaries of the vapour chamber and condenses as it reaches the required concentration and temperature for the phase change. In our model, there are two boundaries; overburden rock at the top and the vapour-oil interface. Both of these boundaries extend over the course of time. As a result, the vapour loses heat at the boundaries. Steam provides heat to the system, and solvent diffuses into the oil zone and dilutes the bitumen. It is believed that a combination of these two mechanisms reduces the bitumen viscosity and supports enhanced recovery and net energy efficiency. The solvent plays a role in reducing oil viscosity if it condenses at the vapour-oil interface. Thus, solvent condensation at any other place is considered to be a loss.

$$\dot{m}|_{out} = \dot{m}|^{top} + \dot{m}|^{front} \tag{7.5}$$

Condensed solvent at top and the front can be related as:

$$\frac{\dot{m}|^{top}}{\dot{m}|^{front}} = \frac{x_H}{L_{int}} \tag{7.6}$$

$$\dot{m}|^{top} = \cos\theta_n \, \dot{m}|^{front} \tag{7.7}$$

$$\dot{m}|_{out} = (1 + \cos\theta_n) \, \dot{m}|^{front} \tag{7.8}$$

We call it conservative design for the solvent loss. The above equation indicates that at the beginning of the process ($\theta_n = \frac{\pi}{2}$), there is no solvent mass loss and all the injected solvent diffuses into the oil zone and is stored in the growing chamber as vapour. Over time, due to increasing solvent loss (retention), mass flux at the front decreases.

$$\frac{1}{2} C_{sol}^{inj} i_{tot} - (1 + \cos\theta_n) \, \dot{m}|^{front} = \frac{1}{2} H \phi S_v \rho_{sol}^{v} x'_H \tag{7.9}$$

$$S_v = 1 - S_{or} \tag{7.10}$$

C_{sol}^{inj} is the injected solvent mass fraction, and S_v is the saturation of the vapour phase in the depleted chamber.

It is assumed that all the condensed solvent at the vapour-oil interface is available to diffuse into the oil zone and contributes to bitumen dilution. The rate of mass diffusion can be calculated based on Fick's law in the direction normal to the interface as:

$$\dot{m}|^{front} = -D_{so} A_{int} \rho_{sol} \left(\frac{\partial C}{\partial \xi}\right)_{\xi=0}$$

(7.11)

For a unit length of the horizontal well,

$$A_{int} = 1 \times L_{int} = \frac{H}{\sin \theta_n}$$

(7.12)

In the above equation, C is the volume fraction of solvent in the fluid mixture, and D_{so} is the diffusivity coefficient of the solvent into the bitumen. Substituting the above equations into the solvent mass balance equation,

$$\frac{1}{2} C_{sol}^{inj} i_{tot} + (\csc \theta_n + \cot \theta_n) D_{so} \rho_{sol} H \left(\frac{\partial C}{\partial \xi}\right)_{\xi=0} = \frac{1}{2} H \phi (1 - S_{or}) \rho_{sol}^{v} x'_H$$

(7.13)

There are two unknowns in the above equation; concentration gradient at the interface, $\left(\frac{\partial C}{\partial \xi}\right)_{\xi=0}$, and vapour chamber velocity, x'_H. The concentration gradient can be obtained based on the vapour chamber velocity as:

$$\left(\frac{\partial C}{\partial \xi}\right)_{\xi=0} = -\frac{0.5}{(\csc \theta_n + \cot \theta_n) D_{so} \rho_{sol} H} \left\{C_{sol}^{inj} i_{tot} - H \phi (1 - S_{or}) \rho_{sol}^{v} x'_H\right\}$$

(7.14)

So, the concentration gradient at the interface is a function of solvent concentration at the injection point, total injection rate, interface angle, reservoir rock and fluid properties and most importantly the vapour chamber velocity. This concentration gradient at the interface will be used as a Neumann boundary condition for the concentration equation in differential form.

One-dimensional advection-diffusion equation in a direction normal to the vapour chamber interface without bulk flow in this direction and assuming a constant diffusion coefficient can be written as:

$$\frac{\partial C}{\partial t} = D_{so}\frac{\partial^2 C}{\partial Z^2}$$

(7.15)

For a diffusive front velocity U_f, the pseudo steady-state concentration equation and the boundary conditions are given by:

$$\frac{d^2C}{d\xi^2} + \frac{U_f}{D_{so}}\frac{dC}{d\xi} = 0$$

$$\left(\frac{\partial C}{\partial \xi}\right)_{\xi=0} = -\frac{0.5}{(\csc\theta_n + \cot\theta_n)D_{os}\rho_{sol}H}\left\{C_{sol}^{inj} i_{tot} - H\phi(1-S_{or})\rho_{sol}^{v} x'_H\right\}$$

$$C(\xi \to \infty) = 0$$

(7.16)

Solving this equation, the concentration distribution ahead of the advancing front is given by:

$$C(\xi, t) = \frac{1}{(1+\cos\theta)\rho_{sol}x'_H}\left\{\frac{i_{tot}C_{sol}^{inj}}{H} - \phi(1-S_{or})\rho_{sol}^{v}x'_H\right\} e^{-\frac{1}{2D_{so}}sin\theta x'_H \xi}$$

(7.17)

Knowing the temperature and concentration profiles ahead of advancing front, the reduced bitumen viscosity can be predicted under the effect of heating and dilution.

7.2.2.3 Viscosity Model

In the solvent-SAGD process, bitumen drainage rate mainly depends on viscosity reduction by heat and solvent mass transfer, apart from gravity as the main driving force. Bitumen

viscosity should be determined based on the temperature and concentration distributions ahead of the advancing front. In this study, a mixture viscosity (solvent and bitumen) model as a function of temperature is developed from the combination of Andrade (1930)'s viscosity-temperature equation and Shu (1984)'s mixture viscosity equation.

Andrade's viscosity model as a function of temperature is given by:

$$\mu = ae^{\frac{b}{T}} \tag{7.18}$$

where *a* and *b* are constants and viscosity in the above equation is calculated in centipoise. A correlation was proposed by Lederer (1933) in which the heavy oil viscosity depends on the volume fraction of the dissolved solvent:

$$ln\mu_{mix} = x_b ln\mu_b + x_{sol} ln\mu_{sol} \tag{7.19}$$

where,

$$x_b = \frac{\alpha V_b}{\alpha V_b + V_{sol}} \quad , \ 0 < \alpha < 1 \quad , \ x_{sol} = 1 - x_b \tag{7.20}$$

$\mu_b$and $\mu_{sol}$are bitumen and solvent viscosities respectively and $V_b$and $V_{sol}$are volume fractions of bitumen and the dissolved solvent. α is also an empirical constant. Shu (1984) proposed the below equation to estimate α:

$$\alpha = \frac{17.04\Delta\rho^{0.5237}\rho_b^{3.2745}\rho_{sol}^{1.6316}}{\ln\left(\frac{\mu_b}{\mu_{sol}}\right)} \tag{7.21}$$

Equation 7.19 can be rewritten as below:

$$ln\mu_{mix} = ln\mu_b - x_{sol}\ln(\frac{\mu_b}{\mu_{sol}})$$

(7.22)

It can be concluded from Equation 7.22 that the mixture viscosity is always smaller than the bitumen viscosity at a certain temperature. A viscosity model as a function of temperature and solvent concentration can be derived by combining these two equations.

7.2.2.4 Oil Drainage Prediction

Volumetric oil displacement as a result of vapour chamber interface movement (x'_H), assuming an inverted triangle approximation for the steam chamber growth is calculated as:

$$q_o = \frac{1}{2} H\phi\Delta S_o x'_H$$

(7.23)

Another equation for calculating oil drainage rate is Darcy's law. Heated and diluted bitumen flows down to the production well in the direction parallel to the vapour-oil interface and the gravity force is the primary drive. Thus, the oil flow rate for a small element parallel to the vapour chamber interface is given by:

$$dq_o = \frac{k_o\, \rho_o g\, sin\theta_n}{\mu_o} d\xi$$

(7.24)

Ahead of a particular vapour-oil interface at a given moment, bitumen viscosity varies significantly in the direction normal to the interface which is the main reason for oil mobility in this zone. It is assumed that the oil density variation with temperature is negligible compared to the viscosity change. The oil rate as a function of temperature and

concentration, and in turn, distance from the interface, for this particular interface position is given by:

$$q_o = k_o\, \rho_o g\, sin\theta_n \int_0^{\infty} \frac{1}{\mu_o(\xi)}\, d\xi \tag{7.25}$$

The viscosity model introduced in the previous section is used to calculate the integral. The primary unknown in this set of equations 7.2, 7.17, 7.23, and 7.25 is the vapour chamber velocity. Because of the non-linearity of the model equations, an iterative method is used to find the vapour chamber velocity (x'_H) which satisfies these equations. By determining the vapour chamber velocity, oil production rate, heat distribution in the system, temperature and concentration profiles, rate of solvent retention, and solvent production rate can be determined and the efficiency of the solvent-SAGD process can be compared with the SAGD process at the same total mass of injection.

7.3 Results and Discussion

7.3.1 Solvent-SAGD Performance Evaluation

The first step in applying the solvent-SAGD approach introduced in the previous subsection is to find the constants in the mixture viscosity model. The constants of Andrade's equation are obtained for bitumen, butane, pentane and hexane using bitumen and solvent viscosities data given in Gupta and Gittins (2011) (See Appendix A) and listed in Table 7.1.

Table 7.1: Andrade's constants used in this study.

	Bitumen	Butane	Pentane	Hexane
a	1.355E-4	2.54E-3	4.3717E-3	0.01772
b	5318.123	1239.98	1184.6	834.89

Using this set of data, the mixture viscosity model introduced is most accurate for temperatures above 130℃. Figure 7.1 shows the results of the mixture viscosity model used in this study. This figure indicates that the mixture viscosity is always lower than bitumen viscosity over the entire range of temperatures. It can also be seen that the higher the solvent concentration, the lower the mixture viscosity. The other point that can be concluded from Figure 7.1 is that the effect of solvent on bitumen viscosity reduction is more significant at lower temperatures. This can also be interpreted as the bitumen viscosity at a high temperature might be lower than the mixture viscosity at a lower temperature.

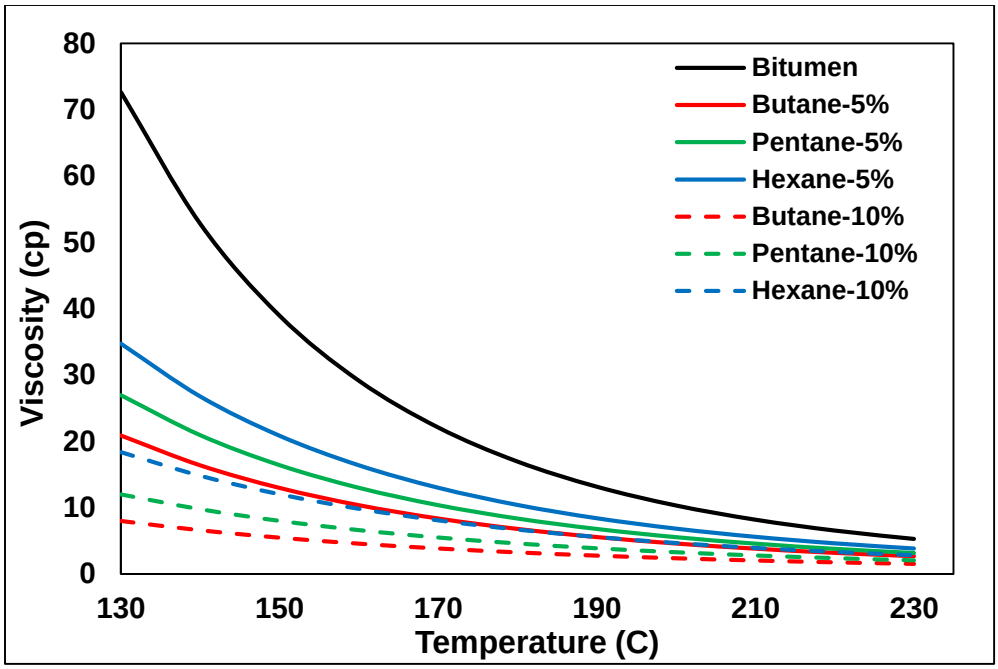

Figure 7.1: Mixture viscosity model as a function of temperature for various solvents, butane, pentane, and hexane and different solvent volume fractions with bitumen; 5 and 10%.

In a solvent-SAGD process, two distinct layers are expected to be formed due to different scales of mass and heat diffusivity. Consequently, two zones ahead of the vapour-oil interface determining oil phase mobility are shaped; the layer (closest to the chamber edge) in which the mobility is controlled by both mass and heat transfer, and the layer in which mobility is controlled by heat transfer only. Over time both of these layers became thicker or in other words, the mass and heat penetrate deeper into the reservoir. However, the length scale of heat and mass transfers are at least an order of magnitude different.

Table 7.2: Rock and fluid properties used in this study.

Porosity	0.35
Reservoir height, m	22
Oil density at reservoir temperature, kg/m^3	1014
Rock density, kg/m^3	2040
Overburden rock density, kg/m^3	2400
Molecular weight of oil, g/mol	500
Specific heat capacity of oil, J/kg.℃	2093
Specific heat capacity of overburden rock, J/kg.℃	837
Specific heat capacity of reservoir rock, J/kg.℃	936
Initial reservoir temperature, ℃	6
Gas constant, J/(K.mol)	8.314
Reservoir rock thermal conductivity, J/(s.m.℃)	1.3
Overburden thermal conductivity, J/(s.m.℃)	1.73
Initial oil saturation	0.75
Residual oil saturation	0.14
Acceleration of gravity, m/s²	9.8
Effective Permeability, m^2	0.8×10^-12

Figure 7.2 compares oil production rate of SAGD and solvent-SAGD for butane, pentane, and hexane (at the same mass fraction 9%). As can be seen, adding solvent increases oil production rate in case of using butane but decreases by pentane and hexane injection. This figure shows that the heavier the solvent, the lower the oil production rate. Bitumen production rate is almost the same when injecting pentane with steam and steam only.

However, it should be noted that in Figure 7.3, it is shown that CSOR in the case of injecting pentane is lower.

The cumulative steam-oil ratio decreases when the solvent is injected with steam. The results are shown in Figure 7.3. In the best case of butane, the steam-oil ratio for a 9% slug is 1.92 which is nearly 17% reduction compared with the no solvent case of 2.32 (m^3/m^3).

Figure 7.4 shows the total solvent and bitumen production rate over a 1000-day time interval. The curves for solvent and bitumen production rate start with much higher initial rates and then decrease sharply compared with SAGD bitumen production rate.

Cumulative steam-oil ratio versus cumulative oil production for different solvents are compared in Figure 7.5. It can be concluded from the curves that at the same cumulative oil production, highest CSOR is for SAGD and the lowest one is for the butane 9%-SAGD. Note that the cumulative oil here means bitumen only. The produced oil in the solvent based recovery methods contains a portion of the injected solvent.

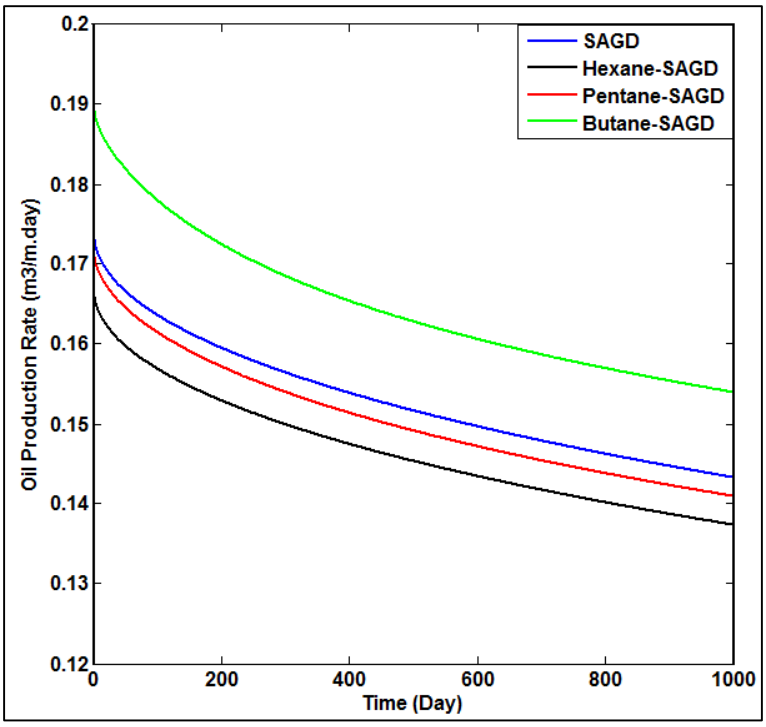

Figure 7.2: Comparison of oil production rate from solvent 9%-SAGD with SAGD.

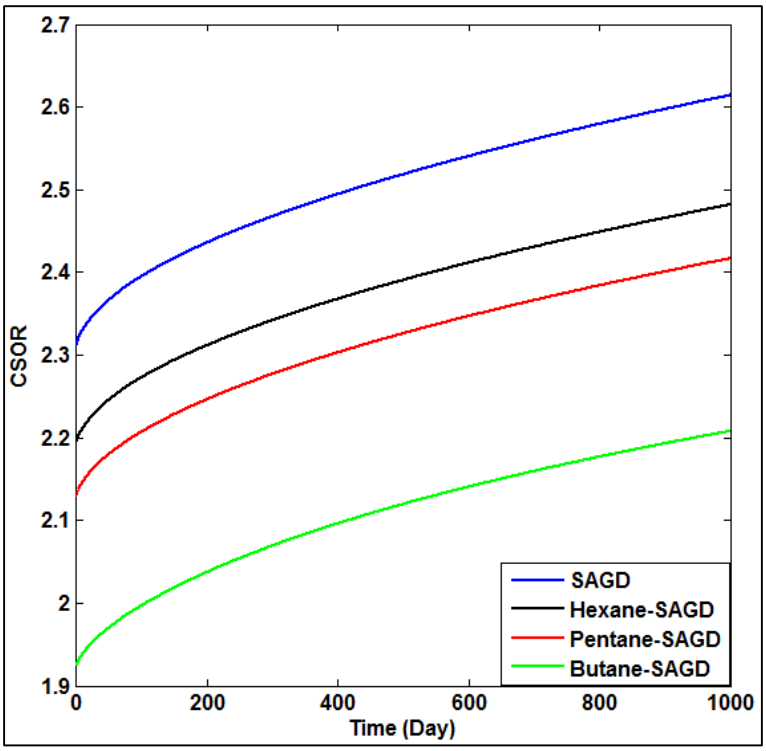

Figure 7.3: Comparison of CSOR of solvent 9%-SAGD with SAGD.

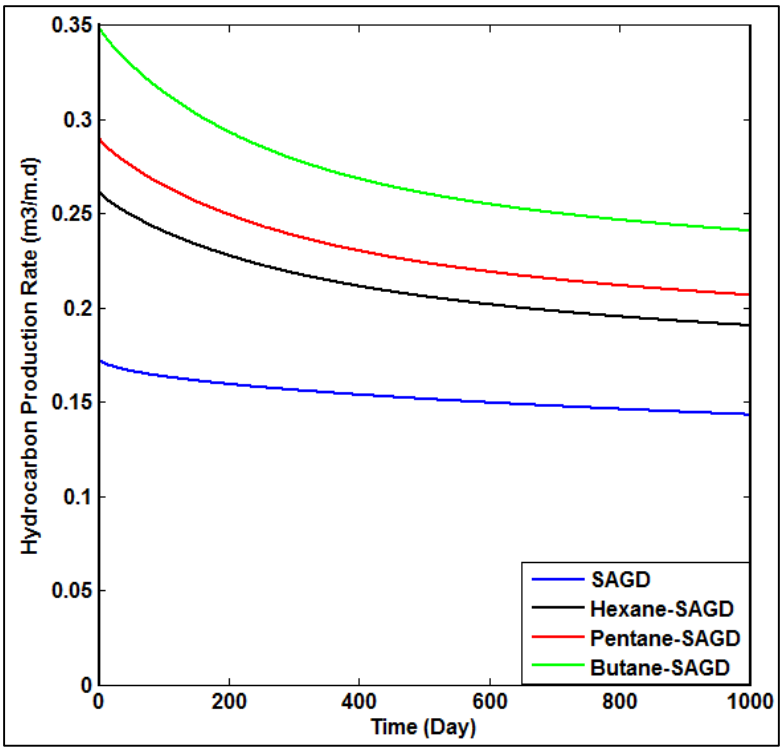

Figure 7.4: Solvent and bitumen production rate over a 1000-day period for different solvent at the same mass fraction (9%).

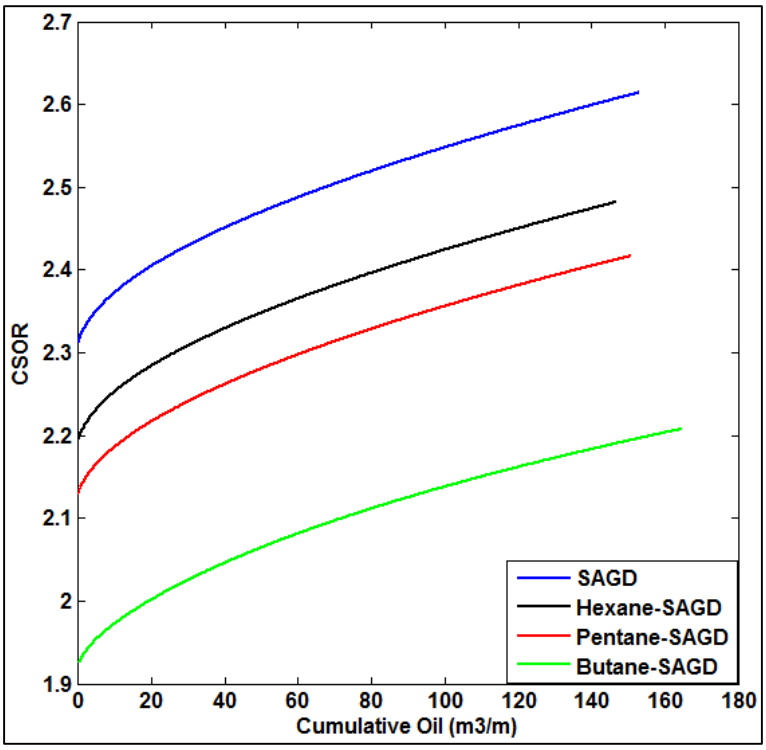

Figure 7.5: Comparison of cumulative steam-oil ratio versus cumulative bitumen production for different solvent co-injection (at the same mass fraction 9%) with steam and steam only.

Effect of the two slug sizes 5%, and 9% is investigated on the performance of the solvent-SAGD process in Figures 7.6, 7.7, and 7.8.

Figure 7.6 shows the oil production rate as a function of time. A higher oil rate is achieved in the case of butane (about 12% increase) and a higher mass fraction of butane, 9% compared with 5%, results in a higher oil rate. When heavier hydrocarbons such as pentane and hexane are employed, the figure shows that oil rate is lower compared with steam only. As can be seen, in the cases of injecting pentane or hexane with larger mass fraction of 9%, a lower oil production results in comparison to the mass fraction of 5%. This behaviour is opposite to the case of butane as a solvent.

Hydrocarbon production rate for two different mass fractions, 5 and 9%, are compared in Figure 7.7. The larger mass fraction results in higher hydrocarbon (solvent and bitumen)

production rate. Solvent production is larger in the case of larger solvent mass fraction in addition to the complex behaviour of oil production rate in all cases (butane, pentane, and hexane). These effects are summarized in Table 7.3.

Figure 7.8 compares the cumulative steam-oil ratio for different solvents with different mass fractions. Cumulative steam oil ratio is defined as cumulative steam injected divided by cumulative bitumen produced. In the case of larger mass fraction, the cumulative steam injected is lower, and but cumulative oil production can be higher or lower depending on the solvent type compared with the smaller one. The combination of these two effects results in lower CSOR in the case of larger mass fraction as can be seen in Figure 7.8.

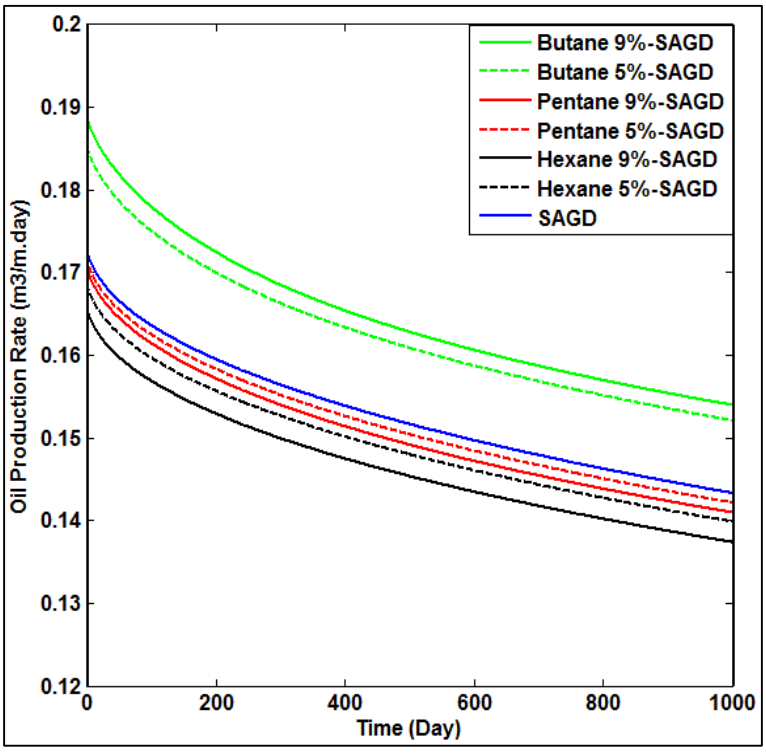

Figure 7.6: Effect of solvent mass fraction on oil production rate for various solvents.

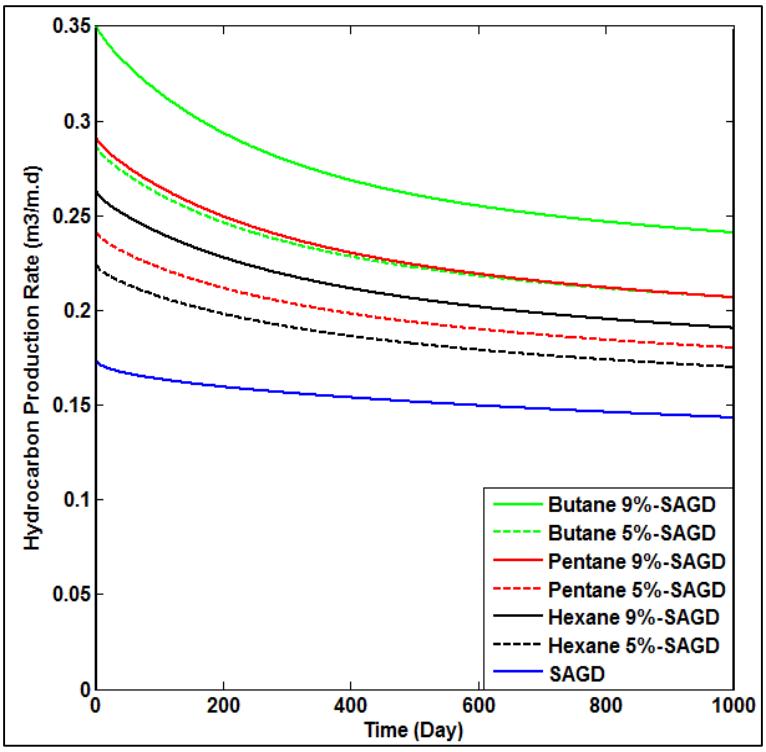

Figure 7.7: Effect of solvent mass fraction on total solvent and bitumen production rate for various solvents.

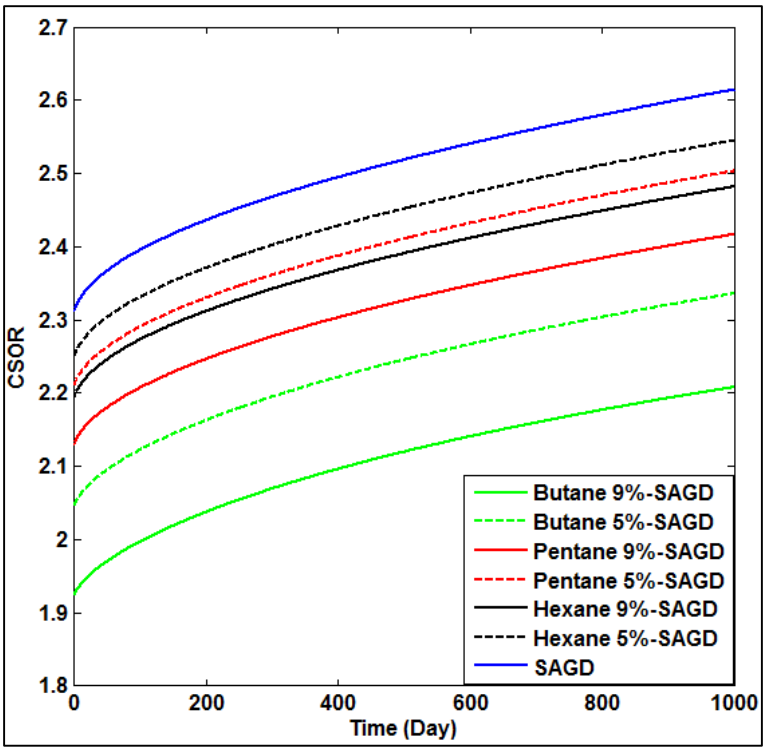

Figure 7.8: Cumulative steam oil ratio over a 1000-day period for different solvents and different solvent mass fraction (5 and 9%).

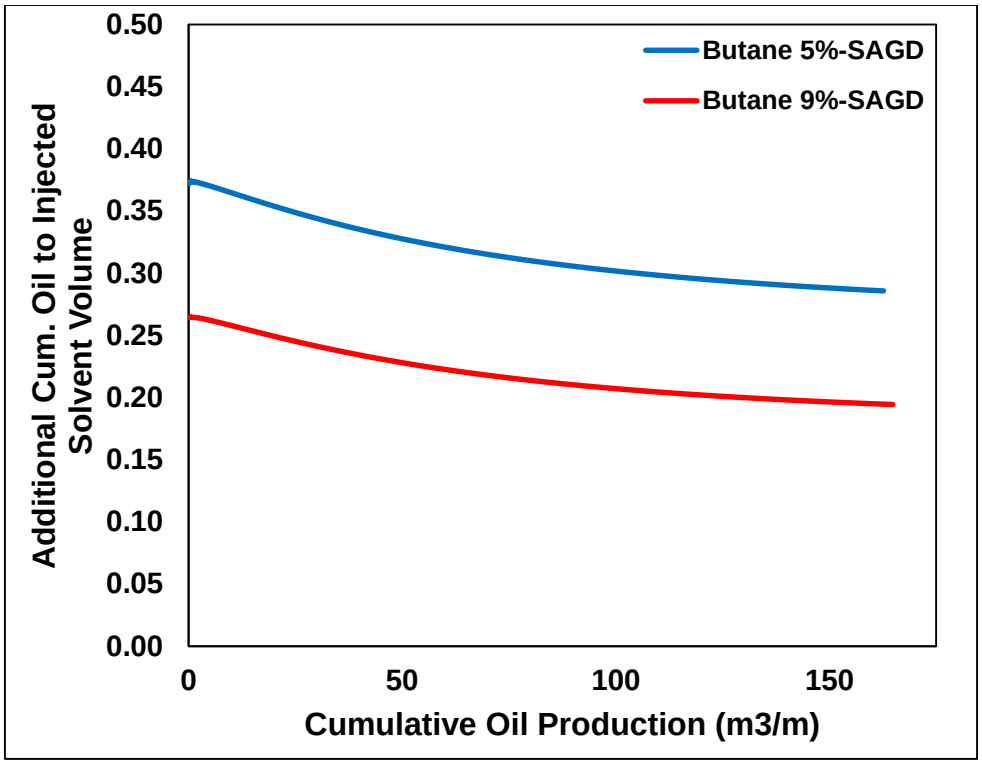

Figure 7.9: Comparison of additional cumulative oil to cumulative injected solvent number versus cumulative oil production for butane at two different mass fractions 5 and 9%.

Figure 7.9 compares the *additional* cumulative oil to injected solvent ratio for butane for mass fraction of 5 and 9%. These curves show that the additional cumulative oil to injected solvent number is positive in case of butane-SAGD process. This indicates that the oil recovery increases when some of the steam in SAGD process is replaced with butane. However, the number is low (much lower than 1) which indicates that the gain in bitumen production is lower than the injected butane volume. The larger mass fraction of butane (9%) results in lower numbers.

Table 7.3 summarizes the results of the solvent-SAGD model for various solvents (butane, pentane, and hexane) and different mass fractions (5 and 9%) using the reservoir properties shown in Table 7.2 which can be explained as follows:

1. Additional oil-to-solvent volume ratio:

   An important number in the solvent-steam injection is the ratio of the additional cumulative oil produced to the injected solvent volume. Additional oil is defined as the oil produced minus the oil produced in the no-solvent case. If this ratio is 1.0, then it means that the gain in bitumen production is same as the volume of solvent injected. This number is seen to be much smaller than 1.0 and is 0.29 and 0.2 in the best case of butane 5% and 9% respectively. In case of pentane and hexane is even negative, indicating that the solvent reduced oil recovery.

2. Effect of solvent on oil recovery:

   Cumulative oil production increases when butane is used as a solvent, compared to no solvent. For a 5% slug, the cumulative oil is highest for butane (162.7 vs. 153 m3 for no solvent). For a 9% slug, the cumulative oil recovery is again highest for butane (165 vs. 153 m3 for no solvent). This behaviour is opposite for the other solvents; lower cumulative oil production and larger the solvent mass fraction lower is the cumulative oil production.

3. Solvent production and loss:

   As expected from the model, solvent production rate decreases over time while solvent loss rate increases. This can be seen from the results shown in the table. Solvent loss and production increase as the mass fraction increases from 5 to 9%.

4. Cumulative solvent-oil ratio:

   The lower the cumulative solvent-oil ratio, the better is the efficiency of the solvent-SAGD process. From Table 7.3, the larger the mass fraction regardless of solvent type, the higher is this ratio. The results also indicate that the heavier hydrocarbons are more desirable in view of the solvent efficiency.

5. Heat injection rate:

Table 7.3 shows that the highest heat injection rate apart from SAGD (6.84E+05 kJ/day-m) is in the case of butane 5% (6.81E+05 kJ/day-m), indicating only a small difference. This is because of the higher latent heat of vaporization of water at the lower saturated temperature or pressure. The heat injection rate decreases from the lighter to the heavier solvents.

Of the 1530 SAGD well pairs in operation (total is about 1800), about 50 are using solvent in some forms (e.g. initial communication between the wells instead of heating, injection with steam as slugs, injection late in a mature project, etc.). The available field results show an increase in bitumen production in some cases, and no gain in others. Often the increase is not defined, i.e. the bitumen volume produced also includes solvent produced. This was observed in the present model results also, viz. the total hydrocarbon (bitumen plus solvent) volume produced increased when a solvent was injected with steam. However, the net gain in bitumen produced (compared to plain SAGD) was invariably smaller than the injected solvent volume.

As regards solvent mixing mechanisms, the present model accounts for actual calculated diffusion only. Effects such as viscous instabilities are not considered (they are difficult to simulate in any case). In miscible displacement works, viscous instabilities are often approximated by use of a dispersion coefficient, arbitrarily increased by a large factor. It has been shown that diffusional mixing is extremely slow compared to heat diffusion. Possibly in some field situations, there was additional solvent-bitumen mixing via viscous instabilities, large scale solvent channelling through thief zones, etc.

Table 7.3: Results of the solvent-SAGD model for different solvents and mass fraction over a 1000-day time interval (day 1 to day 1000).

Injected Solvent	NONE	C4H10	C4H10	C5H12	C5H12	C6H14	C6H14
Injected solvent concentration, w%	0	0.05	0.09	0.05	0.09	0.05	0.09
Solvent molecular weight (g/mol)		58.12	58.12	72.15	72.15	86.18	86.18
Solvent density at reservoir temperature, kg/m^3		591	591	632	632	666	666
Total injection rate (Steam and Solvent), kg/day-m	400	400	400	400	400	400	400
Chamber temperature, °C	232.5	214	205	226	221	229	225.5
Latent heat of vaporization of steam, J/kg	1800000	1881000	1915000	1830000	1853000	1817000	1834000
Steam pressure, MPa	2.94	2.075	1.75	2.6	2.36	2.75	2.55
Oil Production Rate, m^3/day-m	0.1730 to 0.1433	0.1856 to 0.1521	0.1891 to 0.1539	0.1719 to 0.1421	0.1709 to 0.1409	0.1688 to 0.1398	0.1659 to 0.1374
Solvent Production Rate, m^3/day-m	-	0.1007 to 0.0547	0.1605 to 0.0870	0.0693 to 0.0380	0.1199 to 0.0658	0.0548 to 0.03	0.0966 to 0.0533
Solvent Loss Rate, m^3/day-m	-	0 to 0.0462	0 to 0.0737	0 to 0.0314	0 to 0.0543	0 to 0.0248	0 to 0.0436
CSOR, m^3/m^3	2.3 to 2.62	2.05 to 2.34	1.925 to 2.208	2.2 to 2.5	2.13 to 2.42	2.25 to 2.545	2.19 to 2.48
Cumulative Solvent Oil Ratio (CSOR), m^3/m^3	-	0.546 to 0.623	0.8538 to 0.9793	0.4065 to 0.46	0.7068 to 0.8018	0.3272 to 0.37	0.587 to 0.664
Total Hydrocarbon Production Rate, m^3/day-m	-	0.2863 to 0.2068	0.3495 to 0.2410	0.2412 to 0.18	0.2908 to 0.2068	0.2237 to 0.17	0.2625 to 0.1906
Cumulative Oil Production, m^3/m	153	162.7	165	151.8	150.6	149.3	147
Steam chamber Velocity at the top of the Res., m/day	0.0368 to 0.0305	0.0395 to 0.0324	0.0403 to 0.0328	0.0366 to 0.0303	0.0364 to 0.03	0.0359 to 0.0298	0.0353 to 0.0292
Maximum distance vapour chamber traveled at the top of the Res., m	32.5	34.63	35.1	32.1	32.1	31.78	31.2
Heat injection rate, J/day-m	6.84E+08	6.81E+08	6.66E+08	6.63E+08	6.44E+08	6.58E+08	6.38E+08
*Additional cum. oil recovery/Cum. injected solvent ratio	-	0.29	0.2	-0.038	-0.042	-0.12	-0.11

***Additional oil is defined as cumulative oil by steam plus solvent minus oil by steam only.**

7.3.2 Effect of Total Injection Rate

One of the important factors affecting the performance of a solvent-SAGD process is the injection rate. In this section, the performance of a solvent-SAGD process for three different mass injection rates of 300, 400, and 500 kg/ (d-m) are examined. The solvent is butane in all cases at the mass fraction of 9%. A higher total rate of injection at the same mass fraction of the solvent has a higher mass of the solvent plus steam. For instance, a 500 kg/(d-m) of total injection means 45 kg of the solvent and 455 kg of the steam injection rate per day per unit length of the horizontal well.

Figure 7.10 compares the oil production rates for these three cases. It is seen that as the total injection rate increases from 300 to 500 kg/ (d-m), the drainage rate increases about 43%. Higher rate of injection reduces bitumen viscosity because of higher temperature and solvent availability in the oil zone and therefore it results in higher oil production rates.

CSORs are compared in Figure 7.11. Higher injection rate means higher steam injection rate. This means the cumulative steam injection is higher. Higher cumulative oil production is also achieved for a higher injection rate. However, the ratio of these two is greater compared with a lower rate of injection which is undesirable with respect to the process efficiency.

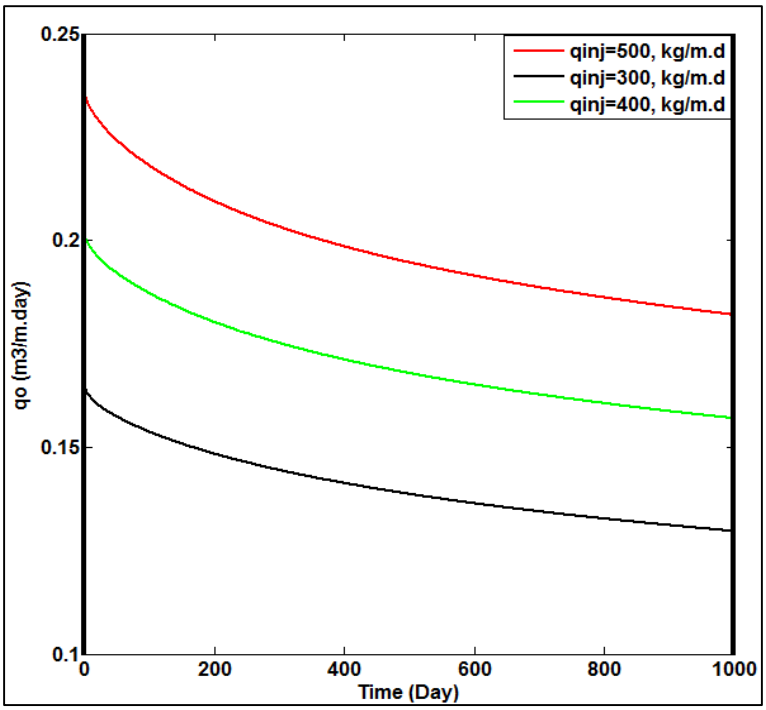

Figure 7.10: Variation of oil production rate with time for three different total injection rates; 300, 400, and 500 kg/day per unit length of horizontal well.

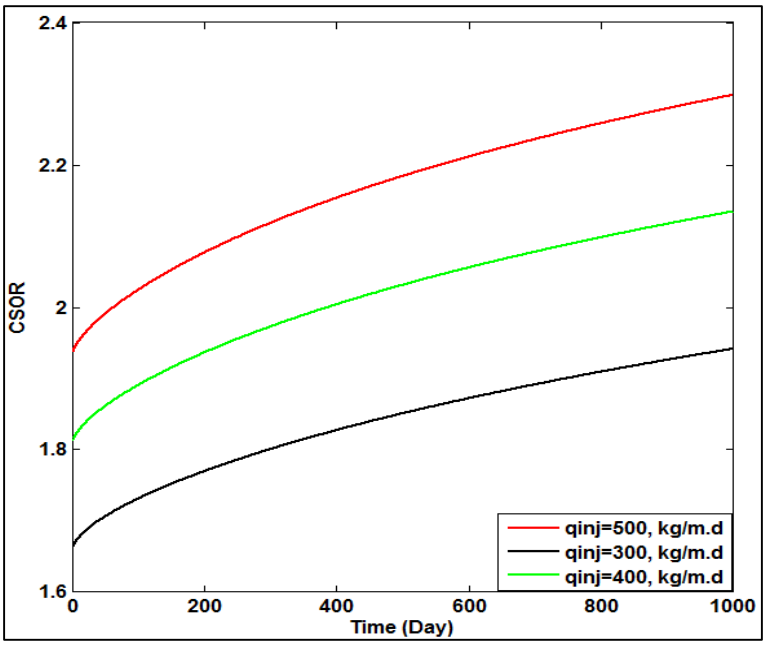

Figure 7.11: Comparison of CSOR as a function of time for three different total injection rates; 300, 400, and 500 kg/day per unit length of horizontal well.

Figure 7.12 shows that the solvent loss rate is zero at the beginning of the process and it increases over time. The solvent-SAGD model predicts a higher solvent loss rate for a higher injection rate condition. Higher total rate of the injection also results in higher CSOR.

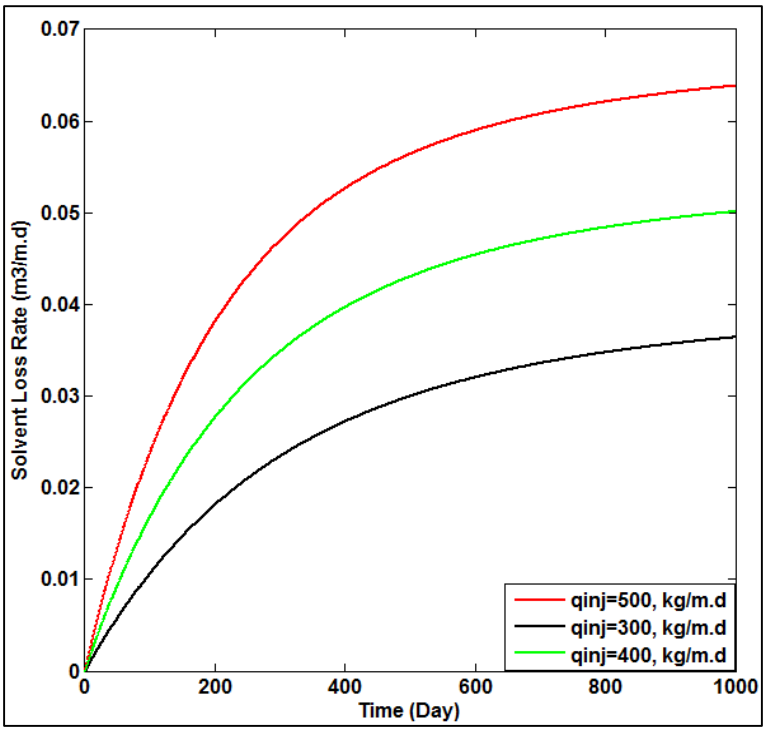

Figure 7.12: Comparison of solvent loss rate as a function of time for three different total injection rates; 300, 400, and 500 kg/day per unit length of horizontal well.

In conclusion, the new mathematical model of solvent-SAGD process shows that a higher injection rate at the same solvent mass fraction results in a higher oil production but higher CSOR, and Cumulative Solvent-Oil Ratio.

7.3.3 Effect of Solvent Diffusion Coefficient

Solvent diffusion coefficient is a controversial parameter in solvent based recovery. Most of the reported experimental diffusivities of hydrocarbon solvents in heavy oil and bitumen are of the order of $10^{-9}$to $10^{-10}\ m^2/s$ (Schmidt, 1989; Upreti and Mehrotra, 2002; Wen and Kantzas, 2005; Afsahi and Kantzas, 2005). In the previous mathematical works in the literature of the solvent-SAGD process, to justify the high oil production rate in a real porous medium, much higher values (almost two orders of magnitude) of the diffusion coefficient than the measured values reported in literature were assumed. Here, the effect

of solvent diffusion coefficient is investigated on the performance of the solvent-SAGD process.

The butane diffusion coefficient into the heavy oil used in the base case is $8.04 \times 10^{-4} m^2/day$. The diffusion coefficients of one and two orders of magnitude higher than the base case are used for this study. Higher diffusion coefficient means that the solvent at the vapour-oil interface can penetrate further. Figure 7.13 compares the cumulative oil production for all three cases. The cumulative oil production is higher for a higher diffusivity coefficient.

Higher diffusivity coefficient at the same rate of injection of the solvent and steam results in lower solvent concentration and temperature due to the limiting effect of constant injection rate, heat and solvent loss.

CSOR is lower in the case of a higher solvent diffusivity coefficient as shown in Figure 7.14. The reason is that in this situation, the cumulative steam injection rate remains unchanged but the cumulative oil production increases.

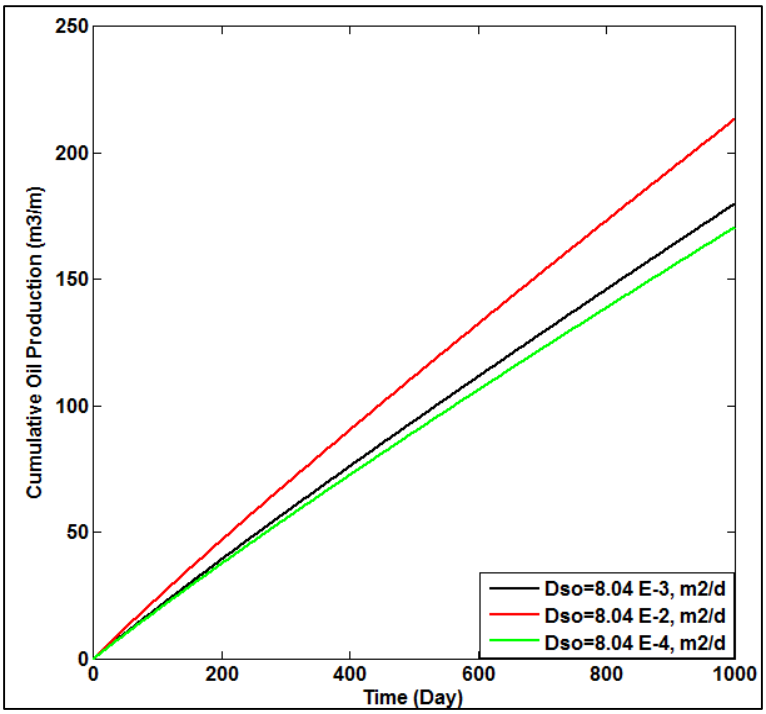

Figure 7.13: Comparison of cumulative oil production as a function of time for three diffusion coefficients; 8.04×10^{-4}, 8.04×10^{-3}, and 8.04×10^{-2}m^2/day.

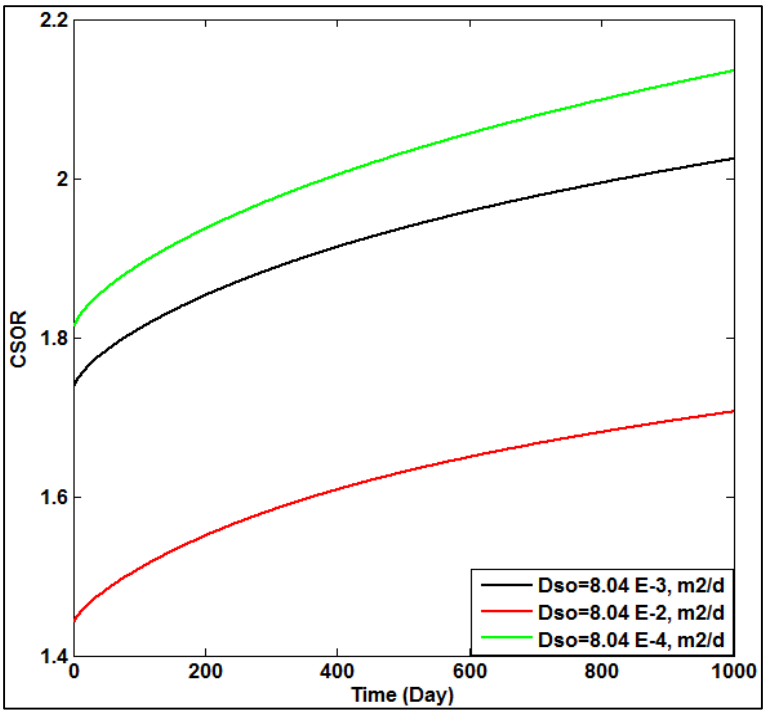

Figure 7.14: Comparison of CSOR as a function of time for three diffusion coefficients; 8.04×10^{-4}, 8.04×10^{-3}, and 8.04×10^{-2} m²/day.

7.3.4 Oil Recovery Mechanism

The important factor in analyzing oil production rate in the present approach is how the bitumen viscosity at and close to the interface is affected by different conditions like injection rate, solvent mass fraction, temperature, etc. A higher oil production rate (at the same solvent mass fraction) is achieved by:

1. Increasing injection rate
2. Higher mass diffusion coefficient for solvent-oil

The bitumen viscosity at and close to the interface is different in these two cases. A higher injection rate results in a higher temperature and concentration at the interface but a sharper decrease close to interface. However, a higher diffusion coefficient results in a lower

temperature and concentration at the interface compared to base case but a slower decrease close to the interface.

The solvent-SAGD model, developed in this chapter, is used to analyze the oil recovery mechanism of the base case; butane 9%, solvent diffusion coefficient of $8.04 \times 10^{-4} m^2/day$, and the total mass injection rate of $400\ kg/day$ per unit length of the horizontal well which will be compared with the two cases below:

1- Higher injection rate, Case A; butane 9%, solvent diffusion coefficient of $8.04 \times 10^{-4} m^2/day$, and total mass injection rate of $500\ kg/(d-m)$.
2- Higher diffusion coefficient, Case B; butane 9%, solvent diffusion coefficient of $8.04 \times 10^{-2} m^2/day$, and total mass injection rate of $400\ kg/(m-d)$.

In Case B, the solvent diffusion coefficient is an order of magnitude similar to that of the thermal diffusivity coefficient.

Figure 7.15 compares the temperature profiles for Case A, and B with the base case. It is clear from the figure that higher and lower temperatures at and close to the interface (distances less than 1 metre) are obtained in Cases A and B compared to the base case, respectively. Considering the effect of heat transfer only, oil viscosity is the lowest in Case A followed by the base case and Case B, respectively.

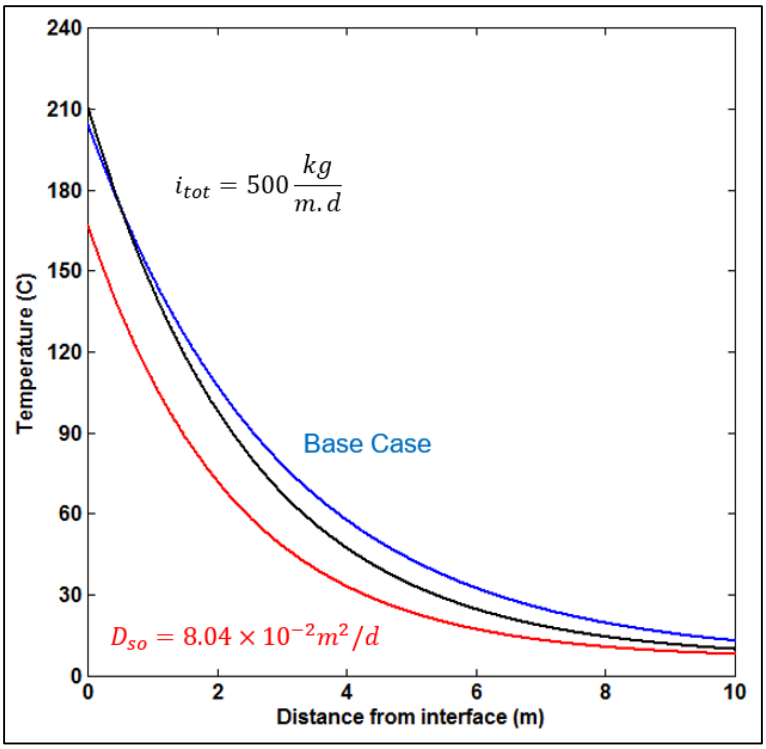

Figure 7.15: Comparison of temperature profiles for two scenarios with the base case ($D_{so} = 8.04 \times 10^{-4} m^2/day$, and $i_{tot} = 400\ kg/(d-m)$.); Case A, higher injection rate, $500\ kg/(d-m)$ and Case B, higher diffusion coefficient, $8.04 \times 10^{-2} m^2/d$ay.

Figure 7.16 shows the solvent concentration distribution beyond the chamber edge. The results of the analytical model as seen in this figure, indicate that solvent concentration rises from 18 to 21% as the injection rate is increased (Case A) from 400 to 500 kg/day per unit length of well, but it drops sharply to almost zero at a distance less than 20 cm from the edge. For Case B, the solvent concentration is smaller, just below 10%, at the interface but it decreases gradually as it moves away from the interface.

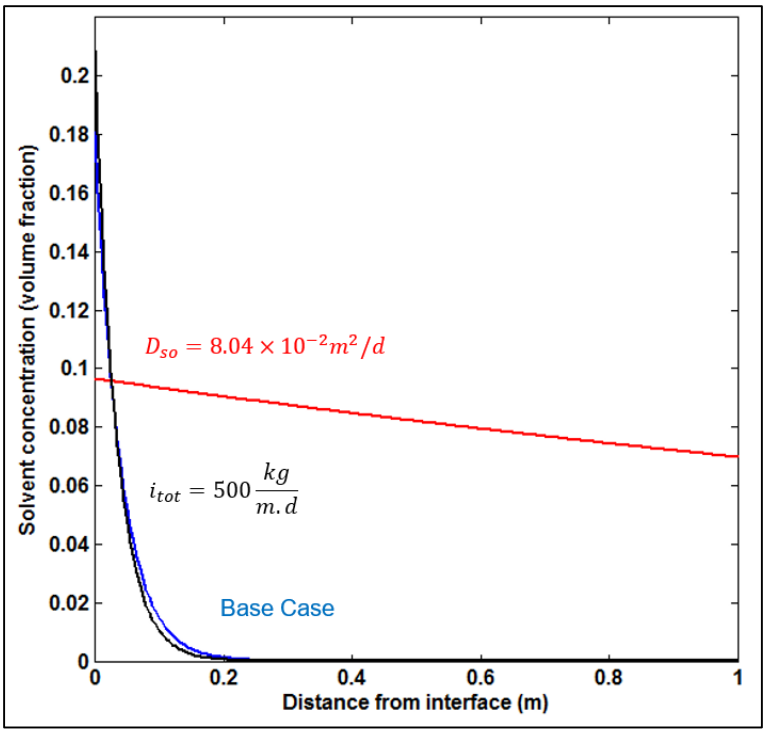

Figure 7.16: Comparison of solvent concentration profiles for two scenarios with the base case ($D_{so} = 8.04 \times 10^{-4} m^2/day$, and $i_{tot} = 400\ kg/(d-m)$.); Case A, higher injection rate, $500\ kg/(d-m)$ and Case B, higher diffusion coefficient, $8.04 \times 10^{-2} m^2/day$.

Bitumen viscosity is predicted from the mixture viscosity model introduced in the previous section. It increases with distance from the vapour-oil interface. As a result, the differential drainage rate decreases with distance. Figure 7.17 shows that bitumen viscosity at a certain distance depends on the temperature and the solvent concentration at that point. In the case of a higher solvent diffusion coefficient, Case B, bitumen is more viscous at a distance less than 10 cm from the edge compared with the two other cases but the situation appears to reverse afterwards. The oil production rate (Equation 7.25) is proportional to the area under the reciprocal curves of the bitumen viscosity which is a representative of the oil phase mobility ahead of the vapour-oil interface. This area is compared for these three cases in Figure 7.18. It is seen that the area is greater in Cases A, and B compared with the base case.

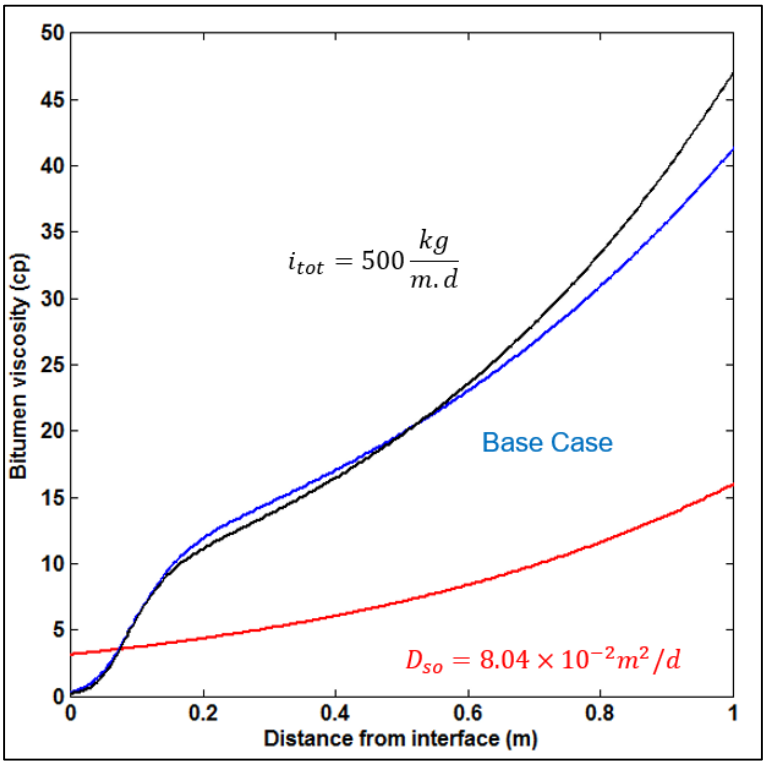

Figure 7.17: Bitumen viscosity variation for two scenarios with the base case ($D_{so} = 8.04 \times 10^{-4} m^2/day$, and $i_{tot} = 400\ kg/(d-m)$.); Case A, higher injection rate, $500\ kg/(d-m)$ and Case B, higher diffusion coefficient, $8.04 \times 10^{-2} m^2/d$ay.

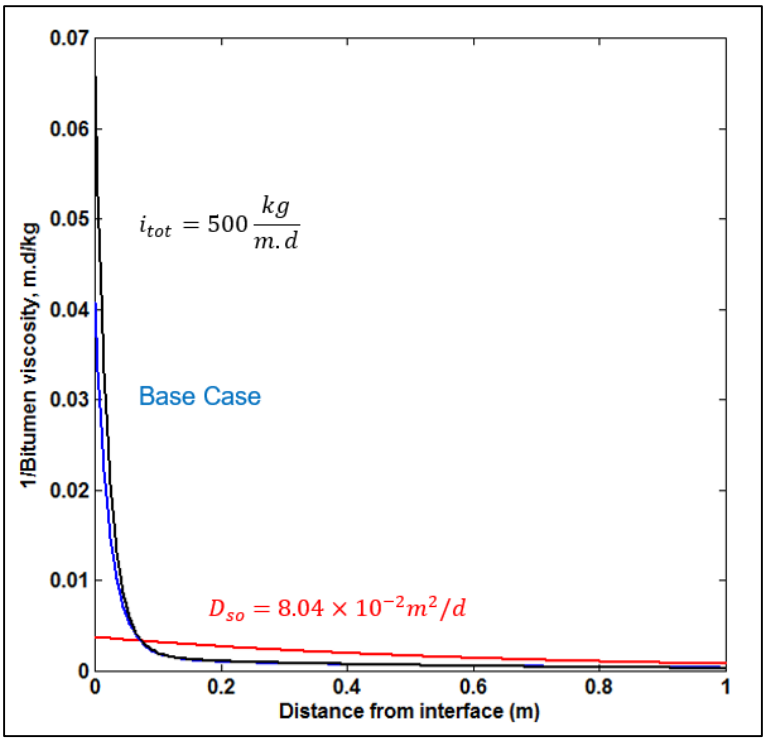

Figure 7.18: Computed reciprocal of bitumen viscosity as a function of distance from the steam chamber edge.

In a low diffusion coefficient case, the solvent penetration depth is smaller (See Figure 7.16). Figure 7.15 shows that the solvent-penetrated zone is at higher temperatures. This results in a lower effect of solvent dilution compared with heating effect on bitumen viscosity reduction. It was shown in the viscosity model that the significant reduction effect of solvent on bitumen viscosity occurs at lower temperatures. In this situation, heat conduction largely controls the bitumen drainage rate.

In this approach, a higher solvent diffusion coefficient results in lower temperature and solvent concentration values but at a larger distance from the chamber edge (See Figure 7.15 and 7.16). Oil recovery mechanism in this situation is mostly controlled by solvent dilution effect on bitumen. The reason is that a lower temperature means a higher bitumen viscosity. However, this negative effect is offset by the positive effect of the bitumen dilution on viscosity reduction. Therefore, the model results indicate that at a larger

assumed diffusion coefficient, the system is forced to be controlled by mass transfer at lower temperatures instead of heat transfer.

It is important to note that a higher diffusion coefficient, $8.04 \times 10^{-2} m^2/day$, results in unrealistic mass diffusion penetration depth changing from several centimetres to several metres (See Figure 7.16). By increasing the injection rate, the oil production rate is dominantly controlled by bitumen viscosity reduction due to the heating effect.

8. CONCLUSIONS

This research presents comprehensive analytical modelling of the SAGD process, encompassing steam chamber rise, lateral expansion, and the confinement phase. The results are validated using experimental data reported in the literature as well as field data. Also, a new mathematical model of the solvent-SAGD process for the sideways expansion of the vapour chamber is developed. The following conclusions are derived from this study; the conclusions are grouped by the model developed.

A. Steam-Assisted Gravity Drainage (SAGD)

1. Steam Chamber Rise Phase

1.1 A new analytical model was developed in this study to predict the steam chamber rise velocity, oil production rate, steam injection rate, and CSOR during the rise period of the SAGD process. The results obtained from this model are in good agreement with experimental and field data.

1.2 The steam chamber rise velocity is of the order of several cm/day. The rise velocity increases with steam temperature and permeability.

1.3 Oil production rate increases linearly with time; CSOR is a strong function of time in addition to rock and fluid properties and decreases with time during this stage.

1.4 The predicted angle between the steam chamber and the horizon for an Athabasca-like reservoir is at its maximum 80 degrees. The model predicts about 7% lower heat consumption than the observed values, based on a comparison with the field values, because heat loss to the underburden is not included in the present model.

2. Sideways Expansion Phase

2.1 Two new models are introduced for assessing SAGD performance during the sideways expansion of the steam chamber for two operating schemes, viz. Constant Volumetric Displacement (CVD) and Constant Heat Injection (CHI).

2.2 It is shown that in the CVD model, injection rate has to be increased continuously to produce at a constant oil rate. The temperature gradient at the interface decreases with time, but the heat penetration depth increases. The predicted oil production rate was in good agreement with experimental and field data.

2.3 The new Constant Heat Injection (CHI) model describes the sideways expansion stage assuming a constant heat injection rate. It is concluded that the coupled heat and mass balances limit steam chamber growth and hence the oil rate, because of heat losses and a constant steam rate.

2.4 The CHI model gives, for the first time, the correct effect of pressure on SAGD, showing a decrease in oil production rate with an increase in pressure.

2.5 Based on the results, it is concluded that the oil production rate and the temperature at the steam chamber interface decrease with time due to increasing heat loss, given a constant injection rate, but the heat penetration depth and CSOR increase.

3. Well Confinement Phase

3.1 A new analytical model is developed, for the first time, to evaluate the well confinement effect in the SAGD process, because of interference with the neighbouring wells, when the effective head for drainage decreases. For a small

lateral well spacing, confinement occurs earlier, heat loss starts decreasing sooner, resulting in a lower CSOR, than for a large spacing.

3.2 For a confined model, it is concluded that after coalescence of the chambers, the oil production rate declines, at a faster rate in the CVD than in the CHI model, because the decreasing steam chamber interface length is offset by a decreasing head. As a result of confinement, CSOR is smaller in the CVD model.

3.3 It is shown that even though oil rate declines faster in a confined model than in the unconfined case, the reservoir depletes faster, as does the angle between the steam chamber interface and the horizon.

4. Comprehensive Approach

4.1 The analytical models developed for the three phases of SAGD, viz. chamber rise, sideways spreading, and confinement were combined to construct the Comprehensive Constant Volumetric Displacement (CCVD) model and Comprehensive Constant Heat Injection (CCHI) model. These were validated with experimental and field data.

4.2 The predicted oil production rate, oil recovery and steam chamber boundaries from the comprehensive analytical approach were found to be in good agreement with the reported experimental work. For two commercial projects, the predicted oil rate and cumulative oil were in good agreement with the field data.

4.3 Based on the CCVD model, it is shown that the oil production rate increases during the rise period and remains constant when the chamber is expanding sideways. Subsequently, it decreases linearly with time

4.4 The good agreement of the predictions of the comprehensive models developed

in this study with the experimental as well as field data serves to corroborate the major postulates of the models.

B. Solvent-SAGD Model

1. The new solvent-SAGD model shows that heat penetrates deeper, the temperature and its gradient at the interface, and solvent concentration decrease with an increase in time. Mass transfer occurs over a scale of centimetres, while heat transfer scale is of the order of metres.

2. It is concluded that the solvent-SAGD process would yield a higher oil recovery, if viscosity reduction from dilution at a lower temperature is greater than viscosity reduction by temperature in the plain SAGD process, for the same total injection rate. For example, 9% wt butane added to steam led to a higher oil recovery than 5% wt butane, or steam alone, while pentane and hexane did not, for the same conditions, resulting in the lowest CSOR for butane. An increase in the mass fraction of butane yielded higher recovery, whereas the heavier hydrocarbons had the opposite effect. Heat loss was lower in the solvent process owing to the lower temperature than for steam alone. Reasons for the aforesaid are discussed in the text.

3. An important number is the *additional* cumulative oil to injected solvent ratio, which was found to be positive for butane only; the number was much lower than 1 which indicates that the gain in bitumen volume produced was lower than the volume of butane injected.

4. It is shown that the total injection rate (steam plus solvent) leads to a higher recovery, because both the temperature and solvent concentration at the interface are generally higher than for a lower rate. However, CSOR and Cumulative Solvent-to-Oil Ratio, as well as solvent retention increase with rate.

5. It is concluded that the solvent diffusion coefficient has a complex effect on performance. A large diffusion coefficient leads to higher oil production, as the depth of penetration is greater than for a lower coefficient, and bitumen dilution is the controlling factor. For a low diffusion coefficient (the real case), depth of penetration is small but the temperature is higher and viscosity reduction by heat is the controlling factor.

9. RECOMMENDATIONS FOR FURTHUR WORK

The following recommendations are offered for further work on the thesis research area:

1. The comprehensive model of SAGD does not include the preheating phase of SAGD. It is recommended to include this phase in the comprehensive model.
2. A uniform steam distribution is assumed along the horizontal well, but annular pressure drop and steam quality along the injector is a major factor. For a more realistic view of SAGD process in practice, this should be considered in the future analytical studies of SAGD.
3. The areal flow ratio of oil to steam in the rise model is a history matching parameter which should be determined in controlled laboratory or field experiments.
4. The diffusion coefficient in a thermal recovery process is concentration and temperature dependent. It is recommended to employ the concentration and temperature dependent diffusion coefficient instead of a constant one.
5. It is recommended to generalize the mathematical model of the solvent-SAGD process into a universal model by applying a mixture viscosity model which covers the whole range of temperature variations accurately to do a quick performance evaluation of the entire spectrum of heavy oil gravity drainage processes from steam only (SAGD) to solvent only (VAPEX).
6. The model equations are derived for a homogeneous reservoir. It is recommended to include the effect of reservoir heterogeneity into the equations.

REFERENCES

Afsahi, B., and Kantzas, A. 2005. Effect of the presence of sand on solvent diffusion in bitumen. Presented at the Canadian International Petroleum Conference, Calgary, Alberta, 7-9 June. PETSOC-2005-092. https://doi.org/10.2118/2005-092.

Akin, S. 2005. Mathematical modeling of steam assisted gravity drainage. *SPE Reservoir Evaluation & Engineering* **8** (05): 372-376. SPE-86963-PA. https://doi.org/10.2118/86963-PA.

Akinboyewa, J., Das, S.K., Wu, Y.-S. et al. 2010. Simulation of expanding solvent-steam assisted gravity drainage in a field case study of a Bitumen oil reservoir. Presented at the SPE Improved Oil Recovery Symposium, Tulsa, Oklahoma, USA, 24-28 April. SPE-129963-MS. https://doi.org/10.2118/129963-MS.

Alikhan, A.A., and Farouq Ali, S. 1974. Heavy oil recovery by steam-driven hydrocarbon slugs from linear porous media. Presented at the Fall Meeting of the Society of Petroleum Engineers of AIME, Houston, Texas, 6-9 October. SPE-5019-MS. https://doi.org/10.2118/5019-MS.

Allen, J. 1974. Gaseous solvent heavy oil recovery. *Canadian Patent* **1**.

Allen, J.C., and Redford, D.A. 1976. *Combination solvent-noncondensible gas injection method for recovering petroleum from viscous petroleum-containing formations including tar sand deposits*, United States Patent and Trademark Office (Reprint).

Alvarez, J., Moreno, R., and Sawatzky, R.P. 2014. Can SAGD be exported? Potential challenges. Presented at the SPE Heavy and Extra Heavy Oil Conference: Latin America, Medellín, Colombia 24-26 September. SPE-171089-MS. https://doi.org/10.2118/171089-MS.

Andrade, E.C. 1930. The viscosity of liquids. *Nature* **125** (3148): 309-310. https://doi.org/10.1038/125582a0.

Ardali, M., Barrufet, M., and Mamora, D.D. 2012. Laboratory testing of addition of solvents to steam to improve SAGD process. Presented at the SPE Heavy Oil Conference Canada, Calgary, Alberta, Canada, 12-14 June. SPE-146993-MS. https://doi.org/10.2118/146993-MS.

Azad, A., and Chalaturnyk, R.J. 2012. An improved SAGD analytical simulator: Circular steam chamber geometry (in English). *Journal of Petroleum Science and Engineering* **82-83**: 27-37. https://doi.org/10.1016/j.petrol.2012.01.003.

Azom, P.N., Kamp, A., and Srinivasan, S. 2013. Characterizing the Effect of Heat Transfer on Multiphase Flow during the Steam-Assisted Gravity Drainage (SAGD) Process. Presented at the SPE Heavy Oil Conference, Calgary, Alberta, Canada 11-13 June. SPE-165494-MS. https://doi.org/10.2118/165494-MS.

Azom, P.N., and Srinivasan, S. 2013. Modeling Coupled Heat Transfer and Multiphase Flow during the Expanding Solvent Steam-Assisted Gravity Drainage (ES-SAGD) Process. Presented at the SPE Annual Technical Conference and Exhibition, New Orleans, Louisiana, USA 30 September-2 October. SPE-166357-MS. https://doi.org/10.2118/166357-MS.

Baker, R.O., Rodrigues, K., Sandhu, K.S. et al. 2010. Key parameters in steam chamber development. Presented at the Canadian Unconventional Resources and International Petroleum Conference, Calgary, Alberta, Canada, 19-21 October. SPE-138113-MS. https://doi.org/10.2118/138113-MS.

Bayestehparvin, B., Abedi, J., and Farouq Ali, S. 2015. Dissolution and Mobilization of Bitumen at Pore Scale. Presented at the SPE Canada Heavy Oil Technical Conference, Calgary, Alberta, Canada 9-11 June. SPE-174482-MS. https://doi.org/10.2118/174482-MS.

Birrell, G., and Putnam, P. 2000. A Study of the influence of reservoir architecture on SAGD steam chamber development at the Underground Test Facility, Northeastern Alberta, Canada, using a graphical analysis of temperature profiles. Presented at the Canadian International Petroleum Conference, Calgary, Alberta, 4-8 June PETSOC-2000-104. https://doi.org/10.2118/2000-104.

Boak, J., and Palmgren, C. 2007. Preliminary numerical analysis for a naphtha co-injection test during SAGD (in English). *Journal of Canadian Petroleum Technology* **46** (1): 13-19. PETSOC-2004-001. https://doi.org/10.2118/2004-001.

BP Global. available at www.bp.com/en/global/corporate/energy-economics/statistical-review-of-world-energy.html. British Petroleum Global.

Butler, R. 1985. A new approach to the modelling of steam-assisted gravity drainage. *Journal of Canadian Petroleum Technology* **24** (03): 42-51. PETSOC-85-03-01. https://doi.org/10.2118/85-03-01.

Butler, R. 1987. Rise of interfering steam chambers. *Journal of Canadian Petroleum Technology* **26** (03). PETSOC-87-03-07. https://doi.org/10.2118/87-03-07.

Butler, R. 2001. Some recent developments in SAGD. *Journal of Canadian Petroleum Technology* **40** (01). PETSOC-01-01-DAS. https://doi.org/10.2118/01-01-DAS.

Butler, R., and Mokrys, I. 1989. *Solvent Analog Model of Steam-Assisted Gravity Drainage*, Vol. 05.p.17, AOSTRA Journal of Research (Reprint).

Butler, R., Mokrys, I., and Das, S. 1995. The solvent requirements for Vapex recovery. Presented at the SPE International Heavy Oil Symposium, Calgary, Alberta, Canada 19-21 June. SPE-30293-MS. https://doi.org/10.2118/30293-MS.

Butler, R., Stephens, D., and Weiss, M. 1980. The vertical growth of steam chambers in the in-situ thermal recovery of heavy oils. Presented at the Proc. 30 th Can. Chem. Eng. Conf.

Butler, R.M. 1991. Thermal recovery of oil and bitumen.

Butler, R.M. 1994. Steam-Assisted Gravity Drainage - Concept, Development, Performance and Future (in English). *Journal of Canadian Petroleum Technology* **33** (2): 44-50. PETSOC-94-02-05. https://doi.org/10.2118/94-02-05.

Butler, R.M., and Dargie, B. 1994. *Horizontal wells for the recovery of oil, gas, and bitumen*, Gulf Pub Co (Reprint).

Butler, R.M., and Jiang, Q. 2000. Improved Recovery of Heavy Oil by Vapex with Widely Spaced Horizontal Injectors and Producers. PETSOC-00-01-04. https://doi.org/10.2118/00-01-04.

Butler, R.M., McNab, G.S., and Lo, H.Y. 1981. Theoretical studies on the gravity drainage of heavy oil during in-situ steam heating. *The Canadian Journal of Chemical Engineering* **59** (4): 455-460. https://doi.org/10.1002/cjce.5450590407.

Butler, R.M., and Mokrys, I.J. 1991. A new process (VAPEX) for recovering heavy oils using hot water and hydrocarbon vapour. *Journal of Canadian Petroleum Technology* **30** (01). PETSOC-91-01-09. https://doi.org/10.2118/91-01-09.

Butler, R.M., and Mokrys, I.J. 1993. Recovery of heavy oils using vapourized hydrocarbon solvents: further development of the VAPEX process. *Journal of Canadian Petroleum Technology* **32** (06). PETSOC-93-06-06. https://doi.org/10.2118/93-06-06.

Butler, R.M., and Stephens, D.J. 1981. The Gravity Drainage of Steam-Heated Heavy Oil to Parallel Horizontal Wells (in English). *Journal of Canadian Petroleum Technology* **20** (2): 90-96. PETSOC-81-02-07. https://doi.org/10.2118/81-02-07.

Cenovus Energy. 2012-2013. Cenovus Christina Lake In-Situ Oil Sands scheme 8591 - Performance Presentation Report available at www.aer.ca.

Cenovus Energy. 2015. *Cenovus Christina Lake In-Situ Oil Sands scheme 8591 - Performance Presentation Report available at* www.aer.ca.

Chalaturnyk, R.J. 1996. Geomechanics of the steam assisted gravity drainage process in heavy oil reservoirs. PhD, University of Alberta, Edmonton, Alberta.

Chow, L., and Butler, R. 1996. Numerical simulation of the steam-assisted gravity drainage process (SAGD). *Journal of Canadian Petroleum Technology* **35** (06). PETSOC-96-06-06. https://doi.org/10.2118/96-06-06.

Chung, K.H., and Butler, R.M. 1987. Geometrical Effect Of Steam Injection On The Formation Of Emulsions In The Steam-Assisted Gravity Drainage Process. Presented at the, 1987/1/1/. PETSOC-88-01-02. https://doi.org/10.2118/88-01-02.

Closmann, P.J., and Smith, R.A. 1983. Temperature observations and steam-zone rise in the vicinity of a steam-heated fracture. *Society of Petroleum Engineers Journal* **23** (04): 575-586. SPE-9898-PA. https://doi.org/10.2118/9898-PA.

ConocoPhillips Canada. 2007. Surmont pilot Performance and Resource Management Presentation to the EUB - Technical Presentation available at www.aer.ca.

ConocoPhillips Canada. 2015. Athabasca ConocoPhillips Surmont SAGD 9426, 11596, and 9460 - Performance Presentation available at www.aer.ca.

Cuthiell, D., Kissel, G., Jackson, C. et al. 2006. Viscous fingering effects in solvent displacement of heavy oil. *Journal of Canadian Petroleum Technology* **45** (07). PETSOC-06-07-02. https://doi.org/10.2118/06-07-02.

Das, S., and Butler, R. 1995. Extraction of heavy oil and bitumen using solvents at reservoir pressure. Presented at the Technical meeting/petroleum conference of the South Saskatchewan section, Regina, Saskatchewan October 16 - 18. PETSOC-95-118. https://doi.org/10.2118/95-118.

Das, S.K., and Butler, R.M. 1996. Diffusion coefficients of propane and butane in Peace River bitumen. *The Canadian journal of chemical engineering* **74** (6): 985-992. https://doi.org/10.1002/cjce.5450740623.

Das, S.K., and Butler, R.M. 1998. Mechanism of the vapor extraction process for heavy oil and bitumen. *Journal of Petroleum Science and Engineering* **21** (1): 43-59. https://doi.org/10.1016/S0920-4105(98)00002-3.

Dehghanpour, H., Murtaza, M., and He, Z. 2013. Modeling Three-Phase Flow during Steam Chamber Rise-Impact of Water Drainage on Oil Production Rate. Presented at the SPE Heavy Oil Conference-Canada, Calgary, Alberta, 11-13 June. SPE-165426-MS. https://doi.org/10.2118/165426-MS.

Dickson, J., Subramanian, S., Shah, P. et al. 2013. Key Learnings from a Simulation Study of a Solvent-Assisted SAGD Pilot at Cold Lake. Presented at the SPE Heavy Oil Conference Canada, , Calgary, Alberta, 11-13 June. SPE-165486-MS. https://doi.org/10.2118/165486-MS.

Dickson, J.L., Clingman, S., Dittaro, L.M. et al. 2011. Design approach and early field performance for a solvent-assisted SAGD pilot at cold lake, Canada. Presented at the SPE Heavy Oil Conference and Exhibition, Kuwait City, Kuwait 12-14 December. SPE-150639-MS. https://doi.org/10.2118/150639-MS.

Dittaro, L.M., Dickson, J.L., and Boone, T.J. 2013. Integrating the Key Learnings from Laboratory, Simulation, and Field Tests to Assess the Potential for Solvent Assisted-Steam Assisted Gravity Drainage. Presented at the SPE Heavy Oil Conference-Canada, Calgary, Alberta, Canada, 11-13 June. SPE-165485-MS. https://doi.org/10.2118/165485-MS.

Doscher, T., Ershaghi, I., Herzberg, D. et al. 1979. An Economic Evaluation of Solvent/Steam Stimulation. *Journal of Petroleum technology* **31** (08): 951-954. SPE-7118-PA. https://doi.org/10.2118/7118-PA.

Dunn, S., Nenniger, E., and Rajan, V. 1989. A study of bitumen recovery by gravity drainage using low temperature soluble gas injection. *The Canadian Journal of Chemical Engineering* **67** (6): 978-991. https://doi.org/10.1002/cjce.5450670617.

Edmunds, N. 1999. On the difficult birth of SAGD. *Journal of Canadian Petroleum Technology* **38** (01). PETSOC-99-01-DA. https://doi.org/10.2118/99-01-DA.

Edmunds, N., and Chhina, H. 2001. Economic optimum operating pressure for SAGD projects in Alberta. *Journal of Canadian Petroleum Technology* **40** (12). PETSOC-01-12-DAS. https://doi.org/10.2118/01-12-DAS.

Edmunds, N., and Gittins, S.D. 1993. Effective application of steam assisted gravity drainage of bitumen to long horizontal well pairs. *Journal of Canadian Petroleum Technology* **32** (06): 49-55. PETSOC-93-06-05. https://doi.org/10.2118/93-06-05.

Edmunds, N., Kovalsky, J., Gittins, S. et al. 1994. Review of phase A steam-assisted gravity-drainage test. *SPE Reservoir Engineering* **9** (02): 119-124. SPE-21529-PA. https://doi.org/10.2118/21529-PA.

Edmunds, N., and Peterson, J. 2007. A unified model for prediction of CSOR in steam-based bitumen recovery. Presented at the Canadian International Petroleum Conference, Calgary, Alberta 12-14 June. PETSOC-2007-027. https://doi.org/10.2118/2007-027.

Farouq Ali, S. 1997. Is there life after SAGD? *Journal of Canadian Petroleum Technology* **36** (06). PETSOC-97-06-DAS. https://doi.org/10.2118/97-06-DAS.

Farouq Ali, S. 2015. Practical Heavy Oil Recovery. ENCH 647 Lecture Notes, Department of Chemical and Petroleum Engineering, University of Calgary.

Farouq Ali, S. 2016. Life After SAGD–20 Years Later. Presented at the SPE Western Regional Meeting, Anchorage, Alaska, USA 23-26 May. SPE-180394-MS. https://doi.org/10.2118/180394-MS.

Farouq Ali, S., and Abad, B. 1976. Bitumen recovery from oil sands, using solvents in conjunction with steam. *Journal of Canadian Petroleum Technology* **15** (03). PETSOC-76-03-11. https://doi.org/10.2118/76-03-11.

Farouq Ali, S., and Snyder, S. 1973. Miscible thermal methods applied to a two-dimensional, vertical tar sand pack, with restricted fluid entry. *Journal of Canadian Petroleum Technology* **12** (04). PETSOC-73-04-01. https://doi.org/10.2118/73-04-01.

Ferguson, F., and Butler, R. 1988. Steam-Assisted Gravity Drainage Model Incorporating Energy Recovery from a Cooling Steam Chamber. *Journal of Canadian Petroleum Technology* **27** (05). PETSOC-88-05-09. https://doi.org/10.2118/88-05-09.

Ferguson, M., Mamora, D., and Goite, J. 2001. Steam-propane injection for production enhancement of heavy Morichal oil. Presented at the SPE International Thermal

Operations and Heavy Oil Symposium, Porlamar, Margarita Island, Venezuela, 12-14 March. SPE-69689-MS. https://doi.org/10.2118/69689-MS.

Frauenfeld, T., Jossy, C., Bleile, J. et al. 2008. Experimental and economic analysis of the thermal solvent and hybrid solvent processes. Presented at the Canadian International Petroleum Conference, Calgary, Alberta 17-19 June PETSOC-2008-149. https://doi.org/10.2118/2008-149.

Frauenfeld, T., Jossy, C., Jossy, E. et al. 2012. Experimental Evaluation of Dispersion and Diffusion in UTF Bitumen/n-Butane System. Presented at the SPE Heavy Oil Conference Canada, Calgary, Alberta, Canada 12-14 June. SPE-157904-MS. https://doi.org/10.2118/157904-MS.

Frauenfeld, T., Jossy, C., Rispler, K. et al. 1998. Evaluation of the Bottom Water Reservoir VAPEX Process. Presented at the Canadian International Petroleum Conference Calgary, Alberta, 8-10 June. PETSOC-2004-241. https://doi.org/10.2118/2004-241.

Gates, I., and Chakrabarty, N. 2006. Design of the steam and solvent injection strategy in Expanding-Solvent Steam-Assisted Gravity Drainage. Presented at the Canadian International Petroleum Conference, Calgary, Alberta 13-15 June. PETSOC-2006-023. https://doi.org/10.2118/2006-023.

Gates, I.D. 2007. Oil phase viscosity behaviour in expanding-solvent steam-assisted gravity drainage. *Journal of Petroleum Science and Engineering* **59** (1): 123-134. https://doi.org/10.1016/j.petrol.2007.03.006.

Gotawala, D.R., and Gates, I.D. 2008. Steam fingering at the edge of a steam chamber in a heavy oil reservoir. *The Canadian Journal of Chemical Engineering* **86** (6): 1011-1022. https://doi.org/10.1002/cjce.20117.

Gotawala, D.R., and Gates, I.D. 2012. A basis for automated control of steam trap subcool in SAGD. *SPE Journal* **17** (03): 680-686. SPE-159170-PA. https://doi.org/10.2118/159170-PA.

Govind, P.A., Das, S.K., Srinivasan, S. et al. 2008. Expanding solvent SAGD in heavy oil reservoirs. Presented at the International Thermal Operations and Heavy Oil Symposium, Calgary, Alberta, Canada, 20-23 October. SPE-117571-MS. https://doi.org/10.2118/117571-MS.

Gupta, S., and Gittins, S. 2005. Christina Lake solvent aided process pilot. Presented at the Canadian International Petroleum Conference, Calgary, Alberta 7-9 June PETSOC-2005-190. https://doi.org/10.2118/2005-190.

Gupta, S., and Gittins, S. 2007. Effect of solvent sequencing and other enhancements on Solvent Aided Process. *Journal of Canadian Petroleum Technology* **46** (09). PETSOC-07-09-06. https://doi.org/10.2118/07-09-06.

Gupta, S., Gittins, S., and Picherack, P. 2002. Field implementation of solvent aided process. Presented at the Canadian international petroleum conference, Calgary, Alberta, 11-13 June. PETSOC-2002-299. https://doi.org/10.2118/2002-299.

Gupta, S., Gittins, S., and Picherack, P. 2004. Insights into some key issues with Solvent Aided Process. *Journal of Canadian Petroleum Technology* **43** (02). PETSOC-04-02-05. https://doi.org/10.2118/04-02-05.

Gupta, S.C., and Gittins, S. 2011. A Semi-analytical Approach for Estimating Optimal Solvent Use in a Solvent Aided SAGD Process. Presented at the SPE Annual Technical Conference and Exhibition, Denver, Colorado, USA, 30 October-2 November. SPE-146671-MS. https://doi.org/10.2118/146671-MS.

Gupta, S.C., Gittins, S., Sood, A. et al. 2010. Optimal amount of solvent in Solvent Aided Process. Presented at the Canadian Unconventional Resources and International Petroleum Conference, Calgary, Alberta, Canada, 19-21 October. SPE-137543-MS. https://doi.org/10.2118/137543-MS.

Heidari, M., Pooladi-Darvish, M., Azaiez, J. et al. 2009. Effect of drainage height and permeability on SAGD performance. *Journal of Petroleum Science and Engineering* **68** (1): 99-106. https://doi.org/10.1016/j.petrol.2009.06.020.

Irani, M., and Gates, I.D. 2013. Understanding the convection heat-transfer mechanism in steam-assisted-gravity-drainage process. *SPE Journal* **18** (06): 1,202-1,215. SPE-167258-PA. https://doi.org/10.2118/167258-PA.

Irani, M., and Ghannadi, S. 2013. Understanding the heat-transfer mechanism in the steam-assisted gravity-drainage (SAGD) process and comparing the conduction and convection flux in bitumen reservoirs. *SPE Journal* **18** (01): 134-145. SPE-163079-PA. https://doi.org/10.2118/163079-PA.

Ito, Y., and Hirata, T. 1999. Numerical Simulation Study of a Well In the JACOS Hangingstone Steam Pilot Project Near Fort McMurray. *Journal of Canadian Petroleum Technology* **38** (13). PETSOC-99-13-38. https://doi.org/10.2118/99-13-38.

Ito, Y., Hirata, T., and Ichikawa, M. 2001. The growth of the steam chamber during the early period of the UTF Phase B and Hangingstone Phase I projects. *Journal of Canadian Petroleum Technology* **40** (09). PETSOC-01-09-02. https://doi.org/10.2118/01-09-02.

Ito, Y., Hirata, T., and Ichikawa, M. 2004. The effect of operating pressure on the growth of the steam chamber detected at the Hangingstone SAGD project. *Journal of Canadian Petroleum Technology* **43** (01). PETSOC-04-01-05. https://doi.org/10.2118/04-01-05.

Ito, Y., and Ipek, G. 2005. Steam fingering phenomenon during SAGD process. Presented at the SPE International Thermal Operations and Heavy Oil Symposium, Calgary,

Alberta, Canada 1-3 November. SPE-97729-MS. https://doi.org/10.2118/97729-MS.

Ito, Y., and Suzuki, S. 1996. Numerical simulation of the SAGD process in the Hangingstone oil sands reservoir. Presented at the Annual Technical Meeting of the Petroleum Society, Calgary, Alberta, CanadaPETSOC-99-09-02. https://doi.org/10.2118/99-09-02.

Ito, Y., Suzuki, S., and Yamada, H. 1998. Effect of reservoir parameter on oil rates and steam oil ratios in sagd projects. Presented at the 7th UNITAR International Conference on Heavy Crude and Tar Sands, Beijing, China.

Ivory, J.J., Zheng, R., Nasr, T.N. et al. 2008. Investigation of low pressure ES-SAGD. Presented at the International Thermal Operations and Heavy Oil Symposium, Calgary, Alberta, Canada 20-23 October. SPE-117759-MS. https://doi.org/10.2118/117759-MS.

Karmaker, K., and Maini, B.B. 2003. Experimental investigation of oil drainage rates in the VAPEX process for heavy oil and bitumen reservoirs. Presented at the SPE annual technical conference and exhibition, Denver, Colorado 5-8 October. SPE-84199-MS. https://doi.org/10.2118/84199-MS.

Keshavarz, M., Okuno, R., and Babadagli, T. 2015. Optimal application conditions for steam/solvent coinjection. *SPE Reservoir Evaluation & Engineering* **18** (01): 20-38. SPE-165471-PA. https://doi.org/10.2118/165471-PA.

Kisman, K., and Yeung, K. 1995. Numerical study of the SAGD process in the Burnt Lake oil sands lease. Presented at the SPE international heavy oil symposium, Calgary, Alberta, Canada 19-21 June. SPE-30276-MS. https://doi.org/10.2118/30276-MS.

Komery, D., Luhning, R., Pearce, J. et al. 1998. Pilot testing of post-steam bitumen recovery from mature SAGD wells in Canada. Presented at the Petroleum Society of CIM, 49th annual technical conference, Calgary, Alberta, Canada.

Leaute, R., and Carey, B. 2007. Liquid addition to steam for enhancing recovery (LASER) of bitumen with CSS: Results from the first pilot cycle. *Journal of Canadian Petroleum Technology* **46** (09). PETSOC-07-09-01. https://doi.org/10.2118/07-09-01.

Leaute, R.P. 2002. Liquid addition to steam for enhancing recovery (LASER) of bitumen with CSS: Evolution of technology from research concept to a field pilot at Cold Lake. Presented at the SPE International Thermal Operations and Heavy Oil Symposium and International Horizontal Well Technology Conference, Calgary, Alberta, Canada 4-7 November. SPE-79011-MS. https://doi.org/10.2118/79011-MS.

Lederer, E. 1933. Viscosity of mixtures with and without diluents. *Proc World Pet Cong London* **2**: 526-528.

Li, Q., and Chen, Z. 2015. A new analysis on the convective heat transfer at the edge of the SAGD chamber. Presented at the SPE Annual Technical Conference and Exhibition, Houston, Texas, USA, 28-30 September. SPE-175063-MS. https://doi.org/10.2118/175063-MS.

Li, W., and Mamora, D.D. 2010. Experimental investigation of solvent co-injection in vapor and liquid phase to enhance SAGD performance. Presented at the SPE Annual Technical Conference and Exhibition, Florence, Italy, 19-22 September. SPE-133277-MS. https://doi.org/10.2118/133277-MS.

Mehrotra, A.K., and Svrcek, W.Y. 1986. Viscosity of compressed athabasca bitumen. *The Canadian Journal of Chemical Engineering* **64** (5): 844-847. https://doi.org/10.1002/cjce.5450640520.

Nasr, T., Beaulieu, G., Golbeck, H. et al. 2003. Novel Expanding Solvent-SAGD Process" ES-SAGD". *Journal of Canadian Petroleum Technology* **42** (01). PETSOC-03-01-TN. https://doi.org/10.2118/03-01-TN.

Nasr, T.N., and Ayodele, O.R. 2006. New hybrid steam-solvent processes for the recovery of heavy oil and bitumen. Presented at the Abu Dhabi International Petroleum Exhibition and Conference, Abu Dhabi, UAE 5-8 November. SPE-101717-MS. https://doi.org/10.2118/101717-MS.

Nasr, T.N., and Isaacs, E.E. 2001. *Process for enhancing hydrocarbon mobility using a steam additive*, US Patent No. 6230814 B1 (Reprint).

Nenniger, E. 1979. Hydrocarbon recovery. *Canadian Patent* **1**.

Nenniger, J., and Dunn, S. 2008. How fast is solvent based gravity drainage? Presented at the Canadian International Petroleum Conference, Calgary, Alberta 17-19 June PETSOC-2008-139. https://doi.org/10.2118/2008-139.

Orr, B. 2009. ES-SAGD; Past, Present and Future. Presented at the SPE Annual Technical Conference and Exhibition, New Orleans, Louisiana 4-7 October. SPE-129518-STU. https://doi.org/10.2118/129518-STU.

Pathak, V., Babadagli, T., and Edmunds, N.R. 2010. Hot solvent injection for heavy oil/bitumen recovery: an experimental investigation. Presented at the Canadian Unconventional Resources and International Petroleum Conference, Calgary, Alberta, Canada, 19-21 October. SPE-137440-MS. https://doi.org/10.2118/137440-MS.

Pooladi-Darvish, M., Tortike, W.S., and Ali, S.M.F. 1995. A New Semi-Analytical Model for Thermal Recovery Processes. Presented at the SPE Western Regional Meeting, Bakersfield, California, 8-10 March SPE-29660-MS. https://doi.org/10.2118/29660-MS.

Rabiei Faradonbeh, M., Harding, T.G., and Abedi, J. 2012. Semi-analytical modeling of steam-solvent gravity drainage of heavy oil and bitumen, Part 1: enhanced flow rate

at mobile zone. Presented at the SPE Annual Technical Conference and Exhibition, San Antonio, Texas, USA 8-10 October. SPE-160316-MS. https://doi.org/10.2118/160316-MS.

Rabiei Faradonbeh, M., Harding, T.G., and Abedi, J. 2014. Semi-Analytical Modeling of Steam-Solvent Gravity Drainage of Heavy Oil and Bitumen, Part 2: Unsteady-State Model With Curved Interface. Presented at the SPE Heavy Oil Conference-Canada, Calgary, Alberta, Canada 10-12 June. SPE-170123-MS. https://doi.org/10.2118/170123-MS.

Reis, J.C. 1992. A steam-assisted gravity drainage model for tar sands: linear geometry. *Journal of Canadian Petroleum Technology* **31** (10). PETSOC-92-10-01. https://doi.org/10.2118/92-10-01.

Reis, J.C. 1993. A steam assisted gravity drainage model for tar sands: radial geometry. *Journal of Canadian Petroleum Technology* **32** (08). PETSOC-93-08-05. https://doi.org/10.2118/93-08-05.

Rezaei, N., Mohammadzadeh, O., and Chatzis, I. 2010. Warm VAPEX: a thermally improved vapor extraction process for recovery of heavy oil and bitumen. *Energy & Fuels* **24** (11): 5934-5946. https://doi.org/10.1021/ef100749z.

Sabet, N., Hassanzadeh, H., and Abedi, J. 2017. Selection of efficient solvent in solvent-aided thermal recovery of bitumen. *Chemical Engineering Science* **161**: 198-205. https://doi.org/10.1016/j.ces.2016.12.031.

Sasaki, K., Satoshi, A., Yazawa, N. et al. 2002. Microscopic visualization with high resolution optical-fiber scope at steam chamber interface on initial stage of SAGD process. Presented at the SPE/DOE Improved Oil Recovery Symposium, Tulsa, Oklahoma 13-17 April. SPE-75241-MS. https://doi.org/10.2118/75241-MS.

Schmidt, T. 1989. Mass transfer by diffusion. *AOSTRA Handbook on Oil Sands, Bitumens and Heavy Oils*.

Sharma, J. 2011. Advanced Analytical Modelling of Steam-Assisted Gravity Drainage and its Variants. PhD, University of Calgary.

Sharma, J., and Gates, I. 2010. Steam-solvent coupling at the chamber edge in an in situ bitumen recovery process. Presented at the Proceedings of SPE Oil & Gas India Conference, Mumbai, India.

Sharma, J., and Gates, I.D. 2011. Convection at the edge of a steam-assisted-gravity-drainage steam chamber. *SPE Journal* **16** (03): 503-512. SPE-142432-PA. https://doi.org/10.2118/142432-PA.

Shu, W. 1984. A viscosity correlation for mixtures of heavy oil, bitumen, and petroleum fractions. *Society of Petroleum Engineers Journal* **24** (03): 277-282. SPE-11280-PA. https://doi.org/10.2118/11280-PA.

Shu, W., and Hartman, K. 1988. Effect of solvent on steam recovery of heavy oil. *SPE reservoir Engineering* **3** (02): 457-465. SPE-14223-PA. https://doi.org/10.2118/14223-PA.

Strang, G., and Aarikka, K. 1986 . Introduction to applied mathematics. Vol. 16. Wellesley, MA: Wellesley-Cambridge Press, pp 538-540.

Suggett, J., Gittins, S., and Youn, S. 2000. Christina Lake thermal project. Presented at the SPE/CIM International Conference on Horizontal Well Technology, Calgary, Alberta, Canada, 6-8 November. SPE-65520-MS. https://doi.org/10.2118/65520-MS.

Upreti, S.R., and Mehrotra, A.K. 2002. Diffusivity of CO2, CH4, C2H6 and N2 in Athabasca bitumen. *The Canadian Journal of Chemical Engineering* **80** (1): 116-125. https://doi.org/10.1002/cjce.5450800112.

Vogel, J. 1984. Simplified heat calculations for steamfloods. *Journal of petroleum technology* **36** (07): 1,127-1,136. SPE-11219-PA. https://doi.org/10.2118/11219-PA.

Wen, Y., and Kantzas, A. 2005. Monitoring bitumen− solvent interactions with low-field nuclear magnetic resonance and X-ray computer-assisted tomography. *Energy & fuels* **19** (4): 1319-1326. https://doi.org/10.1021/ef049764g.

Worldatlas. 2014. available at www.worldatlas.com/articles/the-world-s-largest-oil-reserves-by-country.html.

www.opec.org.

Yazdani, A., and Maini, B.B. 2006. Further investigation of drainage height effect on oil production rate in VAPEX. Presented at the SPE annual technical conference and exhibition, San Antonio, Texas, USA 24-27 September. SPE-101684-MS. https://doi.org/10.2118/101684-MS.

Yazdani, J., and Maini, B. 2004. New experimental model design for VAPEX process experiments. Presented at the Canadian International Petroleum Conference, Calgary, Alberta 8-10 June. PETSOC-2004-263. https://doi.org/10.2118/2004-263.

Zargar, Z., and Farouq Ali, S. 2016. Analytical Treatment of SAGD-Old and New. Presented at the SPE Canada Heavy Oil Technical Conference, Calgary, Alberta, Canada, 7-9 June. SPE-180748-MS. https://doi.org/10.2118/180748-MS.

Zargar, Z., and Farouq Ali, S. 2017. A New Mathematical Model of Solvent-SAGD Process-Importance of Heat and Mass Transfer. Presented at the SPE Canada Heavy Oil Technical Conference, Calgary, Alberta, Canada 15-16 February. SPE-184978-MS. https://doi.org/10.2118/184978-MS.

APPENDIX A

In Chapter 7, the viscosities and densities of bitumen and solvents as functions of temperature used in the solvent-SAGD model are taken from the data given in Gupta et. al (2011). Table 1 through 4 show the data. Andrade's constants listed in Table 7.1 are obtained using these sets of viscosity data.

Table A.1: Bitumen properties as a function of temperature.

Temperature (K)	Density (kg/m^3)	Viscosity (Pa.s)
273.15	1019.441	58522
283.15	1012.324	6456.41
293.15	1005.206	996.915
303.15	998.089	202.798
313.15	990.971	51.8018
323.15	983.854	15.9881
333.15	976.736	5.78021
343.15	969.619	2.38695
353.15	962.502	1.10294
363.15	955.384	0.560677
373.15	948.267	0.309205
383.15	941.149	0.18285
393.15	934.032	0.114824
403.15	926.914	0.0759479
413.15	919.797	0.052547
423.15	912.679	0.037809
433.15	905.562	0.0281516
443.15	898.445	0.0215988
453.15	891.327	0.0170136
463.15	884.21	0.0137166

Table A.2: Butane properties as a function of temperature.

Temperature (K)	Density (kg/m^3)	Viscosity (Pa.s)
273.15	600.679	0.0002371
283.15	591.423	0.0002021
293.15	581.227	0.0001741
303.15	570.091	0.0001515
313.15	558.015	0.000133
323.15	544.999	0.0001177
333.15	531.042	0.0001049
343.15	516.146	9.41E-05
353.15	500.31	8.50E-05
363.15	483.534	7.72E-05
373.15	465.818	7.05E-05
383.15	447.162	6.46E-05
393.15	427.566	5.95E-05
403.15	407.03	5.51E-05
413.15	385.554	5.11E-05
423.15	363.138	4.76E-05
433.15	339.781	4.45E-05
443.15	315.485	4.17E-05
453.15	290.249	3.92E-05
463.15	264.073	3.70E-05

Table A.3: Pentane properties as a function of temperature.

Temperature (K)	Density (kg/m^3)	Viscosity (Pa.s)
273.15	640.279	0.0003333
283.15	632.395	0.000286
293.15	623.79	0.0002481
303.15	614.465	0.0002172
313.15	604.42	0.0001917
323.15	593.655	0.0001706
333.15	582.171	0.0001528
343.15	569.966	0.0001378
353.15	557.041	0.000125
363.15	543.396	0.000114
373.15	529.031	0.0001045
383.15	513.947	9.62E-05
393.15	498.142	8.89E-05
403.15	481.617	8.25E-05
413.15	464.372	7.69E-05
423.15	446.407	7.19E-05
433.15	427.723	6.74E-05
443.15	408.318	6.33E-05
453.15	388.193	5.97E-05
463.15	367.348	5.64E-05

Table A.4: Hexane properties as a function of temperature.

Temperature (K)	Density (kg/m^3)	Viscosity (Pa.s)
273.15	671.816	0.000377
283.15	666.61	0.0003384
293.15	660.645	0.000306
303.15	653.92	0.0002785
313.15	646.434	0.0002551
323.15	638.189	0.0002348
333.15	629.183	0.0002173
343.15	619.418	0.000202
353.15	608.893	0.0001885
363.15	597.607	0.0001767
373.15	585.562	0.0001661
383.15	572.756	0.0001567
393.15	559.191	0.0001482
403.15	544.866	0.0001406
413.15	529.78	0.0001337
423.15	513.935	0.0001275
433.15	497.329	0.0001218
443.15	479.964	0.0001166
453.15	461.839	0.0001119
463.15	442.953	0.0001075

Figure A.1 shows the variation of densities of bitumen, butane, pentane, and hexane with temperature. The relations given below are used in the model to obtain the results. Note that the solvent and bitumen densities in the model equations are assumed to be constant and at the chamber temperature.

$$\rho_b = -0.7117T + 1213.9 \quad \text{(A.1)}$$

$$\rho_{C4} = -0.0047T^2 + 1.689T + 490 \quad \text{(A.2)}$$

$$\rho_{C5} = -0.0036T^2 + 1.214T + 577.2 \quad \text{(A.3)}$$

$$\rho_{C6} = -0.0038T^2 + 1.593T + 520.1 \quad \text{(A.4)}$$

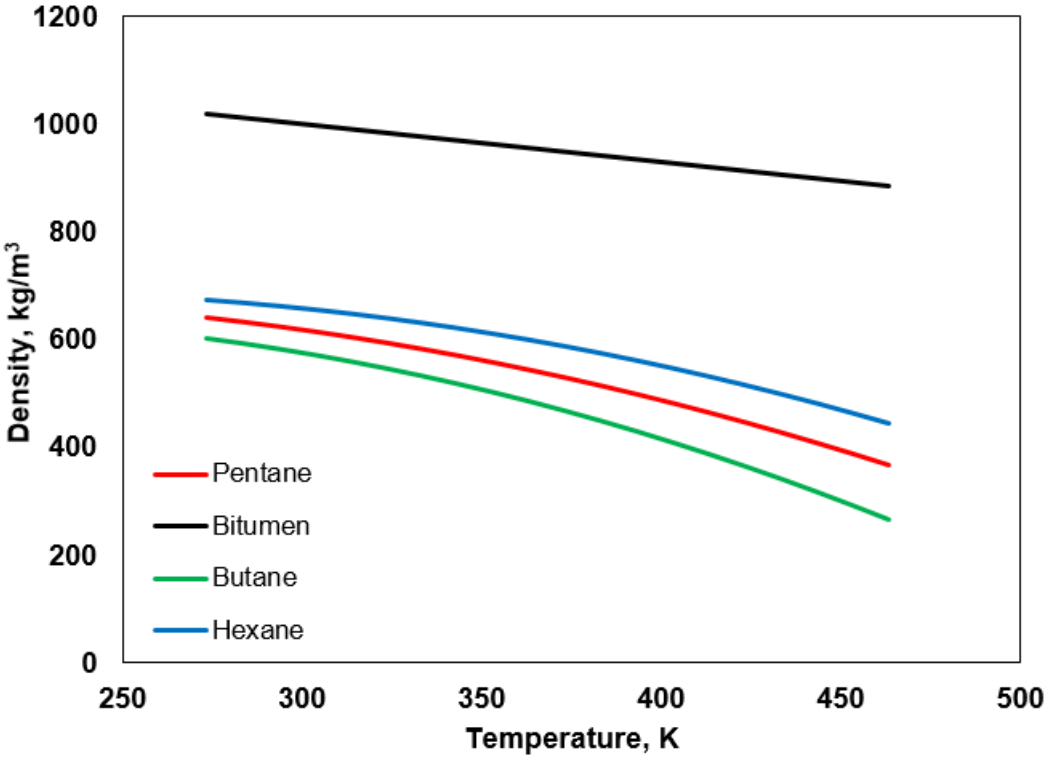

Figure A.1: Density as a function of temperature for bitumen, butane, pentane, and hexane.

APPENDIX B

SOCIETY OF PETROLEUM ENGINEERS LICENSE
TERMS AND CONDITIONS
Sep 28, 2017

This Agreement between Mrs. Zeinab Zargar ("You") and Society of Petroleum Engineers ("Society of Petroleum Engineers") consists of your license details and the terms and conditions provided by Society of Petroleum Engineers and Copyright Clearance Center.

License Number	4196200208681
License date	Sep 25, 2017
Licensed Content Publisher	Society of Petroleum Engineers
Licensed Content Publication	SPE Journal
Licensed Content Title	Analytical Treatment of Steam-Assisted Gravity Drainage: Old and New
Licensed Content Author	Zeinab Zargar, University of Calgary;S. M. Farouq Ali, University of Calgary et al
Licensed Content Date	Jan 1, 2017
Licensed Content Volume	Preprint
Licensed Content Issue	Preprint
Volume number	Preprint
Issue number	Preprint
Type of Use	Thesis/Dissertation
Requestor type	author of the original work
SPE member	yes
SPE member number	
Format	print and electronic
Portion	full article
Will you be translating?	no
Distribution	
Order reference number	

Title of your thesis / dissertation	Comprehensive Analytical Modelling of SAGD and Its Variations
Expected completion date	Sep 2017
Estimated size (number of pages)	250
Requestor Location	Canada Attn: Mrs. Zeinab Zargar
Billing Type	Invoice
Billing Address	Canada Attn: Mrs. Zeinab Zargar
Total	0.00 USD

Terms and Conditions

STANDARD TERMS AND CONDITIONS FOR REPRODUCTION OF MATERIAL

1. The Society of Petroleum Engineers, Inc. (“SPE”) holds the copyright for this material. By clicking "accept" in connection with completing this licensing transaction, you agree that the following terms and conditions apply to this transaction (along with the Billing and Payment terms and conditions established by Copyright Clearance Center, Inc. ("CCC"), at the time that you opened your RightsLink account and that are available at any time at).

2. SPE hereby grants to you a non-exclusive license to use this material. Licenses are for one-time use only with a maximum distribution equal to the number that you identified in the licensing process; any form of republication must be completed within six months from the date hereof (although copies prepared before then may be distributed thereafter); and any electronic posting is limited to the period identified in the licensing process.

3. You may not alter or modify the material in any manner (except that you may use, within the scope of the license granted, one or more excerpts from the copyrighted material, provided that the process of excerpting does not alter the meaning of the material or in any way reflect negatively on SPE or any writer of the material or their employer), nor may you translate the material into another language.

4. Total excerpts from the license material may not exceed thirty percent (30%) of the total text. Not more than five (5) excerpts, figures, tables, or images may be used from any given paper. Multiple permission requests may not be used to exceed these limits.

5. SPE reserves all rights not specifically granted in the combination of (i) the license details provided by you and accepted in the course of this licensing transaction, (ii) these terms and conditions and (iii) CCC's Billing and Payment terms and conditions.

6. While you may exercise the rights licensed immediately upon issuance of the license at the end of the licensing process for the transaction, provided that you have disclosed complete and accurate details of your proposed use, no license is finally effective unless and until full payment is received from you (either by SPE or by CCC) as provided in CCC's Billing and Payment terms and conditions. If full payment is not received on a timely basis, then any license preliminarily granted shall be deemed automatically revoked and shall be void as if never granted. Further, in the event that you breach any of these terms and conditions or any of CCC's Billing and Payment terms and conditions, the license is automatically revoked and shall be void as if never granted. Use of materials as described in a revoked license, as well as any use of the materials beyond the scope of an unrevoked license, may constitute copyright infringement and SPE reserves the right to take any and all action to protect its copyright in the materials

7. You must include the appropriate copyright and permission notice and disclaimer in connection with any reproduction of the licensed material.The copyright information is found on the front page of the paper immediately under the title and author. This statement will then be followed with the disclaimer, "Further reproduction prohibited without permission." Examples:1) Copyright 1990, Society of Petroleum Engineers Inc.Copyright 1990, SPE. Reproduced with permission of SPE. Further reproduction prohibited without permission.2) Copyright 2010, IADC/SPE Drilling Conference and ExhibitionCopyright 2010, IADC/SPE Drilling Conference and Exhibition. Reproduced with permission of SPE. Further reproduction prohibited without permission.3) Copyright 2008, Offshore Technology ConferenceCopyright 2008, Offshore Technology Conference. Reproduced with permission of OTC. Further reproduction prohibited without permission.4) Copyright 2005, International Petroleum Technology ConferenceCopyright 2005, International Petroleum Technology Conference. Reproduced with permission of IPTC. Further reproduction prohibited without permission.If for any reason, the copyright on the paper is missing or unclear, please follow Example 1 above, using SPE as the default copyright holder. SPE administers copyright for OTC, IPTC and other joint events on behalf of all parties in those events.

8. SPE makes no representations or warranties with respect to the licensed material and adopts on its own behalf the limitations and disclaimers established by CCC on its behalf in its Billing and Payment terms and conditions for this licensing transaction.

9. You hereby indemnify and agree to hold harmless SPE and CCC, and their respective officers, directors, employees and agents, from and against any and all claims arising out of your use of the licensed material other than as specifically authorized pursuant to this license.

10. This license is personal to you, but may be assigned or transferred by you to a business associate (or to your employer) if you give prompt written notice of the assignment or transfer to SPE. No such assignment or transfer shall relieve you of the obligation to pay the designated license fee on a timely basis (although payment by the identified assignee can fulfill your obligation).

11. This license may not be amended except in a writing signed by both parties (or, in the case of SPE, by CCC on SPE's behalf).

12. SPE hereby objects to any terms contained in any purchase order, acknowledgment, check endorsement or other writing prepared by you, which terms are inconsistent with these terms and conditions or CCC's Billing and Payment terms and conditions. These terms and conditions, together with CCC's Billing and Payment terms and conditions (which are incorporated herein), comprise the entire agreement between you and SPE (and CCC) concerning this licensing transaction. In the event of any conflict between your obligations established by these terms and conditions and those established by CCC's Billing and Payment terms and conditions, these terms and conditions shall control.

13. This Agreement shall be governed and interpreted by the laws of the State of Texas, United States of America. Regardless of the place of performance or otherwise, the Agreement, and all schedules, amendments, modifications, alterations, or supplements thereto, will be governed by the laws of the State of Texas, United States of America. If any provisions of the Agreement are unenforceable under applicable law, the remaining provisions shall continue in full force and effect.

Other Terms and Conditions:

v1.1

Questions? customercare@copyright.com or +1-855-239-3415 (toll free in the US) or +1-978-646-2777.